CRANFIELD UNIVERSITY

B.TARVER

DEVELOPMENT OF TURBINES FOR USE IN OSCILLATING WATER COLUMNS

SCHOOL OF ENGINEERING

EngD THESIS

This page has intentionally been left blank.

CRANFIELD UNIVERSITY

SCHOOL OF ENGINEERING

EngD THESIS

Academic Year 2012 - 2013

B. TARVER

DEVELOPMENT OF TURBINES FOR USE IN OSCILLATING WATER COLUMNS

Academic Supervisor: Dr. Joao A. Amaral-Teixeira

January 2013

This thesis is submitted in partial fulfilment of the requirements for the Degree of Engineering Doctorate.

This page has intentionally been left blank.

Abstract

Bidirectional impulse turbines for oscillating water column wave power devices have the inherent problem of pressure losses associated with the outlet guide vane, adversely affecting the performance of the turbine. Two methods of guide vane design have been investigated with the aim of improving the performance of bidirectional impulse turbines by reducing these losses. These methods employ the use of optimisation, using computational fluid dynamics as a method of predicting the performance of the turbine.

Numerical results are presented of the performance of the datum turbine, these have been validated using previous experimental data. These results are used as a baseline to measure performance improvements. An optimisation system has been adapted for the guide vanes of the datum turbine, allowing optimisation in bi-directional flows.

Two novel guide vane design concepts were explored and the results of parameterisation studies investigating the effects of specific guide vane parameters are presented. The results of two global optimisation procedures, demonstrating the predicted performance improvements of the optimum guide vane configurations are presented. Both optimisation methods demonstrate reduced losses associated with the OGV of the turbine. The second concept, investigating guide vane profile optimisation in bi-directional flows, resulted in a respectable gain in turbine efficiency.

Acknowledgements

The author wishes to thank his supervisor, Dr Joao Amaral Teixeira for his help, guidance and encouragement throughout the project.

The author is grateful to Dresser Rand Company Ltd for the funding and support provided. The valuable technical assistance of William Maier has been greatly appreciated as has the help of Dr Shahab Natanzi.

Thank you to Dr Kevin Banks for his previous work on the development of the optimisation tool used in the research without which the results presented in this thesis would not have been achieved. The author would also like to thank Joel Ojile for his help with optimisation processes and computer scripting.

Thanks are also due to Michael Lewis for sparking the authors interest in oscillating water columns.

Contents

List of Figures

List of Tables

Notation

Abbreviations

2D	Two-dimensional
3D	Three-dimensional
AFC	Active flow control
BETC	Business Energy Tax Credit
BIMEP	The Biscay Marine Energy Platform
CFD	Computational fluid dynamics
DAWT	Diffuser augmented wind turbine
EU ETS	European Union Emissions Trading Scheme
EVE	Ente Vasco de la Energia
FERC	Federal Energy Regulatory Commission
GA	Genetic algorithm
FIT	Feed-in tariff
GV	Guide vane
IGV	Inlet guide vane
LIMPET	Land Installed Marine Pneumatic Energy Transformer
MEGV	Multi element guide vane
MMS	Minerals Management Service
OGV	Outlet guide vane
OPT	Ocean Power Technologies
OWC	Oscillating water column
PFC	Passive flow control
PG&E	Pacific Gas and Electric
RO	Renewable Obligation
ROC	Renewable Obligation Certificate
RPS	Renewable Portfolio Standards
TE	Trailing edge
TET	Trailing edge thickness
TP	Total Pressure
VRT	Varying radius turbine
WavEC	Wave Energy Centre
WEC	World Energy Centre

Roman letters

A_x	*Axial spacing*	*chord lengths*
b_n	*Axial chord*	*m*
b	*Blade height*	*m*
C_A	*Torque coefficient*	
C_T	*Input power coefficient*	
D	*Characteristic length*	*m*
D_t	*Turbine tip diameter*	*m*
E	*Number of vane rows*	
f	*Frequency of oscillation*	*Hz*
l	*Chord*	*m*
$\dot{m}$	*mass flow rate*	kgs^{-1}
P_T	*Outlet static pressure*	*Pa*
p^*	*Non-dimensional pressure drop*	
P_T	*Turbine power*	*W*
Q	*Volumetric flow rate*	m^3s^{-1}
R	*Vane row chord ratio*	
$r_{TE\,n}$	*Trailing edge radius*	
S	*Pitch*	*m*
S_t	*Strouhal number*	
T	*Wave period*	*s*
T	*Guide vane thickness*	*m*
t_e	*Trailing edge thickness*	*m*
U	*Blade circumferential velocity*	ms^{-1}
V_0	*Flow velocity in*	ms^{-1}
V_a	*Mean axial velocity*	ms^{-1}
V_i	*Flow velocity out*	ms^{-1}
V_y	*Flow velocity Y component*	ms^{-1}
w	*Relative velocity*	ms^{-1}
$y+$	*Non-dimensional first cell height*	
Yt	*Total loss coefficient*	

Greek Letters

β	*Guide vane camber*	*degrees*
δ	*Pitch offset*	*% of pitch*
δ^*	*Nominal deflection*	*degrees*
η	*Turbine total-to-static efficiency*	
θ	*Guide vane camber*	*degrees*
ρ	*Density*	*kg* m^{-3}
Φ	*Turbine flow coefficient*	
ω	*Angular velocity*	*rad* s^{-1}

1 Introduction

1.1 Background and motivation

Current global energy usage is unsustainable. This fact, coupled with predicted growth in energy usage presents a problem both in irreversible climate change and energy security. In the UK, domestic fossil fuel reserve depletion brings reliance on others for continued energy supply through burning fossil fuels. A diverse mix of renewable technologies is required to overcome the supply side issue to the energy problem. The UK has a wealth of energy resources and the exploitation of these resources through renewable technologies will allow a strong contribution to energy needs.

There has long been a desire to harness the power from ocean waves and the current situation has generated renewed interest in the marine renewable sector. Ambitious targets in the UK to install 2 GW of ocean energy generation capacity by 2020 and up to 30 GW by 2050 together with attractive support mechanisms have brought marine renewable energy developers from across the globe. As a result the UK has the highest installed capacity of marine renewable devices in the world at 7.55 MW of which just over 3 MW is wave energy capacity. Despite this fact, the high capital cost of installation and relatively low efficiencies of devices mean that the search for economic generation of electricity continues and on going device development is required to meet the ambitious targets.

One of the most extensively studied wave energy devices is the oscillating water column (OWC), with the focus being on the bi-directional air turbine required to convert pneumatic energy to mechanical energy within the device. Two main types of bi-directional turbine have been studied for this application, one known as the Wells turbine and the main alternative, the bi-directional impulse turbine. Until recently, the

majority of the research had been into the design and performance of the Wells turbine but in recent times, the benefits of the bi-directional impulse turbine have been identified. This is in part due to the HydroAir air turbine development project of which this thesis presents the most recent developments.

The HydroAir air turbine development project is a programme of research that commenced in 2004 as a joint undertaking between Peter Brotherhood Ltd (now Dresser-Rand Company Ltd.) and Cranfield University and was partly funded by the Department of Trade and Industry. The aim of the project was to significantly improve the performance of OWCs by the development of novel, high efficiency turbomachinery and this was achieved with the variable radius turbine (VRT) concept, patented in 2008 (Freeman et al., 2008). The bi-directional impulse turbine, commercially named HydroAir, incorporates the VRT concept and achieved a step change in performance of bi-directional turbines for OWCs with significant performance improvements over existing designs in the literature.

The work presented in this thesis has been conducted by the author as a continuation of the HydroAir air turbine development project, focussing on turbine design with the aim of achieving further performance improvements of the device. Specifically, two concepts of reducing the losses associated with the fixed inlet and outlet guide vanes have been investigated. This has involved optimisation techniques, making use of numerical performance predictions with computational fluid dynamics (CFD). This thesis presents the results of these procedures and describes two novel guide vane solutions for bi-directional impulse turbines resulting in significant performance improvements over conventional geometries.

1.2 Author's contribution

The main contributions in this thesis can be split into two groups and are presented below:

Multi-element guide vane concept:

- An investigation into the concept of replacing conventional guide vane geometry with multiple stator rows in a bi-directional turbine to reduce the pressure losses that occur from reverse flow across the outlet guide vane.

- Definition of a set of design rules for multi-element guide vanes (MEGVs) for bi-directional impulse turbines.

- Optimisation of the MEGV geometry in reversing flows. This resulted in an enhanced configuration for the datum bi-directional impulse turbine, demonstrating the capabilities of the design rules and the potential performance improvements.

Bi-directional profile optimisation:

- Investigation into profile parameterisation methods with the flexibility to produce unconventional guide vane profiles.

- Investigation into the concept of optimising a stator profile for function in reversing flows.

- The development of a novel guide vane profile with significant predicted performance improvement over a conventional profile, produced using profile optimisation in bi-directional flows.

- Demonstration that the design of stators for bi-directional flows, taking into account the bi-directional function of the stator, can result in significant improvement in performance.

An international patent application has been submitted by Dresser Rand on which the author is a named inventor. The patent covers the MEGV concept for bi-directional impulse turbines.

1.3 Thesis structure

The work in this thesis is set out in nine chapters beginning with a literature review in Chapter 2. The review presents a summary of estimated wave energy resource and an up to date review of wave power technologies that have reached the scaled prototype stage, focusing on the UK. The historical development of OWC technology is then reviewed with focus on the bi-directional turbine component of the device and more specifically, the subject of guide vane losses in the bi-directional impulse turbine. Chapter 3 presents an overview of the numerical methods used in the research, covering the optimisation techniques used and geometry generation strategies as well as meshing and processing for CFD.

The datum turbine used as a base for comparison throughout the research is described in Chapter 4, presenting the geometry and an understanding of the function of the device with the help of full scale, 3D simulations. Information is also given on the reciprocating test rig used for validation of CFD results and a description of the experimental method used.

Chapter 5 presents the MEGV concept and the initial design process involved in generating the set of design rules for the configuration prior to optimisation. The parameterisation method is then detailed along with results of a full parameter study. The results of a multi-variable optimisation procedure are then displayed with a graphical comparison of the datum and optimum geometries. The predicted performance of the optimum geometry is then discussed and a comparison is made in full scale 3D CFD for a full characteristic of the turbine with presentation of the results.

Chapter 6 describes the investigation into bi-directional stator profile optimisation commencing with a description of the concept and the reason for conducting the work. A review of parameterisation methods is presented with two methods chosen for further investigation. A parameter study is presented before a global optimisation procedure is conducted. Optimum geometry is again compared with the datum turbine using full scale 3D CFD.

Chapter 7 considers the business environment surrounding wave power technologies, putting the technical content of the research into commercial context. An assessment of the potential market for OWC devices is presented, first at a global scale then specific emerging markets. The information is used to perform an analysis of the external factors affecting a company looking to develop OWC technology. The HydroAir device is then analysed more specifically based on current internal and

external factors affecting its current position. The results are also applicable to other technologies in the early stages of development in the marine renewables sector.

Chapter 8 presents discussions, conclusions and limitations of the work presented in this thesis and Chapter 9 gives some recommendations for further work.

2 Literature Review

The extraction of power from ocean waves has been a long researched topic with literature dating back over 40 years. Despite this volume of research and extensive theoretical analysis and testing, it is not until recent years that successful wave power devices of significant scale have been produced. Even so, the devices that have made it this far are still in the early stages of development and the point of wide commercial deployment has yet to be reached. This review presents the current status of wave power both globally and specifically for the UK with focus on OWC technology. Both historical and current solutions to the turbine assembly of an OWC are presented with discussion of the problems that have contributed to the lack of success of these types of wave power devices. This up to date review, showing the state of the art in OWC turbine technology positions the HydroAir device against the current competition, highlighting the requirements and necessary performance that will take wave power to commercialisation.

2.1 Wave energy

2.1.1 Resource

The reason wave power has seen such a high level of interest over such a long period is due to the huge potential of this energy source from the oceans. Over the years, there have been a number of attempts to estimate the total available wave energy resource in the UK with the aim of understanding the potential for wave energy generation.

Mollison's study (1986), based on a resource frontage model, estimates that the mean power available along the most productive coastlines of the world is above 40 MW/km and if 50% of this resource became economically extractable then the total

resource worldwide is capable of meeting a large proportion of global electricity demand (in 1986). It is also worth noting that electricity is not the only possible use of wave power, there have also been investigations into wave energy devices that work as pumps providing high pressure water for reverse osmosis techniques, producing freshwater from sea water (See, for example, Hicks et al., 1989; Charcosset, 2009). Variations in device design and capability are likely to be suited to different locations, increasing the number of potential sites where wave power can be harvested.

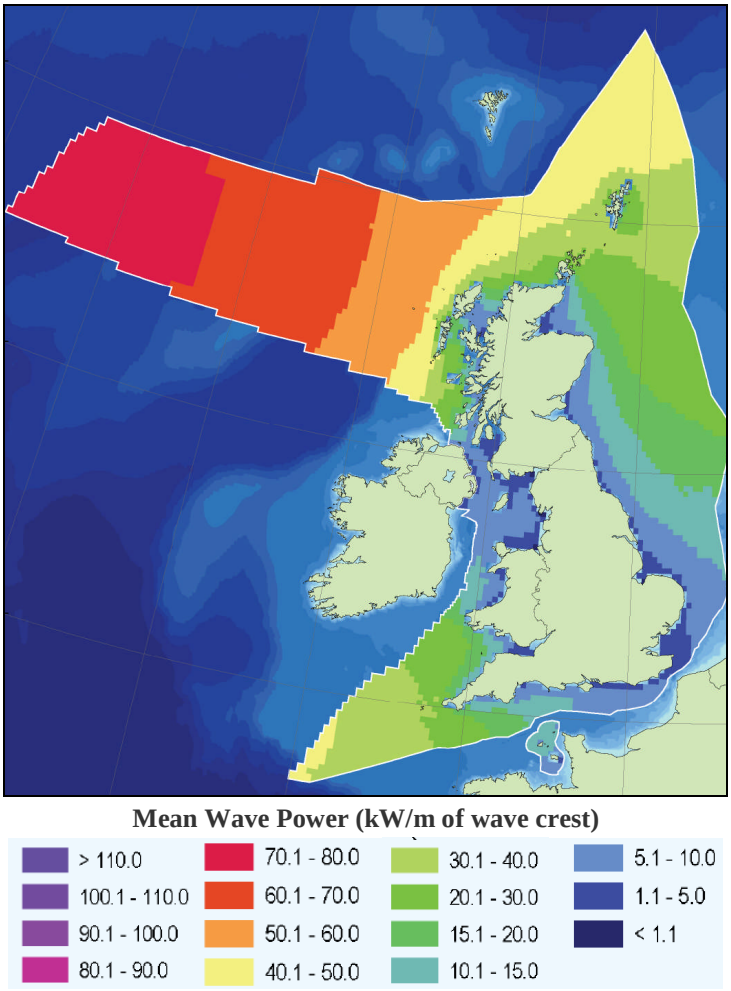

Figure 1: Mean wave power around United Kingdom (kW/m of wave crest) (Jackson, Moore and Cooper, 2008).

The map displayed in *Figure 1* shows the mean wave power around the coast of the UK, based on hourly model hind-cast values over 7 years. These results were published in March 2008 in the Atlas of UK Marine Energy Resources (Jackson, Moore and Cooper, 2008). The data for this publication has been made available by the Met Office, calculating the effective wave power per metre of wave crest using observations of significant wave height (H_s) and wave group speed (c_g).

The data shows that the shoreline of the UK receives significant wave power with the majority coming from the Atlantic Ocean approaching the West coast of Scotland. The range of power available at near-shore locations along these most active coastlines agrees with Mollison's (1986) much earlier resource estimates.

Mackay (2009) performed a more resent study into the estimation of the potential wave energy that could be extracted from the coast of the UK, using Mollison's work as a base but putting into context the length of available coastline, the power available and an up to date estimated efficiency of extraction. This estimation concludes that 40MW/km over an exposed UK coastline of 1000km could realistically supply 4kWh per day per person to the UK (population 60 million). For comparison, this equates to 88 TWh/year.

Mackay's (2009) study estimates that the average energy usage required to supply electricity to one person in the UK is 45 kWh per day per person (only electricity usage, not total energy) showing that wave power has the potential to supply almost 10% of this need for an island like the UK. Even though this study uses rounded figures and the estimates are based on theoretical technology performance that even now has still not been demonstrated at commercial scale, it is useful to put the numbers into context.

The most recent of these studies has been commissioned by the Carbon Trust (Carbon Trust, 2012) and presents an interesting comparison of historical resource estimates of practical resource *(Figure 2).* The practical resource is dependent on a number of both technical and environmental constraints and these are often dependent on assumptions made by the authors. For this reason, it is interesting to see how the practical resource estimates compare as more accurate information about the available resource and the capabilities of technologies has become available.

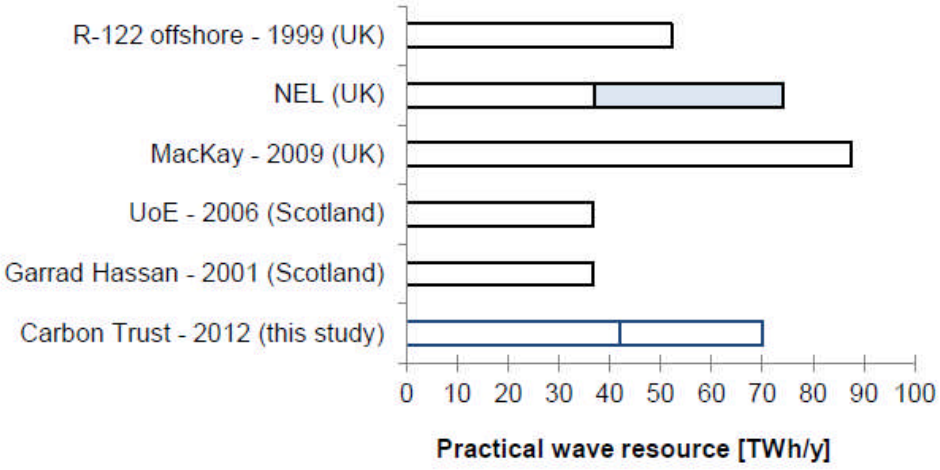

Figure 2: Practical wave energy resource estimates for the UK and Scotland (Carbon Trust, 2012).

In its recent publication the Carbon Trust has paid particular attention to the cost of energy and their model includes estimated costs for capital items, structural costs, installation and project management. Since some of these costs are sensitive to location factors such as distance from shore and water depth, the model enables the identification of areas of least energy cost around the UK. This data is shown graphically in *Figure 3* presenting resource frontages chosen to represent the offshore resource.

The blue bar on the above chart *(Figure 2)* shows a mark at 42 TWh/y which corresponds to the pricing model outlined by the Carbon Trust. This represents resources available at or below three times the most cost effective solution. Looking at the range of resource estimates the majority appear to be around this value suggesting MacKay's estimate is over optimistic. The results indicate that an estimate of almost 5% of UK electricity demand being supplied by wave power may be more realistic.

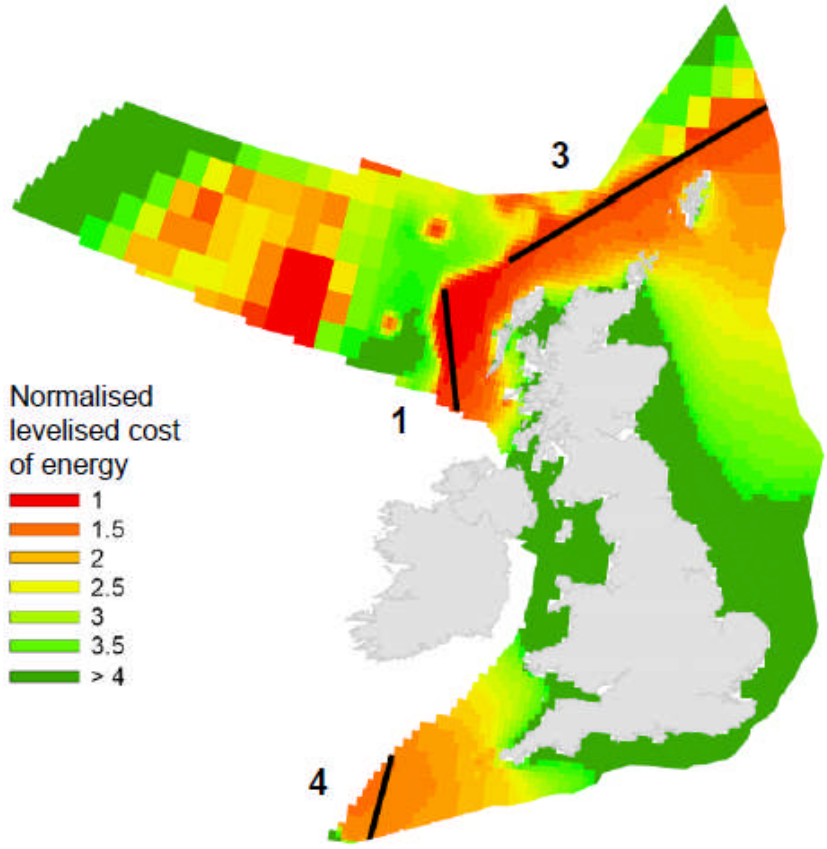

Figure 3: Cost-of-energy model for wave energy
showing areas of relative high and low cost with marked frontages at lowest cost locations
(Carbon Trust, 2012).

2.1.2 Current position

The UK is a leader in wave power technology development due partly to the energetic resource in the surrounding oceans. The UK also has ambitious targets for ocean energy generation capacity and substantial support mechanisms, attracting both wave and tidal energy developers from all over the world to test and establish their technologies in the early stages. A number of test and research centres are also present in the UK, the European Marine Energy Centre (EMEC) in Orkney, Scotland was established in 2003 and offers fully grid connected and instrumented test areas (Morris, 2012). EMEC offers developers the opportunity to test full-scale prototypes quickly and cost effectively and has been instrumental in ensuring the UK continues to lead in the wave power industry. Wave Hub is also a grid connected facility off the coast of south west England, offering wave energy device developers the chance to test full scale devices without the need for high installation costs.

Currently there are 3.05 MW of installed wave energy capacity and over 30 different companies in the UK developing wave energy technologies (Hussey and McNelis, 2012). Total ocean energy installed capacity, including tidal stream and tidal range capacity is currently 7.55 MW with approximately 60 MW of marine energy projects planned for deployment within the next 4 years. These projects are mostly prototype devices with plans for small arrays up to 5MW. However there are larger arrays planned up to 10 MW, following the success of these smaller projects (Khrohn et a1, 2012). Although there are not official targets for ocean energy alone, Figure 4 below shows estimates produced in a number of different studies and roadmaps which indicate an installed capacity between 300MW and 3000MW by 2020.

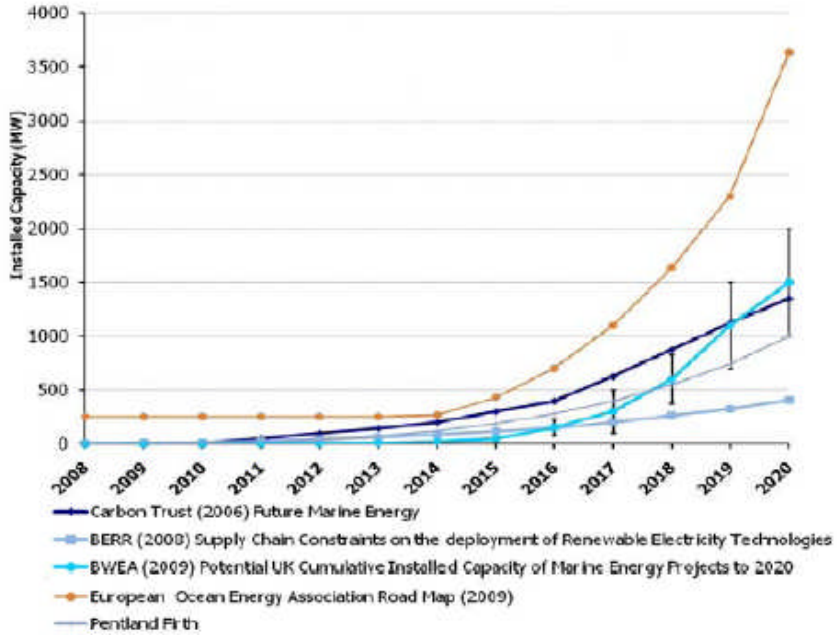

Figure 4: Estimates of Marine Renewable Installed Capacity to 2020 (Hussey and McNelis, 2012)

Of the currently installed capacity, the only OWC device operational in the UK is Voith Hydro Wavegen's (formerly Wavegen) 500kW LIMPET device. This shoreline device was first installed in 2000 and was the world's first grid connected wave energy device (Queen's University Belfast, 2002). LIMPET is run as a test facility for Voith Hydro's Wells type bi-directional turbine. The Voith turbine has also been used in the Mutriku wave power plant in Spain, the first commercial wave power plant in the world. At Mutriku, 16 18.5kW turbines are integrated into a breakwater to produce a 300kW plant. The plant has been running successfully since commissioning in June 2011 clocking up 30,000 turbine hours (Maier, 2012). There have been no recent publications demonstrating the performance of the Voith Hydro Wells type turbine so no comparison as to the efficiencies achieved can be made.

The Irish company, OceanEnergy Ltd, have been successfully testing their scaled OE Buoy OWC in the Irish Sea for over 2 years and have recently been granted a license to test a full scale device at the Wave Hub test site. A partnership has been agreed with Dresser Rand to supply the turbine for the 1MW OWC device, a promising start for OWC technology and the HydroAir turbine in 2013.

2.2 Oscillating Water Columns

An OWC wave energy device is comprised of a chamber and an air turbine connected to a generator *(Figure 5)*.The chamber is open at one end which is submerged beneath the surface of the sea. Above the water level there is an opening that is connected to the turbine duct. As waves move across the chamber, the column of water within the chamber moves up and down, acting like a piston. This movement creates a reciprocating airflow across the turbine. The function of the turbine is to convert this reciprocating airflow into unidirectional rotary motion to drive the generator.

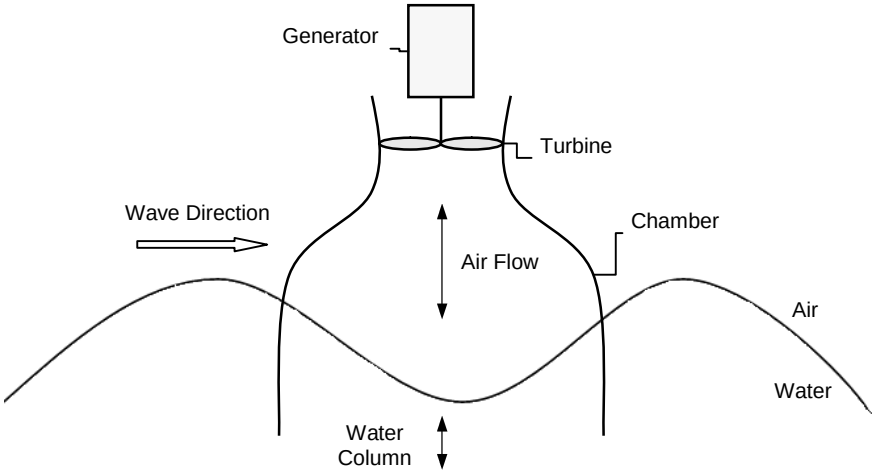

Figure 5: Schematic diagram of an OWC device.

The concept of an OWC is simple but the specific requirement of the turbine to perform in irregular, bi-directional air flow makes the problem difficult. The number of moving parts is minimised to improve reliability, an important factor for a wave energy device as OWCs are sited in active seas making accessibility and maintenance difficult.

The moving parts are positioned above the waterline, reducing the problems associated with submersion in corrosive sea water. The salt and moisture content of the sea air is still a problem for the device as this environment is damaging to traditional materials and components. This has been evident in the large Horns Reef offshore wind project in Denmark, and in the UK, off the Kentish flats, where the gearboxes of the wind turbines have had to be replaced in less than half the expected design life (Wind Power, 2009). This adds further complexity to the problem of extracting power from ocean waves and increases the cost of design, development and manufacture.

Survivability is a key contributor to the development cost of wave power technology. A wave power device must be capable of surviving the extremely high loads associated with high sea states. This means designing the device to withstand the largest wave that could potentially occur at the site where it will operate. This adds considerable cost to the design and manufacture of wave energy devices. The Pelamis wave energy device, a hydraulic actuating wave energy converter, has been designed specifically for survivability but this has compromised the generating capacity of the device. Pelamis, now supported by E.ON Energy, has two second generation 750kW Pelamis P2 devices installed at EMEC with plans for a number of 10MW wave farms in the waters off the Scottish coast.

One solution to the high cost of survivability in high sea states is to design the capability of 'decoupling' into the device if wave energy becomes too great. One device that has this capability is the Oyster wave energy device from Aquamarine Power. This nearshore device comprises a buoyant flap that is hinged at the sea bed and the oscillating action of the flap activates hydraulic rams that pump sea water back to shore. This sea water is then used to drive a Pelton turbine connected to a generator to generate electricity (Whittaker, 2007). The device has the capability to be 'parked' on the sea bed where the buoyant chamber at the top of the flap can be filled with sea water and the flap lowered. Positioning the flap on the sea bed in this way is an effective way of ensuring that even in the highest sea states, the device can be stowed to avoid the risk of damage and loss.

2.2.1 Chain of Conversions

The overall efficiency of an OWC is a result of the combined efficiencies of the components that make up the device. This creates a chain of conversions where the efficiency of each component must be maximised to produce a device of high performance. The capture efficiency of the collector chamber is the amount of energy that is captured by the device compared to the available incident wave energy passing on to the chamber. This gives the efficiency of the transfer of energy from the water column to the airflow in the chamber.

An OWC can be modelled as a mass spring damper, as the column of water must first compress the air within the chamber to then force the air through the chamber orifice, into the duct and past the turbine. The pressure drop across the turbine causes a restriction to the flow, causing a damping effect. This damping effect must be used in the design process to evaluate the efficiency of the device for the known wave activity.

The amount of incident wave energy which is transferred into pneumatic energy in the air is known as the capture efficiency of the chamber. The total efficiency of an OWC device is calculated as the product of the chamber capture efficiency, turbine mechanical efficiency and generator electrical efficiency, known as the wave-to-wire efficiency.

Device		Chamber	Turbine		Generator	Total
LIMPET	Estimated	80%	60%	average	100%	48%
	Actual	64%	40%	average	32%	8%
Mighty Whale	Estimated	50%	50%		-	25%
	Actual	32%	47%		-	15%
Pico	Estimated		50%	average		35%
			75%	peak		
Ocean Linx	Estimated	67%	54%	average	90%	32%
			80%	peak		
Vizhinjam	Actual	50%	25%		50%	6.25%

Table 1: OWC project performance data, estimated and actual (from Webb et al., 2005; Washio et al. 2000)

Table 1 shows estimated and actual efficiencies for components in the chain of conversions of a number of historical OWC devices. These are devices that have reached the scaled prototype stage of production and more information is given about some of them further on in the report. The data shows how the total efficiency of an OWC device is made up of the efficiencies of the individual components of the chain.

The performance data of these devices is poor and there is a large misalignment between the estimated and actual performance of the components. This demonstrates the difficulty in accurately simulating / testing an OWC device and that the actual performance in irregular seas can be very different to predictions. The results for the LIMPET device are dated and it is expected that the performance of the current turbine has improved after over 10 years of testing in real sea conditions but there has been no published data to confirm this.

2.2.2 Location

Sea state and wave activity vary greatly at different locations across the world and it is essential that wave power devices are designed specifically for the location where they are going to function in order to achieve high levels of efficiency. OWCs have been designed to be mounted in a variety of locations and the potential wave resource and the nature of ocean waves varies for different mounting locations.

Shoreline devices are positioned on land, at a coastal location where there is high wave potential. Shoreline devices have the benefit of ease of construction and reduced costs as the majority of the work can be carried out from the land. The LIMPET shoreline wave energy plant (Wavegen, 2003) is situated on the Isle of Islay off the west coast of Scotland and made use of the 'designer gully' concept during construction. In this procedure, the rock is excavated into the cliff from above, leaving a rock bund to protect the construction site from the sea. The concrete chamber could then be assembled using conventional methods on dry land. When the construction is complete the bund is removed by blasting to open the gully to the sea.

This method has benefits in terms of construction but there turned out to be problems with the operation of the device within the gully. Debris from the blasted bund gradually blocked the opening of the chamber over time and the harbour wall effect did not work to benefit the performance of the OWC. This is one of the reasons for the poor performance of the LIMPET device.

There is however a reduction in incident wave power at a site closer to shore due to the decreased depth of water. As the water depth decreases, wave power is reduced due to friction with the sea floor. Shoreline devices are directly affected by this but analysis of two specific Scottish sights by Folley and Whittaker (2009) show that the reduction in incident wave power is limited between nearshore and offshore locations. This study shows that nearshore and offshore sights show similar potential for exploiting wave power, especially when other factors are considered such as construction and connection costs.

Since the LIMPET plant was the first OWC device to be connected to the grid, a shoreline device was the most appropriate due to the reduced costs. The LIMPET device enables an easily accessible test bed for turbine devices to be connected to the chamber and to be tested on real air flows generated from waves. As the technology becomes more established and moves towards larger scale energy production, it would be more economical to move devices offshore to benefit from the larger wave resource (Webb et al., 2005).

Breakwater devices make use of either existing or planned breakwater structures to support the OWC, potentially reducing the capital cost of the OWC project. The Vizhinjam prototype OWC in India is an extension of a pre-existing breakwater and has been used to test a Wells turbine design and variations. The output has been highly variable and the research into improved power conversion systems continues (Khan and Bhuyan, 2009). The problem with installing OWC devices on to existing breakwaters is the suitability of the site. The breakwater will not have been designed with the addition of an OWC in mind and so the wave activity at the location may not

be sufficient to make installing an OWC worthwhile. There has however been research into the combined construction of OWCs and breakwaters with the requirements of both features in mind (Boccotti et al. 2007). The Mutriku wave power plant in Spain made use of a pre-planned breakwater to incorporate a wave power plant.

OWC devices positioned out to sea are classified as either nearshore or offshore depending on distance. These devices can be expected to produce more energy than shore mounted devices due to the increased incident wave power further from the shore. This can be seen from the wave data displayed earlier*(section 2.1.1).* Deployment away from the shore incurs high costs which increase according to how far from the shore the device is positioned. These costs are due to the need for mooring and undersea cabling as well as increased access and maintenance costs as estimated in the Carbon Trust model also discussed earlier *(section 2.1.1).* These extra costs will however be offset by the improved generating capabilities as devices mature and the development of infrastructure, as the wave energy industry becomes more established.

2.3 Turbines for use in Oscillating Water Columns

2.3.1 Requirements

As stated previously, the main requirement of the turbine in an OWC is to efficiently convert the reciprocating airflow produced by the device into unidirectional rotary motion to drive the generator. The turbine is also required to operate across a range of flow rates as the incident wave power for any location varies considerably. The reciprocating airflow produced by an OWC is irregular and not sinusoidal as might be expected. *Figure 6* shows the measured volumetric flow rate with time, produced by the National Institute of Ocean Technology and it can be seen that the negative flow (exhalation) produced by the trough of the wave is much more distorted than the inlet flow and the peak flow in reverse *(negative Q)* is almost half the peak inlet flow *(positive Q)*. This is an example of the flow pattern that the turbine must operate within, converting this irregular, reversing flow to smooth unidirectional rotary motion.

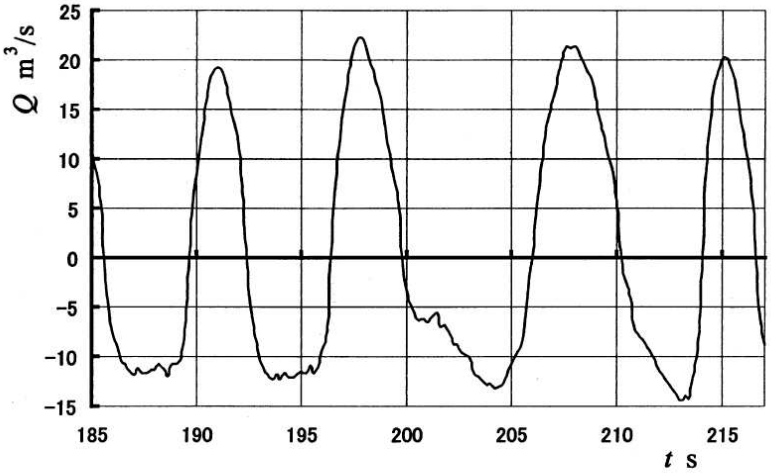

Figure 6: Volumetric flow rate (*Q)* measured with time.
Data from the wave energy plant of National Institute of Ocean Technology of India (Setoguchi et al., 2003).

As OWCs are likely to experience times of zero or very low wave activity it is essential that the turbine is capable of self-starting. If a turbine is capable of self-starting in a short amount of time or a short number of wave cycles, this will greatly improve the overall efficiency of the device.

An OWC puts high demands on the turbine due to the difficult environment created by an ocean wave. The next section displays variations of turbine technologies that

have been designed to meet these requirements, the problems encountered and the performances achieved.

2.3.2 Wells turbine

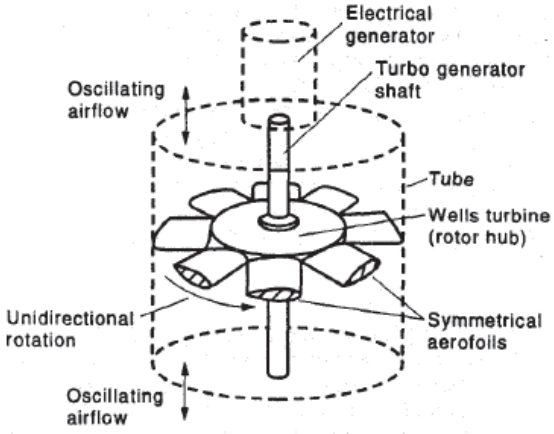

Figure 7: Wells Turbine (Watterson and Raghunathan, 2006)

The Wells Turbine was invented by Professor Alan Wells (Wells, 1976) specifically for the application of the OWC, to convert the pneumatic power of the periodically reversing wave stream to unidirectional rotational motion. The blades of the turbine have airfoil shaped blades of zero camber, symmetrical about the rotational plane and evenly spaced around the rotor *(Figure 7).*

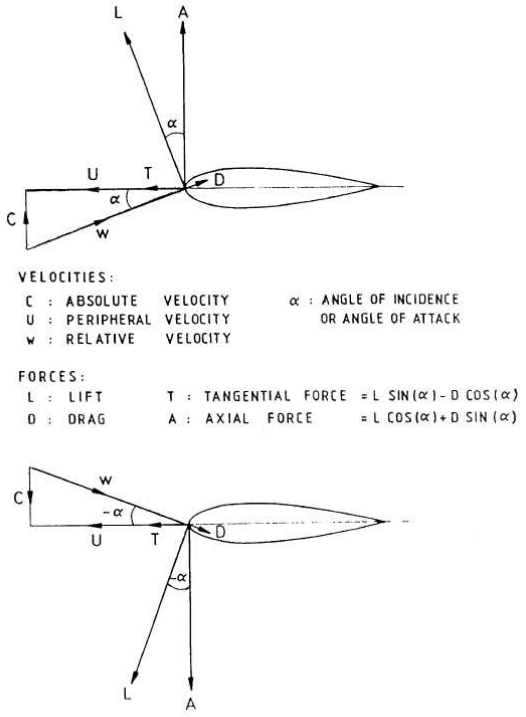

Figure 8: Wells turbine operating principle (Dhanasekaran and Govardhan, 2005).

The airfoil theory behind Wells turbine is displayed in *Figure 8*. The fluid induces a lift and drag force on the airfoil as a result of the incident angle. Resolving these forces gives the tangential forces acting on the turbine blade. It can be seen that a tangential force is generated in the forward direction as a result of fluid approaching the airfoil from both directions.

The simple design of Wells turbine is ideal for an OWC device and for prolonged reliability in a marine environment. There are however a number of fundamental problems with the performance of the design.

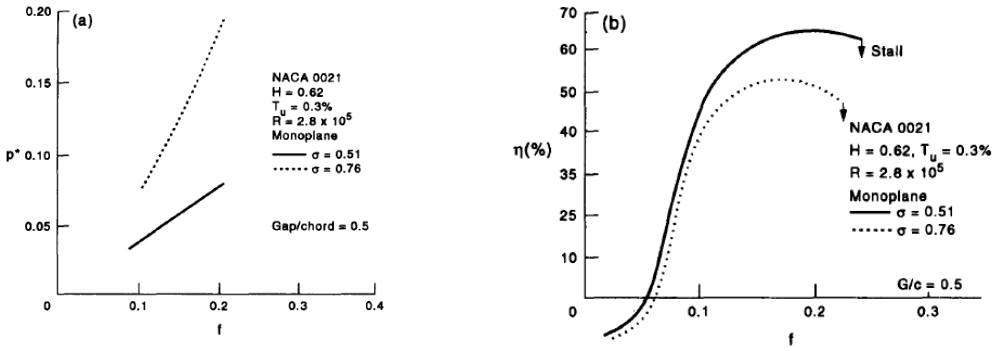

Figure 9: Wells turbine performance characteristics,
(a) Pressure drop – flow coefficient relationship,
(b) Aerodynamic efficiency – flow coefficient relationship (Raghunathan, 1995)

At optimum flow-rate the Wells Turbine performs well with measured efficiencies of up to 70%, but the turbine is sensitive to changes in flow rate. *Figure 9* shows the relationship of non-dimensional pressure drop *(p*)* and aerodynamic efficiency against flow coefficient. Non-dimensional pressure drop is defined as $p^* = \Delta p/(\rho w^2 D_t^2)$ where Δp = the pressure drop across the rotor, w = relative velocity and D^t = turbine tip diameter. It can be seen that although a high efficiency is reached, the flow range at which this level of efficiency is achieved is small. At low flow rates, the drag component of the force transferred to the blade is larger than the lift force, resulting in negative efficiencies (*Figure 9(b)).* At large flow rates, separation occurs at the flow boundary layer on the airfoil resulting in stall and the turbine fails to continue to extract power from the flow. These characteristics mean that the standard Wells turbine will only perform with a high efficiency across a small flow range. This range can be maximised by matching the turbine to the OWC chamber and designing the device specifically for the final location (Brito-Melo et al., 2001), but the range still remains small. Many variations of the Wells turbine have been explored with the aim of increasing the width of the operating range and these are discussed below.

Wells turbine with fixed guide vanes

The addition of static guide vanes was one of the first modifications to be made to the standard Wells turbine design *(Figure 10)*. The guide vanes are positioned so that the fluid approaches the blade at the correct incident angle, improving the tangential force on the rotor blades and extending the operating range by delaying the onset of stall. Govardhan and Dhanasekaran (2001) tested the addition of static GVs to the standard Wells Turbine and improvements in both peak (up to 8%) and overall efficiencies were achieved. Setoguchi et al. (1998) also showed improvement in peak performance. Static guide vanes have also been shown to improve the starting characteristics of the standard Wells Turbine.

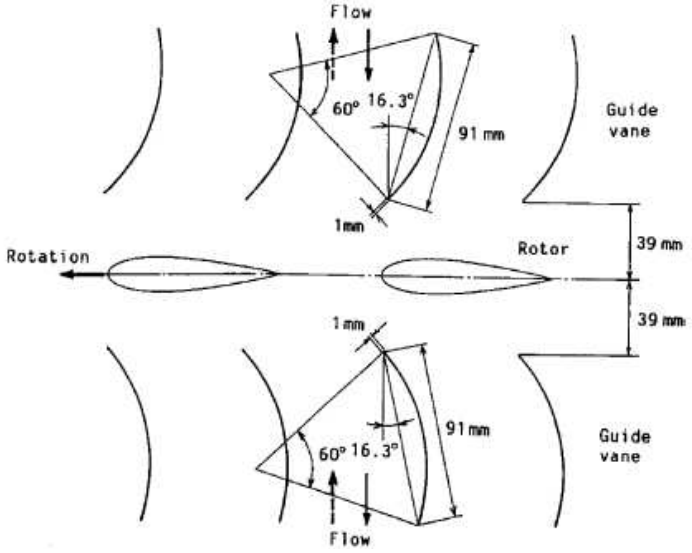

Figure 10: Wells turbine with guide vanes (Setoguchi and Takao, 2006)

The addition of static guide vanes to the standard Wells Turbine maintains the simple design with minimal moving parts, while improving the overall performance characteristics. Other Wells variations, while improving the efficiency, also increase the complexity of the design, which is not beneficial to the application of the device.

Bi-plane Wells turbine

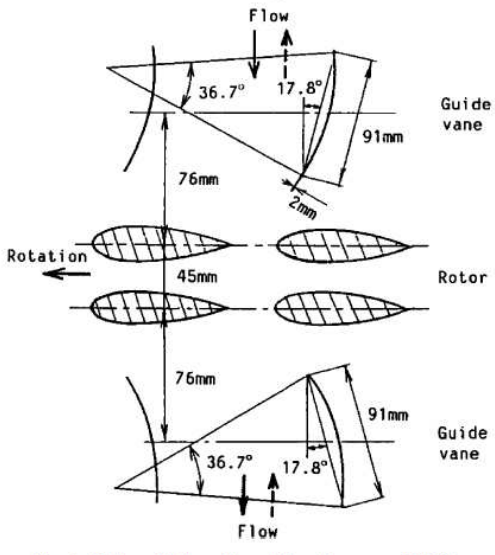

Figure 11: Bi-plane Wells turbine with fixed guide vanes
(Setoguchi and Takao, 2006)

The Bi-plane Wells turbine was developed with the intention of improving the efficiency of the standard Wells turbine, while improving the starting characteristics (Kinoue et al., 2004). The pressure drop across the double set of blades is greater than that for a single blade row arrangement and hence the power transfer to the turbine is greater. The bi-plane Wells turbine has been tested with guide vanes (*Figure 11*) and without. Results show improved performance characteristics over the standard Wells (Raghunathan, 1995). The downside of the design is that the velocity of the rotor must be reduced to prevent the second row of blades becoming supersonic and also downstream swirl is increased, resulting in larger losses downstream.

Contra-rotating Wells turbine

The Contra-rotating Wells turbine is a variation of the Bi-plane Wells turbine, modified to reduce the exit swirl produced by this device. The design still makes use of the double set of rotors, benefiting from increased pressure drop across the turbine, but the second set of rotor blades rotate in the opposite direction. This means that the resultant outlet flow is axial, reducing downstream swirl.

Test results for the Contra-rotating Wells had been promising but when the turbine was installed in the LIMPET plant, the performance was not as expected. Folley et al. (2006) suggest that the poor performance was due to the irregular and unsteady nature of the flow produced by the LIMPET OWC and these conditions had not been sufficiently considered in the predicted performance of the device. The study concludes that biplane or monoplane Wells turbines with GVs are better solutions for OWCs.

Pitched rotor blades

Setoguchi et al. (2003) acknowledged the variation in airflow between peak inlet and peak outlet *(see Figure 6)* and experimented with an asymmetric Wells turbine design *(Figure 12)*. The rotor blade was pitched to accept the inflow (V_0) over a wider range. Through varying the pitch of the rotor blade, the optimum setting angle of 2º was reached. The results showed reduced starting time with shorter time to reach a constant operating speed, showing overall improvement over the standard Wells.

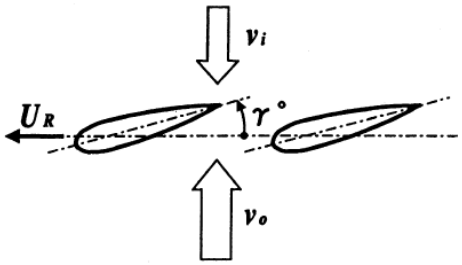

Figure 12: Wells Turbine with fixed asymmetrically pitched rotor blade
(Setoguchi et al., 2003)

Improved performance of pitched rotor blades has led to further investigation into the concept of variable pitch rotor blades that match inlet flow conditions. This has the potential to greatly improve performance as the characteristics of the rotor blade could be altered depending on the current conditions, resulting in improved efficiency across a wider flow range. Investigations have been made into both self-pitching and active pitching rotor blades. Although these types of devices are likely to improve the turbine performance, they require complicated mechanisms or at least large numbers of moving parts which are likely to cause reliability problems in a marine environment.

2.3.3 Impulse turbines for bi-directional flows

The main alternative to the Wells turbine and Wells variants is the impulse type turbine. This device uses the same principle as the unidirectional impulse turbine that has widespread commercial use. In an impulse turbine the pressure change of the fluid occurs in the nozzle of the device that directs the fluid on to the rotor. In an ideal impulse turbine, when the flow is isentropic and the fluid is a perfect gas, this creates the condition of zero enthalpy drop, which implies that there is no change in static pressure across the rotor (Horlock, 1966; Dixon, 2005). In the case of an impulse turbine for bi-directional flows, the nozzles are the stationary guide vanes as shown in *Figure 13*. The flow is accelerated by the inlet guide vane (IGV) in the direction of the rotor, the rotor causes a further change in direction of the fluid, transferring momentum from the fluid to the rotor.

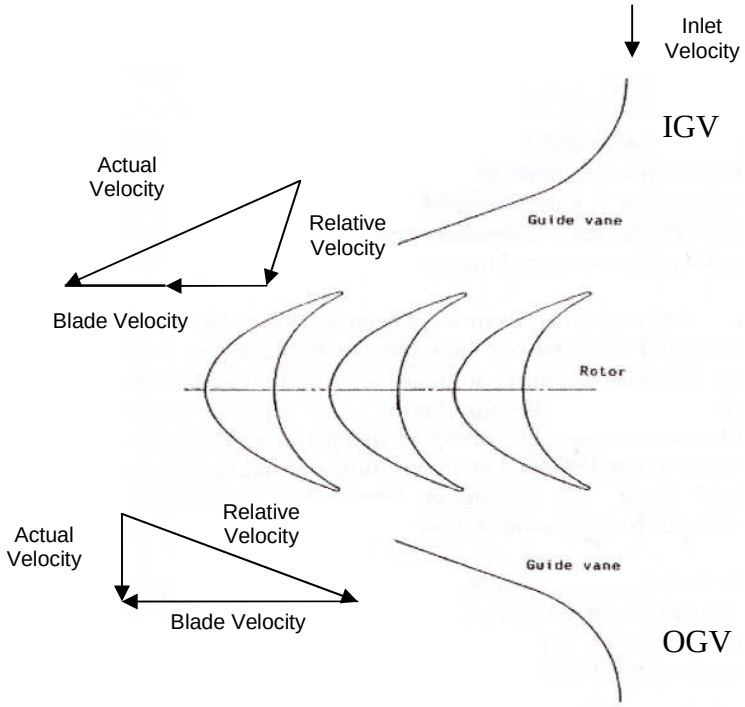

Figure 13: Schematic of standard impulse turbines showing fluid velocity at inlet and outlet.

The impulse turbine has been developed for use in bi-directional flows as the device does not suffer from the inherent disadvantages of the Wells turbine and was first investigated in Maeda et al.(1999) and Setoguchi et al. (1999). Maeda et al. (1999) studied the performance of impulse turbines with fixed guide vanes and compared the results with that of the Wells Turbine for irregular flows. A range of guide vane setting angles were investigated and the results of these tests are shown in *Figure 15*. The results are expressed in the form of torque coefficient C_T, input power coefficient C_A and efficiency η in terms of flow coefficient Φ.

The definitions are:

$$C_T = T/[\tfrac{1}{2}\rho(v_a^2 + U_R^2)b\ell z\gamma_R] \qquad \textit{Eq. 2.1}$$

$$C_A = (\Delta pQ)/[\tfrac{1}{2}\rho_A(v_a^2 + U_R^2)b\ell z v_a] \qquad \textit{Eq. 2.2}$$

$$\phi = v_a/U_R \qquad \textit{Eq. 2.3}$$

$$\eta = (T\omega)/(\Delta pQ) = C_T/(C_A\phi) \qquad \textit{Eq. 2.4}$$

The results demonstrate the wide operating range of the impulse turbine compared to the Wells turbine and the optimum guide vane angle of 30º is compared directly with Wells turbine performance in *Figure 14*. The study concludes that the impulse turbine with guide vanes showed superior running and starting characteristics over the Wells turbine when subject to irregular flow conditions.

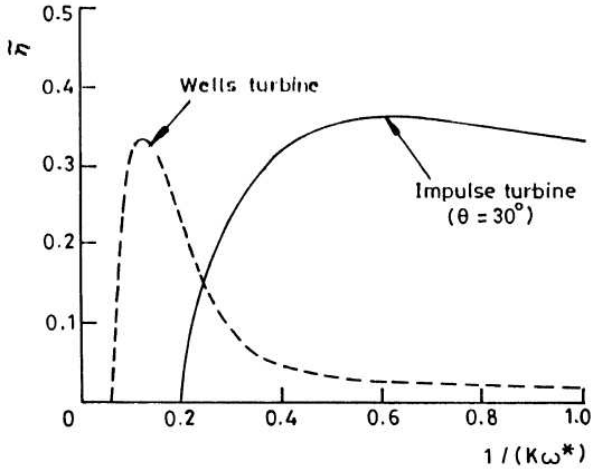

Figure 14: Comparison of mean efficiency under irregular flow conditions of Wells and Impulse type turbines (Maeda et al. 1999).

Despite the improved performance, an impulse turbine with guide vanes suffers losses at the outlet guide vane (OGV), since the turbine assembly must be symmetrical to function in bi-directional flows. The flow leaves the rotor blades axially as displayed in *Figure 13* and as the OGV is designed to direct the flow towards the rotor when coming from the opposite direction, the angle of incidence at which the flow approaches the OGV is poor. As a result of this the flow separates from the OGV, resulting in an area of low pressure across the surface of the guide vane leading to viscous losses. This increases the pressure drop across the whole turbine assembly, reducing the efficiency of the device.

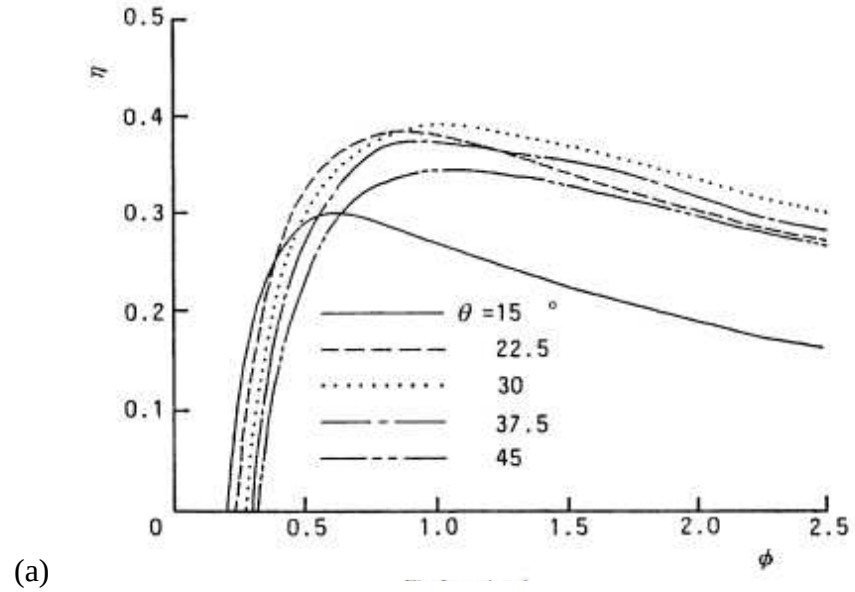

(a)

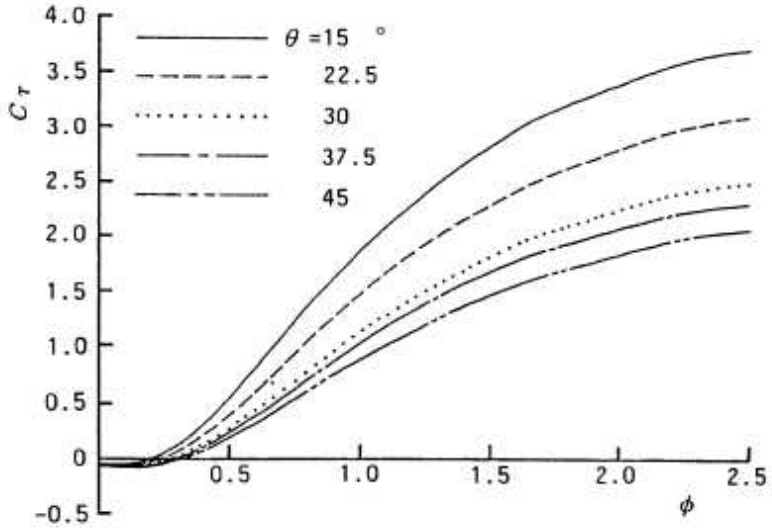

(b)

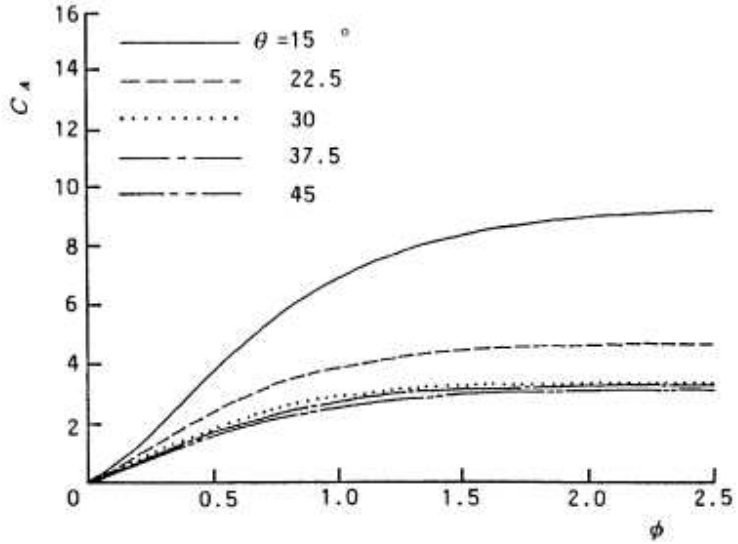

(c)

Figure 15: Bi-directional impulse turbine characteristics.
(a) efficiency, (b) torque coefficient and (c) input coefficient (Maeda et al. 1999).

The pressure losses associated with the OGV have been the subject of much research into the improved performance of impulse turbines for OWCs resulting in several variations of bidirectional turbines with guide vanes, a number of these devices are reviewed in Setoguchi et al. (2001) and Setoguchi and Takao (2006) and the important developments in this area are presented below.

Fixed guide vane impulse turbines

Setoguchi et al. (2001) tested a number of configurations of impulse turbines with fixed guide vanes. Two variations of guide vane profiles were compared. These are plate and airfoil type guide vanes displayed in *Figure 16.* Results showed there is little difference in performance between the two guide vane profiles in terms of mean efficiency. The starting characteristics of these turbine configurations were also investigated with direct comparison with the Wells turbine. Results showed that all types of impulse type turbines tested accelerated faster than the Wells turbine but there was practically no difference in the starting characteristics of the impulse turbine with plate type and airfoil type guide vanes.

The study demonstrates that the difference in guide vane profile has little effect on the performance of the turbine or the losses associated with the downstream guide vane. Despite the thicker guide vane profile, examining the geometries side by side in *Figure 16* shows that the variation has no effect on the trailing edge of the inlet guide vane, the section of the geometry that the flow interacts with as the exit to the rotor. It would be expected that this section of the geometry would have the most effect on the losses at the OGV.

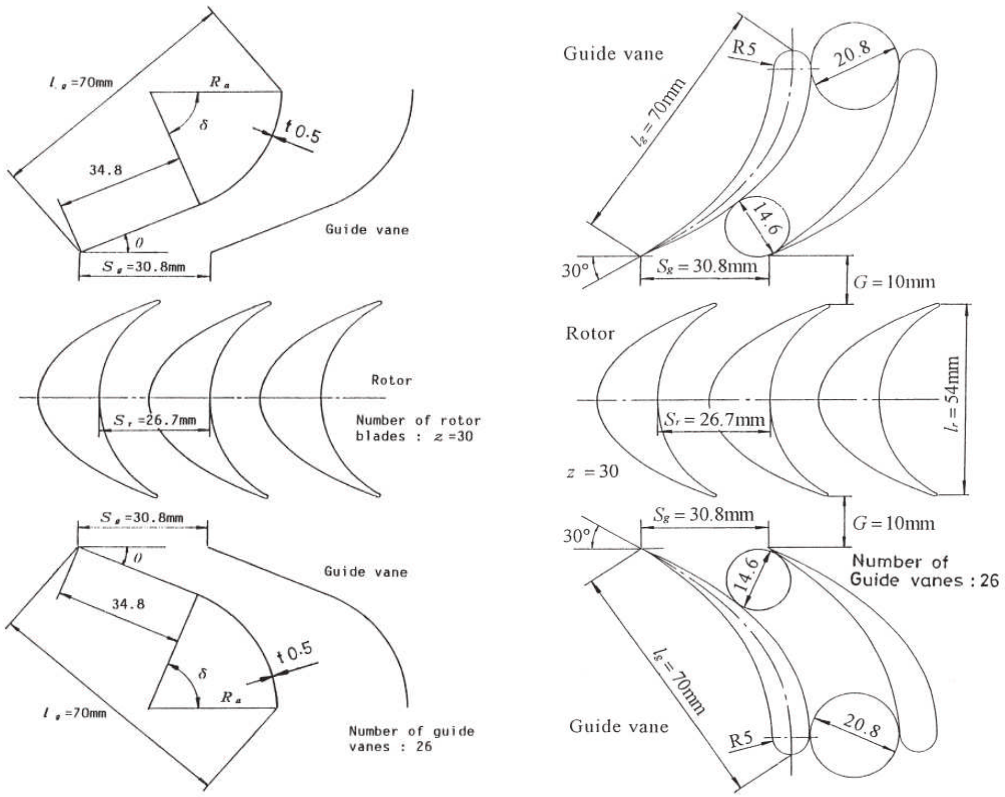

Figure 16: Fixed guide vane impulse turbines
(a) plate type and (b) airfoil type (Setoguchi et al., 2001)

Self-pitching guide vanes

One of the configurations presented in Setoguchi et al. (2001) is the impulse turbine with self-pitching guide vanes *(Figure 17).* In this design the guide vanes are connected to the casing wall by pivots at the end of the chord closest to the rotor. The movement of the reciprocating air flow forces the guide vane to pivot into the correct position depending on the direction of the flow. This self-pivoting capability allows the IGV to be positioned correctly for the incoming flow while the angle of incidence of the fluid on to the OGV is reduced, therefore removing or reducing the separation that occurs. This reduces the pressure drop seen across the OGV, improving the efficiency of the turbine assembly.

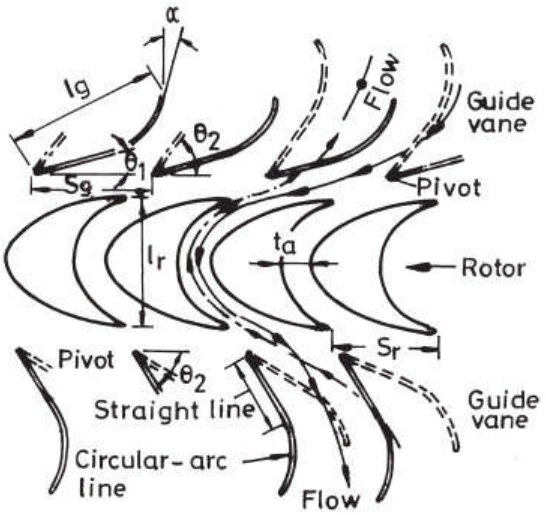

Figure 17: Impulse type turbine with self-pitch-controlled guide vanes (Setoguchi et al., 2001).

A number of variations of the self-pitching vanes were investigated including splitter type and mono vane type guide vanes. After initial monitoring of guide vane movement during testing, the configuration was modified by linking the guide vanes together so that the whole guide vane row would pivot as one. Results showed that the impulse turbine with self-rectifying guide vanes is capable of achieving high levels of efficiency over the range of flow rates produced by an OWC. Of the variations tested, the linked mono-vane type device showed the most promising performance with improved performance over the Wells turbine.

The design is however highly dependent on the perfect functioning of many moving parts and this is not well suited to operation in a marine environment. The pivots are susceptible to interference from sea air resulting in clogging and malfunction. The vast number of cycles alone means that fatigue is a serious concern with this type of device.

2.3.4 Variable Radius Turbine

The VRT concept was developed as part of the HydroAir turbine development project as a solution to the problem of pressure losses associated with the OGV and consists of a varying radius duct, which changes the area through which the air passes upstream and downstream of the rotor *(Figure 18)*.

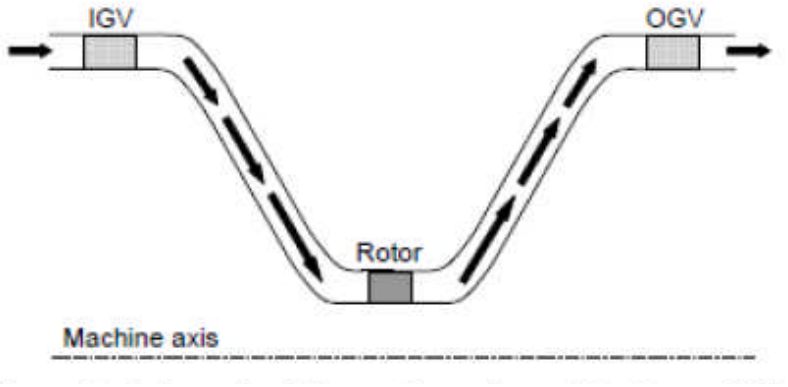

Figure 18: Schematic of VRT layout (Banks, 2009)

The losses incurred at the OGV are proportional to the square of the local flow velocity. Hence reducing the velocity of the flow over the OGV reduces the pressure loss of this component, improving the overall efficiency of the device. Increasing the area of the duct reduces the velocity of the flow and this resulted in the design for the VRT. The area of the duct could not be increased at the initial position of the guide vanes as this would have affected the performance of the guide vanes and their function in directing the flow to the turbine rotor. This resulted in the duct profile shown in *Figure 18.*

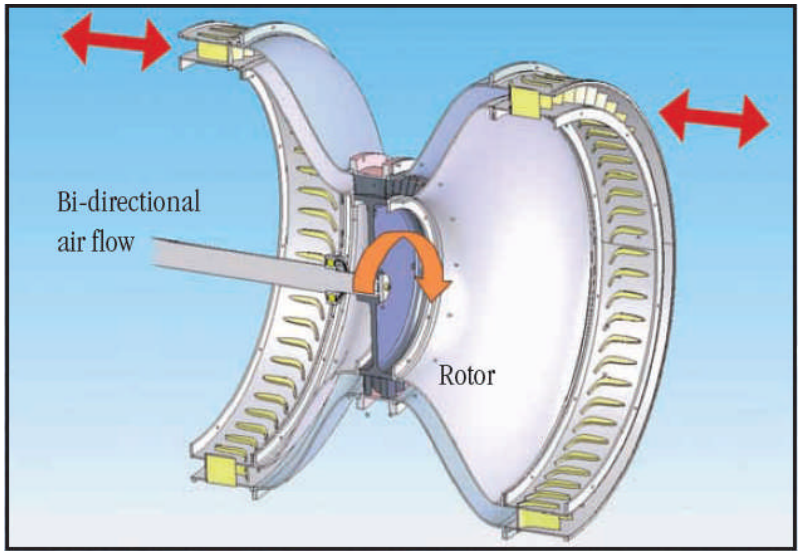

Figure 19: CAD drawing of the datum varying radius turbine installed in the HydroAir Test rig (Dresser Rand, 2009).

The diagram shows the guide vanes either side of the rotor and that they are positioned at a greater radius than the rotor blades. As the air flow passes the IGV at a low speed, the IGV induces turning in the flow. The flow is then accelerated by the reducing area of the duct as it approaches the rotor. After passing the rotor blade, the flow decelerates due to the increasing area of the duct and passes the OGV at a lower speed resulting in a reduced pressure loss across the OGV.

The VRT invention is a simple method of reducing the pressure loss over the OGV and the concept was patented in 2008 (Freeman et al., 2008). Initial numerical results demonstrated a step change in performance over other bi-directional impulse turbines with fixed guide vanes, and experimental results confirmed these predictions.

One main advantage of the VRT is that there are no moving parts except for the rotor and the increase in efficiency does not affect the operating range of the turbine. The turbine is functional over a wide bandwidth and, due to the impulse design, has inherently good self-starting characteristics.

The disadvantage of the VRT design is the required increase in overall size. The size of a turbine in an OWC is highly dependent on the damping of the device however the function of the variable radius duct requires an increase in the outer diameter of the turbine casing. The large final size creates problems in terms of the adaptability of the turbine, as the platform where the device will be positioned must also be relatively large. This also creates problems in terms of transportability, construction and assembly on site as well as cost. Recent, unpublished developments by Dresser Rand have addressed this drawback, reducing the overall size of the VRT by 50%.

HydroAir

The CAD drawing above *(Figure 19)* shows the original VRT geometry Ct14b, installed and tested at the reciprocating test rig at Cranfield University. This was the first VRT device constructed and was used to validate the early performance predictions of the concept.

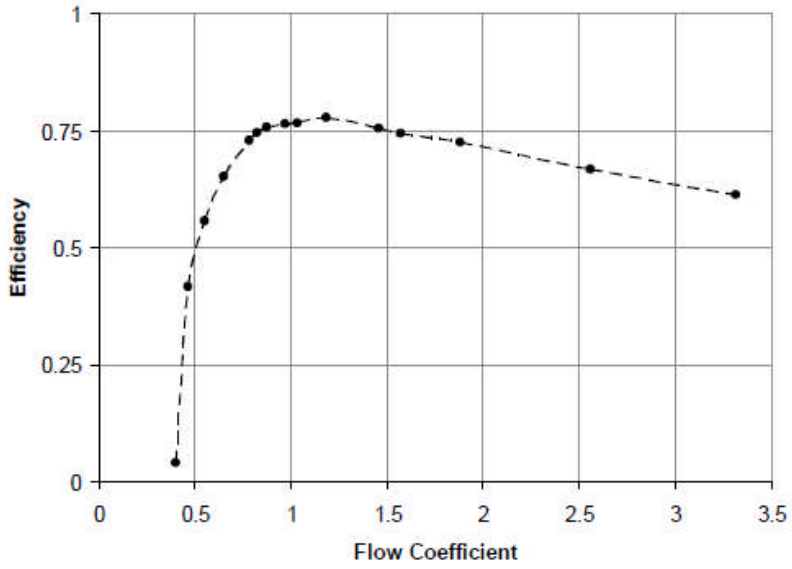

Figure 20: Full scale VRT-2 characteristic
(Natanzi et al., 2011).

Since this time, the commercial turbine, HydroAir has evolved through a number of generations as a result of continued research and optimisation processes carried out by Banks (2009). The most recently published results correspond to the VRT-2 design presented in Natanzi et al. (2011).

A scaled prototype device was manufactured at Dresser Rand's Peterborough facility. A photograph of the turbine during construction shown in *Figure 21*. The device was manufactured for installation on an offshore OWC platform in Australia constructed by Oceanlinx. The 1:3rd-scale floating platform consisted of multiple chambers and was deployed off Port Kembla in 2010. Unfortunately, the mooring of the platform failed in high seas and no performance results were produced from the prototype. The photographs on the following page show the HydroAir turbine mounted on the Oceanlinx buoy next to their own turbine in 2010.

More recently, Dresser Rand Company Ltd. have signed an agreement with Ocean Energy Ltd. to provide the 1MW turbine for their OE buoy to be constructed in 2013 and tested at Wave Hub, the first device to be deployed at the test site off the coast of Cornwall, UK. This is a great opportunity for HydroAir and for the marine renewables sector in Europe.

Figure 21: Part assembled VRT-2 prototype, (Natanzi et al. 2011).

Figure 22: HydroAir VRT-2 prototype
installed on Oceanlinx OWC Platform, Australia 2010.

2.4 Chapter conclusions

An OWC wave power plant puts a unique demand on a turbine for the device and this review demonstrates that the solution for the best turbine for this application has still not been identified. The Wells turbine has been the most widely researched turbine for this application but various methods of increasing the narrow operating range have been unsuccessful. In recent years, more interest has been shown in the bi-directional impulse turbine and published results to date show that this device is currently leading the field.

3 Numerical Methods

3.1 Introduction

The research described in this thesis makes use of optimisation as a design tool with the aid of CFD as a method of performance prediction. This section of the thesis presents the specific details of the optimisation procedures used in the research. Despite the use of optimisation methods, a large number of CFD simulations have been conducted throughout the research and the opportunity to give a brief description of the theory behind the CFD method used is taken in this section.

3.2 Optimisation

Optimisation is the process of identifying the optimum solution to a defined problem. The method of defining the problem is crucial and is usually the starting point of the process. Normally, the problem is defined by a number of design variables which are then adjusted. The overall fitness of the problem is then measured for each of these adjustments and a fitness value assigned to each combination of design variable values. This process is repeated until an optimum combination is reached. This can be defined as the point at which a better set of design variable values does not exist, or the solution meets a predefined performance objective.

The optimisation process starts with the definition of the problem. A single objective optimisation is the process of minimising the objective function and can be defined as:

$$\min\left(f\left(x\right)\right), x = \left(x_1, x_2, \ldots, x_n\right) \in X \qquad \textit{Eq. 3.1}$$

Where $X \subseteq \mathrm{R}^n$ is the n-dimensional design space consisting of real values. The design space is bound by equality constraints $h_i\left(x\right) = 0$ and/or inequality constraints $g_i\left(x\right) \geq 0$. $f\left(x\right)$ is known as the objective function or fitness function and instances of x are called design vectors. These design vectors represent a potential solution to the optimisation problem. All optimisation problems can be considered as problems of minimisation since:

$$\max f\left(x\right) = -\min\left(-f\left(x\right)\right) \qquad \textit{Eq. 3.2}$$

The optimisation tool used in this research was developed by Banks (2009) as part of the HydroAir project at Cranfield University. Banks developed his ImpOpt optimisation system with the capability of performing global optimisation procedures on bi-directional impulse turbines. His method has been adapted for the optimisation conducted in this research and a new geometry module has been written for the concepts investigated. The system makes use of meta-model function approximation methods combined with a Genetic algorithm (GA) to perform the optimisation. The architecture of the optimisation tool is shown *Figure 23*.

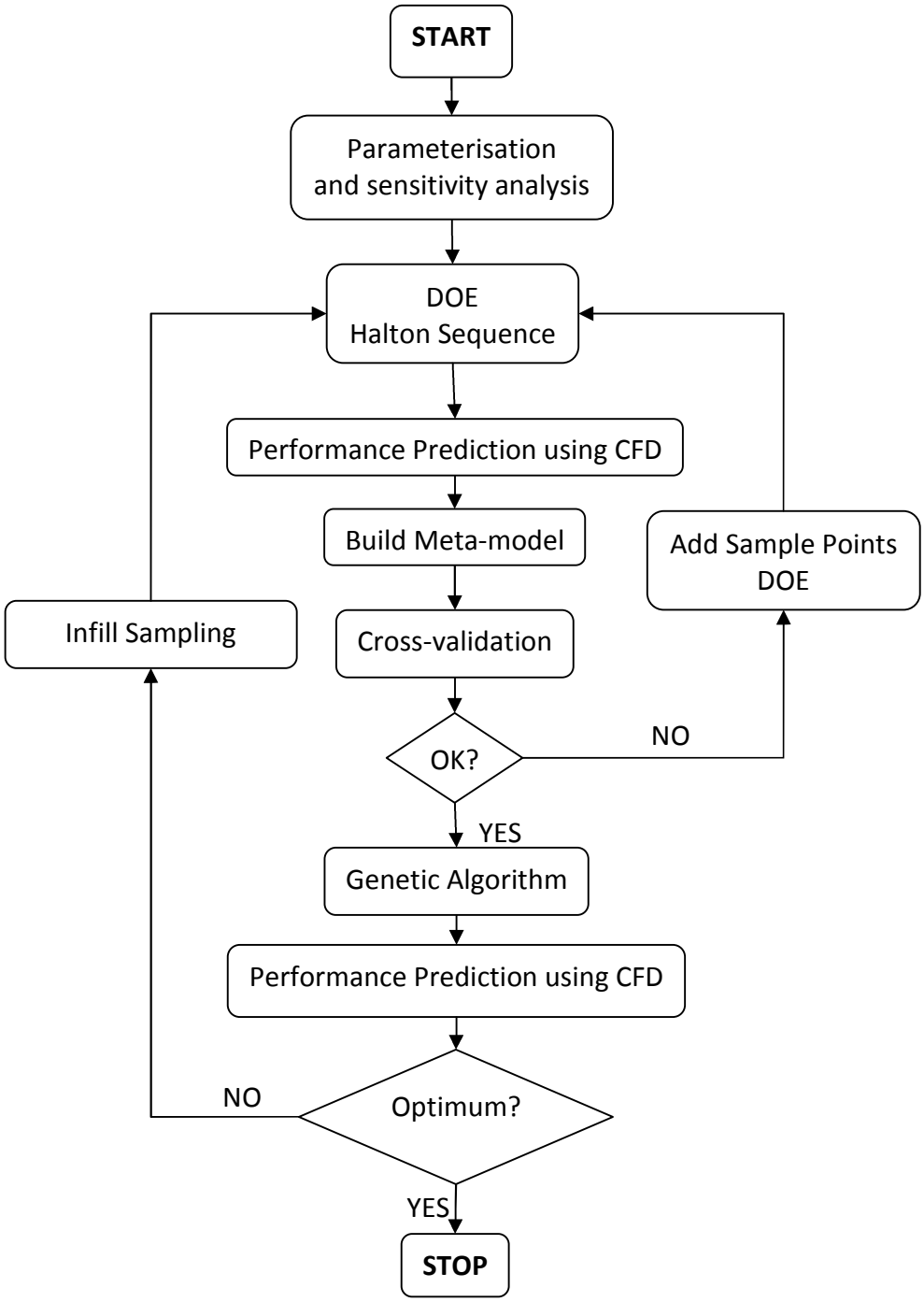

Figure 23: Optimisation Architecture

The first step in the optimisation process is to conduct a full parameter study. This has been done by varying design parameters in isolation and performing CFD simulations to assess the impact of each parameter on the overall function of the guide vane geometry. Details of the results of the parameter study are given below. The parameter study identified the most important parameters in terms of the guide vane function and these parameters were then used for the optimisation.

Design of experiments (DOE) techniques are then used to generate a design space based on the upper and lower limits of the parameters used. These sample points are then output as non-dimensional design vectors to be read for geometry generation and CFD case construction.

The geometry module manipulates the stator profiles and relative positioning based on DOE results. The input values for the geometry module are the non-dimensional design vectors from the DOE sequence that correspond to the geometry parameters. These non-dimensional vectors are interpreted into geometry variations and the resulting geometry profile is output as coordinate data for mesh generation.

A reliable method of automated mesh generation is required in order to automate CFD simulation since accurate CFD results are highly reliant on properly constructed meshes. This is difficult to achieve in an automated fashion, where the aim is to reduce the required manual input per case to zero. A number of meshing procedures have been investigated as part of the research comparing suitability for automation. A reliable method was adopted and this method was used for all optimisation procedures in the research. Once the meshes have been created automatically they are used for CFD simulation. Results are assessed by the performance prediction module and these results are then passed back to the optimiser.

The results are used to build a meta-model to produce a predicted fitness value at any point within the defined design space. This function approximation method is employed to reduce the number of CFD cases that are required to be conducted for the optimisation procedure. The combination of the DOE methods and the Kriging model allows for an initial prediction to span the complete design space. The accuracy of the Kriging model is then cross validated and if necessary, can be improved by adding more points to the design space. CFD cases are then run for these additional points. A meta-model is then built using all the available sample points, this data is then used for the optimisation process by a GA.

The GA determines an optimum value based on the meta-model estimate, this must then be evaluated to find the true fitness. This is done using an adaptation of the performance prediction module that generates the optimum geometry, sets up the CFD case, solves and post processes the solution and outputs the fitness value. This fitness value is then compared to the optimum value and depending on a user defined acceptable error criteria, the optimisation process is either complete or additional points must be added to the design space using infill sampling.

The scheme is developed in Matlab and is fully automated so that once the initial criteria is setup, the procedure can be performed without any interactive user input.

The following sections give more details about the various elements of the optimisation procedure as well as the methods implemented to automate the process.

3.3 Design of experiments

DOE techniques were originally developed as a method of performing experimental or test procedures. The aim being to perform the least number of experiments while generating a large range of data spread. It is important that the method used in generating sample points fills the design space, the computational expense of the function is also an important factor. There are a number of DOE techniques that achieve wide design space coverage for acceptable computational cost and Banks (2009) incorporated a selection of these techniques into the optimisation tool. The source code for these methods was provided by John Burkhardt of Florida State University and is made available on his website *(http://www.csit.fsu.edu/burkardt).*Banks used this source code to develop the DOE component of the optimisation tool. A comparison of the available sequences is presented below in *Figure 24*, displaying 100 sample points in two dimensions, generated using the optimisation code.

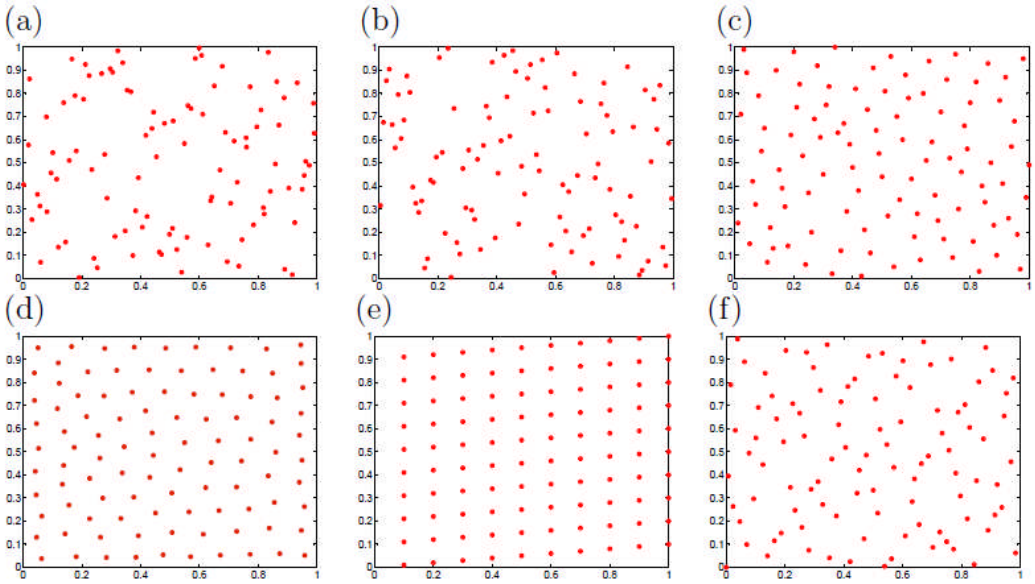

Figure 24: Comparison of DOE methods presenting 100 sample points
in 2 dimensions, generated with: (a) Random LHS, (b) Centred LHS, (c) IDHS,
(d) CVT, (e) Hammersley sequence and (f) Halton sequence.

All presented methods give reasonable coverage of the design space however it can be seen that both versions of Latin Hypercube Sampling (LHS) produce less evenly distributed sample points than the other methods. Improved distributed hypercube

sampling (IDHS) and Centroidal Vorronoi Tessellation (CVT) give much more distributions but this comes at the cost of high computational expense. Hammersley and Halton sequences both fill the design space well with reasonably even distribution and have low computational expense. However, Halton sequences offer the step function which makes them well suited to this type of problem and this is the reason why this method has been implemented for the optimisation procedure. The method is discussed in more detail below.

3.3.1 Halton Sequence

The Halton sequence fulfils the criteria of filling the design space evenly with acceptable computational expense, but this is also achieved by a number of other DOE methods. The main benefit of the Halton sequence, and the reason it has been chosen for the optimisation tool, is the Halton step function. The step function allows the user to specify the starting point of the sequence. This allows sample points to be added to an already calculated distribution without the whole distribution being re-calculated from the beginning and previous results being lost. This is particularly useful when conducting an optimisation procedure since it is unlikely that the initial number of sample points will provide an optimum result. It is then possible to calculate additional sample points and add to the data that has already been predicted.

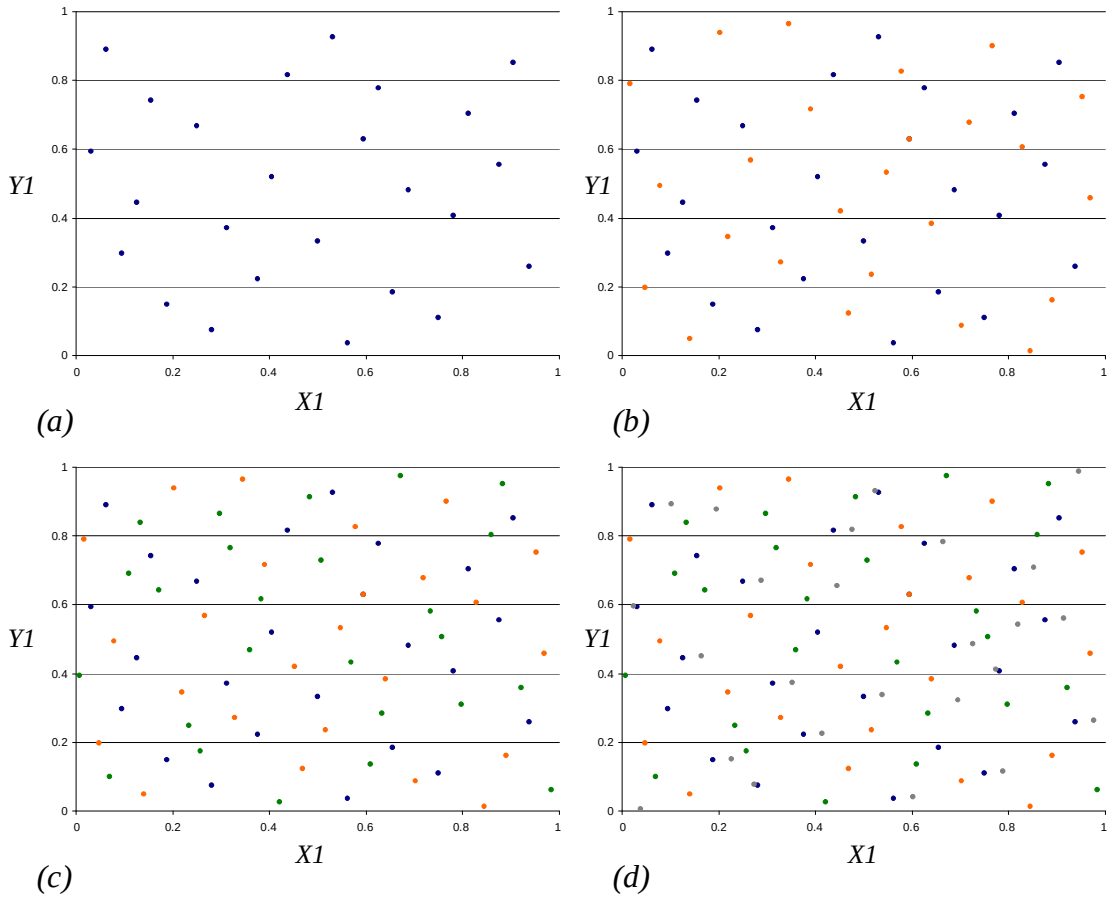

Figure 25: Halton sequence step function in two dimensions.

An example of a two dimensional sequence is displayed on the previous page in *Figure 25* and the step function capability is demonstrated. Initially in *(a)*, 25 sample points are generated, the even distribution across the design space can be seen. The step function is then used to add 25 points to the sample space up to 100 points in plot *(d)*. The even distribution is maintained as points are added.

In order to compute a Halton sequence, the first step is to choose a series of prime numbers to be used as bases for each dimension. Here, an example is given using the prime numbers two and three to produce a sequence in two dimensions. For the sequence *I = 1, 2, 3, 4, 5* each value of I is written in base two. The digits are then reversed, including the decimal and the number is converted back to base 10. This gives the following:

$$\begin{aligned} I = 1, &\quad 1.0 \rightarrow 0.1 = 1/2 \\ I = 2, &\quad 10.0 \rightarrow 0.01 = 1/4 \\ I = 3, &\quad 11.0 \rightarrow 0.11 = 3/4 \\ I = 4, &\quad 100.0 \rightarrow 0.001 = 1/8 \\ I = 5, &\quad 101.0 \rightarrow 0.101 = 5/8 \end{aligned}$$

In the same way, computing the second dimension using base three gives:

$$1/3,\ 2/3,\ 1/9,\ 4/9,\ 7/9$$

Pairing the two gives the following series of points, making up a two-dimensional Halton sequence:

$$(1/2, 1/3),\ (1/4, 2/3),\ (3/4, 1/9),\ (1/8, 4/9),\ (5/8, 7/9)$$

The DOE component is programmed in Matlab as part of the optimisation system and has been compiled to give the user full control over the number of sample points, number of active variables and step size. The user must also assign the upper and lower limits of each of the active variables. Executing the Matlab script reads the input criteria and outputs a sequence of non-dimensional design vectors. These non-dimensional design vectors instruct the optimisation tool of the number of initial sample points and the data required to build the individual cases for the geometry module and the performance prediction module.

3.4 Geometry Module

The role of the geometry module in the optimisation tool is to produce the coordinate data for mesh generation. The input values for the geometry module are the non-dimensional design vectors from the DOE sequence that correspond to the geometry parameters. These non-dimensional vectors are interpreted into geometry variations and the resulting geometry profile is output as coordinate data in the correct format for mesh generation.

Two different design problems have been investigated in this research, each using optimisation as a design tool. The two problems were investigated separately and each required different methods of geometry parameterisation. The setting up of this section of the optimisation procedure makes up a considerable proportion of the research and for this reason, is presented separately in the relevant sections of the thesis.

In both cases, the optimisation process was conducted with the aim of accurately representing the optimisation problem while minimising the number of design variables. This is because a large number of design variables can make the problem difficult for an optimiser to solve and potentially make the computational cost of the process very high.

3.5 Performance Prediction Module

The performance prediction module receives the output from the geometry module and the relevant parameters from the DOE sequence for each sample point. These inputs are used to generate a unique case to be solved and processed using CFD. The output of this process gives the predicted fitness of the individual case, and accompanied with the input data, is output to the meta-model. This process is performed automatically without any interactive user input. Details of the CFD method used are presented in this section along with a description of the automation process that has been implemented.

3.5.1 CFD Computational Method

CFD is widely used in the design process of rotating machines as a method of visualising and analysing flow though devices. The physical testing of devices is expensive and with the availability of modern, powerful computing power, the performance of early designs and modifications can be predicted before rotating machines need to be built.

Much literature has been published on the capability of CFD in producing valid predictions of rotating machine performance see, for example, (Roberts, 2004) and (Denton, 1999). Banks (2009) assesses the capability of CFD to be used as a design tool for bi-directional turbines. This assessment involves a direct comparison of predicted performance from 3D CFD simulations with experimental data from the literature.

First, the Wells turbine without guide vanes and a zero degree setting angle presented in Setoguchi et al. (2003) is chosen for comparison and the CFD prediction is a reasonably good indicator of performance up until the point at which the turbine stalls. After this point, the accuracy of the prediction is poor due to the separation of the flow from the rotor.

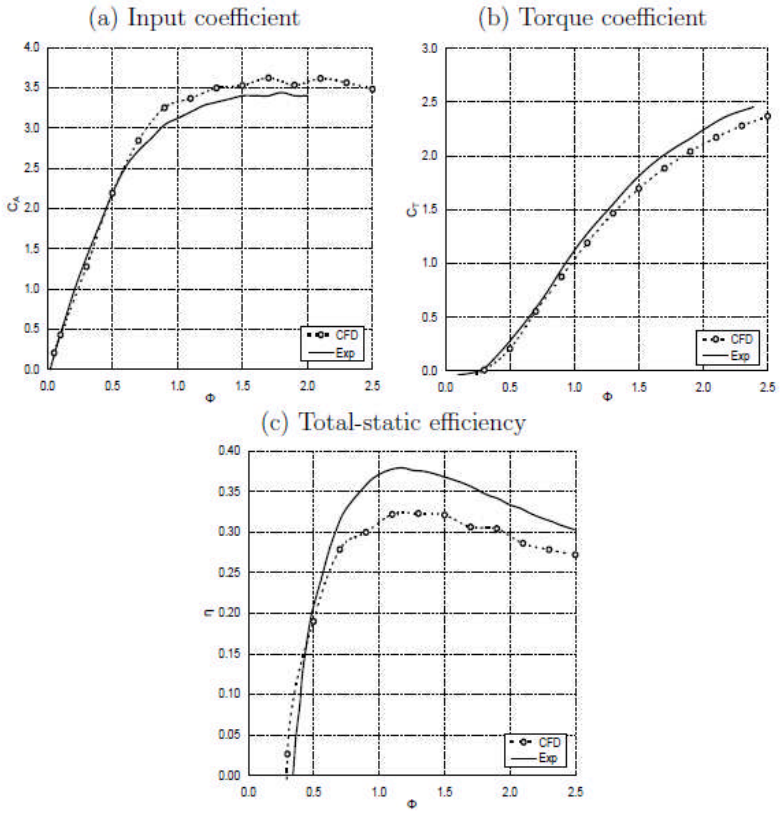

Figure 26: CFD Comparison with experimental results
of Setoguchi's impulse turbine with fixed, splitter type guide vanes (Banks, 2009).

More importantly for this research, Banks also assesses the capability of CFD to predict the performance of a bi-directional impulse turbine *(Figure 26)*. Two fixed impulse turbines were chosen from Setoguchi et al. (2001), these were turbines with fixed guide vanes of 'the splitter' type and 'the airfoil' type *(see Section 2.3.3, Figure 16)*. Results showed reasonable agreement between the experimental results and the CFD results with a notable under prediction of efficiency which it is suggested may be due to an inconsistent definition of static pressure as it was unknown at what point the quoted static pressure had been measured during experimentation.

Despite known separation occurring at the OGV of the impulse turbine with fixed guide vanes, CFD is able to predict the performance of the turbine through the whole characteristic without the large error that was evident for the Wells turbine, post stall. It appears that this is due to the fact that the separation at the OGV has the effect of increasing pressure in the outlet duct so this pressure is calculable despite the separation and the un-steady flow. However when the separation occurs on the rotor, as for the Wells turbine, the prediction of resultant torque on the rotor is inaccurate due to inability to predict the unsteady flow.

Overall, the capability of the CFD method to predict the general trend of the bi-directional impulse turbine performance is promising. On this basis, it was decided that CFD was a suitable method of performance prediction for the optimisation procedure of a bi-directional impulse turbine.

CFD Automation

The CFD process is automated so that once setup, no additional user input is required. This allows for a large number of cases to be simulated efficiently with an output that can be directly compared and evaluated. It is computationally challenging to automate this detailed process and the scripting required to join the different elements of the procedure together is complicated. However, the time invested at this stage is worthwhile due to the high number of simulations that can eventually be performed with little additional human cost.

The automated process is briefly described along with the programming languages used:

The whole process is executed from a Linux Shell script. The Shell script initially counts the number of linear points within the design vector output file, ascertaining the number of sample points being used, this denotes the number of cases that will be setup. Each case is created within an individual directory, the Shell script creates each directory and executes a Perl script to generate each case.

Pre-Processing

The CFD cases were setup using the ANSYS CFX-12 Pre software, run in batch mode from script files. In this process, the boundary conditions are defined as well as the settings for the solver. The process reads in the mesh files created in the meshing procedure, applies the boundary conditions and settings before outputting a definition file ready for the CFD solver.

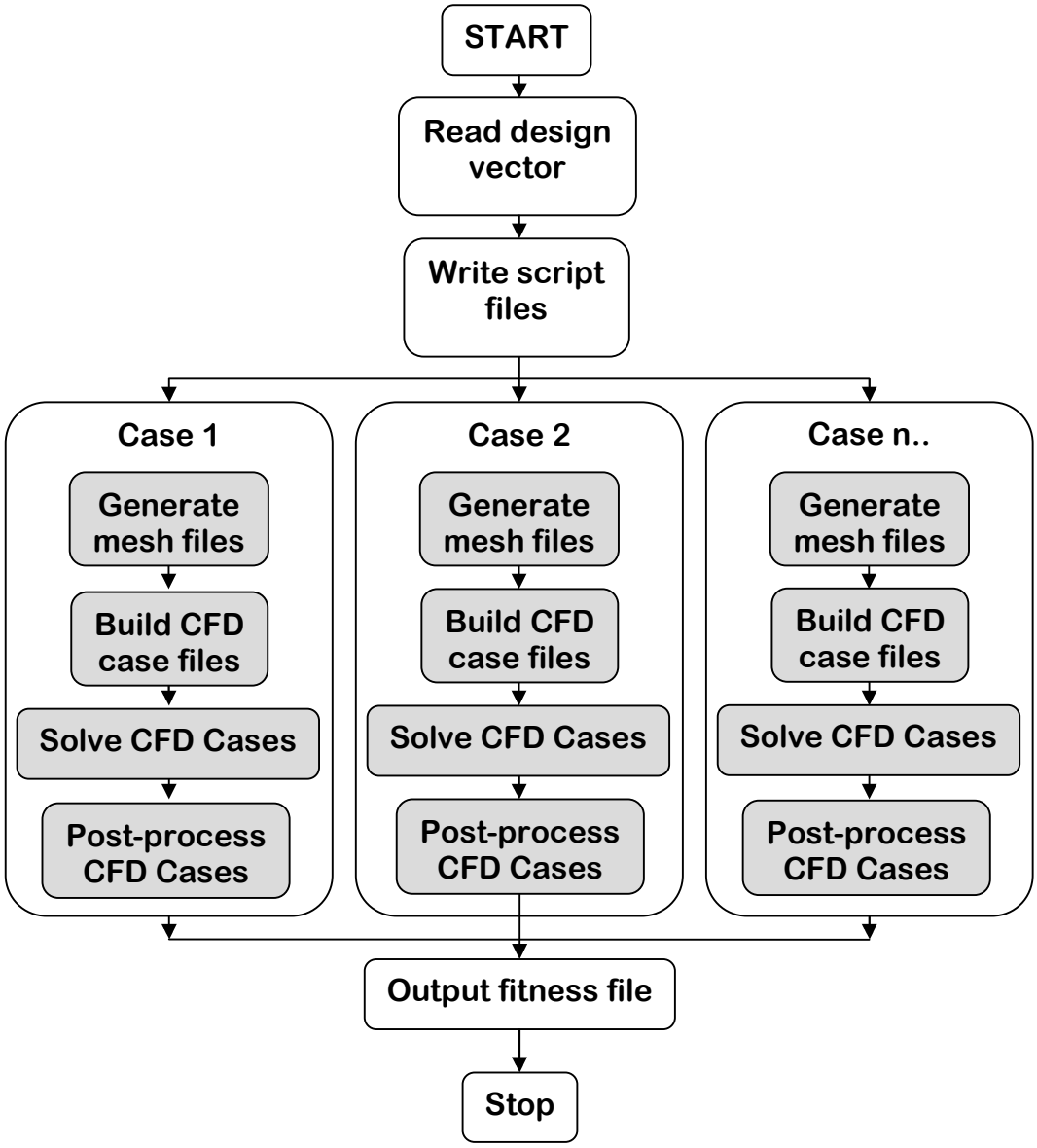

Figure 27: Performance prediction module architecture

The variable parameters output from the geometry module must be incorporated into the mesh generation and setup of each individual CFD case. The CFX Command Language (CCL) uses the existing programming language, Perl allowing Perl statements to be embedded into lines of CCL. A Perl script, making use of the line

input operator, is used to write the script files for case setup in CFX Pre, assigning the relevant variables from the design vector data file. This allows for individual script files to be produced that will generate individual geometries and settings for each case.

Solution

ANSYS CFX-12 Solver was used for the solution of the cases, solving the discretised Reynolds-Averaged Navier-Stokes (RANS) equations. The solutions were carried out in batch mode. The cases were solved using the 'High Resolution' advection scheme which is fully second-order accurate. In all cases, the *k-ω-SST* turbulence model was used, since it is recommended for internal turbomachinery flows of the type investigated in this research. The *k-ω* model requires at least 10 nodes within the boundary layer and a $y^+ \approx 2$ is preferred and the near wall resolution was adjusted in the meshing procedure to ensure these values were met.

A submitter file is written as part of the Perl script with the corresponding identifier for the case. At the completion of the Perl script, the submitter file is executed by means of the over running Shell script. In each submitter file the script file for each process within the CFD run is executed. Each of these processes is automatically assigned to a grid node so that the CFD process is performed in parallel as shown in *Figure 27*. The number of cases running in parallel must be controlled to avoid overloading the grid and prevent resources being exhausted but even so, the ability to run the CFD cases in parallel batches reduces the required time for this procedure.

Post-Processing

The post-processing of the completed solutions was performed using the ANSYS CFX-12 Post software. With satisfactory convergence or an assigned number of iterations, the solver is automatically terminated and the results file is post processed. The use of pre-defined macros written into the CFX-Post script file allow for the results to be assessed for validity and the required data is output. This data is then written to an output data file.

The routine is completed by collating the individual data files to a single fitness data file in the parent directory. This final fitness is then passed back to the optimiser and all sub directories are then deleted.

3.6 Meta-model

Gaussian process modelling or Kriging Models are used as the function approximation method for the optimisation. The function of this process is to produce an estimated fitness value at any point within the global design space. This is constructed using the predicted fitness values produced from the performance prediction module allowing for estimates to be generated at sample points that were not simulated in CFD. The combination of the Halton sequence and the Kriging model allows for an initial prediction to span the complete design space.

The meta-model created for the optimisation tool makes use of the DACE Toolbox for Matlab, developed by the Informatics and Mathematical Modelling department at the Technical University of Denmark. A detailed technical report by Lophaven et al. (2002) gives full details of the mathematics behind the Toolbox. Keane and Nair (2005) also present an extensive explanation of the models used.

The Kriging model reads the fitness values and corresponding design vectors output from the performance prediction module and these values are used to build the meta-model. For a 2D problem, this process can be displayed graphically as a 3D plot as is shown in the example given below in *Figure 28*, with the fitness value on the z-axis. The contour plot in *Figure 28* shows the distribution of the sample points across the design space. It can be seen that the predicted minimum is close to the Y-axis of the plot.

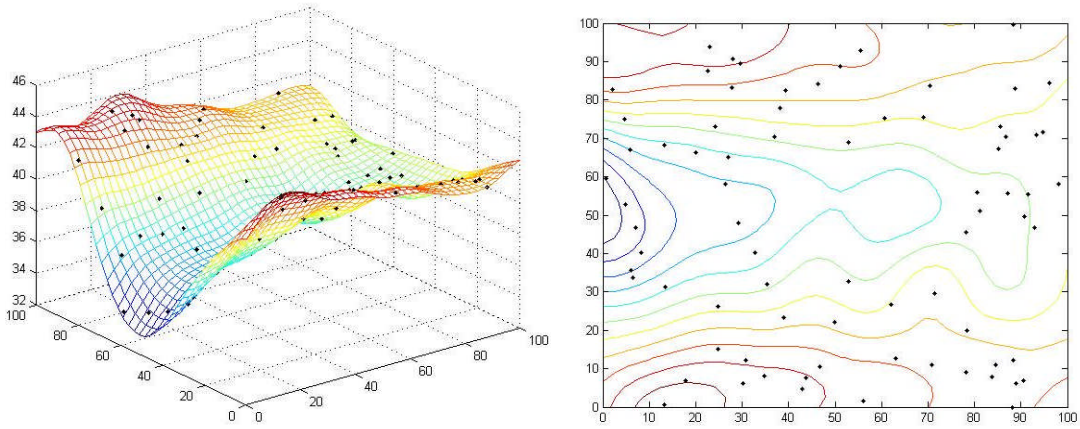

Figure 28: Kriging example 3D plot and contour

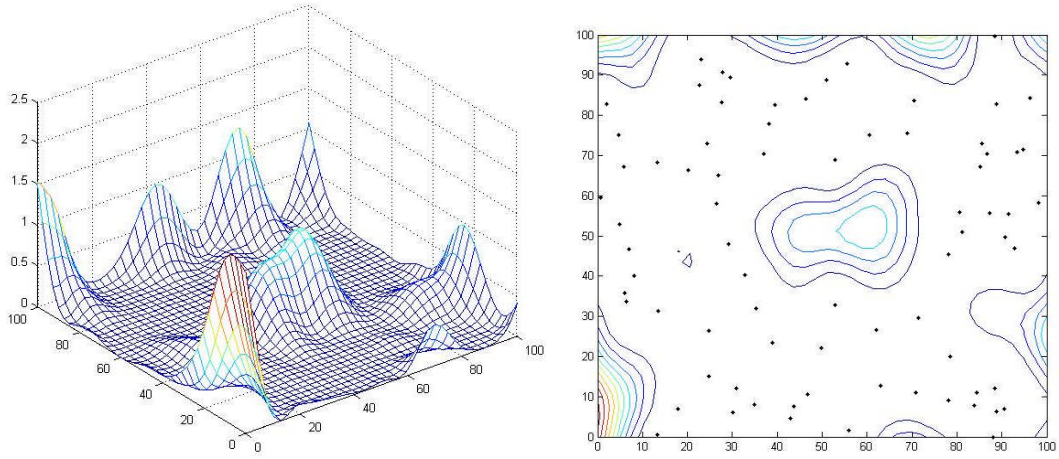

Figure 29: Kriging example MSE 3D plot and contour

An added advantage of the Kriging model is the ability to estimate the mean squared error (MSE) of the estimated fitness based on the initial spread of sample points. This capability, based on the distribution of the sample points is demonstrated in *Figure 29*. It can be seen that the peaks of the 3D plot (higher MSE), around the edge and in the centre, correspond to areas of fewer sample points within the distribution.

Since the optimisation process relies heavily on the Kriging meta-models to reduce the time taken to run the optimisation, the accuracy of these models are important to the success of this approach. A method of cross validation is implemented into the optimisation process to estimate the accuracy of the meta-model before the GA is implemented. In a simple cross validation method, the data is split into two parts, one part is used to construct the meta model while the other is used to estimate the cross validation error. The cross validation error is the difference between the meta-model predictions and the actual values at the design points. The data is then switched to give a second approximation of how well the model predicts a new set of data. A more in depth description of the process and variations of the method can be seen in (Meckesheimer et al., 2002).

In the cross validation method implemented, the averaged root mean squared cross validation error is measured and this is used to indicate how accurately the meta-model is likely to represent the objective function. During the optimisations conducted, a cross validation error of 20% was set. This meant that if the cross validation procedure indicated that the root mean squared error was greater than 20%, the accuracy of the Kriging model was deemed to be insufficient and more points were added to the design space using DOE. If the cross validation error was less than 20%, the Kriging model accuracy was accepted and the optimisation process continued to the next stage.

3.7 Genetic Algorithm

The GA is used to find the absolute minimum within the design space, using the prediction of the meta-model. GAs are well known and widely used evolutionary methods. This is due to their wide adaptability to optimisation problems and their inherent simplicity. GAs are capable of dealing with difficult objective functions that would not be possible with other optimisation methods such as gradient based methods (Gen and Cheng, 2000). Also, the global nature of GAs means that the problem of getting trapped in local minima is less likely to occur.

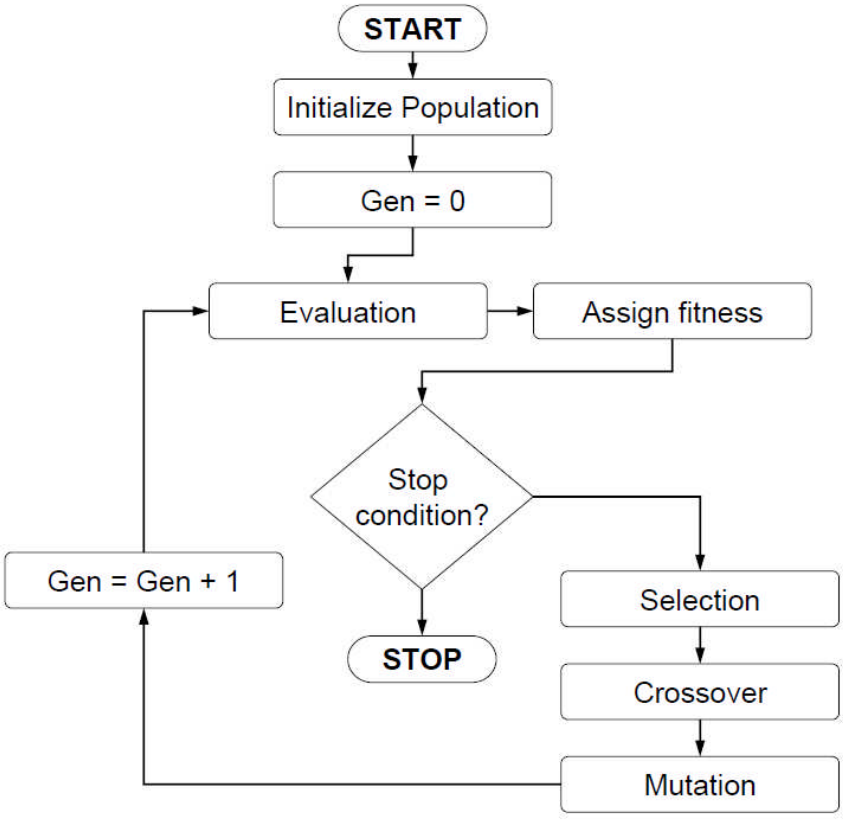

Figure 30: Basic methodology of a genetic algorithm, adapted from Deb (2001)

The basic methodology of a GA is the evolution of a set of candidate solutions towards a better solution. This process is shown diagrammatically in *Figure 30.* The evolution happens in generations, starting from a population of randomly generated individuals from the design space. The individuals are then evaluated and given a fitness score based on the goodness of fit and any design constraints that exist in the

problem. In each generation, candidates are selected based on their assigned fitness. This selection produces a pool from which the next generation will be derived from in the crossover. Selection is usually achieved by one of three main methods, these are Tournament, Proportionate and Ranking (Deb, 2001).

Crossover is the process of combining pairs of the selected, fittest individuals to produce the next generation. Again, there are a number of ways in which crossover can be implemented, the main ones are one-point, n-point or uniform crossover. Mutation is used to maintain diversity in the population by applying random mutations to specific genes or complete genomes, this is set by some user defined scheme. The GA process is repeated until a pre-defined termination condition has been reached.
The GA used in the optimisation system is the standard multi-objective genetic algorithm from the genetic algorithm and pattern search Matlab Toolbox. This is based on the widely used Non-dominated Sorting Genetic Algorithm, NSGA-II described in Deb (2001), Deb et al. (2000, 2002) and more recently Deb (2011). Two options from the Matlab Toolbox were also implemented, “ParetoFraction" and “DistanceFcn" which serve to increase population diversity and to protect against premature convergence.

Although the optimisation procedures undertaken in this research are single objective, the use of the multi-objective algorithm allows for the option of performing multi-objective optimisation in the future. There is a small amount of additional computational power required in using a multi-objective GA for a single-objective problem but it was thought that this was acceptable in the interest of making the tool adaptable for potential future multi-objective problems.

Parameter	**Setting**
Population Size	200
Generations	100
Mutation	Adapt feasible
Elite Count	2
Crossover fraction	0.8
Selection	Tournament
Scaling	Rank

Table 2: Genetic algorithm parameters, adapted from Banks (2009)

The parameters used to control the function of the GA are presented in *Table 2* and are taken from Banks (2009). Adjustments were made to the GA parameters to assess their effect on the optimisation procedures. It was concluded that for the constrained

optimisation procedures conducted, variations to these parameters had little effect on the GA results and as a result, these setting were used for all optimisations presented in this thesis.

3.8 Infill Sampling

When conducting a complex optimisation with a meta-model optimiser, it is possible that the first run will not produce a valid optimum, once the GA output is checked with CFD. In this case, it is necessary to improve the quality of the meta-model by adding more points as the optimisation proceeds and there are a number of ways in which this can be done. One method is to add the result of the predicted optimum to the meta-model and then re-run the optimisation. This method works but has the disadvantage of being slow, adding only one point each time. The other disadvantage is that only the local area around the predicted optimum will be improved. This is not a problem if the initial meta-model is good however, if the optimum result lies in an unexplored area of the design space, it would not be discovered using this method.

Another method of improving the accuracy of the meta-model is to use capability of the Kriging method to estimate the MSE of the area. This identifies areas with low accuracy due to the distance from original sample points. However, improving the accuracy in these areas will not necessarily improve the ability of the model to predict the location of the potential optima.

The optimisation tool uses a method known as the Expected Improvement criterion or ‘infill sampling’ that is capable of adding points in parallel as well as distributing these points around the design space effectively. This distribution balances the need to resolve unexplored regions as well as focusing on areas around potential optima. A detailed overview of the method is presented in the thesis of Sasena (2002).

The optimisation procedure repeats until a pre-defined stopping criteria is met. The stopping criteria could be that a desired value has been achieved, a certain number of generations has been reached or another measure that shows further improvement is unlikely. The main method that was used in the optimisation was the comparison of GA estimated optimum with actual estimates from CFD, a limit was also set on the number of iterations that could be performed.

4 Datum turbine

The starting point for the research into methods of reducing losses at the OGV is the study of the datum turbine. The datum turbine provides a base for comparison for all modifications, allowing levels of performance to be accurately assessed as well as cross validation of CFD simulations, important for trustworthy performance prediction. The datum turbine used for the research is the CT14b HydroAir turbine, installed in the reciprocating test rig facility at Cranfield University.

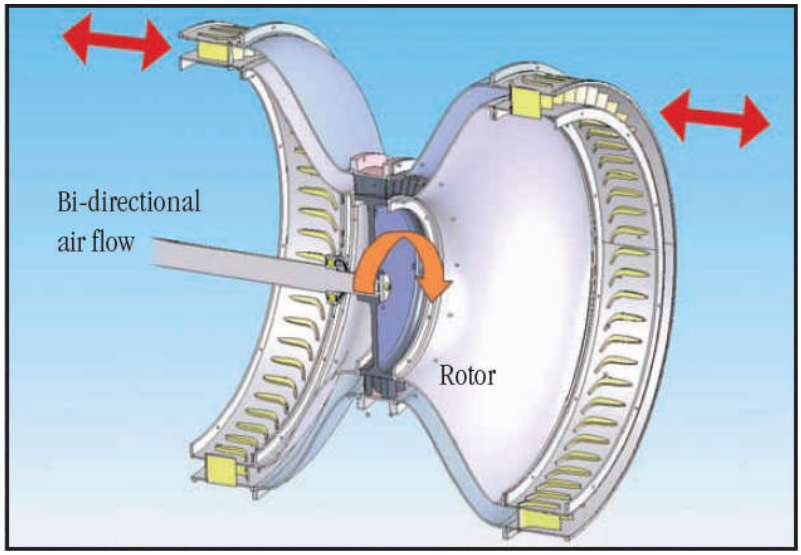

Figure 31: CAD drawing of cut away datum turbine CT14b (Dresser Rand, 2009)

This chapter gives details of the current CT14b turbine geometry *(Figure 31)* as well as information on the previous variations up to this point. The design and capabilities of the reciprocating test rig are also described along with the current limitations of the facility. Numerical analysis of the datum turbine has been performed and this process is described below with specific interest in the flow around the OGV. These CFD results have been compared with simulations previously performed by Banks (2009) which in turn have been validated using experimental data acquired from the reciprocating test rig, these results are displayed below.

4.1 Turbine geometry

The CT14b turbine design is the result of the HydroAir project that started as a collaboration between Peter Brotherhood Ltd. (now Dresser Rand Company Ltd.) and Cranfield University in 2004 with funding from the Department of Trade and Industry (DTI). The project started with the work of Herring, documented in Herring (2007) and then by Banks (2009). This work resulted in the international patent of the VRT design, Freeman et al. (2008). A reciprocating test rig was designed and built at Cranfield University and the original VRT was installed on this test rig. Since this time, there have been a number of modifications made to the turbine, specifically the ducting of the turbine and the profile of the outlet section of the rig. It is this current variation that has been used to gather the experimental data.

4.2 Guide vane geometry

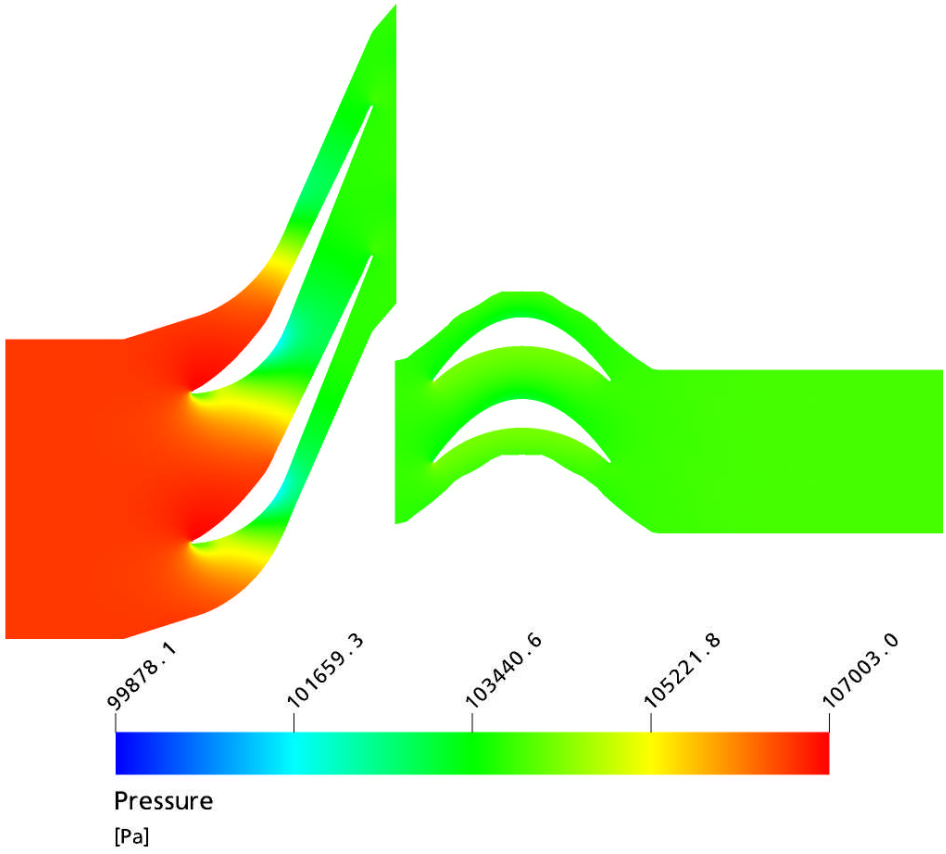

Figure 32: Static pressure distribution around early blading, (Banks, 2009).

The datum guide vane profile, colloquially known as the ‘hockey stick’ from its unusual shape is the result of profile development in the early stages of the datum turbine design by Herring and Banks. The initial design used Setoguchi’s airfoil type impulse turbine as a benchmark, discussed earlier in section 2.3.3. The datum geometry was developed to improve on the performance of this turbine. Early CFD simulations showed improved performance over Setoguchi’s design when the turbine was modelled without an OGV *(Figure 32)*. However, when the complete device was modelled, including the OGV, performance was poor, demonstrating that a superior IGV design is not necessarily an improved OGV design (Banks, 2009).

Up until this point, guide vane profiles with sharp trailing edges had been used but it was evident that this was not helping the OGV performance. It was also noted that the large turning section of the guide vane profile was creating a significant blockage at the OGV stator row due to the axial inlet angle of the flow exiting the rotor. This coupled with the diffusion across the OGV stator row was increasing separation and increasing total pressure loss across the device, resulting in low performance.

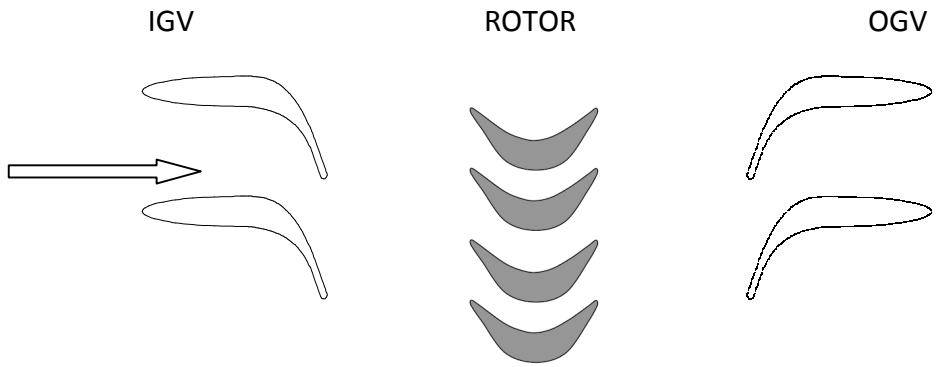

Figure 33: Current ‘Hockey stick’ guide vane arrangement without variable radius duct.

These observations were used to develop a profile with rounded trailing edges and shortened turning section with the aim of reducing the blockage effect caused by the OGV. The resultant guide vane profile can be seen above in *Figure 33* and the method used to define the geometry is shown below in *Figure 34.*

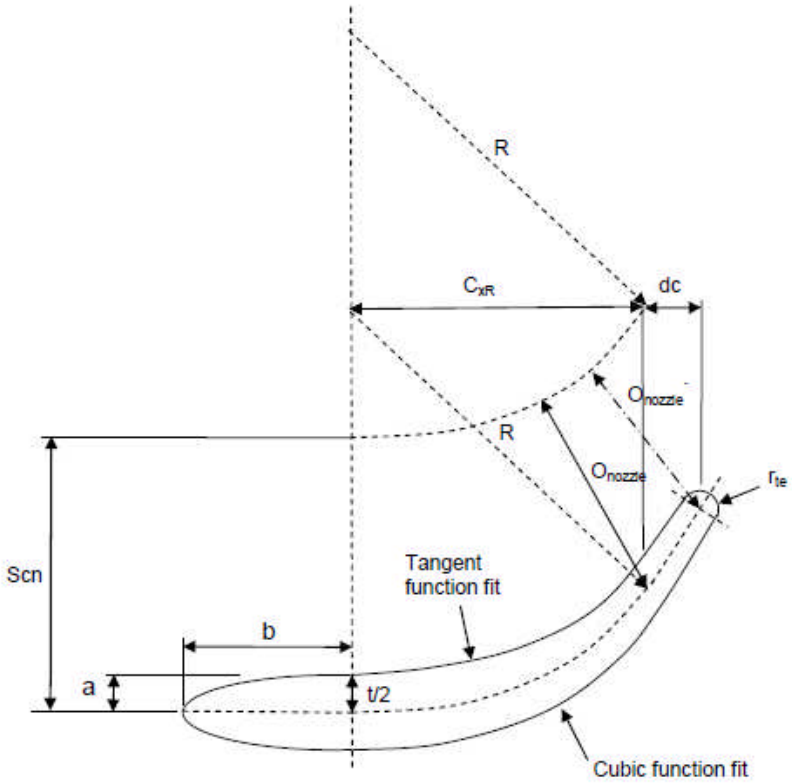

a,b	parameters to define leading edge ellipse
dc	trailing edge extension distance (fraction of distance C_{xR})
O_{nozzle}	distance used to determine maximum thickness of profile
R	radius of camberline arc
r_{te}	radius applied to trailing edge
Scn	space between guide vanes
t	maximum thickness of section

Figure 34: Method of geometry definition for datum turbine guide vanes (Herring, 2007).

Banks performed full 3D CFD simulations to produce the turbine characteristic for the new geometry. These results are shown below in *Figure 35*, compared with Setoguchi's impulse turbine variations. The results show that the new geometry achieved similar performance to the Setoguchi airfoil type impulse turbine with a slightly improved peak performance of 41%. This geometry was used as a baseline design for future development and optimisation procedures that resulted in the VRT. The guide vane profile is still used in the CT14b turbine installed in the reciprocating test rig and is used as a baseline for this research. Defining guide vane parameters are given below in *Table 3*.

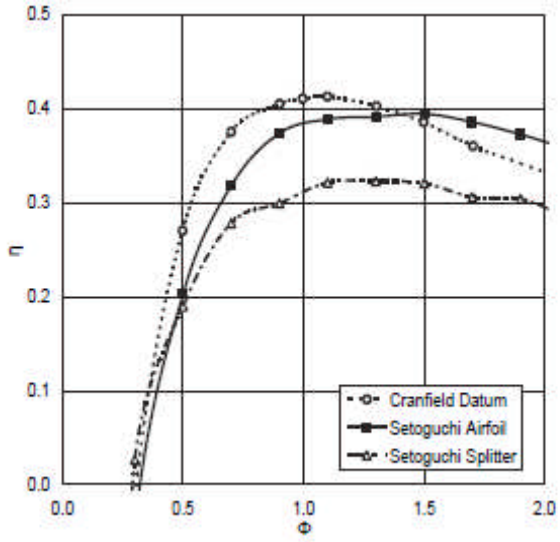

Figure 35: Total-to-static efficiency comparison of Cranfield datum impulse turbine (CT12) with Setoguchi airfoil impulse turbine (Banks, 2009).

Parameter	Value	Units
Guide vane count	59	-
Turning angle	67.2	°
Axial chord	0.110	m
Section thickness / chord	12.56%	-
Pitch	0.061	m
Design Reynolds number	2.15×10^5	-
TE thickness	0.00412	m
Stacking axis	Leading edge	-

Table 3: Datum guide vane parameters (CT14b)

4.3 Variable radius turbine

The breakthrough of the HydroAir project is the VRT concept resulting in a step change in the efficiency of bidirectional impulse turbines. The early guide vane development demonstrated improvement over the Setoguchi design but considerable improvement was only possible with the VRT. This early investigation demonstrated the negative impact of the OGV stator row, reducing turbine total-to-static efficiency by 20% (Banks, 2009).

The theory behind the VRT concept has already been presented in Section 2.3.4 and the design parameters of the Ct14b configuration are given below in *Table 4*. The guide vanes are radially offset from the rotor by 5.55 rotor blade span lengths giving

an outer casing diameter of 1.2m at the guide vanes. Axially, the guide vanes are offset by 5 rotor blade heights giving the profile of the variable radius duct and the relative positioning between guide vanes and rotor. The datum rotor has 43 blades each with an inlet angle of 70º, additional design parameters are given in *Table 5*.

Parameter	Value	Units
Turbine casing diameter	0.60	m
Guide vane outer casing diameter	1.20	m
Hub/tip ratio	0.82	-
Axial gap between blade rows	0.0331	m
Annulus height	0.0540	m
Annulus area	0.0926	m^2
Design mass flow	2.76	Kg s^{-1}
Guide vane radial offset	5.55	Rotor blade span
Guide vane axial offset	5	Rotor blade span

Table 4: General design parameters (CT14b)

Parameter	Value	Units
Blade count	43	-
Relative inlet angle	70	°
Axial chord	0.095	m
Tip gap	0.001	m
Section thickness / chord	12.56%	-
Design Reynolds number	2.37 x 10^5	-
LE & TE radii	0.0052	m
LE ellipse	8:1	-
Stacking axis	Mid pressure surface	-

Table 5: Datum rotor blade design parameters (CT14b)

4.4 Experimental method

The reciprocating test rig was designed and built at Cranfield University to allow scaled turbine devices to be tested in reciprocating flows. The test rig emulates the air flow produced by the chamber of an OWC device and is capable of producing flows associated with monochromatic and polychromatic wave trains. The latter are of the type that an OWC turbine would experience under real ocean conditions. The full design, building and operation of the initial test rig are detailed in Herring (2007) and Herring and Laird (2007). Recent modifications have been made to the test facility to

incorporate polychromatic waves, though the operation of this has still to be published. A short description of the test facility is given here.

The test rig reproduces the piston action of the sea water within the chamber of an OWC by means of a pivoting flap within a sealed circular chamber. The flap acts as the surface of the water and is pivoted about the centre of the circular chamber by an electric motor, through a gearbox. The forwards and backwards motion of this flap produces the reciprocating airflow in the duct that leads to the turbine. The layout is displayed in *Figure 36* below. The motor is controlled by computer and different wave profiles with varied frequency and amplitude can be input into the machine to simulate waves of varying wave height and period. Details of the rigs capabilities are given in *Table 6.*

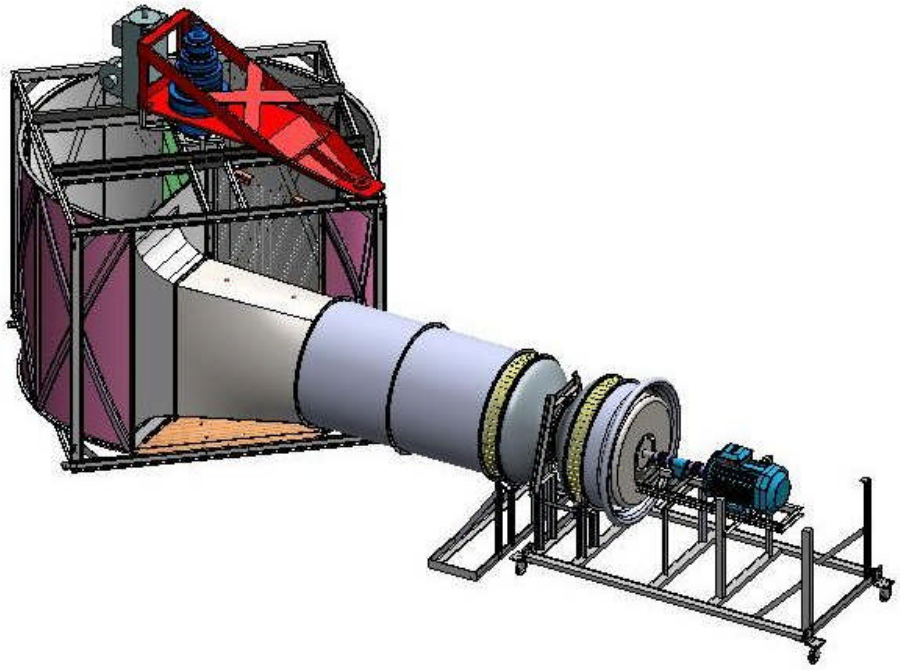

Figure 36: Reciprocating test rig layout
(CAD drawing supplied by D-R)

Parameter	**Value**	**Units**
Total swept volume	16.43	m^3
Max. flow rate	5.88	m^3s^{-1}
Max. RMS flow rate	4.15	m^3s^{-1}
Max. frequency	0.14	Hz
Min. period for full oscillation	7	s
Max. frequency for small oscillation	1	Hz

Table 6: Reciprocating test rig capabilities (Herring, 2007)

The test rig and VRT were designed together to avoid problems as a result of the scaling. Herring (2007) presents the calculations undertaken during the design process to ensure that adequate Reynolds numbers ($\geq 2 \times 10^5$) were maintained across the full range of flows. Scaling issues associated with Mach number effects were not a concern due to the low velocities of the device ($\leq 50 ms^{-1}$). However, due to the reciprocating flow produced by the test rig, it was necessary to achieve Strouhal number similarity during scaling in order to prevent any frequency effects.

Strouhal number is defined as:

$$S_t = \frac{fD}{v_a} \qquad \textit{Eq. 4.1}$$

where v_a is the mean axial flow velocity, f is the frequency of oscillation and D is the characteristic length which in this case is taken as the turbine diameter.

During the design process, the method of theoretical Strouhal number matching was used to ascertain the performance requirements of the test rig. The turbine was originally designed to be a one quarter scale device of which a full scale turbine would be suitable for an OWC similar to the LIMPET where wave periods are around 10s. Using this estimate and a design axial flow velocity of $25 ms^{-1}$, it was demonstrated that the test rig needed to be capable of producing oscillations of period $T = 0.314 \times T_{\text{Full Scale}}$ to achieve Strouhal similarity. The full calculation can be seen in Herring (2007) where it is shown that this performance is achievable with the constructed test rig. However, due to the limitations of the maximum accelerations and velocities that can be achieved with the flap, this performance is only possible for a relatively small range of flows.

During operation, static and total pressure are measured at various positions through the device allowing the flow rate to be calculated. Thermocouple measurements are also made for temperature correction of the pressure. The rotational speed and torque are measured by a torque transducer located on the shaft connecting the turbine to the generator. During testing, the turbine speed is limited to 1500 rpm due to the design constraints of the electrical generator. If the turbine exceeds this speed, additional load is applied to the turbine by increasing the power being taken off by the generator or the turbine is shut down.

The reciprocating test rig allows for the testing of the VRT turbine in reciprocating flows and the measurement of flow rate, turbine rotational speed, torque and the pressure drop across the device, allows for the efficiency of the test turbine to be calculated both instantaneously at given flow rates and as an average for varying flows.

4.5 Numerical method

Full scale, 3D CFD simulations have been performed on the datum turbine with the aim of assessing the performance of the device. This performance is used as a base for comparison for any modifications that are made during this research project. The process also serves as a method of validating the CFD procedure used to represent the VRT. The datum geometry was originally simulated by Banks (2009) and the results presented here are compared to these early simulations. The process was also validated against experimental data from the reciprocating test rig.

Geometry

The original geometry profiles were used to construct the turbine. These were the datum 'hockey stick' guide vane profiles described earlier, the rotor blade and duct profile. The duct and stator profiles are symmetrical about a plane containing the mid chord of the rotor which is itself symmetrical. The domain was extended three guide vane chord lengths upstream and downstream of the IGV and OGV. This was done to reduce the possibility of flow recirculation occurring at the outlet boundary. The turbine domain was constructed using ANSYS Turbogrid and a full representation of the turbine can be seen in *Figure 37*.

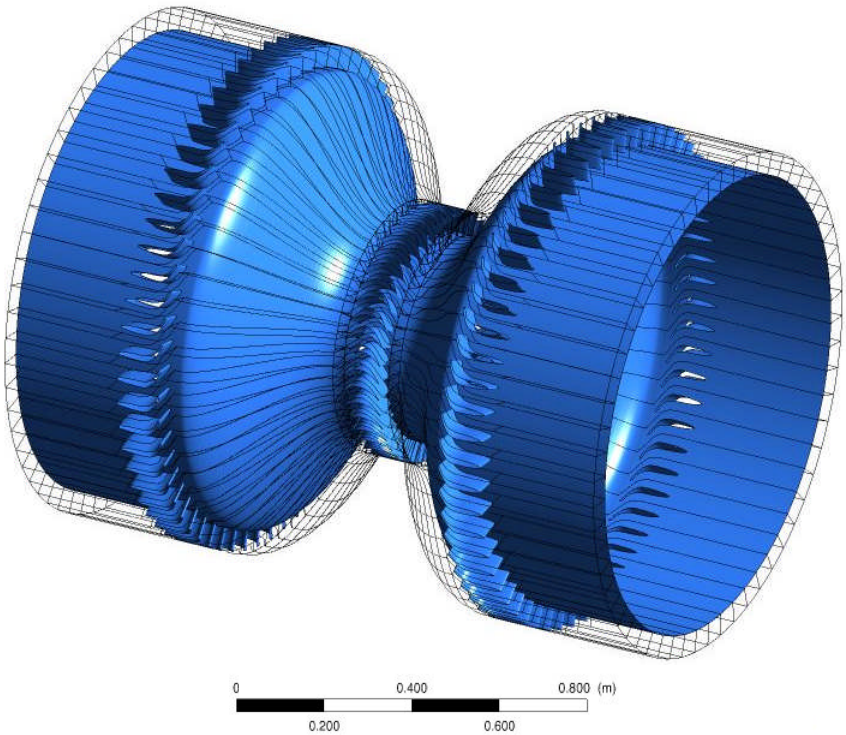

Figure 37: CAD model of datum turbine geometry for CFD simulation showing extended inlet and outlet domains.

The datum turbine simulation is set up with three geometry domains, the IGV, rotor and OGV. ANSYS Turbogrid uses the geometry data to construct a three-dimensional CAD model of the turbine, prescribing the relative blade and duct profile. It also determines the positioning of the periodic boundary either side of the blade profile. The size of the domain is dependent on blade count which is input by the user. The length of the domain is determined by the coordinate data of the hub and shroud profiles. This way, the created domain represents a radial slice of the turbine and the flow within this slice is simulated. The periodic boundaries allow for the flow behaviour of the full device to be represented while minimising the size of the computational domain.

Mesh generation

ANSYS Turbogrid was used to create the computational meshes for the guide vane and rotor blade. The meshes were constructed with O-grids around the blades and H/J/L-type topology. All meshes were body fitted hexahedral meshes. For the rotor blade, the tip region was meshed with a non-matching H-grid. At the blade surface, the first cell heights were set in order to achieve an estimated $y^+ \approx 2$ at maximum Reynolds number and in all cases, maximum mesh angles were > 25º. A mesh dependency study was conducted to examine the degree of dependency of the solution on the mesh density. The results of this study are presented on the following page and examples of the medium density meshed IGV and rotor blade are shown below in *Figure 38*.

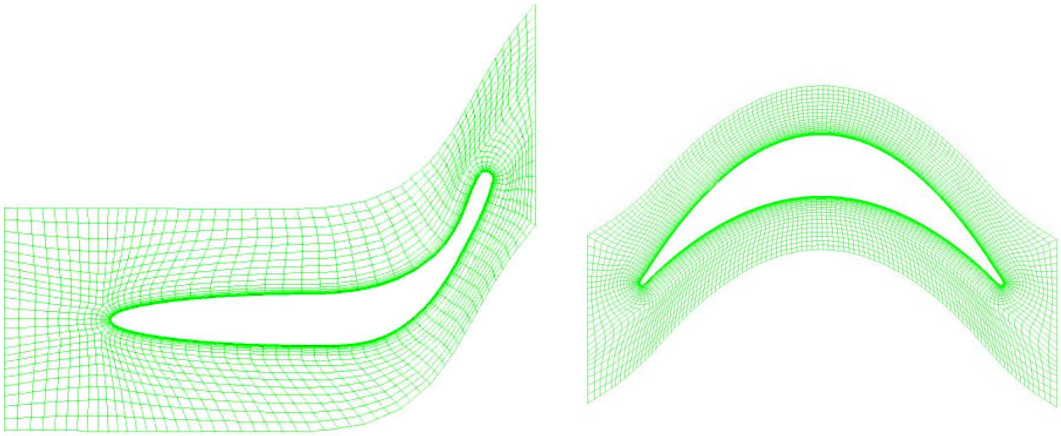

Figure 38: Medium density meshes for inlet guide vane and rotor presented for comparison.

Boundary conditions and settings

ANSYS CFX was used for pre-processing. The complete guide vane and variable radius duct domains were simulated as stationary domains with the hub and shroud boundaries defined as non-slip walls. The rotor domain was simulated as a rotating domain with the shroud defined as a counter rotating wall. A 'Stage' mixing plane type interface was used between the stationary and rotating domains. Using this option within CFX, flow quantities are circumferentially averaged and scaled, allowing for pitch and frame change between domains. The sides of all three domains were set as rotationally periodic boundaries.

3D CFD Parameters	**Value**	**Units**
Avg. Static Pressure at outlet	*0*	*Pa*
Rotor Angular Velocity	*-850*	*rpm*
Working Fluid	*Air @25 º*	
Ref. Pressure	*1*	*atm*

Table 7: 3D CFD Parameters

Boundary conditions of total pressure at inlet and average static pressure at outlet were prescribed as well as rotor RPM. The simulations were run in one direction, from inlet to outlet, in steady state. The effect of reverse flow over the OGV is demonstrated from single direction simulations. Full boundary conditions and flow parameters are given in *Table 7* and the values of total pressure used for each case are shown in *Table 9.*

The *k*-ω-SST turbulence model (Menter, 1994) was used to run the cases, which were simulated as steady state and incompressible with no heat transfer. The High Resolution differencing scheme within CFX was used to solve the simulations which is fully second order accurate (Ansys, 2008).

	Nodes	**ΔP [Pa]**	**T [N m]**
Coarse	568,300	2361.4	1.00
% Change		2.1	1.0
Medium	1,054,720	2410.5	1.01
% Change		1.5	1.0
Fine	1,861,210	2446.7	1.02

Table 8: Results of VRT mesh independence study.

Solution and convergence

A mesh independency study was conducted by running the same simulation three times with increasing mesh densities. A mass flow inlet of 0.05 kg s^{-1} was used and the same convergence limit of 500 iterations was set for each case. This number was based on experience from earlier simulations that the residual values would have reached an acceptable level within 500 iterations. The values of static pressure drop and rotor blade torque were compared. The results are presented in *Table 8* above.

It can be seen from the results that the variation in static pressure drop between the coarse and medium mesh densities was 2.1%. Comparing the medium and fine mesh densities, the variation in static pressure drop reduces to 1.5%. The variation in torque between the coarse, medium and fine meshes is 1%. The results demonstrate the dependence of the solution on the mesh density and that by using the medium density mesh, the error is reduced below 2%. Based on these results, it was decided that the medium mesh density was sufficient to produce accurate solutions and this mesh was used for the simulation of the turbine.

Case	Φ	ω (rad s^{-1})	TP Inlet (Pa)	$\dot{m}$ (kg s^{-1})
1	0.31	89.01	500	0.82
2	0.54	89.01	1000	1.44
3	0.76	89.01	1500	2.02
4	0.94	89.01	2000	2.50
5	1.11	89.01	2500	2.96
6	1.26	89.01	3000	3.35
7	1.54	89.01	4000	4.10
8	2.49	89.01	8000	6.64

Table 9: Values of total pressure inlet for VRT simulations.

CFX-12 was used for solution, pre and post processing of a total of 8 simulations. A full turbine operating characteristic was simulated by varying the total pressure at the inlet to the device. A table of inlet conditions used, along with the achieved range of flow coefficients are given in *Table 9.*

Across the full range simulations, convergence to RMS residuals less than 1 x 10^{-4} was generally achieved after running for 250 iterations. However, continuing the run time of simulations did not achieve lower residual values. The reason for this is thought to be due to the area of separation downstream of the OGV. Despite the VRT concept, separation still occurs at the OGV as it does with all bidirectional impulse turbines with fixed guide vanes. An example of the separated region around the OVG stator row is shown in the contour plot of total pressure presented below (*Figure 39).*

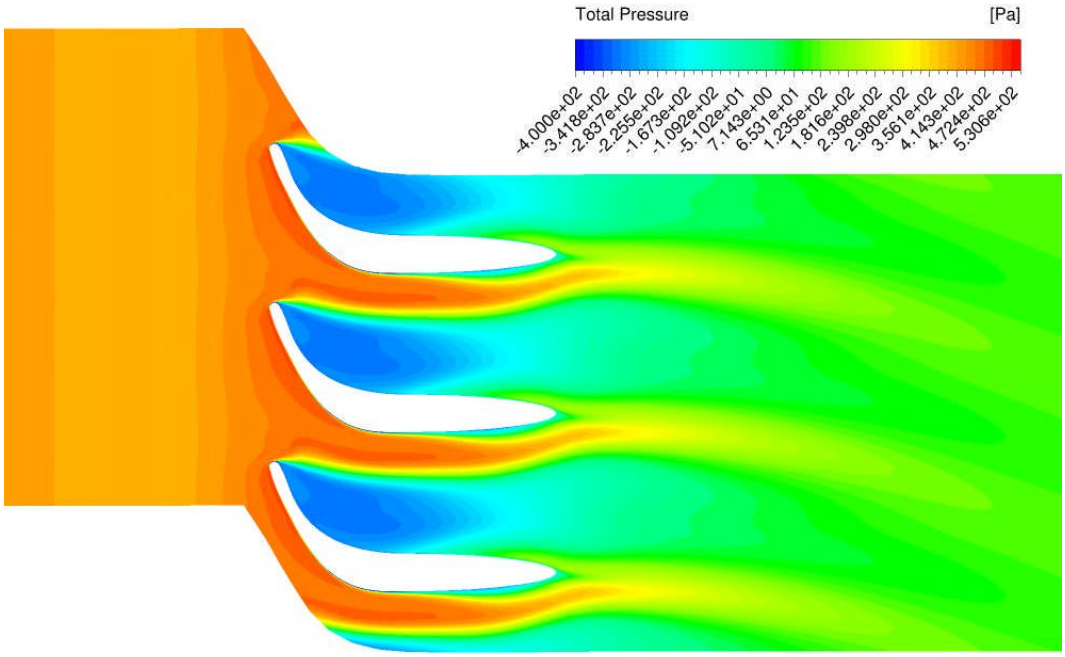

Figure 39: Separation of flow around OGV, results from Case 5.

Results

The numerical results demonstrate the predicted performance characteristic of the datum VRT and plots of static pressure variation through the device are shown below in *Figure 40* for *Case 5*, with a calculated flow coefficient of 1.11. The full turbine characteristic is presented below in *Figure 41* where it can be seen that the predicted peak total-to-static efficiency is 62.8%.

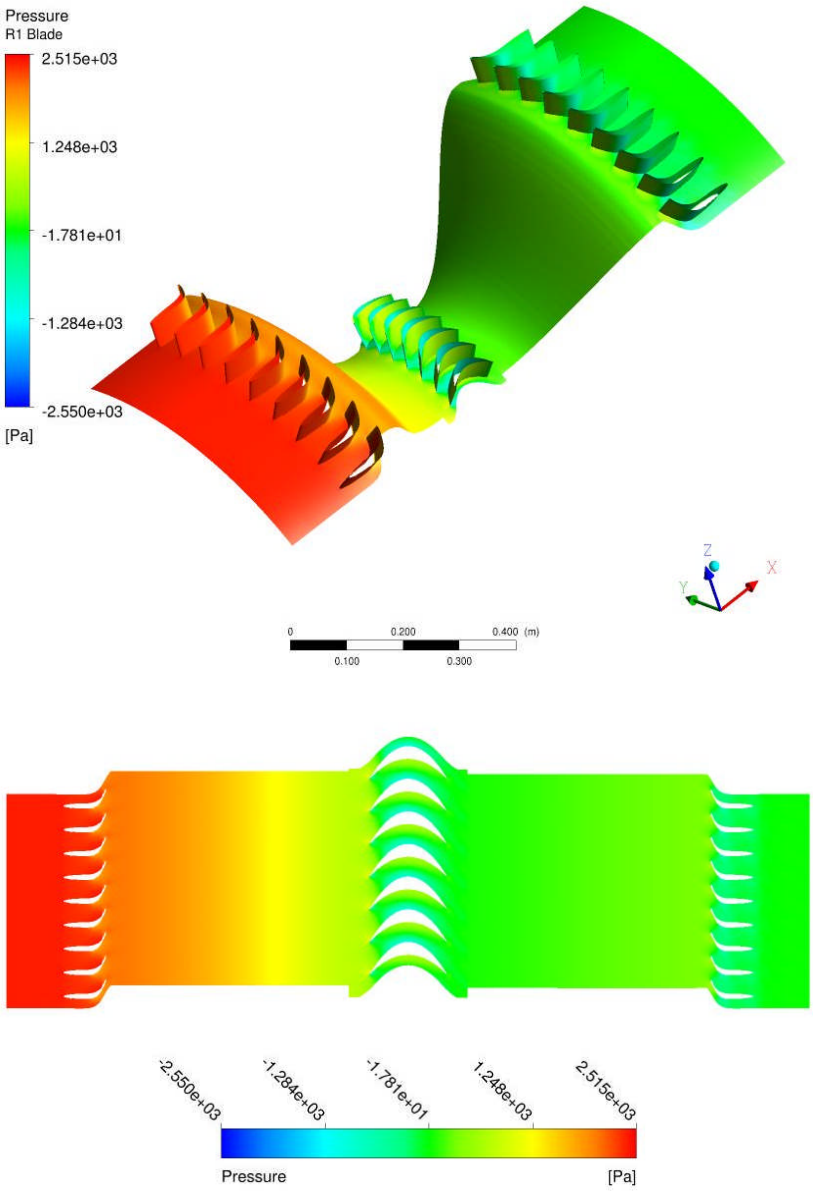

Figure 40: Static Pressure variation through datum VRT design, Case 5.

CFD Comparison

In order to cross validate the CFD method used, these results were compared with the results of simulations performed by Banks (2009) (*Figure 42*). By displaying the plots side by side, it can be seen that the simulations conducted by the author predict slightly higher performance than the results of Banks. Peak efficiency is higher at 62.8% compared with 62.6% by Banks, an error of 0.2%. This error is present for the higher flow rate conditions simulated, above a flow coefficient of 1. Overall, the shape of the turbine characteristic produced by the authors method is a good match to that of Banks, despite the over prediction of performance.

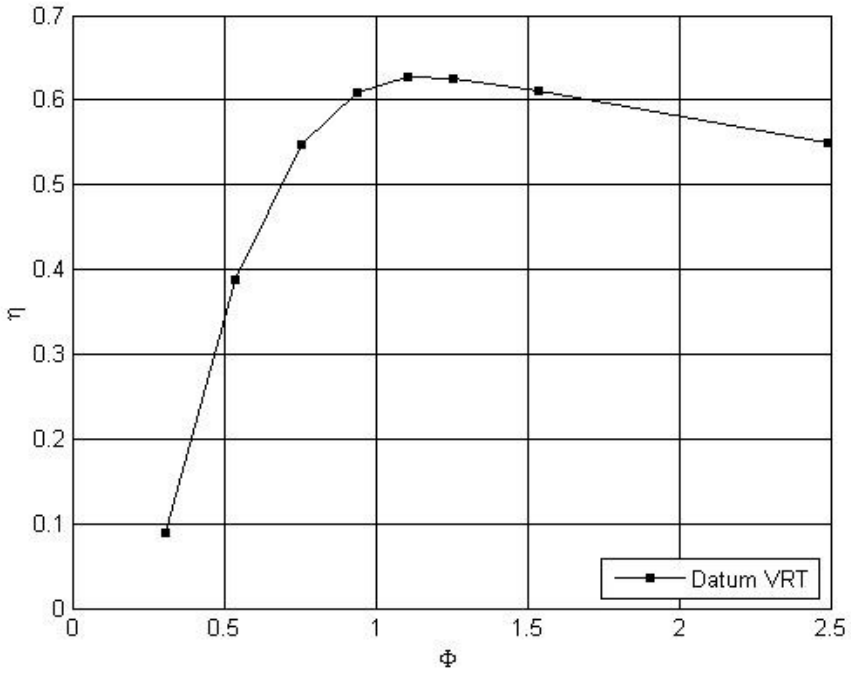

Figure 41: Efficiency prediction for VRT based on CFD results.

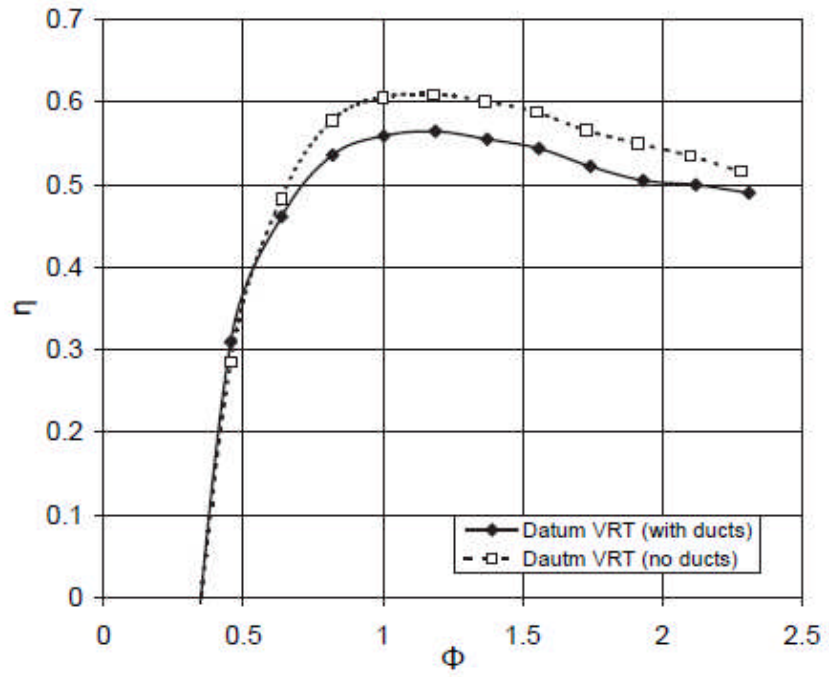

Figure 42: Predicted efficiency characteristics for the datum VRT turbine, comparing with and without the S-ducts, originally required for incorporation into Cranfield test rig (Banks, 2009).

Banks was able to validate these early simulations of the datum VRT design against experimental results from the datum VRT design, tested in the reciprocating test rig at Cranfield University by Herring (2007). The results of some of these tests are shown below in *Figure 43*, showing results for tests carried out at flow rates of 1.84 m^3s^{-1} and 2.32 m^3s^{-1} at wave periods of T = 5s and T = 14s, the shortest and longest periods used during testing.

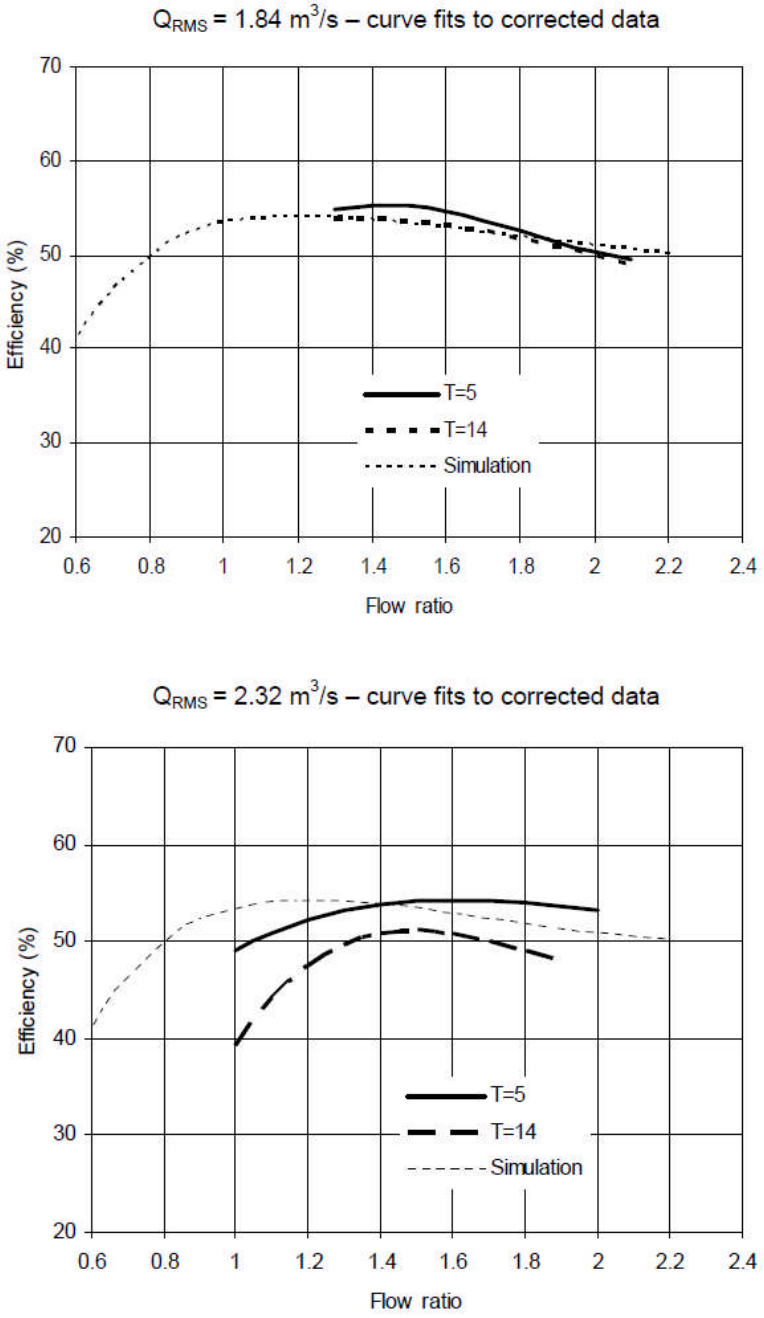

Figure 43: Efficiency characteristic comparison of CFD simulations and experimental data obtained at two different periods for an RMS flow rate of 1.84 m^3s^{-1} and 2.32 m^3s^{-1} for the CT14 VRT datum turbine (Banks, 2009).

Making a comparison between experimental data and the CFD predictions, at the low flow rate of 1.84m^3s^{-1} the results agree well. However, at the higher flow rate of 2.32 m^3s^{-1}, the agreement is poorer. In both cases displayed, the peak efficiency predicted by the CFD occurs at a lower flow coefficient than the experimental measurements. Banks suggests that the reason for this was due to uncertainties regarding the accuracy of the boundary conditions representing the actual experimental conditions. Overall, Banks concluded that performance prediction from steady-state RANS CFD was a suitable tool for use in the design of bidirectional impulse turbines. The fact that the quantitative agreement was not especially good meant that caution should be taken when quoting absolute values but as a method of measuring relative performance of design modifications, this method was suitable.

The fact that the CFD results of the datum turbine show good agreement with simulations performed by Banks which in turn, were validated with experimental data, demonstrates the capability of the method. The error of 0.2% of the peak efficiency in the results is acceptable and the results presented here are used as a base for comparison for all modifications made in the research presented in this thesis. The CFD method used is also used as a model for all simulations performed in the research.

4.6 Conclusion

This chapter presents a study of the datum turbine that is used as the starting point for the research in this thesis. The study has given insight into the design of the turbine and the development process that took place over the course of the HydroAir project to reach the datum design. The design and capabilities of the reciprocating test rig are also presented here as well as the method used for testing the datum turbine in reciprocating flow conditions.

A numerical study has been undertaken, conducting full scale 3D CFD simulations of the datum turbine. This has been used to gain understanding of the function of the datum turbine as well as to test the CFD method used. The results of the simulations demonstrated the flow conditions within the turbine, giving important understanding of the function of the device. This is especially important for the OGV, the main focus of study for this research.

The results of the numerical study have been compared with previous CFD simulations performed by Banks which have also been validated against experimental data, produced using the reciprocating test rig. The performance characteristic produced from the simulations shows good agreement when compared to previously documented results from numerical analysis of the same turbine geometry. The error of 0.2% is deemed acceptable for the application of the CFD method.

In the research presented in this thesis, CFD is being used as a method of performance prediction for optimisation and so the main requirement of the tool is to estimate relative performance variations. The fact that the method used here is able to re-produce previous results, with a small error, has given confidence in the method used and demonstrates that it is capable of performing this function.

The performance results from the 3D CFD presented in this section are used as a baseline for turbine developments in this research from this point forward, as is the CFD method described here.

5 Multi-element guide vanes

5.1 Introduction

The idea of using multi-element guide vanes (MEGVs) to reduce the losses at the OGV of a bi-directional impulse turbine has been previously suggested by Banks (2009). The concept was presented as an area for potential performance improvement in the continued development of the HydroAir turbine. The concept involves the use of a number of airfoil shaped elements which when combined, perform the function of the IGV. Each element provides a small amount of turning so that as a whole, the set of the elements will change the direction of the inlet flow. The benefit of the design is that the relative positioning of the guide-vane elements creates a channel for the outlet flow to pass through with reduced restriction. The principle of the design proposed by Banks is presented schematically in *Figure 44*.

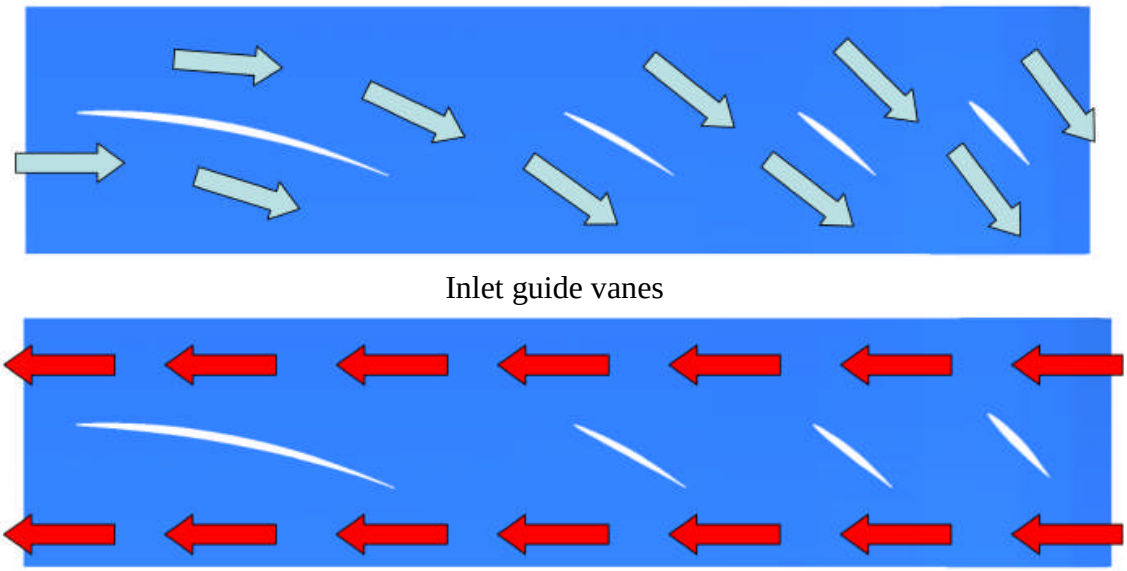

Figure 44: The multi-element guide vane concept of Banks (2009)

Banks (2009) carried out preliminary CFD and experimental work on the multi-element arrangement with initial results indicating that the configuration had the potential to outperform the existing guide vane geometry with further work but this could not be confirmed. It is this concept that has been further investigated in this research, starting with a literature review of relevant applications that incorporate multi-element airfoils in their design and continuing to further develop the concept with the employment of MEGVs on bi-directional impulse turbines.

5.2 Literature review

5.2.1 Aeronautical applications

A modern aircraft is required to cruise for long periods of time with minimum drag in order to achieve acceptable levels of efficiency. An aircraft is also required to take-off and land within the distance set out by the length of an airport runway. In terms of wing profile, these two requirements cause a conflict in design, as a wing designed for high lift would look very different to a wing designed solely for cruising.

The distance required for take off is determined by the stalling speed of the aircraft wing, a lower stalling speed requires a shorter runway and less acceleration to provide enough lift for the aircraft to take off. The stall speed of the wing can be reduced by increasing the area of the wing but this has the negative effect of increasing drag which is not desirable for cruise flight. There is also the increased weight associated with increasing the area of the wing.

Figure 45: Aircraft wing with single slat and flap (Abbot and von Doenhoff, 1949)

This problem is overcome by changing the shape and area of the wing according to the aircraft flight condition. This enables a good high-speed, cruising performance to be obtained while at the same time achieving a high lift coefficient at the low speed of take-off and landing. This has led to a multi-element wing design with an adjustable flap at the trailing edge and an adjustable slat at the leading edge of the main airfoil *(Figure 45)*.

Extending the adjustable components of the wing allows a maximum lift coefficient to be achieved over a smaller area of the main body of the wing. This has the incurred benefit of reduced weight from reduced area and when the flaps are retracted, drag is minimised for efficient cruising.

A correctly positioned slat increases the overall lift coefficient by altering the forward camber of the wing. This reduces the build up of pressure that occurs on the leading edge at high angles of attack. Reducing the pressure build up improves the flow of air around the leading edge and over the upper surface of the main body of the wing, delaying the onset of stall (Abbot and von Doenhoff, 1949).

The ‘Plain Flap’ or ‘Aileron’ and the ‘Split Flap’ *(Figure 46)* achieve increased lift with adjustment of a hinged section at the rearmost part of the wing section. This effectively changes the camber of the whole wing section and can be effective for flap deflections of 10 to 15 degrees. At greater flap deflections the flow separates from the upper surface of the flap.

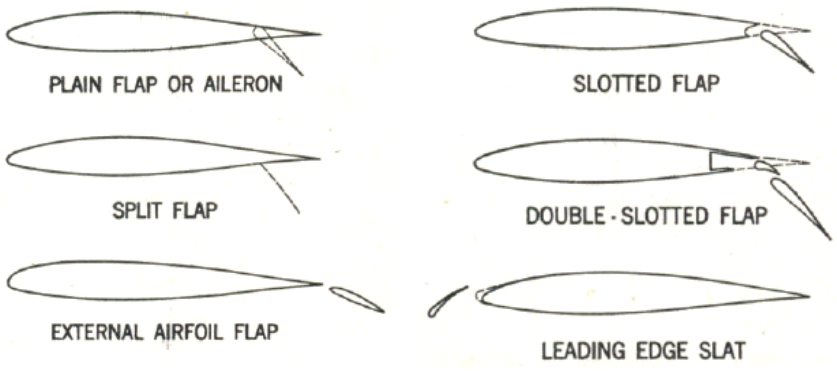

Figure 46: Typical high-lift devices (Abbot and von Doenhoff 1949)

The other trailing edge flaps displayed in *Figure 46* are positioned so that there is a gap between the main body of the wing and the adjusted flap forming a slot along the span of the wing. These flap designs, including the slot allow for the camber of the wing section to be increased and in some cases, the effective chord length of the wing profile is increased as well. Due to the pressure difference between the upper surface of the wing, air travels from the lower surface, to the upper surface through the slot. The slot acts like a nozzle, producing a jet of air which, due to the phenomenon known as the Coanda effect, attaches to the upper surface of the flap. The result is that the boundary layer of the fluid on the upper surface of the flap has high energy and remains attached through a larger angle of deflection than would be possible without the slot. The existing boundary layer, after passing over the main body of the airfoil, has become too depleted to remain attached over a large deflection. The jet of air from the slot re-energises the boundary layer, preventing separation across the surface of the adjusted flap allowing for higher adjustability.

The requirement of a high-lift wing section to change the direction of the working fluid without separation is similar to that of the IGV of an impulse turbine. The wing section accelerates the fluid over the upper surface, changing the direction across the flap at the rear and this generates lift. The IGV changes the direction of the air flow, accelerating the fluid towards the rotor blade. Multi-element, high-lift devices are able to achieve greater turning angles than single airfoil designs and it may be possible to incorporate this capacity into the guide vane design. If the required amount of turning of the flow can be achieved over a reduced frontal area, the solidity of the guide vane row and the restriction to the outlet flow could be reduced.

A correctly positioned leading edge slat is able to reduce the peak pressure occurring on the leading edge of the main wing body. This could be adapted to the design of the IGV where a slat would allow the main guide vane to be positioned at a higher angle of attack, reducing the peak pressure on the foremost section of the GV preventing separation occurring at the upper surface.

5.2.2 Compressor blades

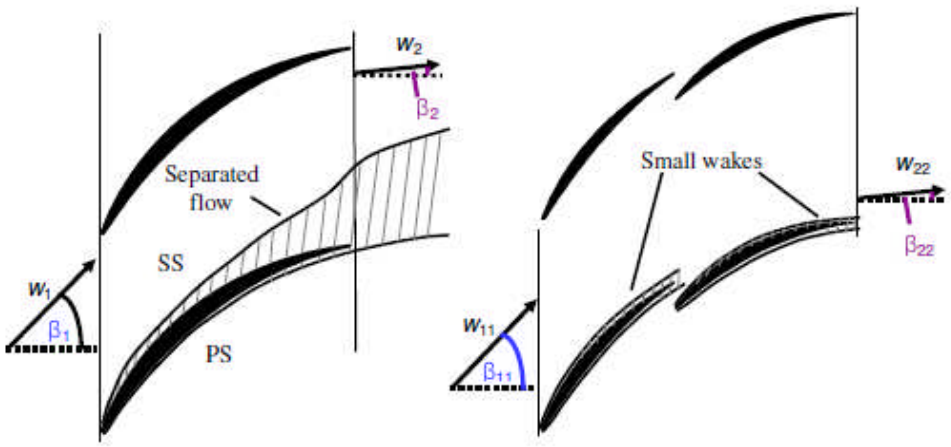

Figure 47: Profile view of single (Left) and Tandem (Right) airfoil arrangement at high loading (McGlumphy, 2008).

McGlumphy (2008) conducted research into the use of tandem airfoils to act as rotor blades in a core axial-flow compressor *(Figure 47).* A two-dimensional (2D) CFD study was conducted, assessing the performance of the tandem airfoils in different positions and then three-dimensional (3D) CFD was developed based on the best case from the 2D simulations. The overall outcome of the research indicates that a tandem airfoil design can perform better than a single airfoil with the correct deign. The 2D CFD clarified that the positioning of the airfoils is highly sensitive as although the configuration showed improved performance at optimum positioning, incorrect

positioning can result in the tandem arrangement performing more poorly than a single airfoil blade. McGlumphy (2008) observed fluid flow characteristics that are also seen on multi-element airfoil arrangements where locally accelerated fluid flow occurs through the gap between the two airfoils, reporting that this effect was beneficial to the flow at the leading edge of the aft airfoil.

The 3D CFD simulations confirmed that the tandem arrangement performed better than the single blade, attaining a higher working coefficient. Analysis of the results showed that the flow around the forward blade behaves as a single blade would, whereas the flow around the aft blade is much more complicated, non-uniform and three dimensional. The resulting flow of the aft airfoil depends strongly on the flow that is received from the forward blade. This confirms that the interaction of flow around two airfoil shapes is complicated and difficult to predict as stated earlier.

As the positioning of the geometry is so significant to performance, it is important to examine how McGlumphy (2008) conducted the experiment. A simple design rule was adopted to calculate the overall loading and associated losses for the elements of the tandem blades in terms of the *Lieblein diffusion factor*. By using an airfoil shape that had a large amount of published experimental data and simplifying the design rule to assume that there is no interaction between the flow fields of the tandem blades, the loading to loss ratio could be predicted. Using these predictions and ensuring the airfoils were close to equally loaded, seven different airfoil configurations were modelled that would produce a wide range of minimum loss factors. This was achieved by altering the combination of percent pitch and axial overlap, measured as a percentage of the chord length. All other parameters were kept constant and the tandem blades were of identical airfoil shape to reduce the number of variables. The airfoil shape was also geometrically similar to the single airfoil blade tested to aid the accuracy of the comparison.

McGlumphy's (2008) method takes into account the importance of the relative positioning the tandem blades and the potentially large number of variables associated with the position. The design rule enables a performance prediction to be made before investing in CFD simulation and limiting the positioning variables to two factors reduces computing cost. This approach may not produce the optimum result but the research shows that an improved performance was achieved and the 2D CFD identified the geometry with highest performance which could then be further investigated in 3D.

5.2.3 Other multi-element applications

Multi-element airfoil configurations are used in a number of applications and a few of the more relevant scenarios are presented here.

Formula 1 car design makes use of advanced aerodynamics to minimise air resistance and increase the downwards force of the car on to the track in order to improve traction. The visible wings on the front and rear of the cars are solely designed for this purpose. The front wing is designed to divert the air in front of the car past the front tyres as the large tyres create a large amount of air resistance. The other function of the front wing is to create down-force. The FIA F1 regulations limit the size of the front wing and so designers and developers have to achieve the desired amount of downwards force from a limited area. This restriction has led to multiple element airfoils being used in the front wing design (Mortel, 2003).

In the same way that multiple elements are used in aircraft wings for high lift, the airfoils in the F1 wing are used to achieve an increased down-force. Adjustability is also incorporated into the design to allow the team to make adjustments to the downwards force created by the front wing and adapt the function to particular race conditions or the cars performance. This is done by having the front airfoil fixed and the second airfoil adjustable. The adjustment of the second airfoil is restricted so it can only be adjusted within the capability of the design as if the wing was adjusted further, the flow would separate and the down-force would be lost.

This demonstrates the use of multi-element airfoils to achieve increased lift (in this case down-force) over a reduced area. It may be possible to adapt this concept to the IGV as achieving turning of the flow over a reduced area will benefit the outlet flow, reducing the solidity of the OGV row.

Renewable technologies

The addition of ducts to devices that extract energy from fluid flows has been widely investigated due to the potential improvement in power extraction. Two of the technologies where this has been investigated are hydrokinetic energy conversion systems and wind turbines. In both technologies the application is similar in that the duct is designed to influence the conditions of the fluid after it has passed the rotor. This manipulation of the flow involves aerodynamically designed duct profiles and designs for multi-element geometries have been suggested.

Wind turbines extract power from air flowing past them. As the air passes the rotor blades, the velocity of the air decreases and this causes the static pressure to increase

before and after the turbine while the static pressure drops at the rotor as energy is extracted from the air. The air flow after the rotor blade widens due to the flow deceleration and the increase in static pressure. The maximum power that a windmill can extract from an air flow is 16/27 of the available power or 59%, known as the Betz efficiency. This is due to an amount of kinetic energy that must remain in the airflow to carry the air past the rotor.

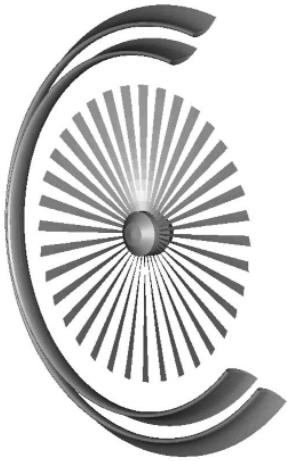

Figure 48: Multiple airfoil profiled rings around wind turbine rotor.
(Bet and Grassmann, 2003)

There have been attempts to increase the potential efficiency of conventional wind turbines by controlling the diffusion of the air stream at the outlet of the rotor using wings or diffusers (see, for example; Lawn, 2003). Bet and Grassmann (2003) modelled a wind turbine with an airfoil profiled ring around the rotor *(Figure 48)*. The ring is designed to capture some of the kinetic-energy of the exhaust, drawing additional air through the turbine. The development of the concept resulted in the multiple-element profiled ring shown above.

The multi-element design is used to change the direction of the flow, using a wing of minimum area. The design allows maximum manipulation of the flow using the smallest area possible. This is necessary as the addition of a wing to a wind turbine creates a very large device and any saving in size weight will be beneficial.

The Vortec 7 diffuser augmented wind turbine (DAWT) incorporates a multi element design for a different reason. The multi element design creates a nozzle at the leading edge of the duct profile and a secondary slot towards the trailing edge as can be seen in *Figure 49*. The initial nozzle adds energy to the boundary layer of the fluid, keeping the flow attached. The increasing area of the duct accelerates the flow after the turbine, drawing more air in through the front of the turbine blade. The secondary slot ensures attachment of the flow, fed by the airstream that has not passed through

the turbine, this jet of air maintains the energy level in the boundary layer towards the exit of the duct.

Scale testing of the Vortec 7 DAWT show that the diffuser draws more air through the blade plane, increasing the power capabilities of a wind turbine (Phillips, Flay and Nash, 1999). The design demonstrates the use of a multi element configuration to maintain flow attachment and manipulate fluid flow successfully.

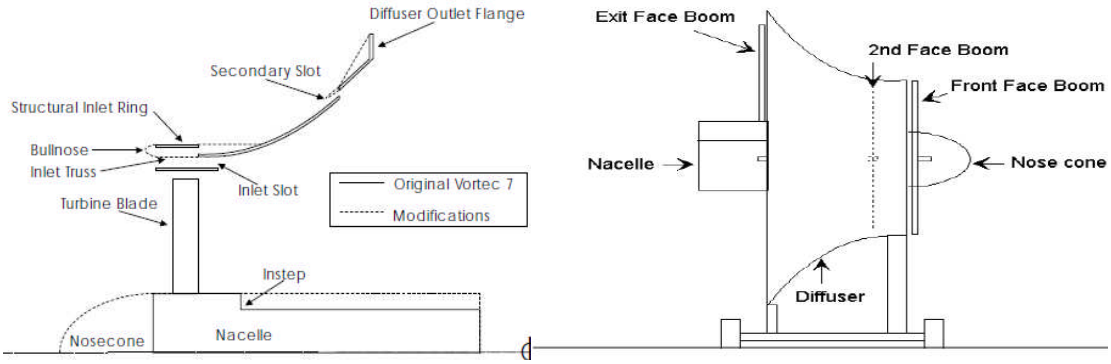

Figure 49: Cross section and side view of the Vortec 7.
(Phillips, Flay and Nash, 1999)

Hydrokinetic energy conversion systems function in the same way as wind turbines, extracting energy from a free fluid stream. The use of ducts or channels in hydro kinetic energy conversion systems has been broadly investigated and has resulted in a number of multi element designs. The advantage of a multi element design over a single element is the ability to be able to bring in fluid from the flow stream that has not passed by the rotor of the device. This allows the capture area of the device to be increased, allowing greater power extraction.

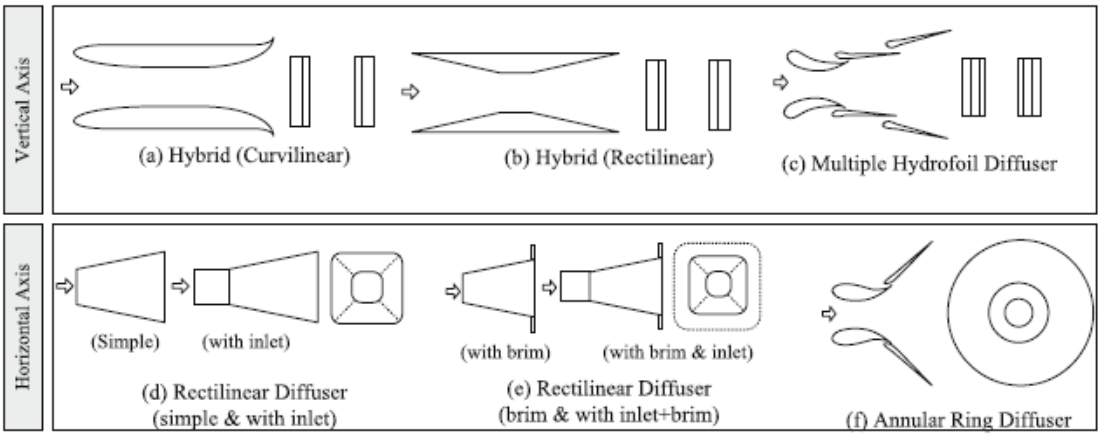

Figure 50: Duct shapes for Hydrokinetic energy conversion systems
(top and front view) (Khan et al. 2009)

Khan et al. (2003) investigate system design and duct augmentation for hydrokinetic energy conversion systems, stating that multiple hydrofoil and annular ring diffusers *(Figure 50, (c) and (f))* are possible when higher efficiencies are required and both are capable of exceeding the Betz limit of 59%.

All the multi-element applications presented in this literature review are designed for uni-directional flow. The application of MEGVs for bi-directional impulse turbines is unique in the fact that the concept is being employed for bi-directional operation.

5.2.4 Multi-element CFD, Parameterisation and Optimisation

Early multi-element design problems relied solely on empirical methods as no adequate theory had been developed that was capable of predicting the aerodynamic characteristics of the flow. Even though there has been a large accumulation of experimental data across a wide range of configurations, the sensitivity of the geometry makes the design process difficult (Abbott and von Doenhoff, 1949).

Despite significant advances in CFD, the prediction of the maximum lift coefficient of multi-element configurations is still not satisfactory (Cebeci et al. 2005) and the geometry sensitivity and large number of variables mean that the design process is still complicated and unreliable.

The configuration of airfoils in a multi-element array means that the flow leaving the trailing edge of an upstream airfoil will then interact with an airfoil downstream. It is this interaction of the viscous wake of an upstream airfoil which creates the complicated flow and the unreliability of CFD to predict the outcome. Separation and unsteady flow are also usually present in the early design stages of a multi element configuration and this adds to the complexity of the problem.

The way that multi-element airfoil geometries interact is governed by a number of geometric variables. In a 2D problem, the most important variables are the size of the gap between elements, the axial overlap and the ratio of the elements chord length. There are however many more variables that can be introduced to the design such as orientation and variations in the airfoil shape. This also adds to the complexity and the difficulty of achieving the optimum design for the specific problem. This has lead to the use of optimisation techniques in conjunction with CFD simulation. These techniques reduce the number of required CFD simulations to produce a solution as well as the accompanied need for repetitive grid generations when making small geometry alterations. This process can be automated, while analysing the results

produced, in order to make adjustments to the geometry and manipulate the performance of the design towards the desired outcome.

There is a large amount of literature on the subject of optimisation techniques using CFD and a number of these have already been discussed. Slawig (2001) focuses on optimisation of multi-element airfoil arrangements and uses automatic differentiation techniques to study the effect of lift and drag on a four element configuration with respect to flap positioning. In this study, Slawig defines the flaps position by the angle of rotation around a fixed point, allowing systematic adjustments to be made and the resulting effect simulated. Deng et al. (2007) present one method of optimising the gap, overlap and deflection of a multi-element airfoil arrangement using a genetic algorithm. This experiment focused on take off and landing configurations and wind tunnel validations of the CFD analysis shows that the optimisation had been successful in improving performance.

Manufacturability

While considering the possibility of adding multiple stator elements to the HydroAir turbine the implications on manufacturability and cost need to be considered along with the expected performance improvements. The current datum turbine has 59 stators made from a composite material. Adding an extra element to the individual guide vane profile doubles the number of guide vane components, naturally adding to the cost of manufacture and construction.

The use of flow control has also been suggested as a way of reducing separation at the OGV and improving overall performance. Herring (2007) considered this requirement and after consultation with the manufacturers, a minimum thickness of 4mm was deemed necessary to incorporate some method of flow control into the guide vane profile. Since the addition of flow control is still possible in the continued development of the HydroAir device, this minimum thickness requirement has been maintained in the geometry investigation of the MEGVs.

Due to the commercial nature of the project, it is important that these factors are kept in mind while investigating the MEGV concept. While the primary aim of this section of the research is to investigate the MEGV concept for bi-directional turbines, the solution must be appropriate for the specific application.

5.3 MEGV Concept

The MEGV concept works by splitting up the stator profile into two or more separate elements. This has the effect of reducing the frontal area of the stator row, hence reducing the obstruction to the flow in the exit duct. The turning requirement of each stator element is reduced, resulting in a reduced axial chord length. The combined axial chord length is greater but the stacking effect of combining the stator elements reduces the frontal area of the stator row. The arrangement also allows for a free passage to be present between stators for the flow to pass through.

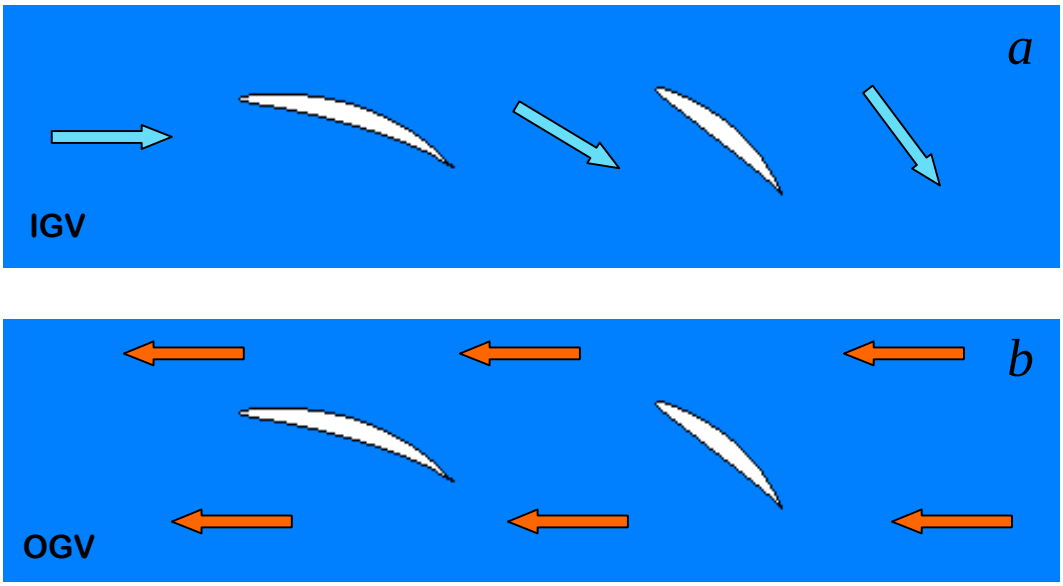

Figure 51: MEGV Concept

When performing as an IGV *(Figure 51a)*, each stator element acts independently, gradually inducing turning to the flow until the desired turning angle is achieved. When performing as an OGV *(Figure 51b)*, the flow passes freely between the stator elements. Since the angle of incidence between the rotor exit flow and the OGV is poor, the flow separates from the surface of the stator creating a wake of low pressure. The size of this wake is minimised due to the reduced frontal area of the upstream element of the MEGV configuration. The additional pressure loss associated with an increased number of profiles is reduced by the shadowing effect of the wake. The wake of the upstream element encloses the downstream element, reducing the overall area of low pressure, improving turbine performance.

5.3.1 Initial investigation

The initial approach into the MEGV investigation was to define the problem. The aim was to reduce the total pressure loss across the OGV, improving the overall performance of the bi-directional turbine. The main constraint was that the turning angle of the IGV had to be maintained. As a result of the literature review on multi element airfoil applications, two MEGV configurations were selected for early investigation. These two methods were investigated using 2D CFD methods to enabled a large number of variations to be investigated in a relatively short time scale.

This approach allowed greater understanding of the problem to be gained within the time allowed. After this initial investigation, a decision was made as to which concept would be taken further. A brief description of these two approaches is given below and the investigation methods used before moving on the improvement and development of the chosen concept.

MEGV Cascade

The MEGV cascade concept uses the theory of airfoils with flaps from the literature, with the intention of achieving the desired amount of turning over a reduced surface area. Initially a configuration was set up using a standard airfoil profile with a single flap of 30% chord length applying the same method as McGlumphey (2008). 2D CFD simulations were conducted using ANSYS FLUENT to assess the performance of the early geometry configurations. It quickly became apparent that it was not possible to achieve the desired inlet turning angle of 67.2° with a single flap.

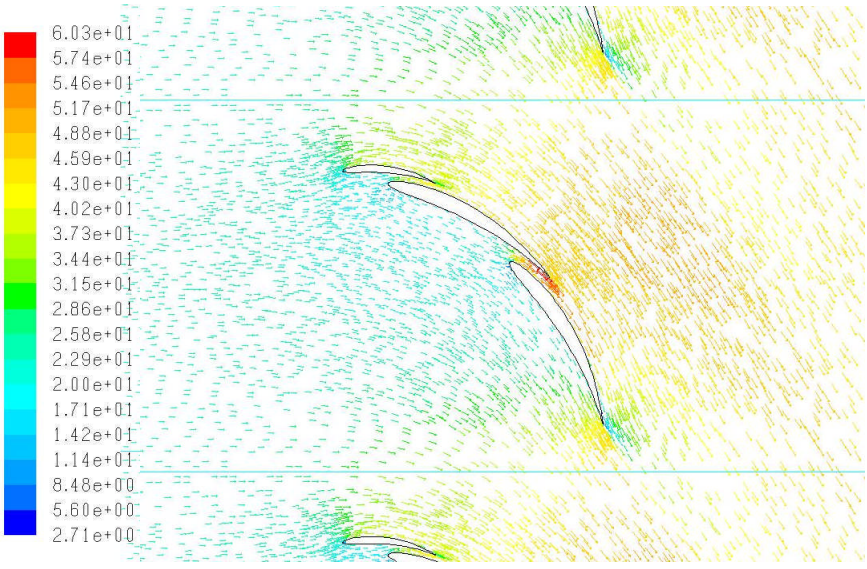

Figure 52: MEGV Cascade OGV, velocity vectors coloured by velocity

A number of further geometries were investigated using thin airfoil profiles with increased camber. It was necessary to increase the angle of attack in order to achieve the turning angle but this resulted in separation from the suction surface of the main body of the configuration. At this point, a slat was introduced at the leading edge. This allowed the angle of attack to be increased further such that the desired turning angle was achieved. This resulted in the geometry displayed below in *Figure 52*. In the reverse direction, the flow separates from the sharp trailing edge of the final airfoil and this creates a large wake downstream of the guide vane. The flow becomes attached to the upper surface and the gap between the guide vanes allows the air to pass freely *(Figure 53).*

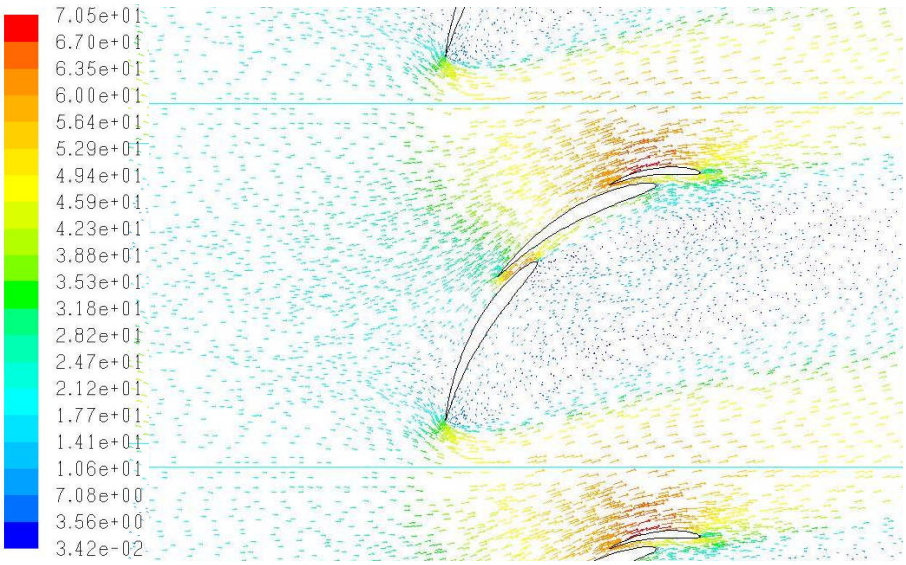

Figure 53: MEGV Cascade OGV, velocity vectors coloured by velocity

The initial investigation demonstrated the complexity of this guide vane configuration as the cooperation of a large number of parameters was required for this configuration to function. A comparison was made with the datum geometry by comparing the total pressure loss across the guide vane geometry at the design condition. The comparison estimated an improvement in the total pressure loss across the OGV due to the reduced solidity of the stator row. This was owing to the fact that the slots between the guide vane elements strengthened the boundary layer attachment, allowing for increased turning to be achieved at increased pitch.

CFD simulations were only performed at a single operating condition and there was concern that the parameters controlling the relative positions of the guide vane elements would be sensitive to variations in flow rate. If this was the case the performance improvement would not be achieved across the full operating range of the turbine resulting in an overall reduction in performance. This could have been overcome by having adjustable geometry as in aircraft wings but this is not a viable option for a marine energy device.

Axially staggered MEGVs

The second MEGV configuration investigated the method of axially staggering stator elements to form multiple stator rows. Initially, to reduce the number of variable parameters, identical NACA 0012 airfoil profiles were used for each element. Much literature exists on the behaviour of the NACA 0012 airfoil (see for example: Abbott and von Doenhoff, 1949; McCroskey, 1987; Sheldahl and Klimes, 1981) and this information was used in the initial setup of this configuration. Initially, five airfoil elements were used, the initial airfoil was set at an angle of attack of 12°, below the know stall angle of ≈16° of the NACA 0012 profile. The angle of the remaining stators was then increased up to the required turning angle of 67.2°.

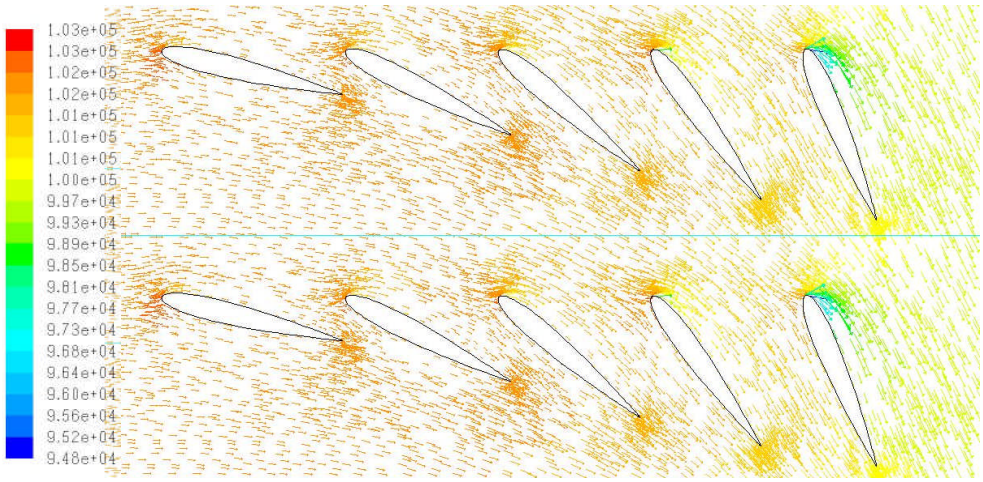

Figure 54: Results showing velocity vectors coloured by static pressure of IGV geometry

Again, 2D CFD simulations were conducted using ANSYS FLUENT to assess the performance of these early geometries and through making adjustments to the axial spacing and rate of overall turning, the IGV turning requirement was met. *Figure 54* shows the vector flow pattern produced using FLUENT and it can be seen that the flow is turned by the IGV configuration, with the flow interacting with the individual airfoil elements as had been intended. The turning angle, calculated using FLUENT was 64.4º at the stator exit.

Reversing the flow for this configuration to simulate the OGV highlights the fact that due to the high angle of the final airfoil required for IGV turning, the passage left for the flow is small, and this resulted in a large restriction of the flow. *Figure 55* shows that there is separation of the flow around the airfoil closest to the rotor *(Point A)* with the largest angle of attack but the reverse flow around the other airfoil elements appears steady with no separation. Overall performance was poor when compared to the datum geometry due to the high solidity of the first stator row.

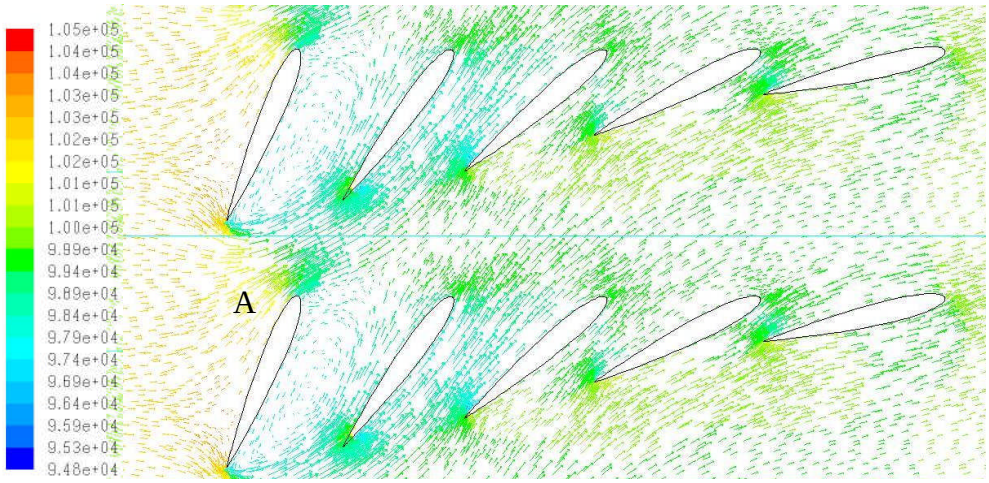

Figure 55: Results showing velocity vectors
coloured by static pressure of OGV geometry

These early investigations highlighted the difficulty in producing a functioning MEGV design. At this point, due to the time constraints on the research project, it was necessary to decide on one MEGV concept to investigate further as there was not enough time to pursue both configurations. The complex interaction between the guide vane elements in the cascade arrangements and uncertainty of performance in variable flows meant that this configuration was not preferred. The more simple axially staggered MEGV arrangement maintained the required simplicity of the device, good for operation in the marine environment and manufacturability.

Concept development

It was necessary to assess the main objective of the GV function, this is to produce turning of the flow at the IGV while minimising restriction to the flow at the OGV. Analysis of the 2D results highlighted the way that the design of the guide vane elements could help these main function objectives.

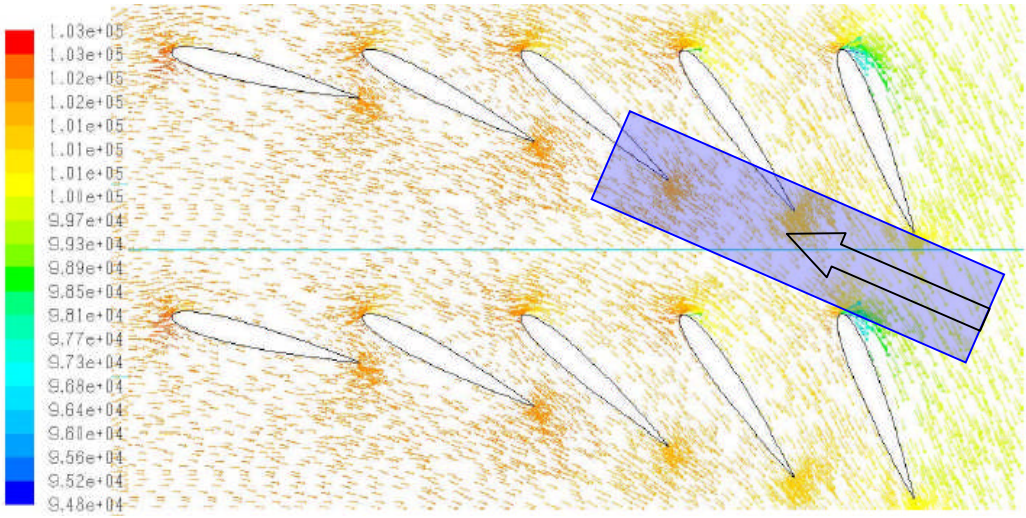

Figure 56: An Initial MEGV design

Figure 56 shows one of the early MEGV designs. The blue shaded region shows the passage of the flow when the stator is acting as an OGV. This demonstrates the high solidity of the stator design and the small passage the flow must pass through. The improved design is shown in *Figure 57*. The red shaded box shows the flow area of the new design when acting as an OGV, this passage is greater, reducing solidity and improving flow past the OGV.

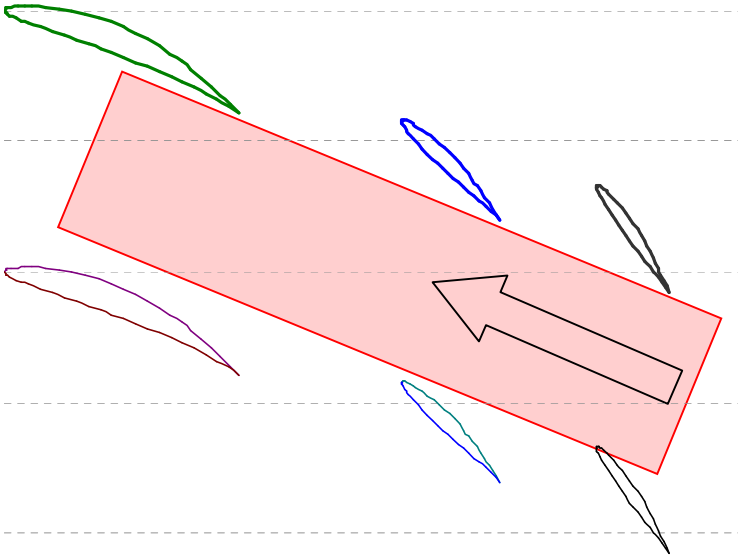

Figure 57: Improved MEGV design

The improved design uses standard NACA 65 series airfoil profiles with circular arc mean camber lines for each vane. In order to maximise the reverse flow area, each vane row has approximately the same circumferential chord, this ensures that in the reverse direction, downstream vanes are shadowed by the obstruction of the upstream vane. The ideal situation is that one wake is created and all three vanes are enclosed within this wake, acting as a single vane in the reverse direction. The width of this

wake should be minimised to ensure that the unobstructed passage between vanes is as large as possible; this is achievable by maintaining approximately the same circumferential chord. For each vane to have approximately the same circumferential chord, the turning of each vane reduces as the average camber angle increases. This means that the majority of the turning is done in the first vane row. The chord for each row is set using the Zweifel blade loading criteria. Pitch remains constant between vane rows.

Analysing the flow over the OGV from the 2D CFD plots showed that a turning angle was being induced. This is due to the angle of the final vane which has been designed to achieve a turning angle of 62 degrees when performing as an IGV. In the reverse direction this metal angle induces a turning of 25 degrees in the flow. This turning is undesirable and accounts for losses in the reverse flow however it is necessary to have a trailing edge metal angle of approximately 62 degrees to achieve the desired amount of turning for the IGV. The vane rows are offset radially at an angle of 25 degrees allowing the flow to pass along an unobstructed passage at this nominal back angle.

The axial spacing between vane rows is initially set at one axial chord length, this is to minimise the interference between the vane rows. Ideally, each vane row acts independently as an IGV, each row adding increased turning to the flow. This greatly simplifies the simulation of the problem since the interaction of a vane wake with downstream geometry would cause complex and unpredictable fluid behaviour.

The initial design was simulated in FLUENT using identical boundary conditions to previous simulations to give an accurate comparison.

5.3.2 Inlet Guide Vane

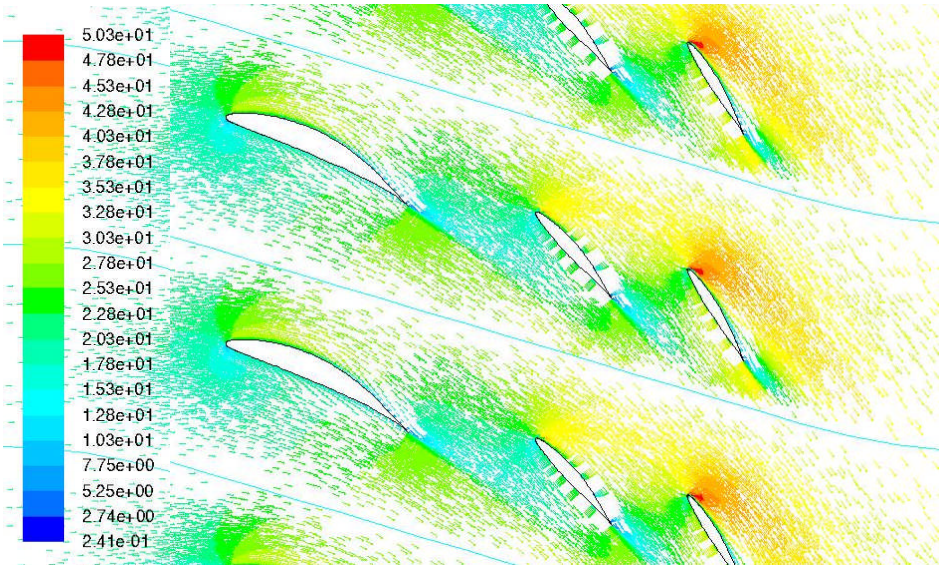

Figure 58: IGV – Vectors coloured by Velocity

The results of the 2D FLUENT simulation are shown in *Figure 58*. It can be seen that the desired turning angle of 62 degrees has not been achieved despite a final metal angle of 64 degrees; the velocity vector display shows the reason for this. The first vane is too highly loaded and the fluid separates from the suction surface at approximately two thirds of the chord. The result of this is that the exit angle from the first vane row is measured at approximately 20 degrees, half the desired amount of turning. This has a knock on effect and the angle of incidence of the second vane row is reduced, the impingement region occurs on the suction surface of the second vane. The flow then accelerates around the leading edge of the second vane and the flow becomes detached from the suction surface at about 50% chord length. This effect is then magnified on the third vane and the losses are visible as the high velocity of the flow accelerating around the leading edge of the third vane.

5.3.3 Outlet Guide Vane

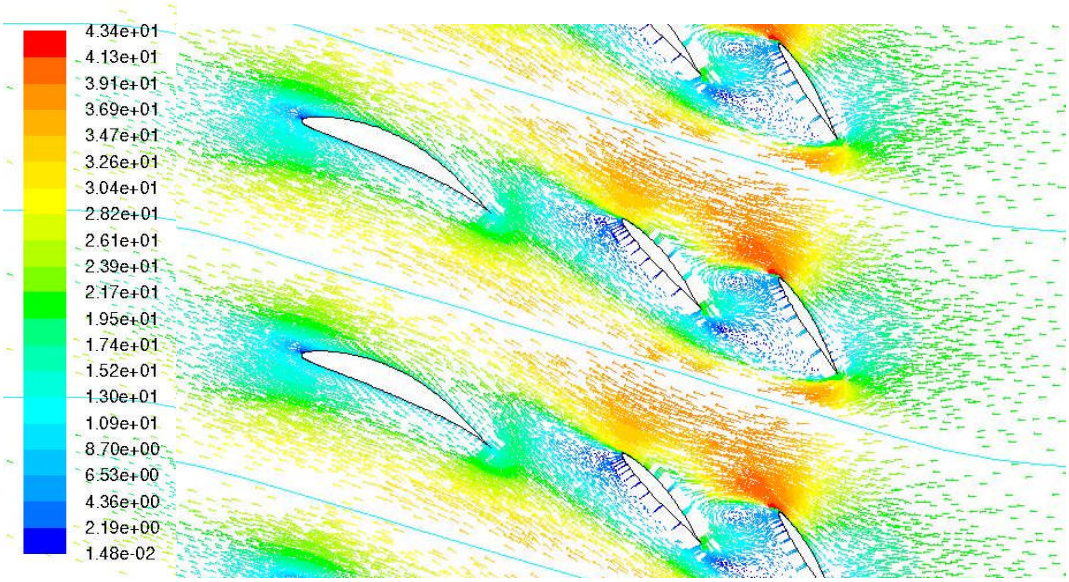

Figure 59: OGV – Vectors coloured by velocity

Simulation of the improved geometry as an OGV displayed promising results; *Figure 59* shows the velocity vector results. The flow behaves as expected with close correlation to the initial guess shown above in *Figure 57*. The fluid passes unobstructed between the vanes with an initial upwards deflection of approximately 25º as predicted. The wake generated by the upstream vane shows areas of unsteady flow but the downstream vanes are mostly contained within the wake, acting almost as a single guide vane. Ideally the second vane would be positioned so that it was completely contained within the wake, this should not affect the performance of the IGV since each vane is acting independently.

Comparing the results of the CFD simulations of the MEGV design with the datum guide vane geometry showed a 6% reduction in total pressure loss. Although this is not an overall improvement due to the poor function of the IGV, the OGV performance shows significant improvement.

Discussion and modifications

The modified MEGV arrangement did not achieve the necessary turning at the IGV and this is where the design needed to be improved initially. CFD results showed that pressure losses across the IGV were greater than the datum geometry and this was due to the separation occurring at the leading stator row as well as the additional friction and mixing losses from the increased number of profiles. Despite this fact, combined total pressure losses are reduced demonstrating the superior performance of the OGV over the datum geometry.

The setting up and analysis of the improved geometry highlighted the number of variables associated with the design and the potential for using optimisation as a method of improving the geometry. A number of further modifications were made to the geometry until a satisfactory baseline setup was achieved, ready for optimisation.

The modifications to the geometry are briefly discussed below:

Trailing edge thickness

The NACA 65 profile that was used in the early investigations had a final trailing edge thickness (TET) of zero. This profile was used for simplicity of setting up initial CFD cases but to enable realistic performance prediction a rounded trailing edge was added to the profile. The Ainley and Mathieson (1957) loss model *(Figure 60)* has been used to calculate the TET. The model states that if the TET to blade pitch (t_e/S) varies from 2% then the plotted correction factor can be used to calculate the total loss coefficient of the TET, Y_t is the estimated variation of the total loss coefficient. *Figure 60* shows that 0.02 is the nominal value but anywhere between this and 0.05 is acceptable in terms of minimising losses. An arc of radius 0.002m was added to the base NACA 65 profile. This allowed for a limited range of pitch variation while maintaining acceptable losses due to TET. The initial geometry had a pitch of 0.1m giving a (t_e/S) of 0.04. This equates to an acceptable loss coefficient of 1.1. The TET of 4mm is also the minimum requirement for flow control to be added to the guide vane trailing edge as discussed earlier and set by Herring (2007).

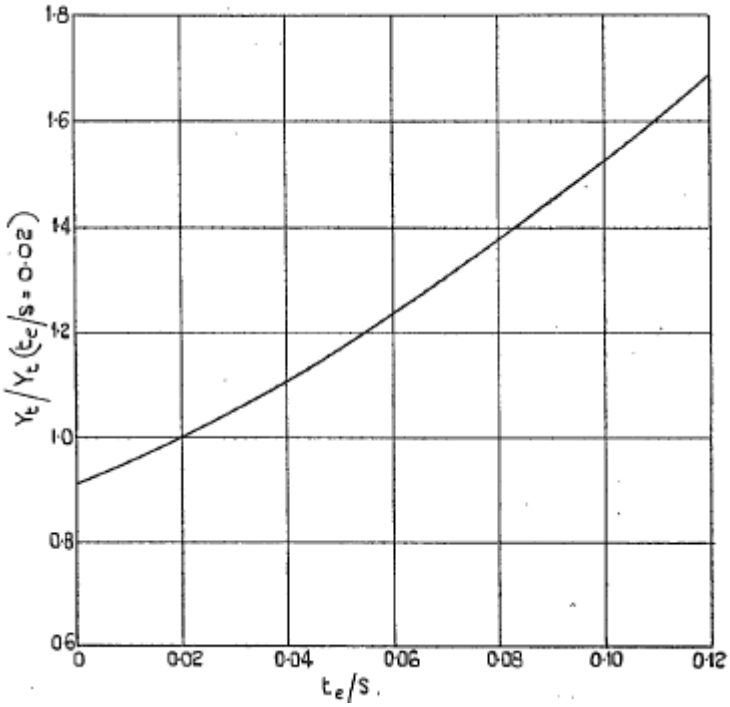

Figure 60: A&M loss model
Effect of trailing-edge thickness on blade loss coefficients,
Ainley and Mathieson (1957).

Blade Loading

High loading on the first stator row results in separation. This loading can be reduced by variation of a number of parameters such as pitch, camber and stagger. The reduction of pitch has the negative effect of increasing the solidity of the stator rows, reducing the passage for the flow past the OGV and increasing total pressure loss. Initially, the blade loading was assessed by modelling each vane of the IGV in isolation, looking at the nominal upstream conditions for each vane and matching the characteristics of the vane to the inlet and outlet flow for each row. This allowed for the turning to be distributed across the rows according to blade loading. These variable parameters need to be optimised in order to maximise the performance of the geometry when functioning as an IGV and an OGV.

Reduced stator rows

During this investigation it became apparent that is was possible to achieve the desired amount of turning using two vane rows. This has the positive effect of reducing friction and mixing losses with a reduced number of elements. There is however, the negative effect of the increased axial chord length of the second vane due to the increased turning requirement of each element. At this point, it was decided to continue the geometry investigation using two stator rows and to continue to adjust

the design until the desired amount of turning could be achieved at the IGV. This resulted in the geometry displayed in *Figure 61*. This geometry forms the base case for the optimisation procedure detailed in the next section of the report.

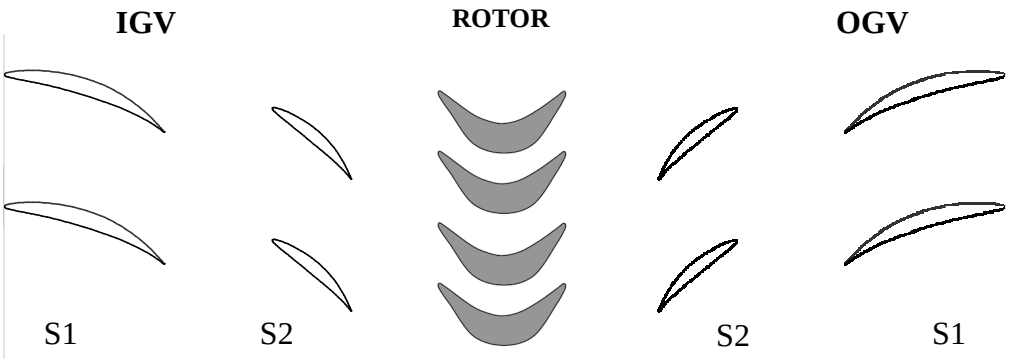

Figure 61: MEGV arrangement without variable radius duct.

Design Constraints

The successful operation of the MEGV concept is dependent on the relative positioning of the stator rows and these early investigations allowed for the following set of design constraints to be defined. These design constraints must be met for the concept to function correctly.

1. Stator elements have approximately the same circumferential chord to maximise the reverse flow area and produce a constant area passage for the reverse flow.
2. Turning requirement for the IGV are split across the stator rows. The first stator row performing the largest amount of turning with reducing turning requirements for subsequent rows, closer to the rotor.
3. Relative positioning between stator rows is important to allow unobstructed reverse flow, stator rows must be clocked circumferentially to create a free passage at the nominal back flow angle.
4. Axial spacing between rows is greater than one chord length of the lead stator to minimise interference between stator rows for forward flow.

Although these design constraints seek to constrain the geometry and define the function of the GVs, there are many variable design parameters within the design. The successful function of the MEGVs is reliant on the correct combination of these parameters and optimisation methods have been used in order to find the optimum performance criterion for reduced pressure loss across the guide vanes for bi-directional flow.

5.4 Datum geometry

A datum geometry was created as a result of early CFD simulations which helped gain understanding of the required function of the MEGV concept. This has resulted in a geometry made up of two stator rows using modified NACA 65 series profiles with circular arc mean camber lines. Further details of the datum geometry are given in *Table 10*. This datum geometry is used as the starting point for all subsequent optimisation and parameter studies unless otherwise stated.

Parameter	**Symbol**	**Value**	**Units**
Geometry Assembly			
Number of Stators	*N*	*44*	-
Diameter at mid span	*D*	*1.150*	*m*
Pitch	*s*	*0.082*	*m*
Pitch Offset	*δ*	*0*	*% of pitch*
Axial Spacing	*Ax*	*1.40*	*S1 chord lengths*
Number of Vane Rows	*E*	*2*	-

Guide Vane Geometry		***S 1***	***S 2***	
Axial Chord	b_n	*0.100*	*0.080*	*m*
Thickness / chord ratio	$(t/b)_n$	*0.120*	*0.120*	-
Trailing edge radius	$r_{TE\,n}$	*0.004*	*0.003*	*m*
Turning angle (Camber)	*β*	*41.0*	*29.0*	*degrees*
Vane Row Chord Ratio	*R*	*1.00*	*0.80*	-

CFD Parameters			
Inlet mass flow (whole machine)	$\dot{m}$	*2.88*	*Kg/s*
Outlet Static Pressure	P_s	*100*	*kPa*

Table 10: Datum geometry parameters

5.5 Mesh Generation

Once the datum geometry for the MEGV optimisation had been produced, it was necessary to investigate the method of automated mesh generation for the optimisation process. Two methods of mesh generation, using different meshing software, were investigated. The aim of the investigation being to assess the suitability and controllability of the software for automated mesh generation with controlled variables.

5.5.1 ICEM CFD

One method of mesh generation has been investigated using the Ansys mesh generation software ICEM. The software is very versatile with the capability of being adapted to generate meshes for a wide variety of geometries and applications. The software is also capable of generating either structured or unstructured mesh in either 2D or 3D. ICEM Hexa 3D has been used to create a structured mesh in 3D. A 3D mesh is required to use the CFX solver.

The domain geometry was defined as a thin slice, simulating a section of the stator geometry, mid-way along the span of the stator. This allows for a 3D mesh to be generated with the minimum number of nodes, this reduces required computing power and processing time. The slice was constructed as a flat plane and although this is not an exact representation of a slice at mid span, modelling the area as a flat plane greatly simplifies the generation of the domain, an important consideration for meshing automation. Each case was split into 4 separate domains, inlet and outlet, and stator vanes 1, and 2. This allows for adjustments to be made to each stator element geometry individually without re-generating the whole mesh each time.

ICEM CFD has an inbuilt scripting function that allows the user to record commands while constructing a mesh, this is useful in interactive mode when repetitive commands are required. The script can also be used to create a batch job, where the geometry can be recreated, from the command line without the use of the GUI. This allows the grid generation to be performed more quickly due to the reduced computing power required in batch mode. The script also allows the mesh to be generated without added manual intervention, once the batch job has been submitted.

The base geometry was used to build a script to automatically generate the mesh in batch mode. Since the mesh was generated specifically for the base geometry, a mesh of high quality is produced. This is confirmed by monitoring mesh characteristics such as cell length ratio, skewness and y^+ at the stator boundary. The case was passed through the CFX solver to confirm the viability of the mesh against previous results for the base case.

The procedure demonstrated the capability of ICEM CFD to automatically reproduce a quality mesh in batch mode with no manual intervention. This is a desirable quality for automating an optimisation process and the software is very capable. It is however more important that the software can reproduce a quality mesh over a range of input geometries. This requires the mesh to be recreated around a geometry that has varied from the base case.

The ability to mesh varied geometry was tested by modifying the initial geometry of the stator vanes, this was originally done for vane S2. The geometry was modified to position S2 at the upper and lower limit of the parametric adjustment, the position was then output as coordinates to be read and interpreted by ICEM. The script was then modified to read the new coordinate data as part of the mesh generation procedure. This modification tests the ability of the software to mesh the S2 stator domain at the upper and lower limit so that the mesh can be analysed to see if it is of an appropriate quality.

The results showed that automating the mesh generation in this way is unreliable. This is due to the blocking approach used in ICEM. This approach works well in interactive mode as the user positions the blocks to allow different combinations of grid arrangements to be fitted to a specific geometry. The problem arose in automation when the blocking nodes had to be repositioned to fit the adjusted geometry. Small adjustments to the geometry meant that the blocks did not have to be moved and the script executed with no errors. Greater adjustments closer to the upper and lower limits resulted in errors in the script due to misplaced blocking nodes and incorrect interaction between the blocking framework and the geometry.

The need for the blocking to be pre-set to avoid these errors in reproduction reduced the potential range of the pitch offset parameter since the blocking framework must be within the domain geometry. Added complications were also being incorporated into the problem with the risk or an error developing and the mesh not being generated successfully.

5.5.2 CFX Turbogrid

CFX Turbogrid is a mesh generation software specifically designed for rotating turbomachinery. The software was investigated in terms of suitability for automated mesh generation for optimisation. The investigation was approached in the same way as for ICEM. A thin slice of the base MEGV geometry and duct was modelled using Turbogrid, generating a mesh for the datum geometry, once the mesh was of a required standard, adjustments were made to the geometry, testing the ability of the software to reproduce the mesh at the upper and lower limits of the parameter variation.

Turbogrid generates a radial slice of the geometry and uses periodic boundaries to simulate the function of the whole machine *(Figure 62)*. For this reason it was necessary to modify the initial geometry coordinates so that they would be accepted by the software. The initial profile coordinates are plotted on a flat plane but it was necessary to manipulate the profile, effectively plotting it on to a radial curve.

Turbogrid then projects the hub and shroud profile to form a slice of the machine, the vane profile must then be within a small tolerance of the hub and shroud projections so that the software can trim the extrusion of the vane profile and generate the 3D geometry of the machine.

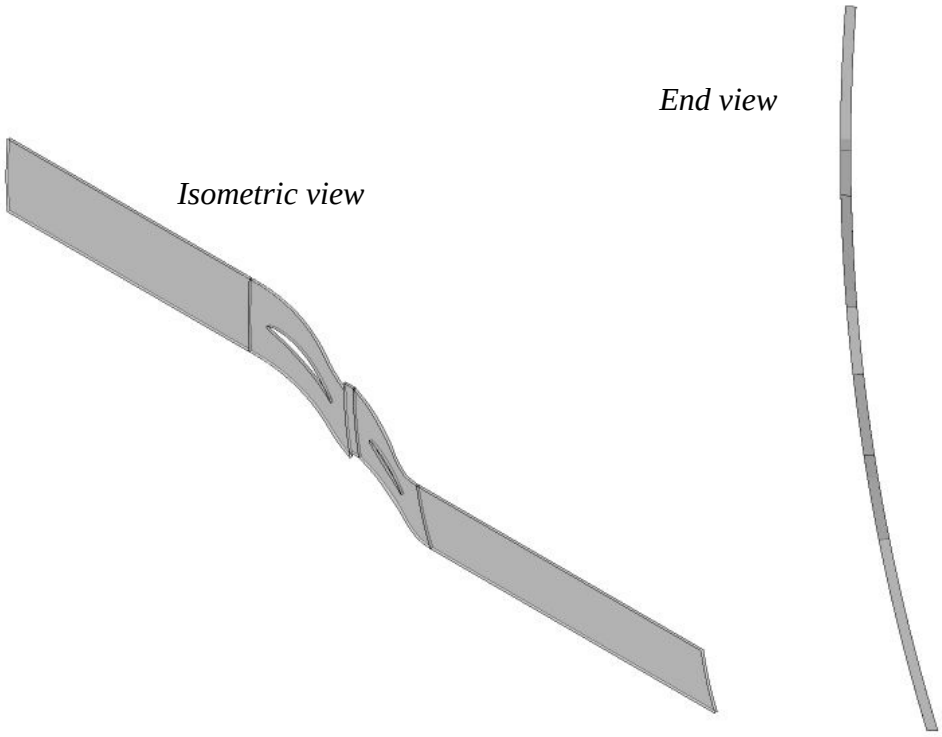

Figure 62: Turbogrid radial slice configuration

Modelling the geometry in this way is more realistic than the flat plane approach used in ICEM since the radial fluid velocity is simulated. In modelling a thin slice with free slip walls the improvement in accuracy is likely to be small but it is worth considering when comparing the two methods. It must also me noted that an extra stage is required in the geometry generation to modify the final coordinates to the correct format for Turbogrid, this is a small additional calculation but does add complexity to the procedure.

The guide vane configuration was split into two stationary domains, one for each vane, the first and second vane incorporated the inlet and outlet domain respectively. The length of the inlet and outlet domain was set to two chords length of the whole guide vane assembly. This allows for the same case file to be used as an IGV and an OGV by reversing the inlet and outlet boundary conditions.

While generating the initial mesh and constructing the script for the batch process, it could be seen that the speciality of the software helped to reduce the complexity of the procedure. Important parameters, such as number of stators, could be input as a value

and the software automatically adjusted the pitch of the stator row. This allows for reduced complexity in the scripting of the procedure.

Once meshing parameters had been set, Turbogrid was able to cope with variation in the geometry and successfully generated mesh files for the parameter extremes that were tested. The required scripting was also more compact that the equivalent script required for ICEM. An added benefit was the consistent programming language used for Turbogrid and CFX. Batch process scripts for these programmes also use the Perl programming language and the consistency reduces complexity during construction.

One difficulty that was encountered using Turbogrid was the discontinuity between domains. Since each vane of the GV assembly was generated separately, Turbogrid automatically generates the duct domain around each vane. The duct is positioned at the mid-pitch value for each stator row and since the pitch for each row is kept the same, this did not cause a problem. The problem was caused by the projected inlet and outlet domain for each vane. Since these domains were generated independently, they were not aligned when the domains were compiled in CFX Pre. In CFX Pre it is necessary to align the domain geometry for the solver, this is a simple task but in doing so, the relevant stator geometry becomes misaligned.

Two options were explored to overcome the geometry misalignment, the first was to have no projected inlet and outlet domains at the stator domain interfaces. This would mean that the domain follows the mid-pitch line for each vane, creating a continuous duct profile. The downside of this approach was that the whole domain is meshed as an extension of the O-Grid mapped around the vane profile. The mesh is extended from the profile using the defined expansion factor based on the y+ value at the profile wall. This reduces the control of the mesh density and of the distribution of nodes at the domain interface. It is necessary to be able to control the number of nodes at the domain interface for mesh continuity between domains.
The other option was to align the geometry in CFX Pre and then use the offset pitch command with the frozen rotor boundary setting to re-align the vanes. This allowed for the default inlet and outlet domains to be used for each vane. This reduced the need to interfere with the mesh generation process.

In the interest of minimising the complexity of the mesh generation procedure, the second method of re-aligning the vanes in CFX Pre using the ‘frozen rotor’ interface was used.

5.5.3 Mesh Generation Study Conclusion

The investigation into the mesh generation software to be used for the optimisation procedure thoroughly tested both ICEM and Turbogrid for suitability for the mesh generation procedure for the optimisation problem. Both software packages were assessed in terms of capability of re-producing accurate mesh files and the scripting complexity required. For the specific application of guide vanes for a turbine, Turbogrid proved to be the most suitable. The specialisation of the software to turbomachinery allows for accurate meshes to be reproduced across the full range of tested parameters using easily adapted script functions.

Using Turbogrid as the mesh generating software for the optimisation tool does limit the optimiser to turbomachinery optimisation problems. At this stage this is not a problem since that is all that is planned for the scope of the project. At a later date however, the optimisation tool could be adapted to problems outside turbomachinery, such as an OWC chamber design, in which case a different mesh generation package would be necessary and ICEM may well be suitable.

5.6 Optimisation Procedure

The optimisation tool has been used to perform a number of two variable, single objective optimisations as well as a three variable optimisation on the MEGV arrangement. These optimisation procedures have served two purposes, to obtain an optimum configuration of the MEGV geometry by freely varying multiple parameters simultaneously and also to test and develop the function of the optimisation tool. Both these objectives have been accomplished; an optimum geometry has been produced using a functioning optimisation tool. This section gives details of the optimisation procedure that has been undertaken.

5.6.1 Parameterisation

The datum geometry has been simulated with the variation of each parameter in turn, between the initial upper and lower limits. The parameter study has been performed in order to test the weighting of each of the parameters in terms of their individual effect on the overall pressure loss. This process has also been useful to test the limits of the automated meshing procedure and to ensure that a complete and accurate mesh can be produced across the full range of geometry variations.

Number of Stators

The analysis has been conducted by varying the number of stators for each case; this varies the pitch of the stator rows. The number of stators has been varied between 30 and 60 stators with the upper and lower limits displayed in *Table 11*. Pitch is defined as the spacing between stators at mean blade height and is varied by altering the number of stators in each vane row.

		Variable	**Parameter**			**Zweifel Number**	
	Case	**No. GVs**	**Pitch [m]**	**S1 s/b_1**	**S2 s/b_2**	**S1**	**S2**
Lower	1	30	0.120	1.20	1.70	1.19	0.85
Datum	8	44	0.082	0.82	1.16	0.81	0.58
Upper	16	60	0.060	0.60	0.85	0.59	0.43

Table 11: Pitch parameter limits

The initial datum geometry has been set using the optimum space-chord ratio, calculated using Zweifel's loading criterion, from the initial blade count of 44 stators per row see e.g. Dixon (2005) for a detailed explanation. A Zweifel number of

approximately 0.8 has been used as a useful starting point but it is expected that this is not the optimum value for this configuration. Horlock (1966) writes that Zweifel's optimum space chord ratio is only valid for outlet angles of 60º – 70 º, the S1 turning angle in this case is only 41 º. However, this value has been used as a starting point for the investigation. Varying the stator row pitch alters the Zweifel number as can be seen in *Table 11* above.

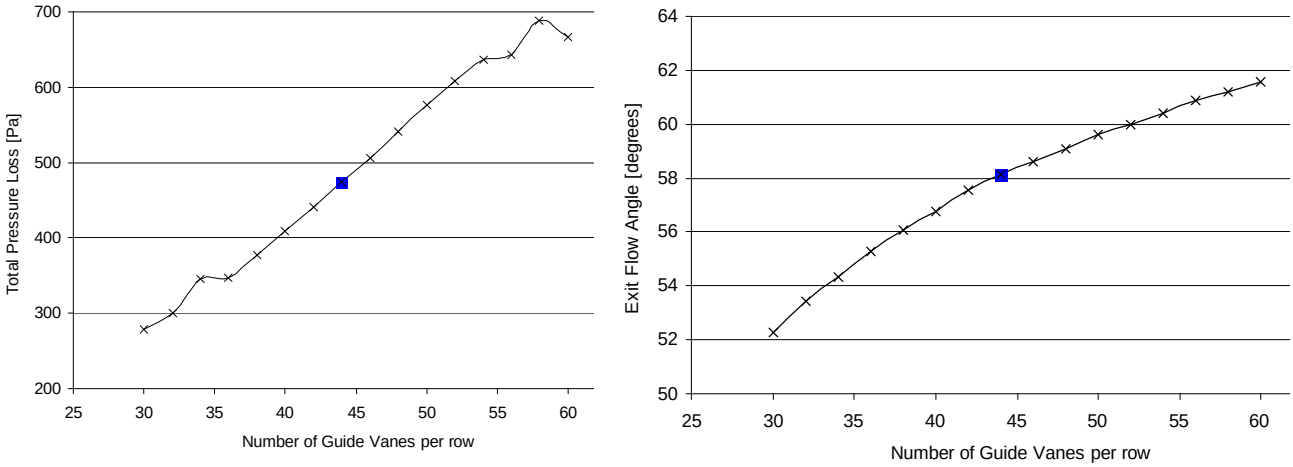

Figure 63: Plots of total pressure loss and IGV exit flow angle.

Results are shown in *Figure 63* above. Decreasing the number of guide vanes, increases pitch, resulting in lower total pressure loss as well as a reduced IGV exit flow angle. The results for the datum geometry are marked by the blue square.

Discussion

Results are as expected for variation of the pitch parameter; increased pitch reduces friction losses at the IGV but reduces guidance of the flow, reducing the turning angle that is achieved. At the OGV, the increased pitch presents a greater passage for reverse flow, reducing total pressure losses. Since the turning angle of the IGV is a necessary design constraint, the apparent improvement in performance is not valid. This study demonstrates the importance to maximise the pitch parameter within the design since large reductions in total pressure can be achieved.

Pitch Offset

The pitch offset of the stator rows is the relevant positioning between the first and second stator row. Pitch is kept constant with 44 stators in both the first and second stator row. Varying the pitch offset has the effect of rotating the second stator row, relative to the first. *Figure 64* shows the pitch offset parameter, *(a)* is the datum position, *(b)* shows the second stator row offset rotationally from the datum position.

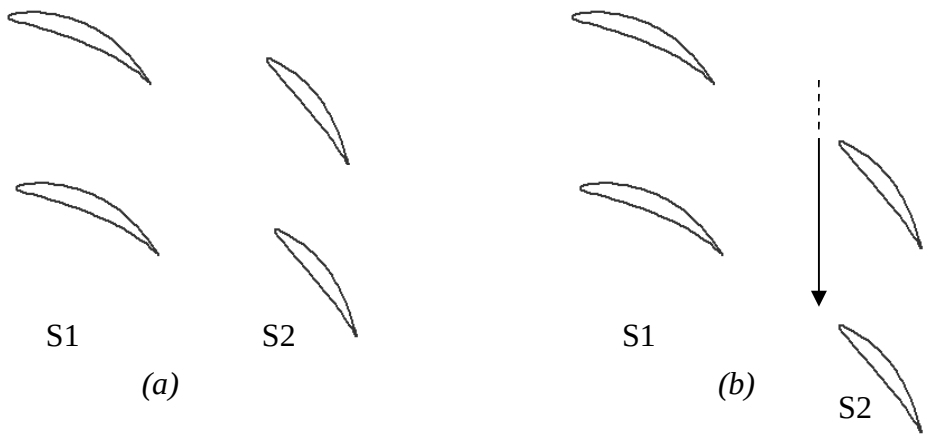

Figure 64: Pitch offset

The rotational offset between vane rows is calculated as a percentage of pitch, disassociating the parameter from the pitch variation. This adjustment is performed using the *pitch offset* function in CFX Pre at the setup of each case, using a frozen rotor boundary between the two stator domains.

Clocking the vane rows circumferentially, relative to each other varies the alignment of the free flow passage between pairs of vanes. Pitch offset has been varied across the full range of the cyclic parameter at 10% intervals and total pressure loss and turning results recorded below.

Results

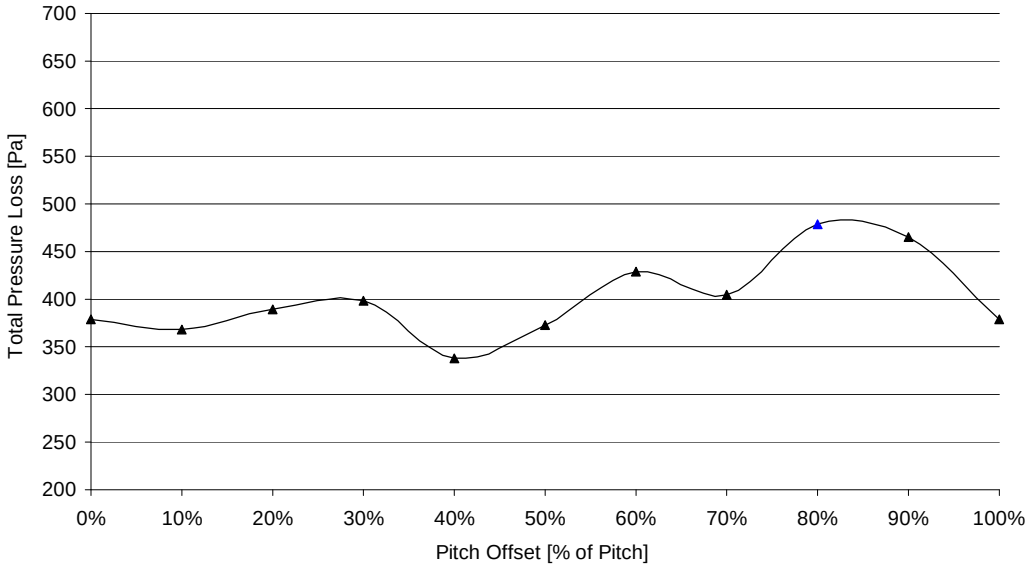

Figure 65: Plot of Pitch Offset against Total Pressure Loss
for Pitch Offset parameter study.

Total pressure loss across the IGV remained constant, as did the turning angle at the IGV. There is variation in the total pressure loss across the OGV resulting in the variation in combined total pressure loss between 338.45 Pa and 478.29 Pa displayed graphically in *Figure 65*.

Discussion

The cyclic nature of the pitch offset parameter can be seen in the results with 100% pitch variation returning to the same total pressure loss vales as 0% pitch. There is however variation across the full range of the parameter. Further analysis of the flow patterns shows the reason for this variation across the range and the interaction between the stator rows in the reverse direction.

The total pressure contour plot of the OGV of Case 5 below (*Figure 66*) shows the function of the stator design. At 40% pitch offset, the wake of the first element of the stator encloses the upstream element. The path of least resistance shown by the high pressure (red) contour passes through the row of upstream stators, missing the stator geometry and resulting in a reduced total pressure loss.

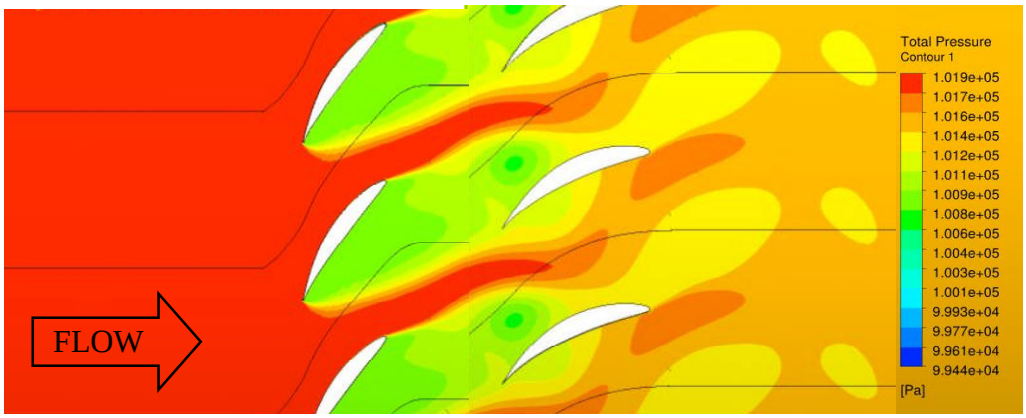

Figure 66: Pitch Offset - Case 5 - OGV Pressure Contour Plot

Comparing this case with Case 1 (*Figure 67*), the reason for the poor performance can be seen. The main flow path is obstructed by the downstream stator row and an area of high pressure builds up on the suction surface, showing the source of the losses in the flow.

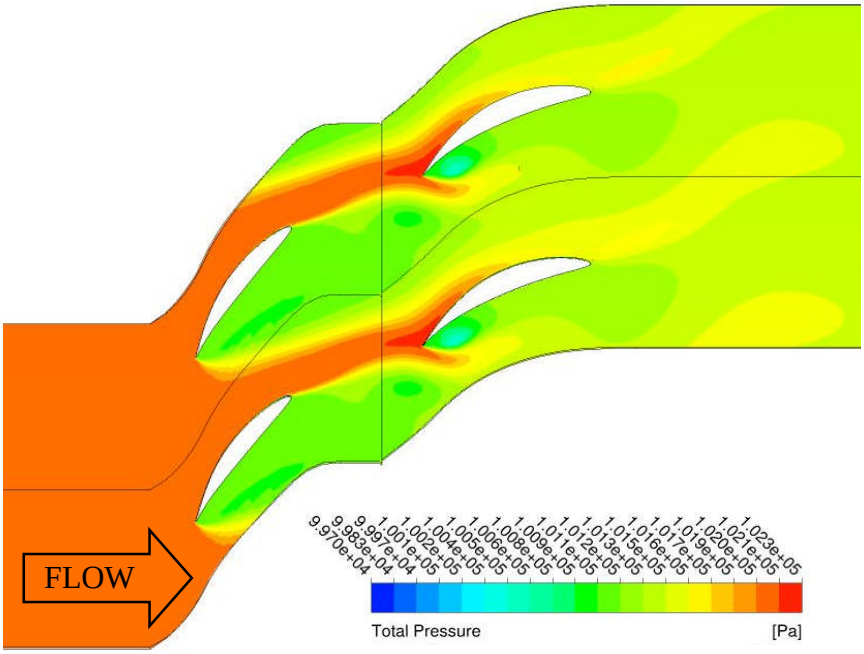

Figure 67: Pitch Offset - Case 1 - OGV Pressure Contour Plot

S1 turning parameter

The overall turning required of the IGV is a fixed objective however the amount of turning that is performed by each blade row is not. Variation of the S1 turning parameter controls the camber of the first stator row, changing the amount of turning that is done across the first row so that the flow exit angle changes. This in turn affects the turning of the second stator row, controlling the angle of incidence of the

stator row S2 as well as the camber so that the overall turning of the inlet guide vane is maintained. Varying the turning in this way, also changes the chord length of the S2 stator element since these are calculated using Zweifel's loading criterion.

Initially the axial chord is fixed and the Zweifel number is calculated using the inlet and outlet flow angles for each vane row at a given pitch. This theoretical Zweifel number is then used to calculate the actual axial chord length of the second vane row based on the remaining turning that is required of the second row. This results in a variation of the weighting of the turning across the vane rows and as the turning is distributed, the axial chord length of the second vane row changes. This ensures that the blade loading on the second vane row remains acceptable so that the overall turning can be achieved. Combining these geometry variations into one parameter maintains flexibility in the geometry while reducing the number of variables in the optimisation process.

Results

Varying the S1 turning parameter in isolation had little effect on total pressure loss with a variation of 4% across the full range. The combined turning was kept constant so there was also no variation in IGV exit flow angle. Towards the upper limit of the parameter range, when the most turning was being performed by the first stator row S1, reverse flow was unsteady and convergence was not achieved. It appeared this was due to the small axial chord length and high angle of attack of stator S2. This caused flow separation and oscillating flow downstream which then impinged on the downstream element, S1. The code was unable to predict this complicated, unsteady nature of the flow.

Discussion

The IGV exit flow angle is unvarying as expected since the combined turning is kept constant and the axial chord of S2 is set using the Zweifel criterion. This demonstrates that this is an effective way of calculating blade loading for this profile, despite the small turning angle of 44 degrees and less.

This parameter study highlighted the fact that the initial range is too large. The range of this parameter has been reduced with the upper limit being constrained to 62 degrees of turning. Within these new limits, steady state simulation gives accurate performance prediction and a sufficient range is maintained. Observation of the geometries being tested in the upper range of the parameter are not in alignment with

the original design rules and the reduction of the range makes the optimisation more robust without hindering the generation of potential optimum geometries.

When varied in isolation, the performance variation across the range of results is small. However, the axial chord length of S2 is important since at a higher angle of attack, this vane causes the most obstruction to the flow. Combined with other parameters, the variation of the vane geometry has the potential to produce further performance improvements.

Axial Spacing

Initial constraints state that the axial spacing should be at least one chord length of the first stator row. This constraint is maintained. Increasing the axial offset does not affect the performance of the IGV since the guide vane elements are acting independently, it does however effect the interaction of the reverse flow with S1.

In the reverse direction, S2 induces turning in the flow. The wake created by S2 then interacts with S1 and the combination of the flow angle and the axial length between stators effects how the wake interacts with S1. Like the pitch offset parameter, it is ideal for the wake to completely enclose S1 and this will only occur at a certain combination of these parameters.

The axial spacing between blade rows S1 and S2 has been increased from 1.1 to 2.6 S1 Chord lengths at equal intervals of 0.1. A total of 16 cases were simulated across this range. It was necessary to extend the length of the exit duct of S2 to ensure that there was sufficient length between the trailing edge of S2 and the exit boundary condition for accurate results to be achieved. The full range of the parameter is displayed in the results table below.

Results

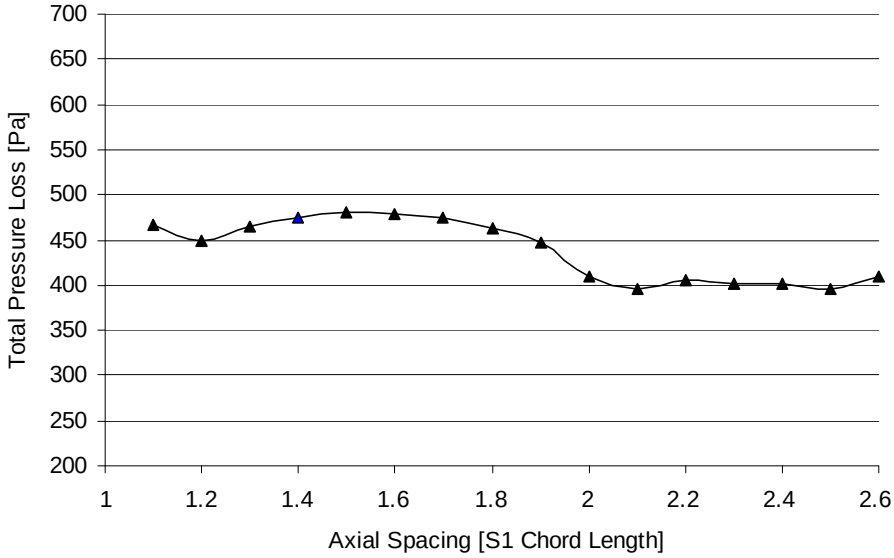

Figure 68: Plot of axial spacing parameter results.

The turning angle achieved by the IGV remains constant across the range of axial spacing investigated. The total pressure loss across the IGV also remains constant. The combined total pressure loss, displayed graphically in *Figure 68* shows that as axial spacing is increased, total pressure loss increases up to 1.5 chord lengths. After this point, the total pressure loss reduces until two chord lengths of spacing at which point the losses remain constant for the remainder of the range. The lowest total pressure loss occurs at this constant value of 395 Pa giving a 17% variation from the datum value shown in blue.

Discussion

The constant turning angle and total pressure loss occurring at the IGV confirms that in forward flow, the stator elements are acting independently. Increasing the axial spacing has no effect on the turning effect of the IGV or the total pressure loss across the IGV.

The variation in total pressure occurs across the OGV. Turning is induced in the reverse flow as it passes stator row S2. Examination of the CFD results used in the parameter study show that a turning angle of ~20degrees is induced in the flow and this angle remains constant as the fluid passes on to stator row S1. Since all other parameters are fixed, this flow angle effects the interaction of the wake of low pressure downstream of S2 with the stator row S1. This is demonstrated in the total pressure plot of Case 11 (*Figure 69*) below where the flow angle can be seen and the passage of flow passing between the stators of S1.

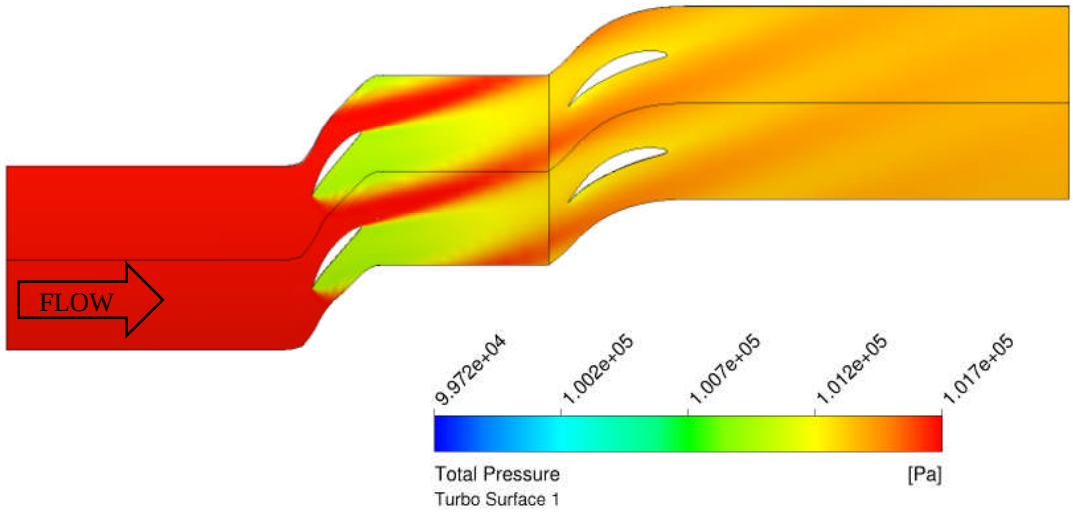

Figure 69: Axial Spacing - Case 11 - OGV Pressure Contour

This parameter investigation demonstrates the importance of the axial spacing parameter. Viewing the plot of the results above (*Figure 68*) it could be interpreted that increasing the axial offset above two chord lengths would give the optimum, reduced total pressure loss but investigation of the flow path demonstrates that this is not the case. It is the interaction of the wake with the downstream geometry which has the effect on total pressure loss and this is governed by the nominal reverse flow angle and the axial spacing. Increasing the axial offset has the same effect as clocking the stator rows circumferentially and there will be an optimum positioning of the two parameters that will ensure that the best reverse flow passage can be achieved.

Parameter study conclusions

The parameter study demonstrates the effective range of the chosen variable parameters and gives a quantitative value of the overall effect of these parameter variations on the performance of the geometry. The study also demonstrates that the scripting process of mesh generation and CFD simulation is capable and has been used to improve and refine this process. As a result of this, it can be confirmed that the scripted procedure and meshing functions are capable of meshing and simulating any geometry within the parameter range and that results achieved from these simulations are reliable.

5.7 Two-variable optimisation

The parameterisation study demonstrates the effect of varying each parameter individually but it can be seen that greater performance can be achieved by varying more than one parameter simultaneously. The optimisation process described in section 3 has been used to investigate the effect of varying pairs of parameters. The objective of each optimisation procedure is to minimise the total pressure loss across the guide vanes. Not all pairs of parameters have been performed; just the combinations that are expected to have the largest influence on performance. These are displayed in the following section.

Nominal Backflow Angle

Investigation of the Axial spacing parameter showed how the nominal backflow angle interacted with the upstream stator row of the OGV. Similarly, circumferential clocking of the stator rows changed the interaction of the reverse flow stream with the upstream stator row. Both parameters showed definite areas within the range where reverse flow passage was improved when varied independently. It was decided to vary the parameters simultaneously, keeping the same constraints. This will investigate if there is a relationship between the two variables for controlling the backflow through the OGV and if simultaneous variation will further reduce the total pressure losses.

Parameter	Min	Datum	Max
Axial Offset (Ax)	1.3	1.4	2.6
Pitch Offset (δ)	0%	90%	100%

Table 12: Variable parameter limits

The optimisation procedure was started with 21 initial sample points, distributed evenly within the design space by the Halton sequence. No additional points were required to build a Kriging model of sufficient accuracy. The resultant Kriging estimate is displayed as a 3D plot and contour plot in *Figure 70*.

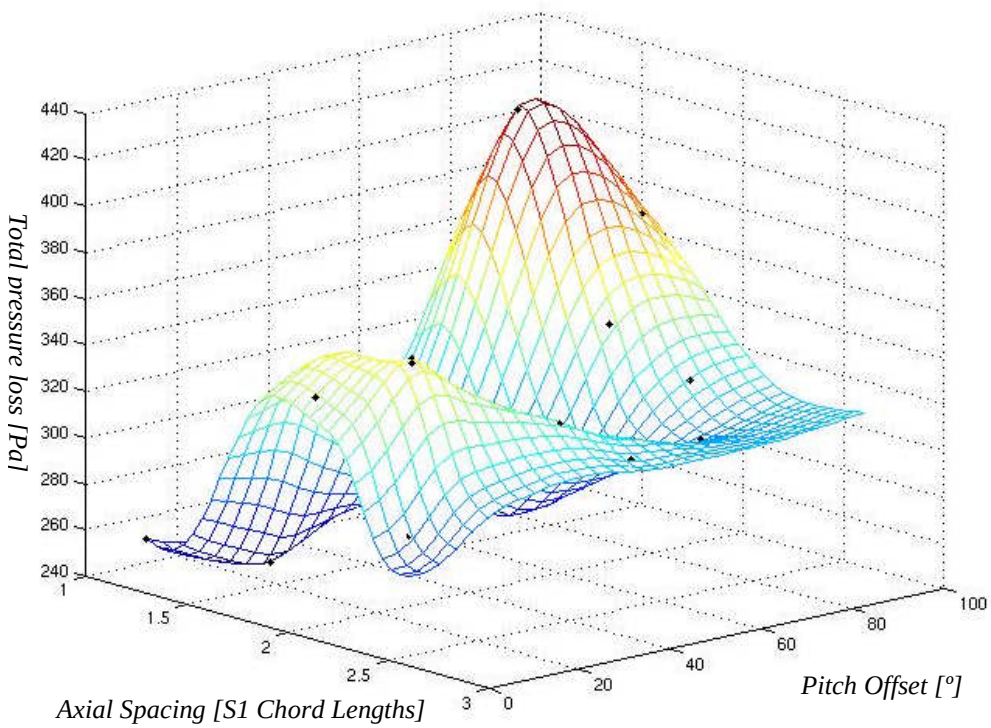

Figure 70: Kriging estimate response surface for nominal backflow optimisation.

The optimum combination occurred at an axial offset of 1.46 S1 chord lengths and a pitch offset of 17.74% giving a total pressure loss of 249.13 Pa. This gives a 26% and 37 % reduction in total pressure loss compared to varying the pitch offset and axial spacing parameters individually. The predicted minimum value occurs at the lower end of the range for both parameters and demonstrates that combined variation can greatly improve performance. This is a multi-variable problem.

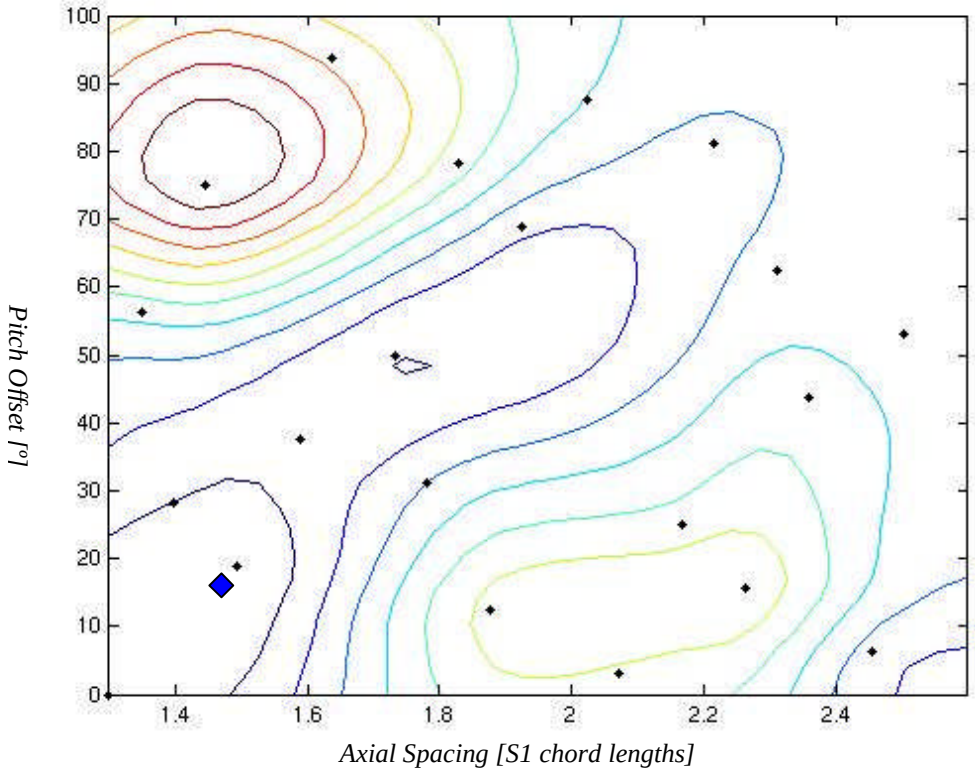

Figure 71: Total Pressure Loss contour plot of response surface.

Turning parameter optimisation

The S1 turning parameter controls the characteristic airfoil geometry of both stator rows S1 and S2. The result of this is that this parameter gives the potential to maximise the back flow area by ensuring that the wake produced by S2 of the OGV fully encloses the upstream stator row, S1. This coupled with the capability of ensuring the main reverse flow passage is clear gives potential for high performing geometry. The S1 turning parameter has been coupled with the pitch offset parameter to assess the importance of the interaction between these two parameters.

Parameter	Min	Datum	Max
S1 Turning (St)	44 º	56 º	62 º
Pitch Offset (δ)	0%	90%	100%

Table 13: Dependent Parameters

Again 21 initial sample points were used and no additional sample points were required for the optimisation. A contour plot of the predicted Kriging model is shown below in Figure 72 with the optimum point marked in blue. The optimum combination of these two parameters occurred at *St = 58.67 º, P= 43.75%* which corresponds to a

3.58 º pitch offset. This geometry combination produces a predicted total pressure loss of 225.38Pa. Again this is a large improvement over the individual parameter studies conducted above. It can be seen from the contour plot that another sample point shares the minimum total pressure loss contour of 240 Pa. This shows there is a large area of the design space where this low pressure loss can be achieved by different combinations of these parameters. This shows flexibility in the geometry and potential for greater pressure loss reduction with additional freedom from the use of more variable parameters.

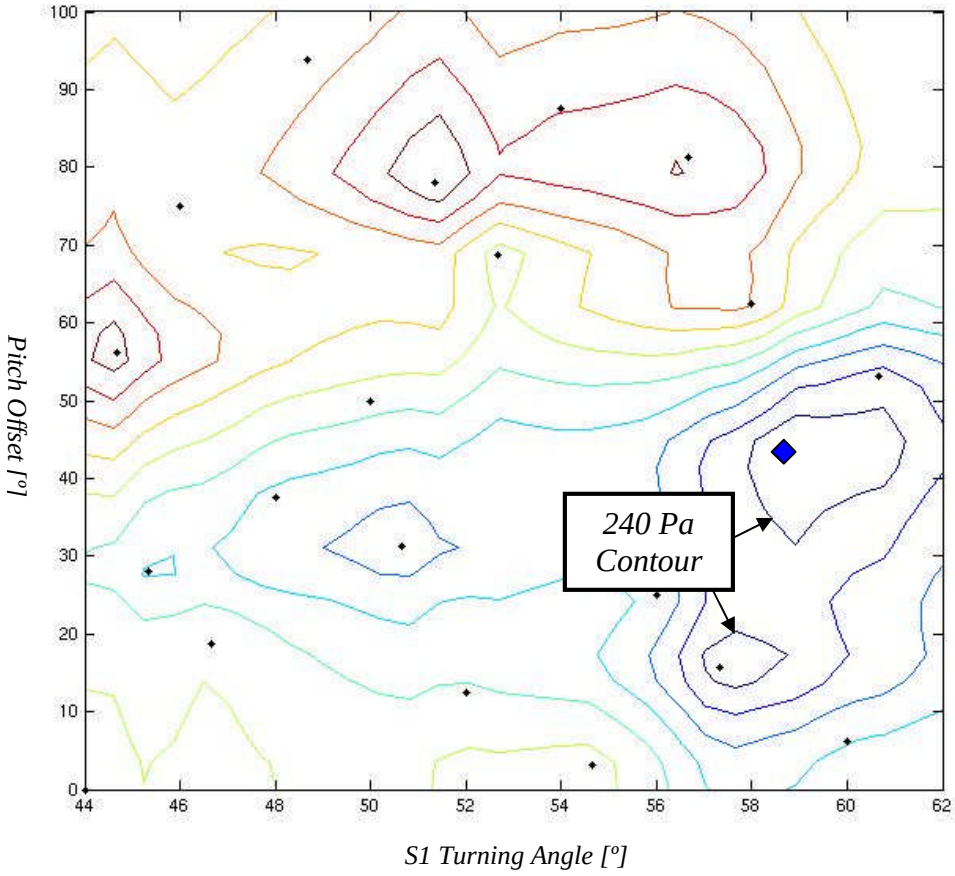

Figure 72: Total Pressure contour plot of turning parameter optimisation.

Pitch optimisation

Investigation of the pitch parameter in the early parameter study demonstrated large reductions in total pressure loss at the expense of the turning angle achieved by the IGV. This is down to the optimum space-chord ratio of blading with large deflection angles. The Zweifel criterion has been used to set the required axial chord for a given pitch and has been successful in achieving the desired turning angle of 58º over a range of stator weightings. In order to maintain this desired turning angle over a range of blade pitch values would require large variation in the geometry of the stator

elements which would in turn greatly increase the complexity of the optimisation procedure. A number of two-variable optimisation procedures have been performed using pitch as one of the variable parameters but since these have not been successful in achieving the desired IGV turning angle, they have not been included here.

The aim of this investigation is to prove the concept of MEGVs by direct comparison with the current single element guide vane and it has been decided that reducing the number of independent parameters by fixing the pitch parameter will aid this endeavour. This allows the geometry of the vane profile to be manipulated in a way that will benefit the reverse flow passage rather than attempting to achieve the correct blade loading for variable pitch which may prevent the best reverse flow geometry being achieved. In this way the blade loading for the given pitch is fixed but the amount of turning done by each vane row is controlled by the S1 turning parameter.

5.7.1 Global Optimisation

The results of the parameter study and two-variable optimisations show interesting results as well as performance improvements over the datum geometry. It is apparent however that the MEGV configuration is a multi-variable problem and it is necessary to combine these design variables to understand the full complexity of the design. This has been achieved by varying the parameters simultaneously using the same optimisation techniques. Three parameters have been varied within the constraints shown in *Table 14* with the objective of minimising the total pressure loss across the guide vane geometry.

Parameter	**Min**	**Datum**	**Max**
Axial Spacing (Ax)	1.3	1.4	2.6
Pitch Offset (δ)	0%	90%	100%
S1 Turning (β)	44 º	56 º	62 º

Table 14: Parameter Limits for Global Optimisation

An initial starting point of 30 sample points was used to generate a Kriging model of sufficient accuracy for the global design space. With the increased complexity of three independent parameters it was suspected that this number may not be adequate in which case, more points would be added during the optimisation process.

A further 13 points were added during the optimisation process before an MSE error of 13.95% of the Kriging model was reached. The GA performed 80 generations and predicted an optimum total pressure loss of 208.13 Pa based on the Kriging model estimate. A CFD simulation of the optimum geometry was carried out and output a total pressure loss of 201.3 Pa. Optimum parameter results are shown in *Table 15*.

Parameter	Datum	Optimum
Axial Spacing *(Ax)*	1.4	1.3
Pitch Offset *(δ)*	90%	35.3%
S1 Turning *(β)*	56 º	59.62 º
Total Pressure Loss	474.69 Pa	201.3 Pa

Table 15: Results of Global Optimisation

A wire frame of the optimum MEGV geometry coloured blue is shown in *Figure 73* compared with the datum geometry coloured orange. The diagram shows the final adjustments in the geometries as a result of the varied parameters, the increased turning angle in S1, reduced axial chord of S2 and the variation in circumferential clocking. Comparison in this way makes the variations look small but the 58% reduction in total pressure loss demonstrates the sensitivity of this arrangement to geometrical variation. The improvement also demonstrates that the parameters used did indeed have a large influence on the performance of the geometry and that varying these parameters simultaneously could have a large performance improvement over optimisation of two variables with constrained geometry.

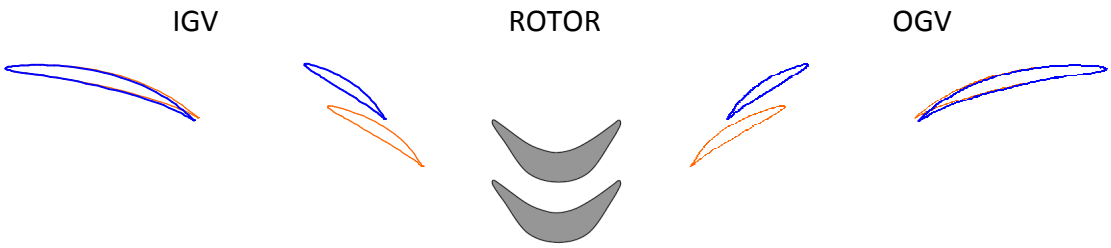

Figure 73: Comparison of datum geometry (Orange)
with Optimum Geometry (Blue)

Comparing the optimum geometry with the baseline ‘hockey stick’ geometry shows an improvement of 19.2% over the 2D CFD simulation. A 3D comparison is required to find the actual performance improvement for the test rig geometry.

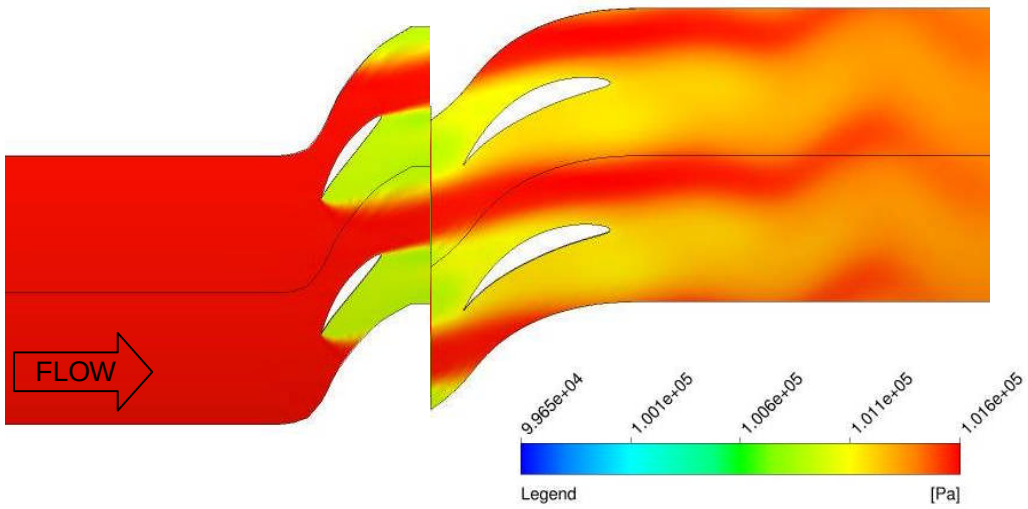

Figure 74: Total pressure plot of optimum OGV geometry

5.8 3D Comparison

The optimum guide vane geometry was used to generate a 3D case for comparison. The datum guide vane was directly replaced with the double stator rows of the optimum MEGV configuration, all other conditions of the simulation have been kept the same so that a direct comparison in performance can be made, parameters used for both cases are given in *Table 16*. As with the datum geometry, a mesh dependency study was conducted for the turbine with the MEGV geometry. The results show that the error between the medium and fine density meshes 0.1%, measured torque at the turbine did not change with mesh density indicating that this value is mesh independent at this level of accuracy. The medium mesh density was used for the 3D analysis, the results of the mesh dependency study are shown in *Table 17*.

3D CFD Parameters	**Value**	**Units**
Avg. Static Pressure at outlet	*0*	*Pa*
Number of Rotor Blades	*43*	-
Rotor Angular Velocity	*-850*	*rpm*
Working Fluid	*Air @25 º*	
Ref. Pressure	*1*	*atm*

Table 16: 3D CFD Parameters

	Nodes	P [Pa]	T [N m]
Coarse	822,758	1555.0	0.39
% Change		2.1	0
Medium	1,149,128	1538.7	0.39
% Change		0.1	0
Fine	3,517,583	1523.5	0.39

Table 17: Results of MEGV mesh dependency study.

The performance of the guide vanes has been compared in two ways, firstly by measuring total pressure upstream and downstream of the guide vanes to work out the pressure loss across the guide vane geometry. Secondly, the total – static efficiency of the turbine has been calculated for each guide vane configuration.

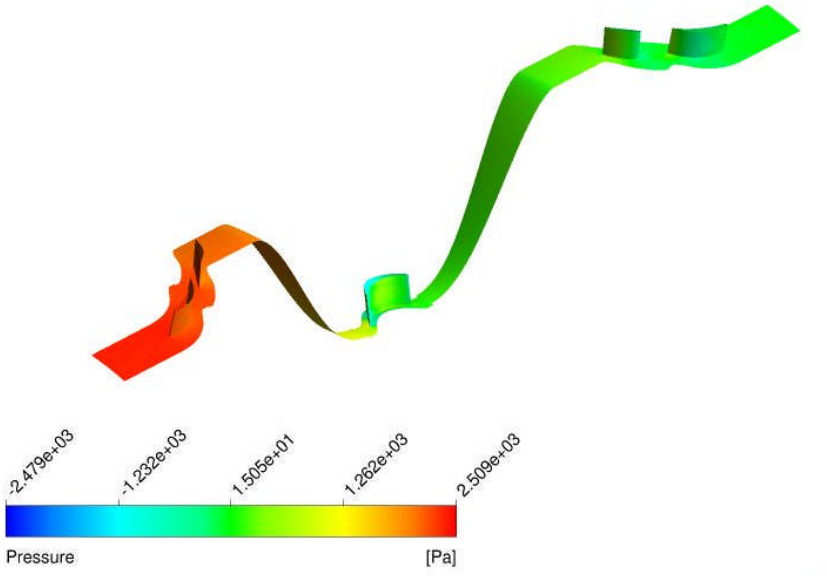

Figure 75: MEGV geometry simulated in 3D, coloured by Total Pressure.

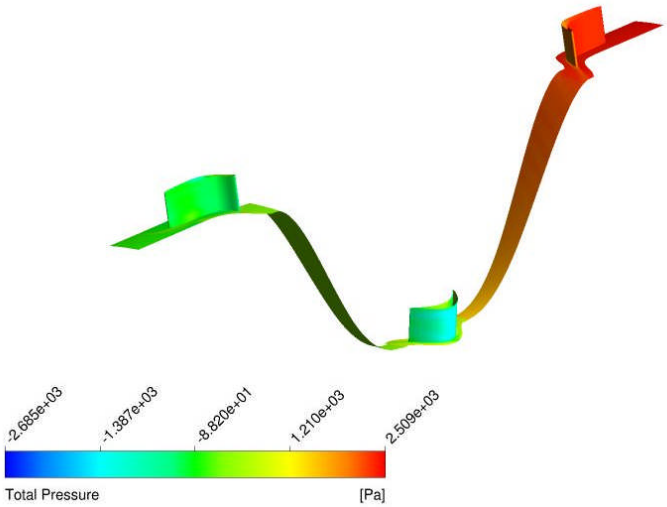

Figure 76: Test rig geometry simulated in 3D, coloured by Total Pressure.

Results

Results of total pressure loss across the guide vanes is shown in *Table 18* and although there is a performance improvement between the test rig geometry and the MEGV configuration, the improvement is small compared with the 2D comparison.
A plot of static pressure through the turbine geometry is displayed in *Figure 75* with a plot of the datum geometry presented in *Figure 76* for comparison. These plots demonstrate the layout of the components in full turbine.

Parameter	IGV	OGV	Total	% of Total
Test rig-geometry	38.1 Pa	277.8 Pa	315.9	13.0%
Optimum MEGV	35.8 Pa	161.4 Pa	197.2	8.4%

Table 18: Total pressure loss across the guide vane at 2500 TP inlet.

The full turbine efficiency characteristic is shown in *Figure 77* compared with the datum turbine. The results show an overall improvement however, this is by a smaller amount than the 2D simulations suggested. The MEGV geometry has a peak efficiency of 62.8% whereas the optimum MEGV geometry has a peak efficiency of 64.5%, a predicted improvement of 1.7%. MEGV peak performance occurs at a higher flow coefficient of 1.3 as opposed to the datum geometry peak of 1.1.

CFD simulation of the optimum geometry demonstrates that the 3D flow pattern is behaving differently to the ideal 2D simulation of a slice at mid span. The complex flows occurring in the variable radius duct mean that the flow is not uniform as it approaches the OGV and for this reasons, the parameters from the 2D simulation do not translate directly to the 3D geometry.

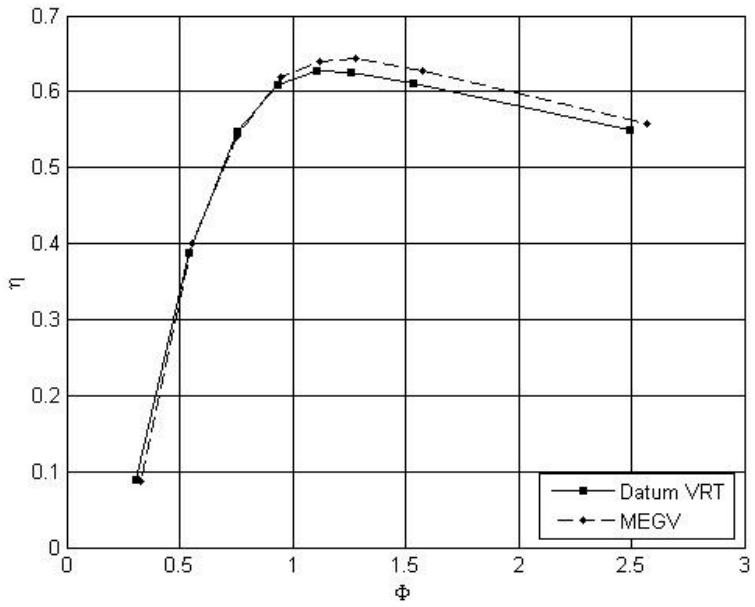

Figure 77: MEGV turbine characteristic comparison with datum VRT

5.9 Conclusions, discussion and limitations

A novel method of reducing the losses occurring at the OGV of a bi-directional turbine, using MEGVs has been investigated. This has resulted in a set of design constraints. These design constraints have been used to produce a datum geometry that can be controlled by the variation of design parameters. A full parameterisation study has been conducted to investigate the effect these design parameters have on the performance of the guide vane geometry and based on these results, a number of optimisation procedures have been conducted.

The optimisation code has been adapted for the optimisation of the MEGV problem and the results of the investigation prove the functionality of the optimisation tool. An overall improvement of 58% was achieved from the initial datum geometry to the optimum configuration. This proves that the tool works and that the parameters that were chosen had sufficient influence on the performance of the geometry.

The use of the optimisation tool has allowed a wide design space to be explored and an optimum configuration to be identified within the design space. The tool reduces the required user input for this procedure and allows the problem to be systematically tackled, ending with an optimum result. This is an efficient way of tackling multi-variable problems such as the MEGV concept.

The aim of the investigation was to prove the concept of the MEGV and demonstrate performance improvement over the test rig geometry. In ideal 2D simulations, the concept was shown to have improved performance over the hockey stick guide vane, showing an improvement of 19.2% in terms of total pressure loss.

The optimum guide vane geometry has been modelled in 3D CFD, directly replacing the datum guide vane with the MEGVs. The optimum parameters determined from the optimisation procedure in 2D do not correspond to the 3D performance of the geometry and although an improvement in total to static turbine efficiency has been achieved it is small.

Further investigation is required into the performance in 3D. It may be necessary to perform a three variable optimisation in 3D, using total-to-static efficiency as the global objective. It is likely that the correct parameters for 3D performance could then be found with the potential to improve the performance of the HydroAir device.

Limitations

Conducting 3D simulations using the optimum 2D geometry demonstrated the limitations of the method of representing the geometry in 2D during the optimisation. The optimum geometry generated using the 2D CFD as a method of performance prediction did not meet the requirements of the 3D turbine.

There are a number of reasons why this could be. This could demonstrate that the flow within the turbine is three dimensional and cannot be accurately represented as a slice at mid span. Further investigation of the 3D results show that the velocity flow angle at rotor inlet was lower than expected. This shows that the guide vane geometry is behaving differently when simulated in 3D. This reduced turning angle would have a negative effect on the performance of the turbine.

Another reason for the misalignment between the 2D and 3D simulations could also have been that the 2D domain was not a true representation of the 3D case in terms of the boundary conditions and settings used. This could have been improved by regularly cross-validating the 2D representation with a 3D case during the investigation.

Due to a tight project timescale, there was insufficient time to re-run the MEGV optimisation process once the 3D comparison had been conducted. The experience gained from the design process was carried forwards to the next section of the project, primarily ensuring accurate representation of the geometry in 2D throughout the design process.

The MEGV concept is recommended for further investigation as the potential of this method has been identified and with the experience gained in this research, it is anticipated that greater performance improvements can be achieved.

An international patent application for a new configuration of bi-directional impulse turbine was submitted by D-R in 2012 with the author as a named inventor. The new configuration incorporates the MEGV concept and sets out the design constraints presented here in this thesis.

6 Bi-directional stator profile optimisation

6.1 Introduction

The guide vane profile in a bi-directional impulse turbine is designed primarily as an IGV, with the main purpose of the component being to meet the rotor inlet turning requirements. The mitigation of the losses across the stator profile in reverse flow are currently an afterthought in the design process. Measures such as increased trailing edge radius and reduced turning angles have been applied to conventional stator profiles to try and reduce the total pressure losses but the main focus has always been on the function of the IGV in the profile design.

A method of stator design is suggested which takes into account both the forwards and reverse flow requirements of the profile. The aim being to produce a stator that performs well as an IGV, producing the required turning angle while at the same time, reducing the reverse flow losses through novel stator profile design.

The requirement of the stator to function in bi-directional flows is unique and requires an unconventional profile design. Optimisation methods are implemented, using a locally free profile generation tool in reversing flow. The profile is optimised for flow in both directions with the objective of meeting the required inlet turning angle as well as reducing pressure losses across the profile in reverse flow.

6.2 Datum geometry

The test rig turbine Ct14b is used for the investigation, in order to give direct comparison with the MEGV research detailed in the previous section. It was decided however not to use the CT14b stator geometry for the optimisation since this unusual stator has been designed specifically for the prescribed application and does not give opportunity for modification. A more conventional ‘curved plate’ type stator profile is used allowing greater possibilities for optimisation of the profile shape.

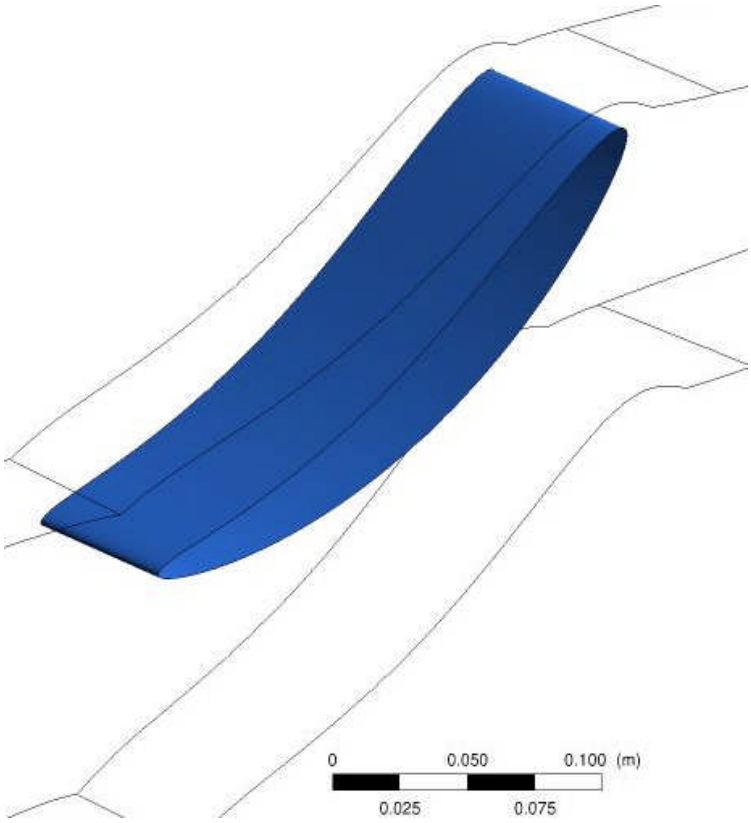

Figure 78: VRT2 datum guide vane profile

The initial stator profile used is based on the current VRT2 stator *Figure 78* but with an increased turning angle. The decision to use the CT14b test rig turbine geometry for the optimisation means that the IGV turning requirement of 67.2° of turning must be met.

The VRT2 stator has a low turning angle of 35° with constant turning along the full length of the stator. The leading edge of the stator has a rounded section profile perpendicular to inlet flow at the design condition. In modifying the stator profile the leading edge section was kept similar while the trailing edge section was pivoted

around a point located at 40% chord to achieve the increased turning angle. The two sections were then joined using two cubic splines, one for the pressure surface and one for the suction surface.

This resulted in a stator with a high degree of turning, and matching TE and LE profiles to the VRT2 stator. The turning produced by the profile of the suction surface is low on the forwards section of the stator and increases around 30% chord where the majority of the turning occurs. Maintaining the trailing edge section of the VRT2 stator profile means that the profile is not straight backed and the suction surface has 20° of uncovered turning from the throat to the trailing edge. This is high, Saravanamutto et al. (2009) state that modern steam turbine blades usually have as much as 12° of "uncovered" or "unguided" turning.

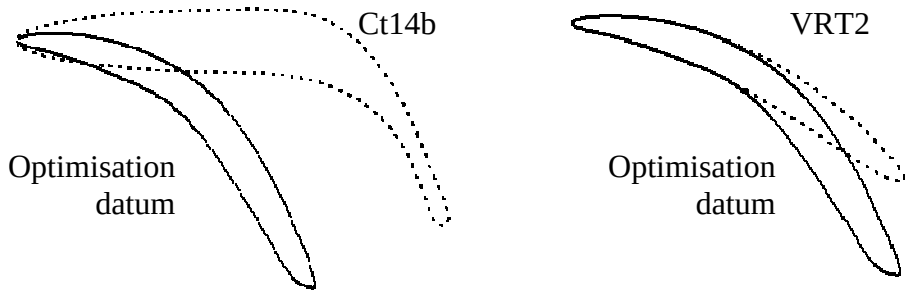

Figure 79: Stator profile comparison

It is necessary that the modified profile meets the requirement of the IGV, turning the flow to provide the correct inlet angle at the rotor. It is expected that the stator will perform poorly as an OGV but the initial profile provides a starting point for the profile optimisation with the potential for improved overall performance.

Parameter	Ct14b	VRT2	NGV	Units
Guide vane count	59	60	50	
Turning angle	1.17	0.611	1.17	rad
	67.2	35.00	67.2	deg
Chord	0.117	0.0843	0.0902	m
Stacking axis	Leading edge	Leading edge	Leading edge	
Space / chord ratio	0.45	0.62	0.67	

Table 19: Defining Guide vane parameters

Figure 79 shows the modified stator profile used as a base for the optimisation, for comparison, it is shown next to the CT14b and VRT2 stator profiles, demonstrating the modification and the final turning requirement. *Table 19* gives design parameter values for the three profiles for direct comparison.

6.2.1 Fluid Deviation

Fluid deviation is the variation between the actual fluid angle at the exit to the stator row and the metal angle at the trailing edge. At inlet, the deviation between these two values is easy to control and it is set by the designer. At outlet however, the deviation is a function of blade camber, blade shape, space-chord ratio and stagger angle (Dixon, 2005). The effect is that the deflection of the fluid is reduced and in this instance would result in a reduced turning angle at the rotor inlet, reducing power transfer to the rotor. When modifying the datum profile using the method described above, it was insufficient to match the trailing edge metal angle with the Ct14b design as the deviation may be of considerable size due to the relationship with other profile parameters. It was necessary to achieve an estimate of the fluid deviation when designing the datum stator for optimisation to ensure that the desired fluid angle at the rotor inlet could be achieved.

Howell (1945a) relates deviation to the camber and space/chord ratio using the empirical rule below:

$$\delta^* = m\theta(s/l)^n, \qquad \textit{(Eq. 6.1)}$$

Where δ^* is nominal deflection in degrees and m = constant = 0.19 for accelerating flow. θ is the camber of the guide vane measured as $\theta=\alpha_1 - \alpha_2$ and s/l is the space chord ratio. n, in this case is taken as 0.5 for inlet guide vanes.

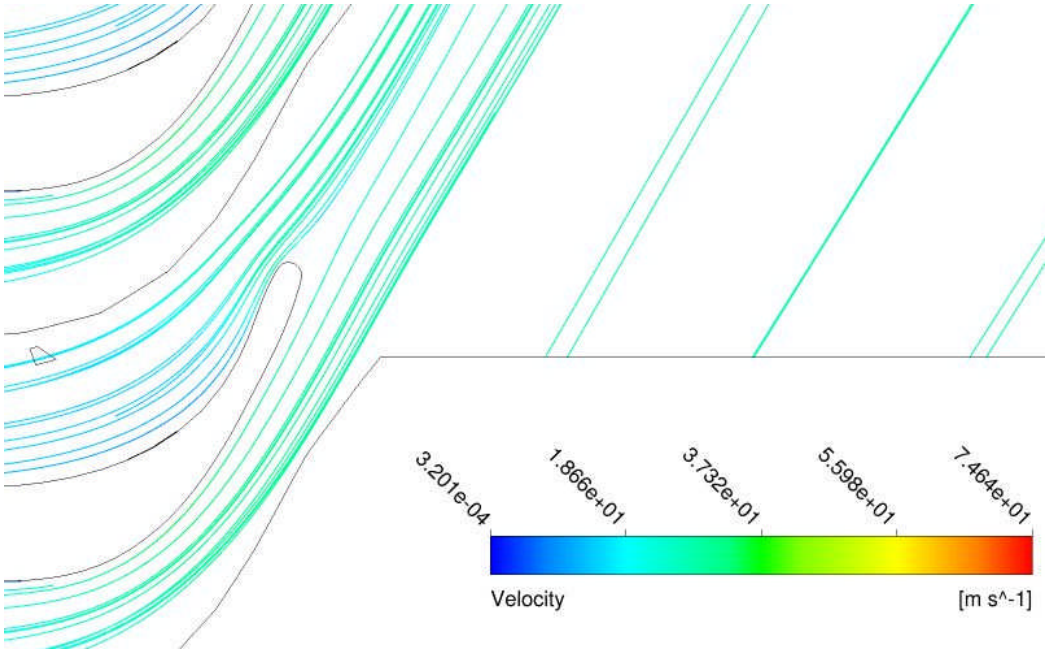

Figure 80: Streamlines coloured by velocity showing fluid deviation at trailing edge of Ct14b geometry.

Using the above rule, an estimate for fluid deviation for the Ct14b geometry was calculated as 8.6º. Since CFD simulations of the Ct14b geometry had been produced, it was possible to compare this estimate with the predicted fluid deviation from the simulations. *Figure 80* shows a plot of stream lines, coloured by velocity, at the trailing edge of the Ct14b stator geometry. This is a full 3D case run at the design condition with a flow coefficient of 1. The deviation between the stator metal angle and fluid stream can clearly be seen and has been measure as 7.2 º giving a fluid flow angle of 60 º at the exit to the stator row. This demonstrates that the deviation is in fact considerable but due to the unusual profile of the Ct14b stator it is not surprising that there is slight variation between the CFD prediction and the estimate using Howells rule.

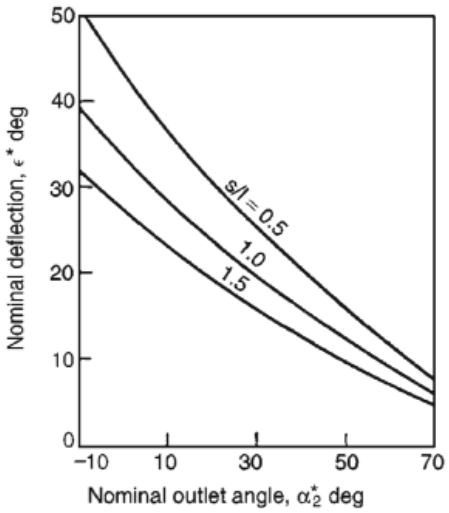

Figure 81: Nominal deflection with nominal outlet angle
for a range of space-chord ratios. (Dixon, 2005, adapted from Howell 1945a and 1945a)

The plot in *Figure 81* shows the relationship between nominal deflection and nominal outlet angle for three values of space chord ratio, adapted from Howell's work by Dixon (2005). The estimate calculated above corresponds to the above relationship for the high nominal outlet angle and low space chord ratio.

Estimated fluid deviation was then calculated for the NGV profile giving a result of 10.5º, higher than for the Ct14b profile. This indicated that it would be necessary to increase the metal angle of the NGV stator greater than the 67.2º to account for the increased deviation. An additional 1.9º was added to the turning of the NGV profile by pivoting the trailing edge section as described above giving a final metal angle of 69.1º. A 3D CFD simulation was then run to measure the turning angle achieved by the IGV.

A plot of streamlines coloured by velocity is shown in *Figure 82* and the deviation between the fluid and the stator trailing edge can clearly be seen. This was measured as 8.5º, giving a flow angle of 60.6º at exit to the stator row. At this stage this variation between fluid flow angle of 0.6º was deemed acceptable for the datum profile for the optimisation. Due to the variable nature of the flow through the turbine, it is expected that this stator row exit angle and hence rotor inlet angle will vary and the turbine must be able to tolerate variations across the operating range. It is also expected that modifications made to the guide vane profile will have an effect on the exit flow angle and although this will be constrained as much as possible, variations are inevitable. For these reasons, 0.6º was deemed acceptable.

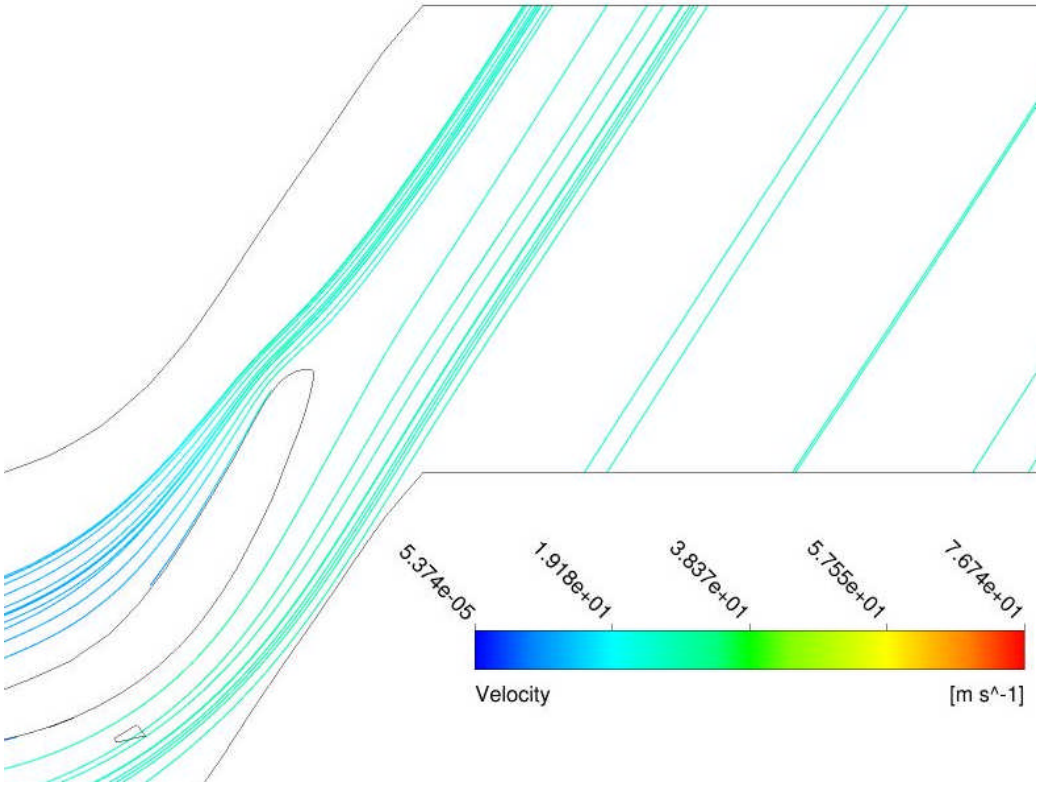

Figure 82: Streamlines coloured by velocity
showing fluid deviation at trailing edge of NGV geometry.

For further clarity, a plot of flow angle along the full length of the inlet duct was produced for both geometries and is presented below *(Figure 83)*. The plot shows the flow entering the duct domain at 90º (horizontal), passing the IGV row where turning is induced and then flowing through the duct to the rotor inlet.

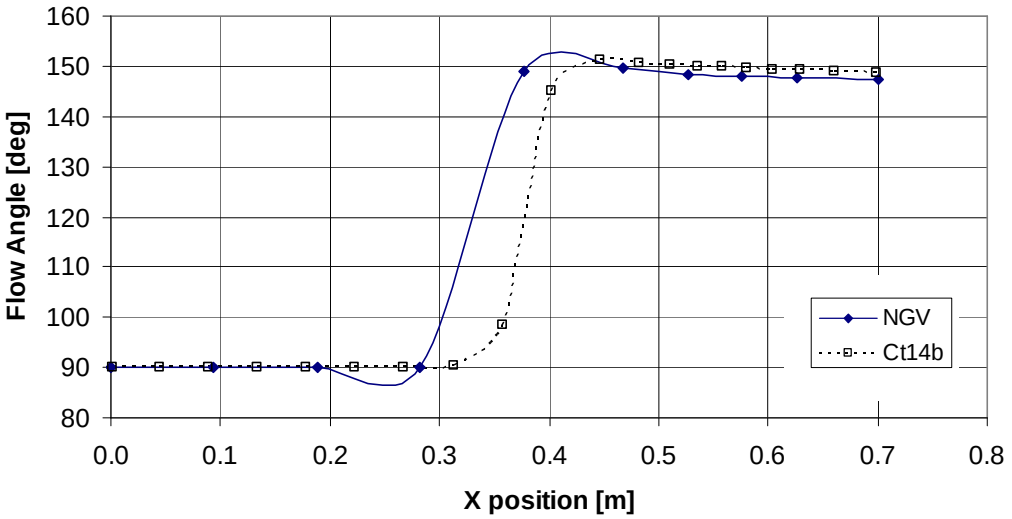

Figure 83: Plot of flow angle along inlet duct
for NGV and Ct14b stator geometries.

It can be seen that there is a variation in the amount of turning that each guide vane produces. At rotor inlet, the Ct14b stator produces 148.79° of turning whereas the NGV profile produces 147.26° a variation of 1.53°. This variation is greater than the 0.6º variation measured at the exit to the stator rows. The plot also shows the slight reduction in turning angle through the inlet duct as the radius of the duct profile reduces, this can be seen between the X positions of 0.45m and 0.7m.

Overall, this reduction in turning angle produced by the NGV profile will have a negative effect on the turbine but due to the nature of the variable operational requirements of the turbine discussed above, it was decided that this variation was acceptable. The aim of this investigation is to test the hypothesis that profile optimisation in bi-directional flows can produce a superior profile to one that has been designed solely for uni-directional operation. The NGV profile has been used as a base for the optimisation procedure from this point forward and all performance measurements will use this turbine configuration as a datum.

6.2.2 Mixing Losses

Guide vanes are designed to change the direction of the flow to ensure the correct angle of incidence at the turbine blade to produce maximum power transfer to the rotor. As the flow passes over the guide vanes, it accelerates as it changes direction

and this results in pressure losses in the flow. Well-designed guide vanes minimise these pressure losses. The overall stator aerodynamic losses are made up of components profile loss, mixing losses, secondary losses and annulus losses.

Profile loss is the result of skin friction or separation losses at the surface of the profile. The boundary layer is the layer of stationary or slow moving flow on the surface of the profile. When the adverse pressure gradient at the profile surface becomes too steep, the boundary layer grows causing separation resulting in increased frictional losses on the flow stream.

Mixing losses are caused at the trailing edge of the stator by rapid dissipation of the wake. The wake interacts with the free stream until the flow is completely mixed out at some point downstream. This is evident by a uniform velocity profile in the duct.

Secondary losses result from non-uniformity of flow across the span of the stator. The interaction between blade ends and annulus walls have an effect on these losses.

Annulus loss is the result of skin friction and resulting boundary layer at the hub and shroud of the stator row.

The procedure of profile optimisation aims to minimise these aerodynamic losses by modifying the stator profile for improved performance in bi-directional flow. For this reason, it is the profile loss and mixing loss components of the total loss that will be reduced. All other components of the turbine will not be changed, including span and duct dimensions so it is expected that secondary loss and annulus loss will not be largely affected by the variation in stator profile. It is important to understand the loss components associated with the stator to ensure that the CFD modelling and performance measures are correct for the desired performance improvements.

6.2.3 Datum profile performance

Full 3D CFD simulations were run, replacing the Ct14b stator geometry with the new stator profile. Axial guide vane positioning, duct and rotor geometry and mesh density were maintained for direct comparison with the datum turbine. The stator count was adjusted, altering pitch to a point where the space/chord ratio was close to that of the VRT2 geometry. This resulted in a count of 50 stators. A full turbine characteristic was simulated and a direct comparison is presented below in *Figure 84*.

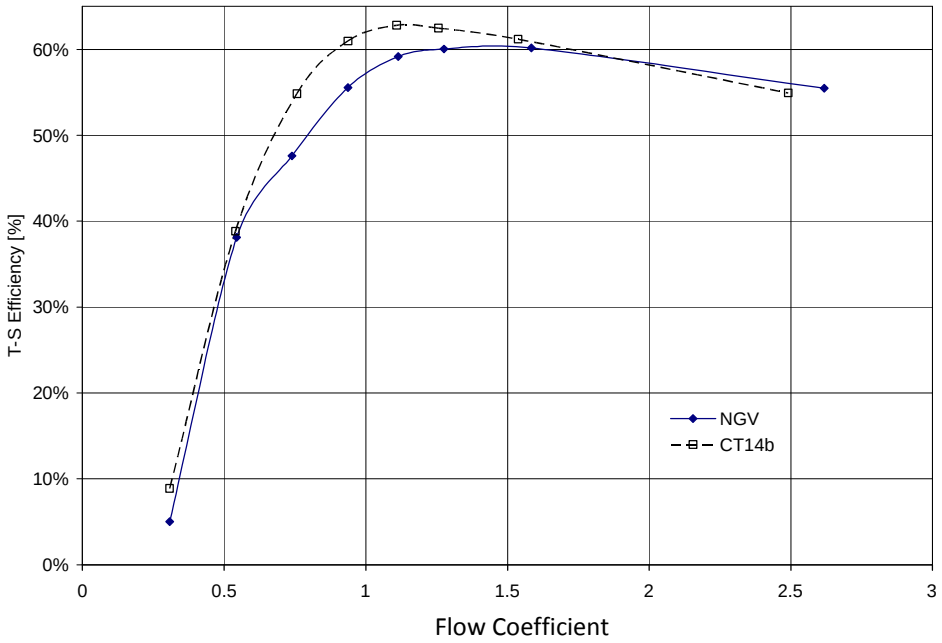

Figure 84: Comparison of efficiency
for new guide vane profile and datum CT14 geometry.

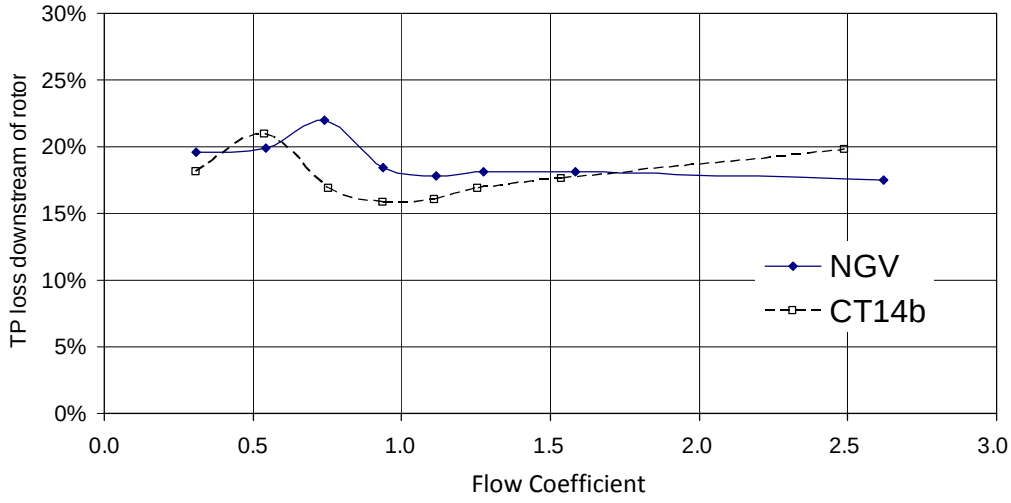

Figure 85: Comparison of total pressure loss
downstream of the rotor due to OGV.

Comparing the characteristics of the turbines with the two different stator geometries shows that the new guide vane profile has a negative effect on the turbine. Efficiency is reduced by 3.5% across the main operating range. Since the only difference between the two sets of data is the guide vane geometry, this variation in performance must be down to the guide vane profile. It is known that the IGV produces a slightly reduced turning angle which will result in reduced power transfer to the rotor. It is

also predicted that the NGV profile will show reduced performance as an OGV when compared to the Ct14b profile.

The performance of the OGV stator profiles was observed, analysing the performance of each stator profile in reverse flow. *Figure 85* presents a plot of the total pressure losses downstream of the rotor. This has been calculated by measuring the difference in total pressure between the outlet of the rotating domain and the exit of the outlet duct. This data is displayed as a percentage of the total pressure loss across the whole turbine, equivalent to the percentage of energy loss in the fluid. Measuring the data in this way includes the losses associated with the outlet duct, but since the duct geometry has remained unchanged, the difference between the two is a result of the difference in the OGV profile.

The results show similarity between the two profiles with distinct peaks in total pressure losses occurring. However, these peaks occur at different flow conditions with losses for the Ct14b stator profile occurring at a flow coefficient of 0.54 and the NGV losses peaking at 0.74. Generally the total pressure losses across the NGV profile are greater than that for the Ct14b profile and a direct comparison between *Figure 84* and *Figure 85* demonstrates that the reduction in turbine performance is a result of the total pressure losses associated with the OGV since the variations seen on both plots correspond to the same flow conditions.

Contour plots of total pressure are presented below in *Figure 86* for a qualitative comparison of the reverse flow over the guide vane profiles. The plots show two stators from the outlet stator row plotted with identical total pressure range of -250 Pa to 450 Pa. Both cases have been simulated with identical boundary conditions, this run shows a flow coefficient of 1.11 and corresponds to the turbine characteristic plots discussed above in this section.

The first thing that is apparent is the difference in the size of the wake produced by each profile, the area of low pressure, shown in blue, downstream of the stator profiles. The constant arc suction surface of the NGV profile, required to produce the high turning requirement of the IGV, results in a large amount of uncovered turning. This uncovered turning section of the profile creates a large obstruction to the incoming flow, increases the solidity of the stator row. Despite a lower vane count and resulting increase in pitch, the area of the flow stream and size of the nozzle produced between stators is very similar for the two profiles. If the area of the stream passing between stators is the same but the number of stators is reduced then this results in an overall reduced area for the flow to pass through.

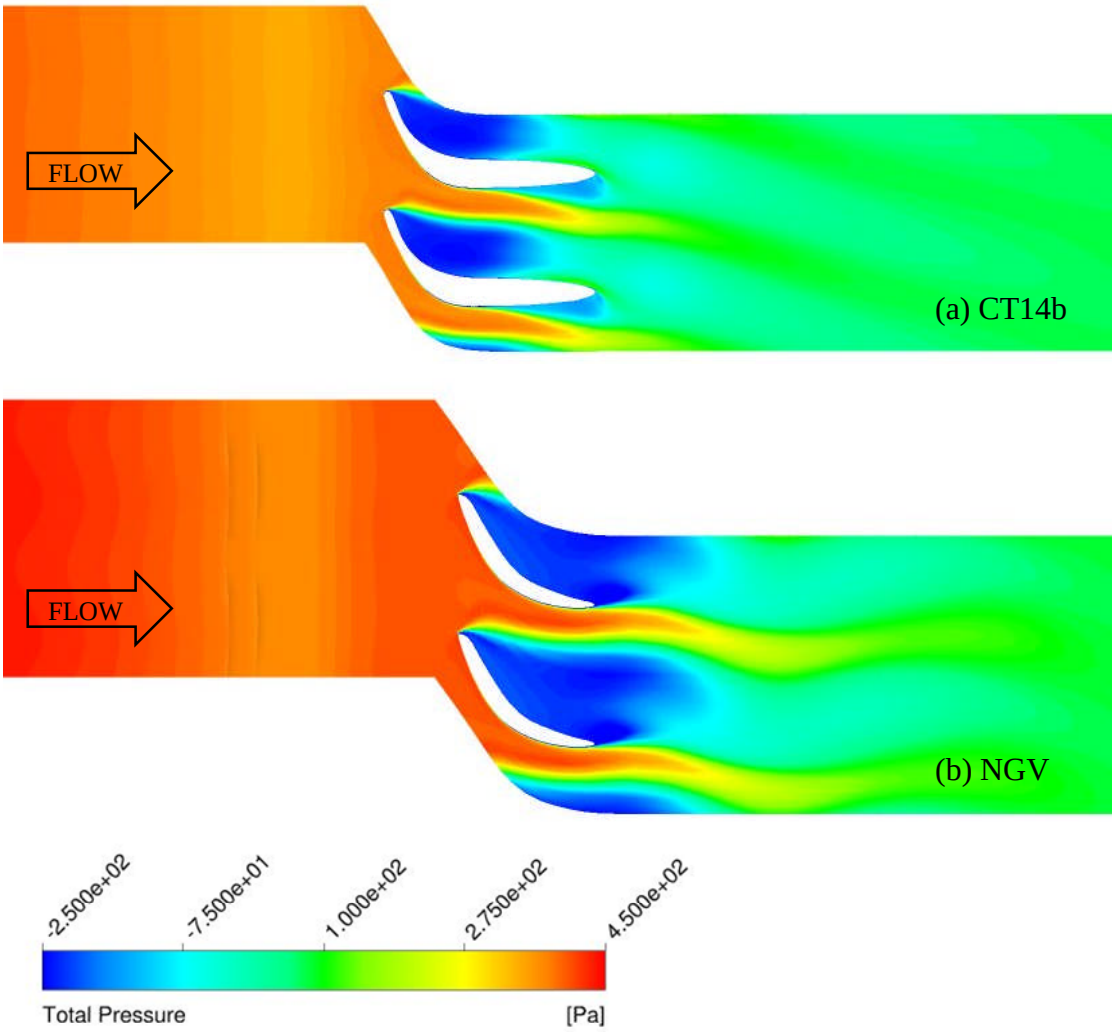

Figure 86: Total pressure contour plot of flow around OGV for CT14b and NGV geometry at $\Phi = 1.11$.

Downstream of the NGV profile, it can be seen that the stream of air is demonstrating oscillating motion suggesting unsteady characteristics in the flow. A transient simulation was conducted at the design condition, inlet total pressure of 2500Pa and this indicated that the flow downstream of the OGV was indeed mildly unsteady. However, in this instance, when simulating the whole turbine, global integrated values such as total pressure drop, were capable of adequately predicting the turbine performance from the steady state results.

Despite the reduced performance, the NGV profile is suitable for the starting point of the optimisation procedure. The profile performs well as an IGV, generating the required amount of turning for the rotor inlet with minimum losses. In the reverse direction, the profile performs poorly as the fluid flow separates from the narrow

trailing edge, creating a large wake and area of low pressure resulting in large mixing losses. However, the simple profile lends itself to profile parameterisation with potential for modification on all sections of the stator.

6.3 CFD Representation

The meta-model approach to the optimisation process is used to reduce the number of CFD cases required to reach a desired optimum. The process will however still require a large number of CFD case to be run and it is necessary to minimise the run time of each of these cases to reduce overall computational cost. Despite this requirement it is essential to ensure accuracy is maintained in the results produced.
As before, a 2D representation is used, modelling the domain as a slice at mid span. However, this time measures are taken to ensure the accurate representation of the 3D flow characteristics in 2D.

Only the guide vane and outer radius duct are modelled. The duct length is maintained at the outer diameter and extended to allow for complete wake development downstream of the guide vane. Since the domain will be used to simulate both the IGV and OGV, the duct was extended in both directions by three chord lengths. The stator profile and duct assembly are modelled as a slice at mid span, effectively modelling the flow as a 2D scenario. It was necessary to verify this representation by comparison with the results of the full 3D case and this comparison is presented below.

In setting up the domain for representation as a slice at mid span, the hub and shroud are modelled as free slip walls so no secondary losses occur as a result of boundary layer growth. The result is a simulation of the fluid flow at mid span, ignoring secondary losses. To simulate the stator row, a control surface is created, bound by median stream lines between vane profiles. These are modelled as periodic boundaries simulating the domain as a single component while modelling the effect of a complete stator row on the whole turbine assembly. The inlet and outlet boundaries are positioned five chord lengths upstream and downstream of the stator row. This configuration is setup using ANSYS Turbogrid.

	Span [m]	**% of Span**	**Inlet mass flow [kg s^{-1}]**	**Outlet Static Pressure [Pa]**
Full 3D Case	0.050	100	0.058	0
IGV	0.004	8	0.0046	2040
OGV	0.004	8	0.0046	0

Table 20: Boundary conditions for 2D simulations, calculated from 3D results.

The boundary conditions used for the 2D representation were calculated from the 3D case conducted at a flow coefficient of 1 and are given in *Table 20*. Inlet mass flow was measured for the full 3D case, given as 0.058 kg s^{-1} per component. Since the thin slice represents a span of 8% of the total span of the original geometry, 8% of the measured total mass flow for the 3D case was used. Due to boundary layer effects within the turbine duct, it is unlikely that the flow would be exactly 8% of the total mass flow through the turbine. However, it was thought that this was an acceptable value for the 2D representation.

For the IGV it was necessary to set the static pressure at the outlet since the rotor and the remainder of the device was not present to provide this pressure. Initially a measurement was taken from the 3D case for this value but since the position of the outlet at 2D is not present on the 3D simulation, it was necessary to make an initial guess. The 2D simulation was then run with this initial guess of outlet static pressure and the overall pressure profile through the domain was compared with the 3D case. It was then necessary to adjust this value until the 2D case gave an accurate representation of the flow over the stator in the 3D case.

Similarly, for the OGV it was necessary to induce an angle in the inlet flow entering the domain. This was to ensure that the angle of incidence at the OGV was the same in the 2D and 3D case as a result of the rotor exit angle and the effect of the outlet ducting. This was achieve using the same method as is described above and resulted in an OGV domain inlet angle of 20º described in cylindrical components of velocity in CFX Pre. The same mass flow was used in reverse flow and an outlet static pressure boundary condition of 0 Pa, as for the 3D case. To simulate the flow over the OGV, the same domain was used as for the IGV but the inlet and outlet locations were reversed. This meant that during the optimisation procedure, only one domain is generated for each geometry variation, this is then used to simulate both IGV and OGV and the overall performance ascertained.

Steady state simulations of the 2D IGV domain in isolation showed good comparison with the 3D results with fast convergence, demonstrating that steady conditions had been reached. However convergence difficulties were experienced when the inlet and outlet boundaries were reversed to simulate flow over the OGV.

A transient simulation of the OGV domain was run and demonstrated that the flow downstream of the OGV was in fact unsteady and that the results of the partially converged steady state CFD were not able to predict the performance of the OGV. Since the domain had been modelled as a thin slice at mid span, it was possible to run unsteady CFD simulations at reasonable cost however this would increase the run time of the optimisation. At this time, a time step dependency study was undertaken to ascertain the time step intervals needed to achieve accurate results.

6.3.1 Timestep independence

In order to analyse this time dependent behaviour it is necessary to specify the correct timestep and time duration when setting up the CFD case. This allows the solver to calculate the flow field at different time intervals. The time dependent behaviour will only be resolved if the time step size is correct as if the time is too large, an inaccurate representation of the flow will be determined (ANSYS, 2009).

	Number of Timesteps	Timestep size [s]	T – S Pressure Loss [Pa]
Low	25	0.060	466.0
% Change	100	100	5.2
Initial	50	0.030	441.6
% Change	100	100	0.7
High	100	0.015	438.5

Table 21: Results of OGV timestep independence study.

A timestep independence study was conducted with the aim of determining the effect of the timestep size on the accuracy of the computed results. An initial timestep size is specified covering a set time duration. In this case, 50 timesteps of 0.03 seconds were chosen covering a duration of 1.5 seconds. Fixing the time duration, the simulation was re-run with half and double the number of timesteps. The results of the study are presented above *(Table 21)*, measuring total to static pressure across the whole domain at each timestep and taking an average of the results. This is the performance measure that will be used for the optimisation.

The results demonstrate the level of error due to timestep size selection. A significant difference of over 5% between the low and initial timestep demonstrates that a timestep size of 0.06 seconds is too large. The difference between the initial and high value is below the acceptable solution tolerance of 1%. As a result, the initial value was used as the higher accuracy of halving the timestep size was not necessary.

Doubling the number of timesteps increases the running time of the simulation as results are computed for each timestep value, as set by the user. This study not only identifies the error due to timestep size, but also shows the minimum number of timesteps required to compute the unsteady flow behaviour for a given time duration. This streamlines the simulation, minimising the computing power required for a given error. If running a small number of transient simulations, this is less important, but in the case of optimisation where possibly hundreds of simulations will be run, case streamlining is important. As a result of this study, 50 timesteps of 0.03 seconds were used for all OGV simulations from this point on.

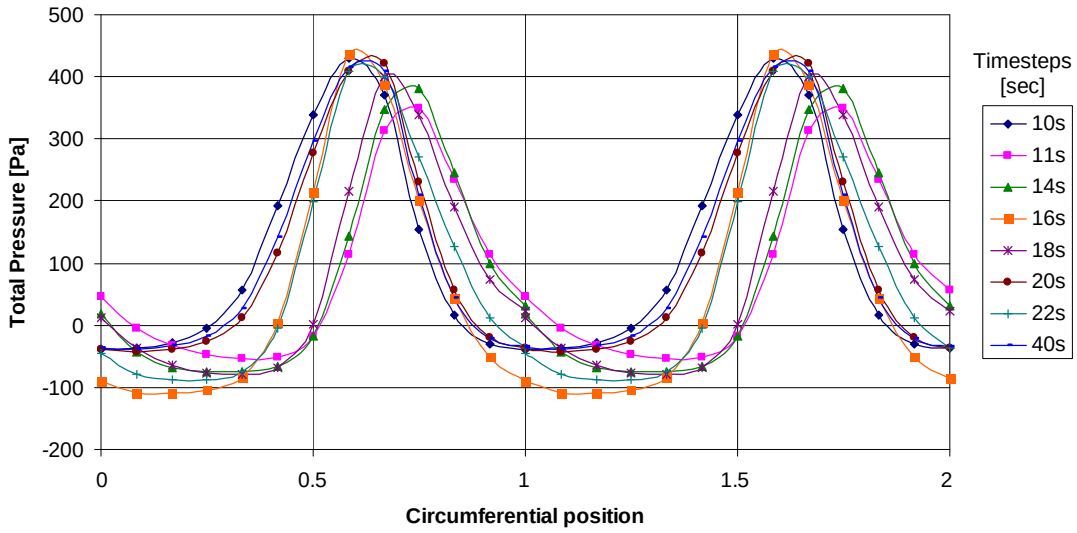

Figure 87: Circumferential plot of wake profile at different timesteps.

To demonstrate the unsteady behaviour of the flow downstream of the OGV stator row, measurements were made to assess the wake profile at various timesteps. This involved positioning a reference frame at a position downstream of the stator row and measuring the total pressure across the wake, from one periodic boundary to the other. The data is presented in *Figure 87* where the total pressure is plotted against the non-dimensionalised circumferential positioning across two wake profiles, covering two individual stators. Each line demonstrates data recorded at a different timestep, the times of which are presented in the legend on the right. A random set of timestep results are displayed to ensure that different positions within the oscillatory cycle are displayed without the results becoming in-sync with the oscillations. The variation between the circumferential total pressure plots at different time steps demonstrates the unsteady nature of the flow and the time dependent behaviour.

6.3.2 CFD Comparison with 3D results

Once the 2D CFD simulations had been set up, it was necessary to compare the representation of these simulations to the full 3D case. This was done using the design case with total pressure of 2500 Pa at inlet and 0 Pa static pressure at outlet. Data was recorded for fluid velocity, static pressure, flow angle and total pressure, measured through the device from inlet to outlet. This data is presented on the plots below compared with the 2D representation of the design case. In each plot, the 3D case is presented in blue, the 2D IGV representation is presented in green and the OGV is represented in orange. The 2D cases use the boundary conditions that have been discussed above and in the case of the transient case, an average of the results was used.

In reading the following collection of plots, the discrete nature of the 2D results must be noted. One domain is used to simulate the IGV and OGV in 2D by reversing the inlet and outlet boundary conditions. In order to compare the 2D and 3D results, the 2D OGV results have been reversed and adjusted for x positioning so that they correspond to the OGV section of the 3D plot.

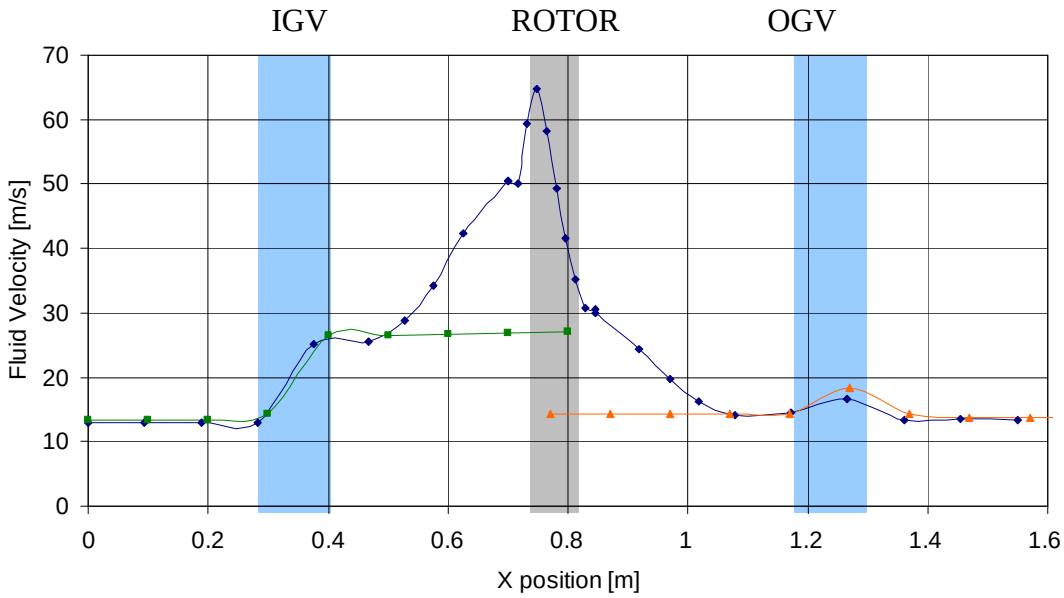

Figure 88: Plot of fluid velocity from inlet to outlet through the turbine showing 2D and 3D comparison.

Figure *88* shows the plot of fluid velocity through the device from inlet to outlet. The results for the IGV, shown in green, show slightly higher fluid velocity at exit to the stator row. Flow velocity over the OGV row shows good comparison between 2D (orange) and 3D (blue).

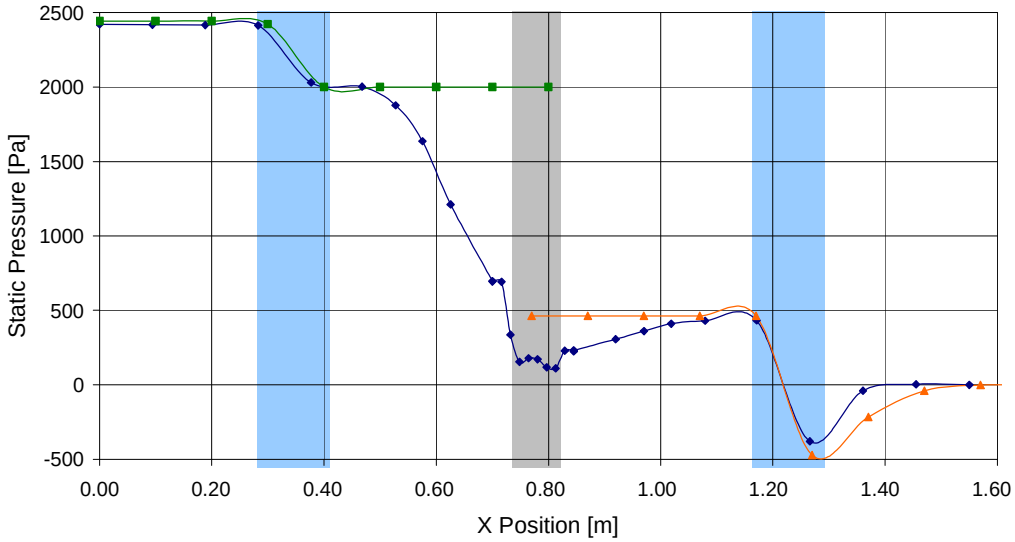

Figure 89: Plot of static pressure from inlet to outlet through the turbine showing 2D and 3D comparison.

Figure 89 shows the comparison of static pressure variation through the device for the 2D and 3D CFD. Both IGV and OGV show good comparisons between the two, with the static pressure loss across the stator rows being accurately represented.

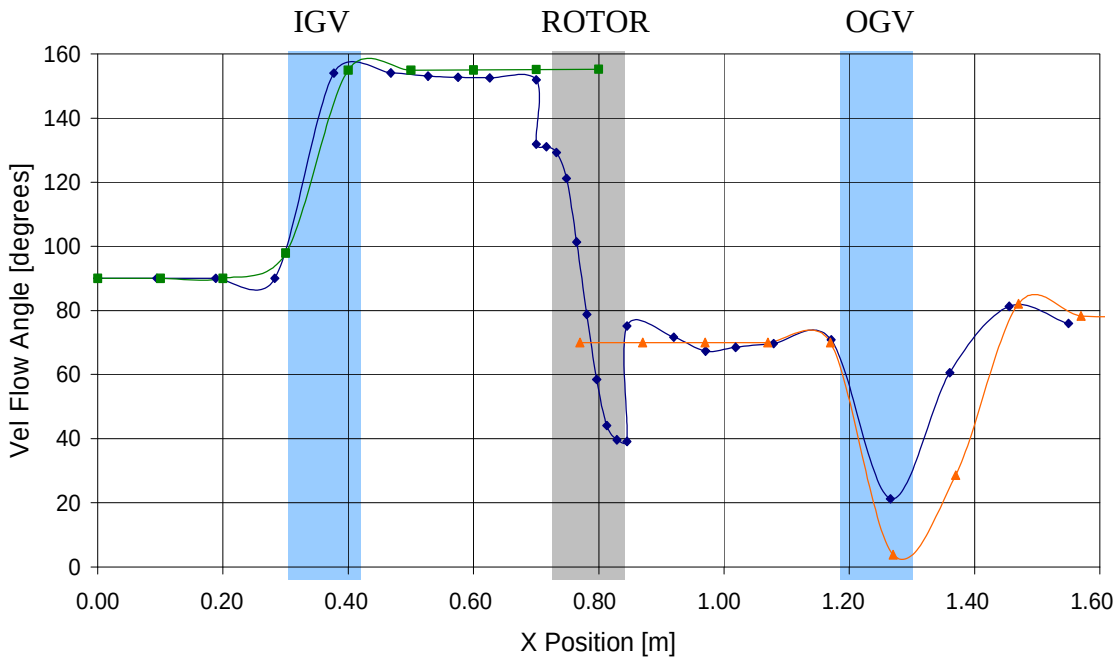

Figure 90: Plot of velocity flow angle from inlet to outlet through the turbine showing 2D and 3D comparison.

A plot of velocity flow angle through the device is shown in *Figure 90*. The results show that the 2D IGV case, in green, achieves a higher inlet turning angle than the 3D case. For the OGV, overall turning angle is similar however the prediction of turning angle passing the OGV row varies greatly.

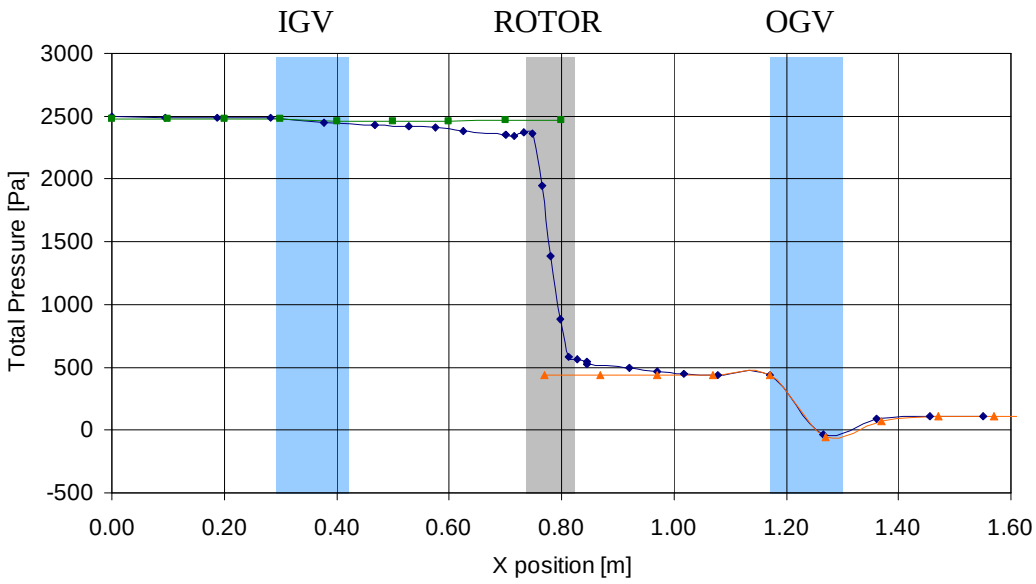

Figure 91: Plot of total pressure from inlet to outlet through the turbine showing 2D and 3D comparison.

Figure 91 is a plot of total pressure through the turbine. The plot of the 2D representation of the IGV shows that there is a variation between the total pressure drop predicted in 2D and the 3D prediction. Total pressure drop across the OGV shows accurate prediction for total pressure drop with very good representation between 2D and 3D.

Overall the representation of the guide vane geometry as a 2D slice at mid span shows highly similar predictions to the full 3D case. However there are variations and these were to be expected when simplifying a 3D problem into a 2D representation. The variations are present due to the mitigation of secondary losses in the 2D representation by using free-slip wall boundary conditions. Also the fact that the flow is fully 3D in the turbine and the flow at mid span is unlikely to be uniform as it is being simulated, especially due to the variable radius duct. The above plots demonstrate the capability of the method and this is satisfactory for the optimisation process. This method allows a great many geometry variations to be investigated and measured for improvement from the datum geometry. It is the estimated improvement that is important in the optimisation procedure rather than the actual performance result. The final result will be simulated in 3D for final performance prediction.

Representing the guide vane geometry and domain in this way reduces the computational cost of running each CFD case. A full 3D case takes roughly 6 hours to run using 4 processors. A 2D representation can be complete in 20 minutes, 40 minutes for both forwards and reverse flow. This reduces the overall time to simulate each geometry variation by 9 times. Greatly reducing the computing cost and the

necessary time for each optimisation procedure. This allows for a great many more geometries to be investigated in the time available for the research project.

6.4 Profile parameterisation

The method of parameterisation used for an optimisation procedure can have a major effect on the final results as well as the efficiency and effectiveness of the system used. For this reason it is important to choose the most suitable parameterisation method, matched with the capability to produce the desired objective. A study into various methods of profile parameterisation was conducted and a number were selected for further investigation. The most suitable method for the application was then selected, the review and selection are discussed in the following section.

There has been much research into the parameterisation of airfoil geometry and although there are differences between this scenario and that of the guide vane parameterisation, this was the starting point of the investigation. Various methods have been used to represent airfoil geometry and these methods are generally suited to different situations depending on the goal of the parameterisation. Bezier curves and Spline curve variations are used to directly fit airfoil shapes using interpolated coordinates see, for example, work by Venkataraman (1998), Lépine. et. al. (2001), Tang and Désidéri (2002), Sóbester and Kean (2007) and Sóbester and Barrett (2008).

Another method uses analytical functions such as Hicks-Henne functions (Hicks and Henne, 1978) where a number of functions are combined to define the airfoil profile. The profile is then optimised by assigning specific function parameters to design variables. Generally, these methods have been employed for either global parameterisation for conceptual designs or for local modification where the interest lies in the detail of a specific area and different methods are suitable for different applications (Song and Keane, 2004). Keane and Nair (2005) suggest that in the early stages of a design process, global optimisation techniques should be adopted to allow for radically different designs to be considered. Then, in subsequent stages of the design process, local parameterisation techniques can be implemented, incorporating increased surface control in local areas of interest. To this end, Hoyle (2006) discusses a general purpose, multi-stage parameterisation strategy that is capable of both local and global variations, employing different parameterisation methods at each stage.

Apart from different parameterisation methods being suitable for either local or global techniques, the reason for splitting up these methods into multiple stages is due to the need to minimise the complexity of the optimisation. Increasing the surface control of

a parameterisation method increases the number of design variables required to describe that surface. This does create an increase in dimensionality but it also increases the complexity of the problem. In the case of automated optimisation, this results in an increase in computational cost since an increased number of expensive calls to the solver will be required for an effective design search. For this reason, it is necessary to employ an efficient parameterisation technique, suited to the problem at hand, to minimise the cost of the optimisation procedure.

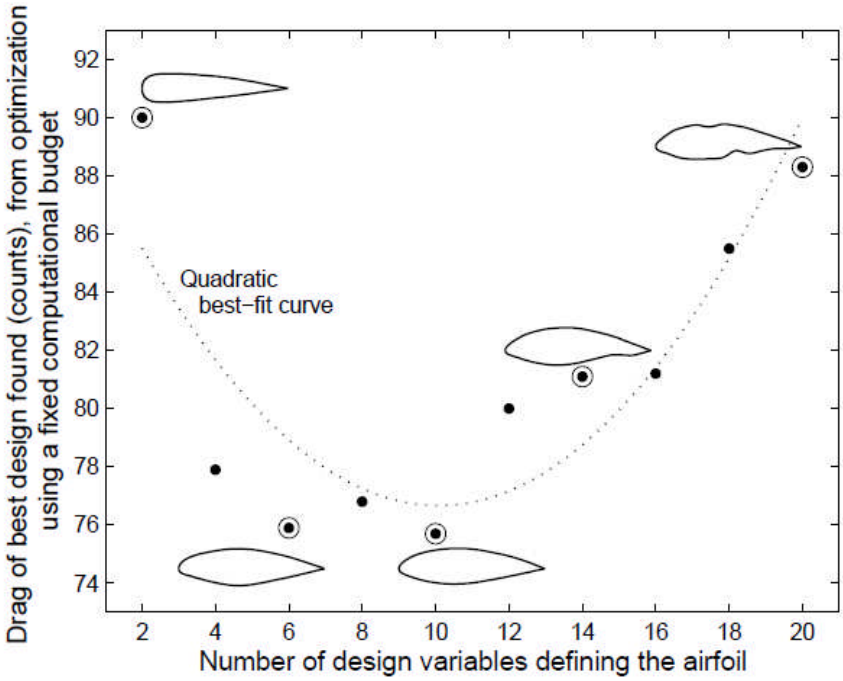

Figure 92: Example of airfoil design parameterisation (Barrett, 2007).

Barrett (2007) displays the compromise between the need to achieve detail and local control while minimising complexity *(Figure 92)*. In this example, an optimisation procedure is performed to minimise drag on an airfoil. The airfoil is parameterised by two cubic splines where the control points lie on the surface of the airfoil profile. Along the x axis is the number of design variables used to represent the airfoil, the data ranges from 2 to 20. The y axis shows a measure of the drag of the produced airfoil. A genetic algorithm is used for the optimisation and for each optimisation run, 10 iterations are performed so that each run has the same computational cost.

The results show that with 2 design variables, a smooth airfoil shape is produced however, the drag is poor due to the limited controllability of the design. In contrast, with 20 design variables, a large amount of local control is possible but the number of GA iterations is not sufficient to achieve an optimum profile. An irregular airfoil shape is produced, again resulting in poor drag values. It can be seen that the optimum profile, with minimum drag, occurs with 10 design variables. In this case, the profile

has sufficient controllability to be able to manipulate the airfoil enough to reduce drag while having few enough design variables to be able to achieve this optimum within the permitted computational cost. This example emphasises the need for efficient parameterisation methods that allow for complex shapes to be generated in sufficient detail while at the same time using a minimum number of design variables in order to minimise computational cost.

6.4.1 Standard airfoil geometry definition

Initially, the possibility of defining the guide vane geometry using standard airfoil definition was considered, such as the method used for the NACA series airfoils. In its simplest form this requires parameters such as maximum thickness and maximum camber with relevant positioning of these values along the percentage of the chord. Despite the fact that additional parameters can be included, such as designed lift coefficient in the NACA five digit airfoil series, the end result is a variation of a standard airfoil shape.

The idea behind optimising the guide vane profile in two directions is to produce a novel guide profile that performs well in two directions. Airfoils are designed for operation in one direction and the way they have been defined is also reliant on this fact. As a result of this, it was though that standard airfoil geometry definition was an inadequate method of parameterising the guide vane profile for bi-directional optimisation since it would be difficult to produce unconventional, purely bi-directional profiles.

6.4.2 Bezier parametric curves

A Bezier parametric curve is specified by prescribing the vertices of a defining polygon *(Figure 93)*. This method allows for complex curves to be defined using a minimum number of points or coordinates.

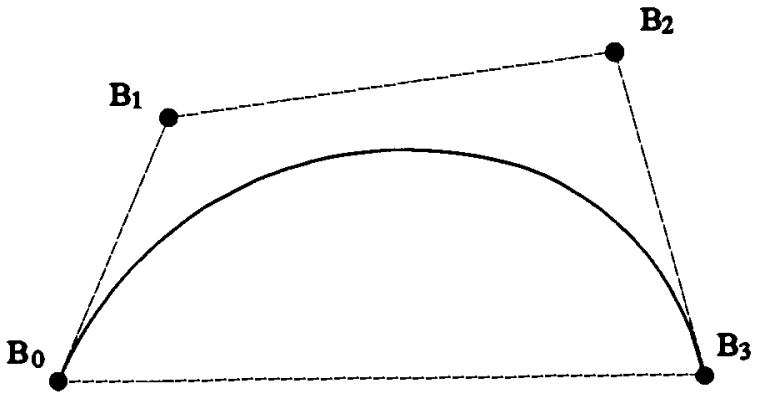

Figure 93: A cubic Bezier curve showing the defining polygon and control points, (Rogers and Adams, 1989).

Mathematically, the general description of the Bezier curve is given below in the binomial form:

$$P(t) = \sum_{i=0}^{n} \binom{n}{i} (1-t)^{n-i} t^{i} B_i$$

$$= (1-t)^{n} B_0 + \binom{n}{1} (1-t)^{n-1} t B_1 + \ldots \qquad \textit{(Eq.6.2)}$$

$$\ldots + \binom{n}{n-1} (1-t) t^{n-1} B_{n-1} + t^{n} B_n, \qquad t \in [0,1],$$

The cubic Bezier curve or *third order* Bezier curve above *(Figure 93)* is described mathematically as:

$$P(t) = (1-t)^{3} B_0 + 3(1-t)^{2} t B_1 + 3(1-t) t^{2} B_2 + t^{3} B_3, \qquad t \in [0,1], \qquad \textit{(Eq. 6.3)}$$

A method of generating airfoil geometry employs four Bezier parametric curves, each using a 6th order polynomial. In this method there are two curves for the pressure surface and two curves for the suction surface. By enforcing slope continuity at all curve joints and second derivative continuity between the for and aft curves, as well as second derivative direction continuity at the leading edge, an airfoil profile can be produced that is controlled by 27 design variables.

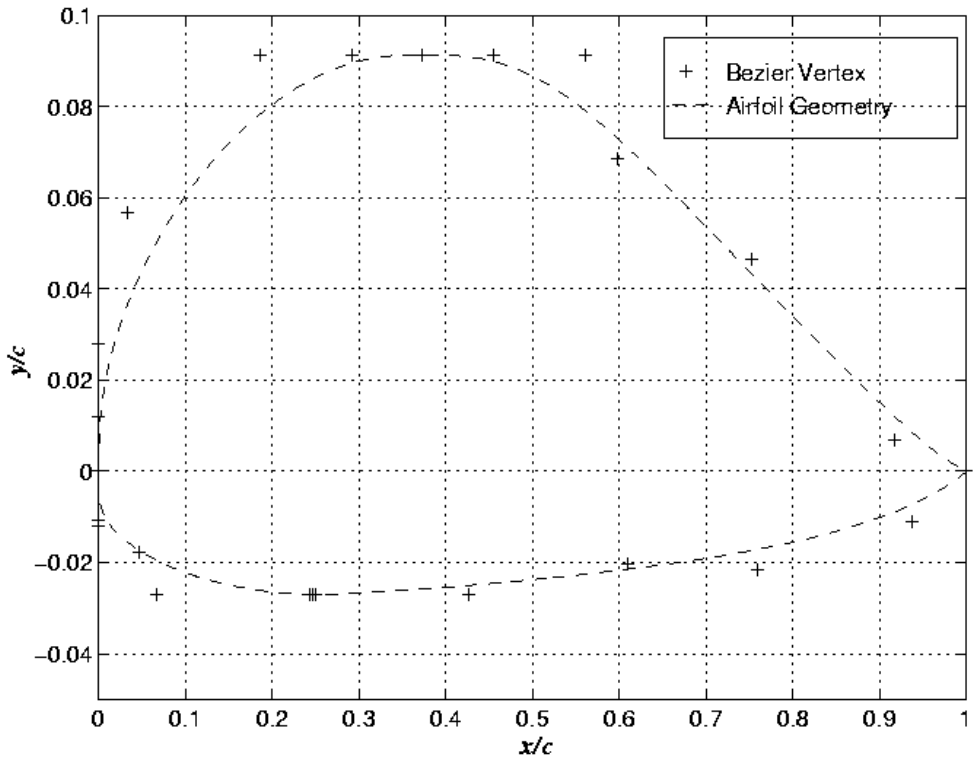

Figure 94: Airfoil profile defined by four Bezier curve method
(Venkataraman, 1998)

Venkataraman (1998), states that it should be possible to reproduce all existing single element airfoils using this procedure. *Figure 94* shows an example of an airfoil produced in this way, showing the control points *(Bezier Vertex)* positioning required for this profile. This capability does however come at a price of a large number of design variables and complex design space.

Tang and Désidéri (2002), simplify the problem by representing an airfoil profile using two 8th order Bezier curves, reducing the total number of design variables *(Figure 95)*. Although this inevitably reduces the range of airfoil profiles that can be produced but depending on the problem at hand, this may be acceptable depending on the application.

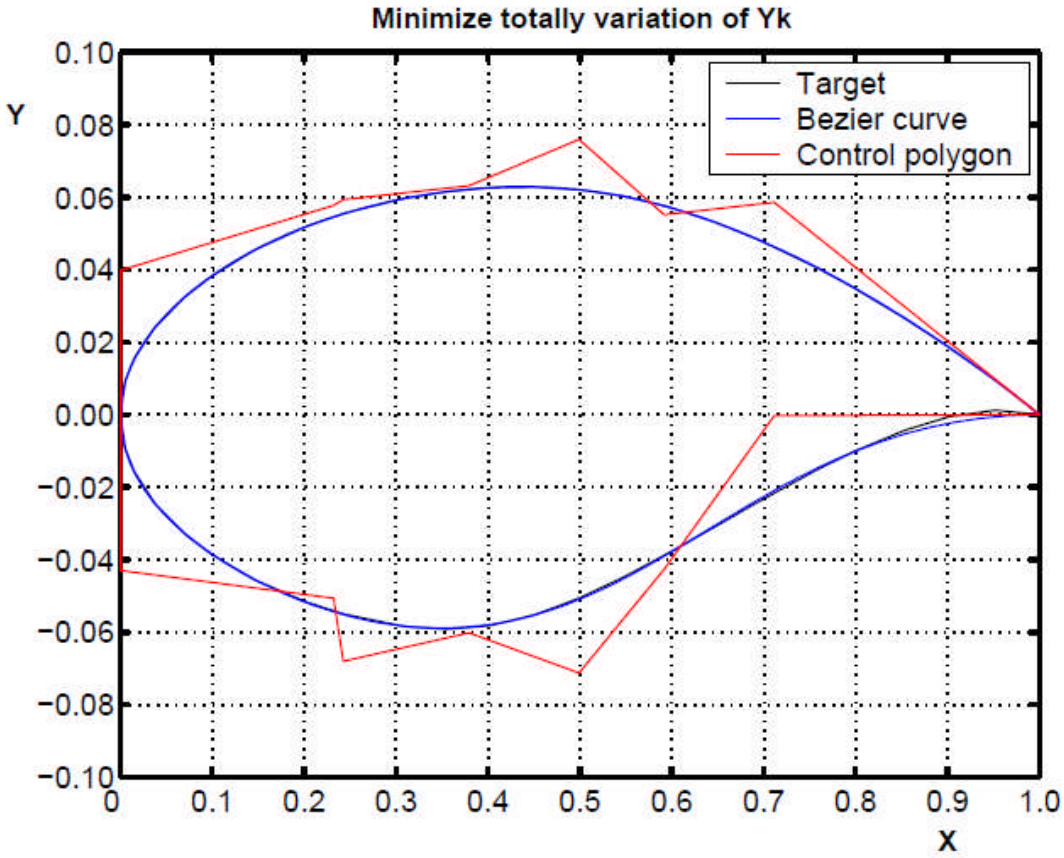

Figure 95: Airfoil profile represented by two 8th order Bezier curves,
(Tang and Désidéri, 2002)

A requirement of the geometry parameterisation was to minimise the number of parameters used to define the guide vane profile. For this reason, it was thought that the above method of airfoil definition, requiring 27 design variables would necessitate too many optimisation calls to find an optimum geometry.

The potential of the Bezier curve definition did however seem promising and the possibility of reducing the number of curves and hence the number of design variables was investigated. A single 8th order Bezier curve was generated using Matlab. This was done by first prescribing the coordinates of the control points and using the above equation *(Eq. 6.1)* to plot the Bezier curve.

The starting point of the investigation was to plot an ellipse using a minimum number of control points *(Figure 96).* From this starting point, the position of the control points were varied, adjusting the defining polygon and hence the final profile *(Figure 97 a and b).*

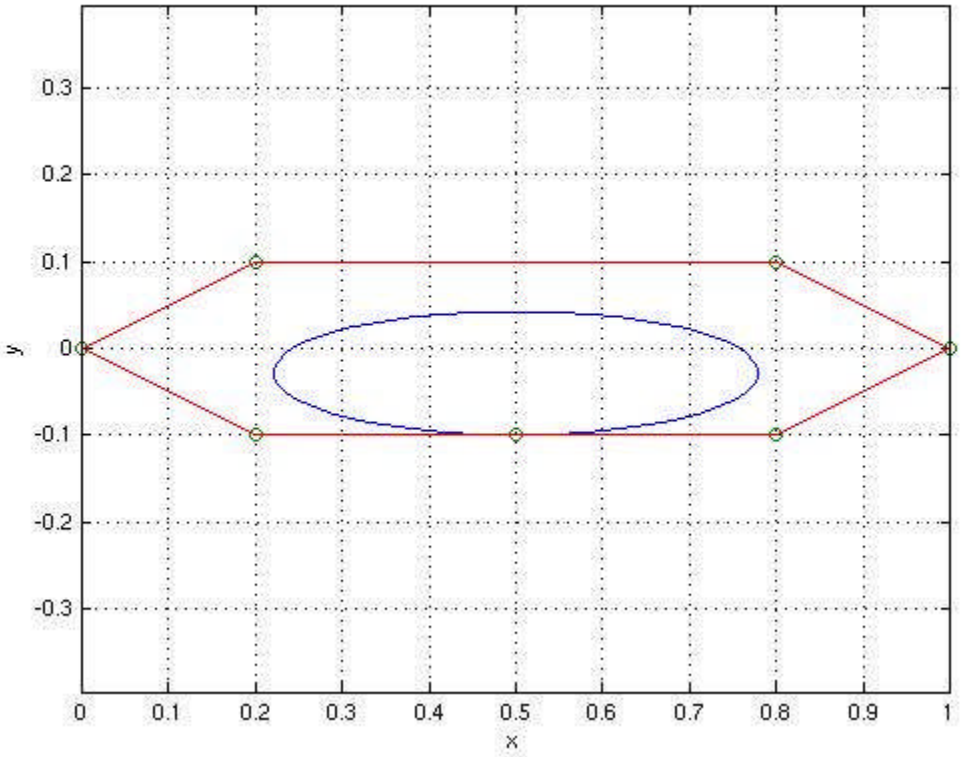

Figure 96: Ellipse plotted using 8th order Bezier curve
showing control points in green and defining polygon in red.

(a)

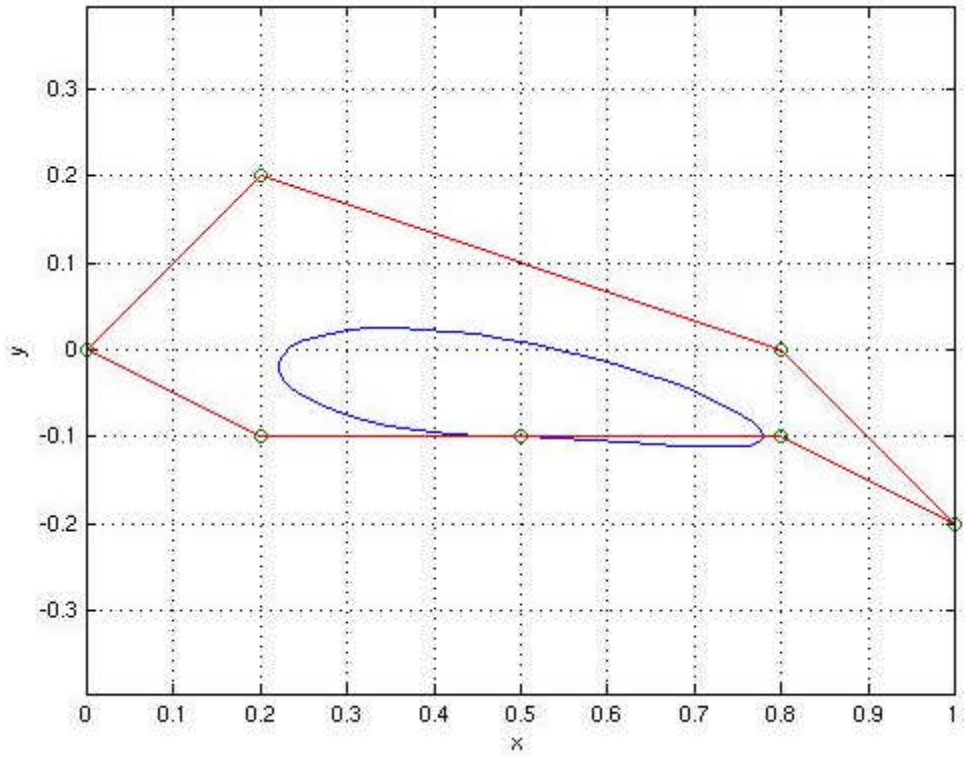

(b)

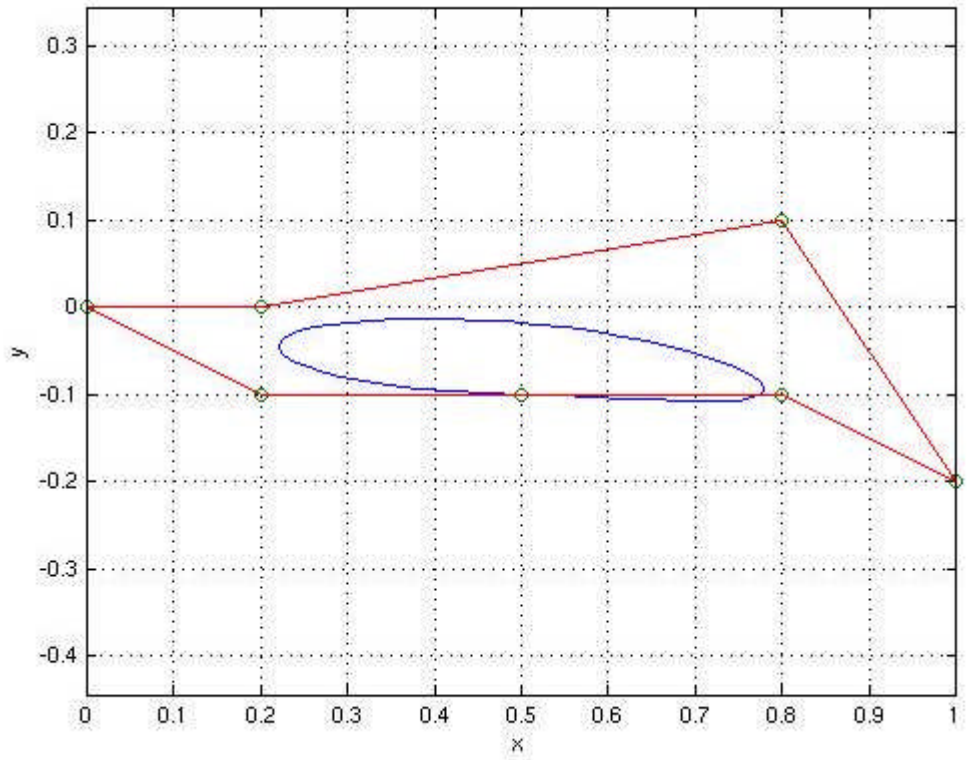

Figure 97: Variations of single Bezier curve profile (blue)
by manipulation of defining polygon (red).

The initial investigation into the single Bezier curve profile demonstrated that the minimum number of control points required to produce an ellipse were not sufficient to produce a more complex profile so more control points, or a combination of more, connected curves would be required to produce a guide vane profile using this method.

A defining property of a Bezier curve is that the first and last points on the curve are coincident with the first and last points of the defining polygon (Rogers and Adams, 1989). When defining a complete ellipse with a single curve, the first and last points are located at the same position so that the curve starts and finishes in the same place, completing the ellipse. This can be seen in *Figure 96* and *Figure 97*above at x = 0.5, y = -0.1. When producing a profile using a Bezier curve, these end points behave differently to the other control points as they are located on the profile, i.e. the profile point must pass through these end points. As a result, the variation of these end points has a much larger influence on the overall positioning of the plotted profile compared with the other control points. When parameterising a profile using Bezier curves, this factor presents difficulty in the manipulation of these points as the weighting or influence of the end point must be taken into account.

Trailing edge constraint

The inlet guide vane has the requirement of turning the flow through the desired turning angle to ensure correct incidence angle at the inlet to the rotor. This factor must remain and is a fixed objective in the function of the guide vane profile. For this reason, the trailing edge of the IGV had to be constrained to ensure that this turning angle is achieved for all permutations of the modified profile during the optimisation.

The potential of maintaining the angle of the trailing edge of the IGV was investigated, initially by positioning a higher concentration of control points at the trailing edge and fixing their relative position to the required angle. The start and end point of the curve was positioned at the trailing edge with these additional control points positioned close to and either side of the joining section. This can be seen below in *Figure 98*. In the above Bezier curve generations, the beginning and end point of the Bezier curve occurs in the middle of the lower section, by positioning this point on the suction section, towards the aft trailing edge, the metal angle can be controlled and the rest of the profile is produced by a constant curve.

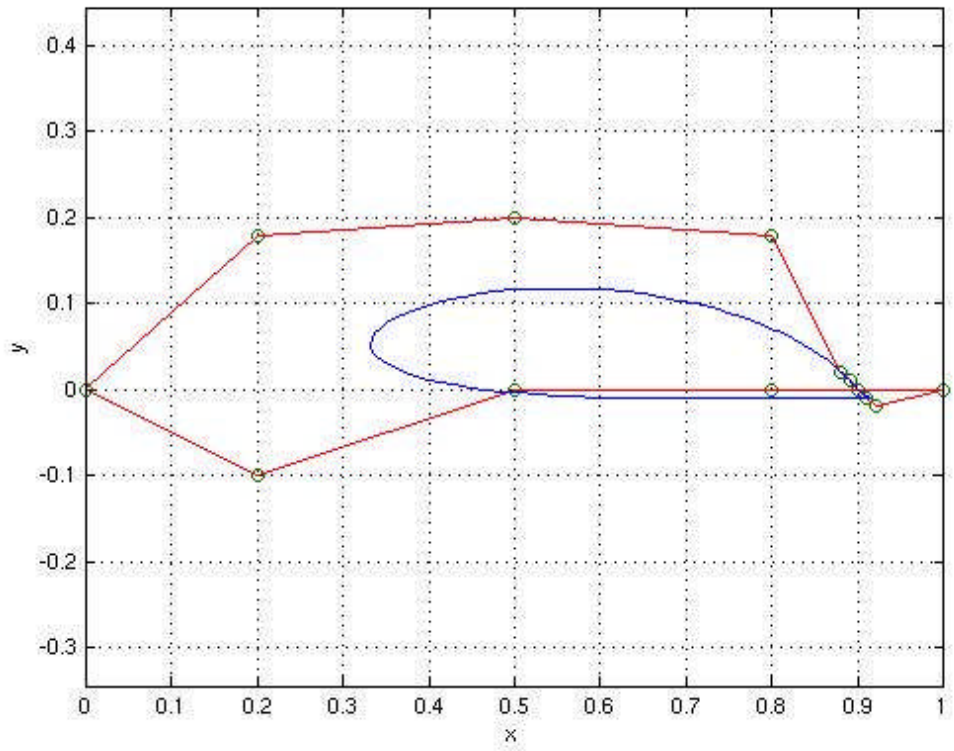

Figure 98: Single Bezier curve airfoil profile with defining polygon,
note additional control points and beginning/end point at trailing edge.

Observations of Bezier curve method

The single Bezier curve was used to construct an airfoil profile, constraining the aft-section of the suction surface using a higher density of control points with fixed relative positioning. Attempting to produce a profile in this way, using a single Bezier curve highlighted a number of characteristics about the way that Bezier curves function. The first is that a large variation in single control point positioning is required to have a significant effect on the profile. When control points are moved together, they have more of an effect on the profile curve showing that the relative positioning of the control points is significant. This adds complexity to an optimisation problem as the positioning of a single control point may be beneficial or non beneficial depending on the relative position of other control points.

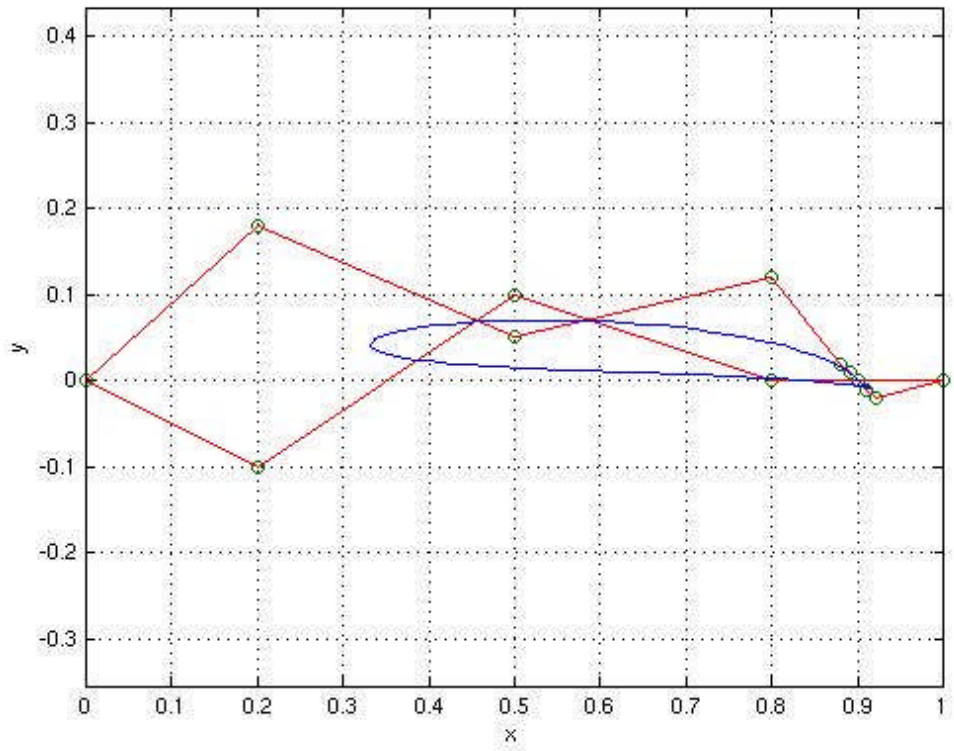

Figure 99: Single Bezier curve with self-intersecting polygon and valid profile.

The large variable range required for each control point also adds complication to the parameterisation of the profile. Each control point requires a large range in both the positive and negative direction in order to influence the profile, the result of this is that the defining polygon has the potential to self-intersect as in *Figure 99*. In this instance, this is not a problem since the profile curve does not self-intersect, resulting in a positive geometry. However, with full variation of control points, there is the problem of self-intersection which would result in a negative geometry being produced *(Figure 100)*. It was necessary to ensure that these invalid profiles were not produced as they would cause errors in the geometry generation procedure and resulting in failed CFD runs.

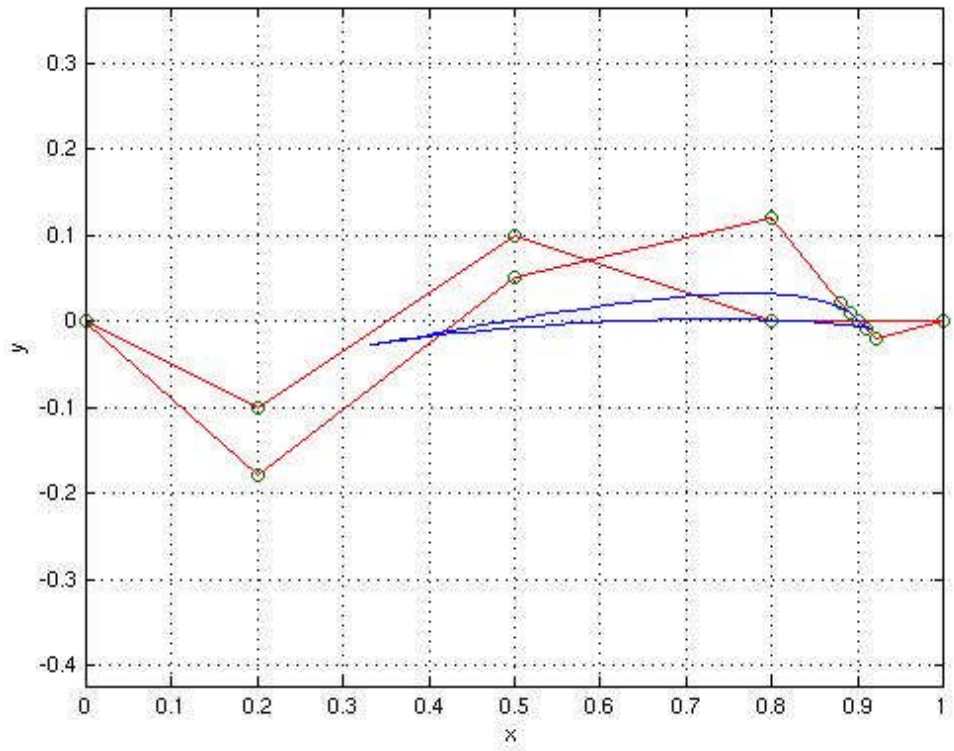

Figure 100: Invalid geometry showing self-intersecting defining polygon and self-intersecting profile.

Self-intersection

A method was devised to test for self-intersection of each profile generated by variation of the control points. This was done by first dividing the profile into pressure and suction surfaces by locating the leading and trailing edge (minimum and maximum x values). The y-values of the pressure surface were then subtracted from the corresponding y-values of the suction surface. A negative value in the output identifies a self-intersecting profile, identifying a combination of control point coordinates that do not produce a valid geometry. This method was then be used to discard this data sample point, during optimisation, to prevent geometry errors further down the procedure.

Bezier curve testing

Initial investigations into the capabilities of single Bezier curve profile representation appeared promising despite a number of concerns as to the controllability. The next step was to test the controllability of the single Bezier curve with 18 control points. This was done by first producing a datum airfoil, the profile shown in *Figure 98* was used.

Each control point was assigned an equal range of +/- 0.5. The two control points either side of the beginning and end points were given relative positioning. This resulted in a complete airfoil with 7 design variables. An array of sample points was generated using a Halton sequence and each of these points with corresponding control point coordinates was sampled by generating the profile curve and measuring its fitness. Fitness was measured as the variation between the produced profile and the datum profile and a specific tolerance was assigned to each run to act as the optimisation objective.

The plots below *(Figure 101 to Figure 104)* show the solution converging towards the datum geometry as different tolerances are met. The blue solid line shows the datum airfoil and the red dashed line shows the generate profile.

This method of investigating the single Bezier curve demonstrates the number of iterations necessary to get within a small tolerance of the datum profile and the job of the optimisation process to reduce this number of sample points in order to find the optimum solution. This method took over 39,000 generations to produce a solution within a tolerance of 0.02 of the datum profile. This experiment was only possible as the solution calculation took under a second to compute, despite this fact, this number of calculations took 8 hours to run. This would not be possible if CFD was used to predict the performance of the solution demonstrating the necessity of the optimisation procedure in the research.

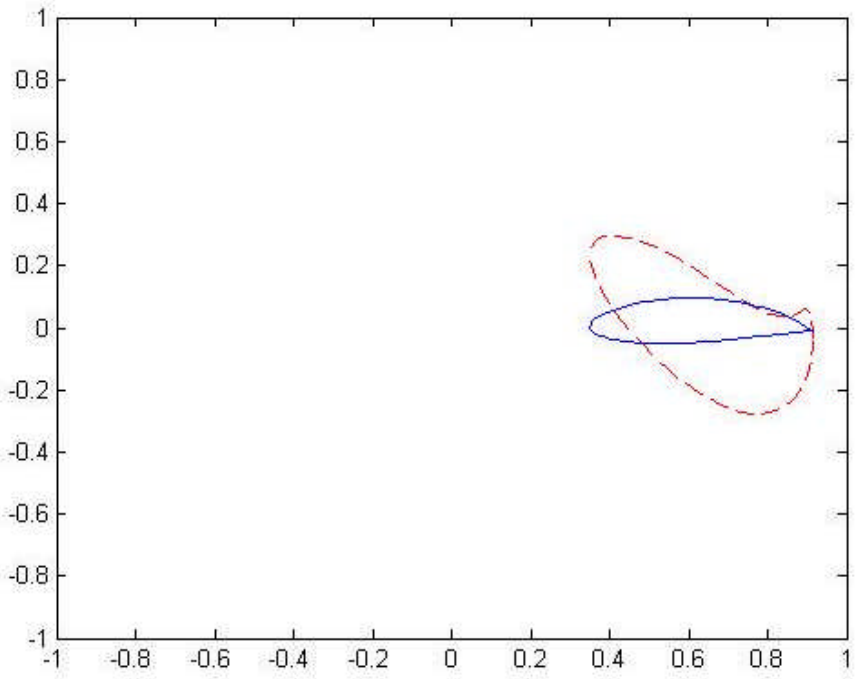

Figure 101: Bezier curve reproduction
of datum profile with tolerance value of 0.3

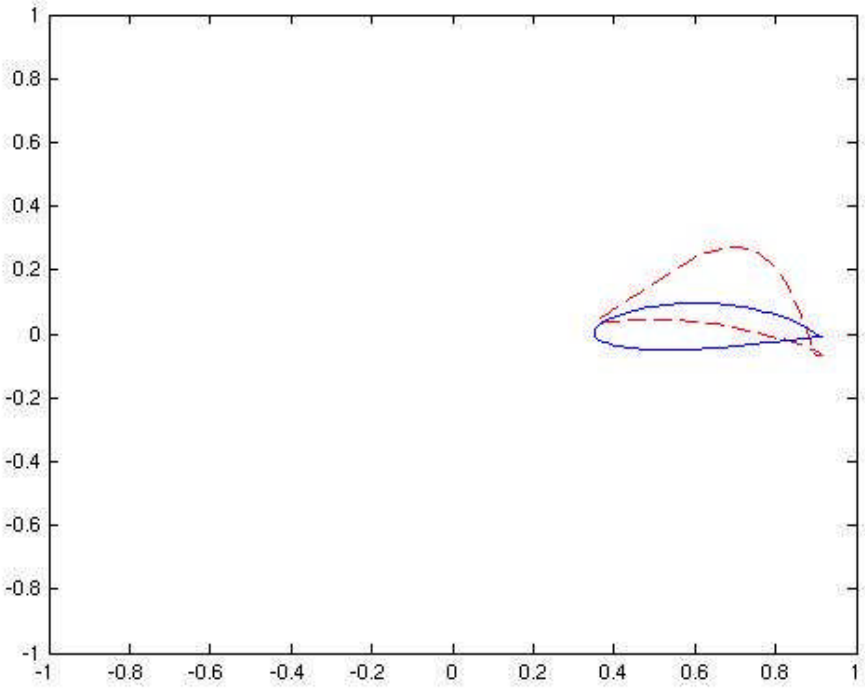

Figure 102: Bezier curve reproduction
of datum profile with tolerance value of 0.2

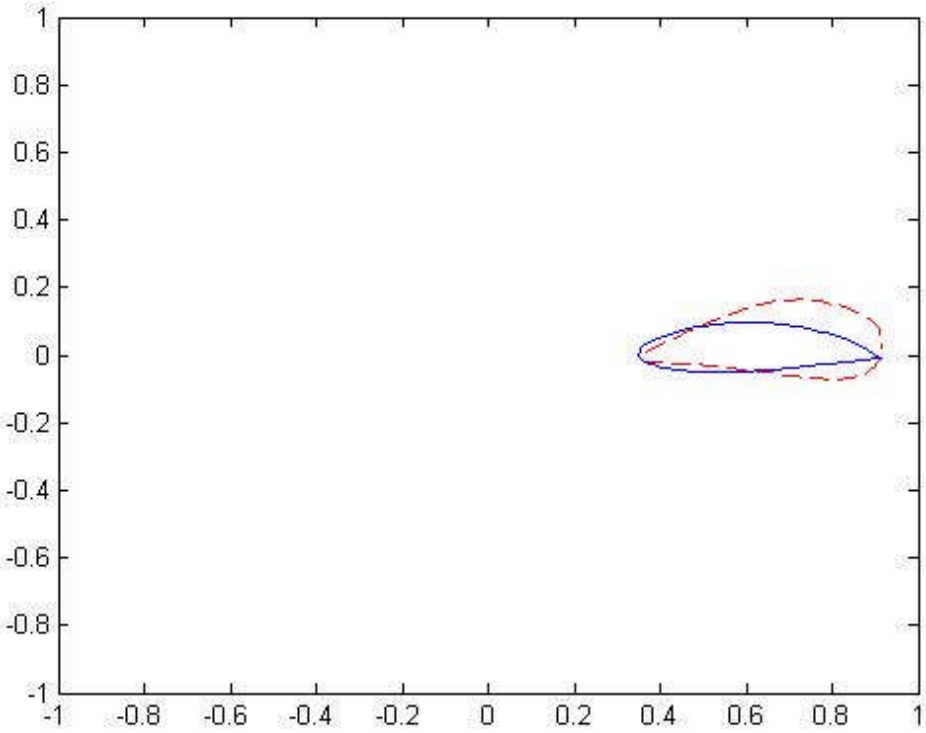

Figure 103: Bezier curve reproduction
of datum profile with tolerance value of 0.1

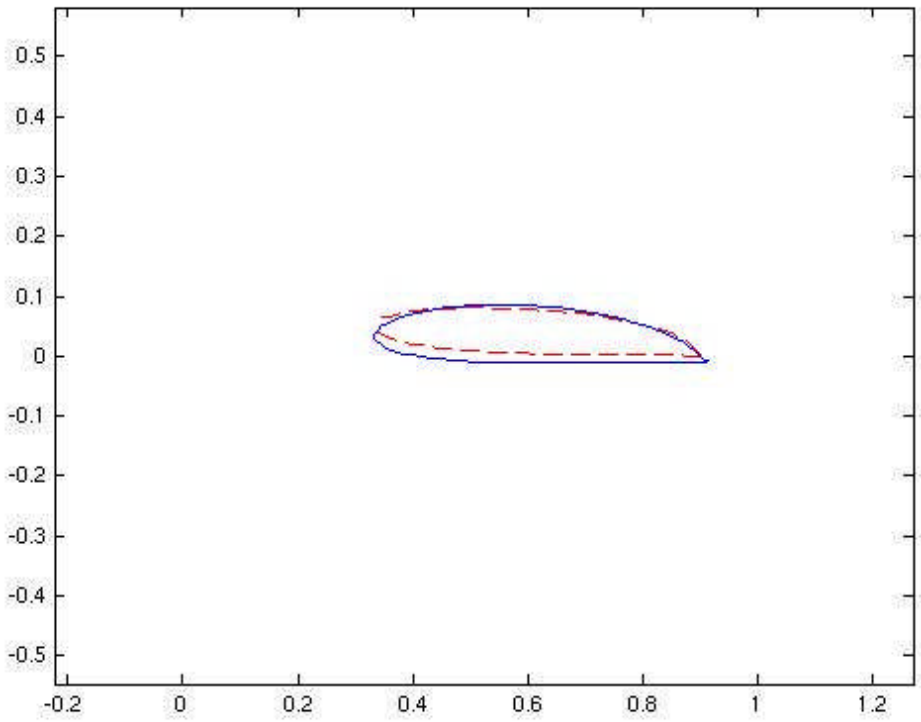

Figure 104: Bezier curve reproduction of
datum profile with tolerance value of 0.02

Bezier Curve Optimisation

In order to test the compatibility of the single Bezier curve with the method of optimisation used in the research, an optimisation procedure was conducted. The objective of the optimisation was to reproduce the datum profile. The number of control points was kept the same and the variation between the produced profile and the datum profile was measured in the same way as above and interpreted into a final fitness value. The range of the control points was reduced to +/-0.2 in the y direction, the x coordinate of the control point positioning was fixed.

The datum profile is shown below in Figure 105 where the profile curve is displayed in blue and the control points shown as green circles.

Optimisations were run with increasing number of initial sample points and estimated optimum profiles were produced at the end of the run. The plots below show the results of these optimisation runs with the optimum profile plotted in red with corresponding control points *(Figure 106 to Figure 110).*

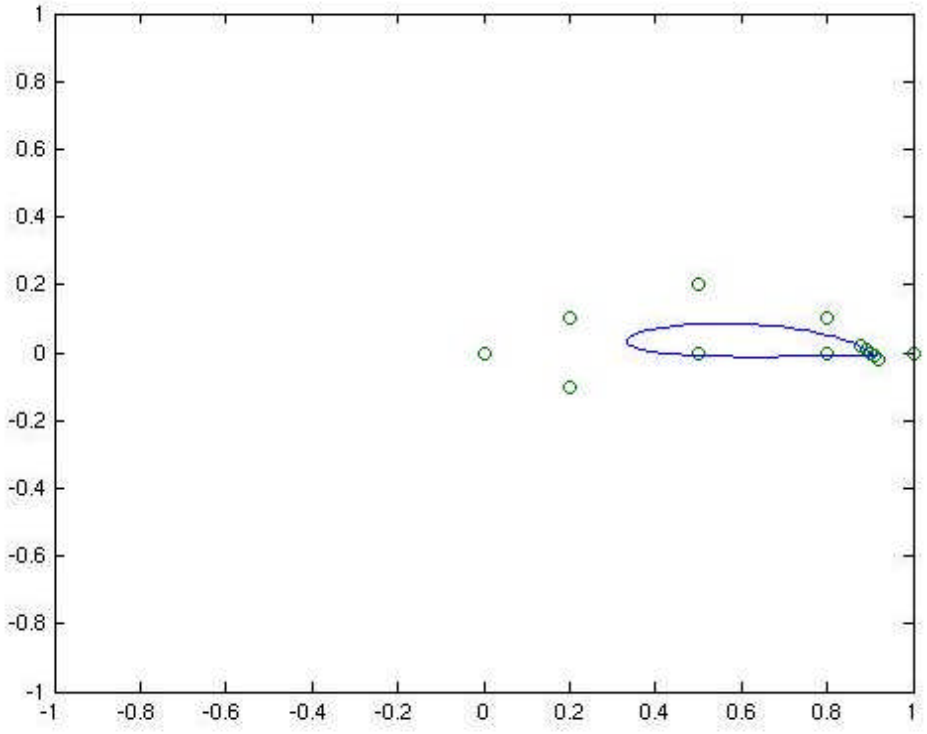

Figure 105: Datum profile described by single Bezier curve
with 7 control points

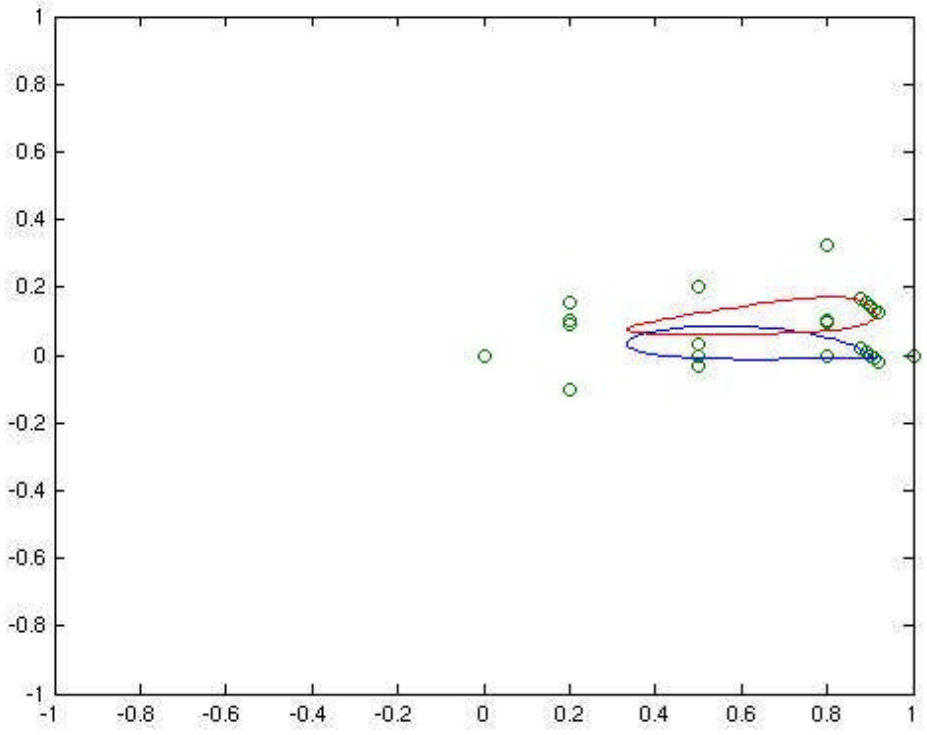

Figure 106: Optimum profile representation
after 10 initial sample points and 150 iterations.

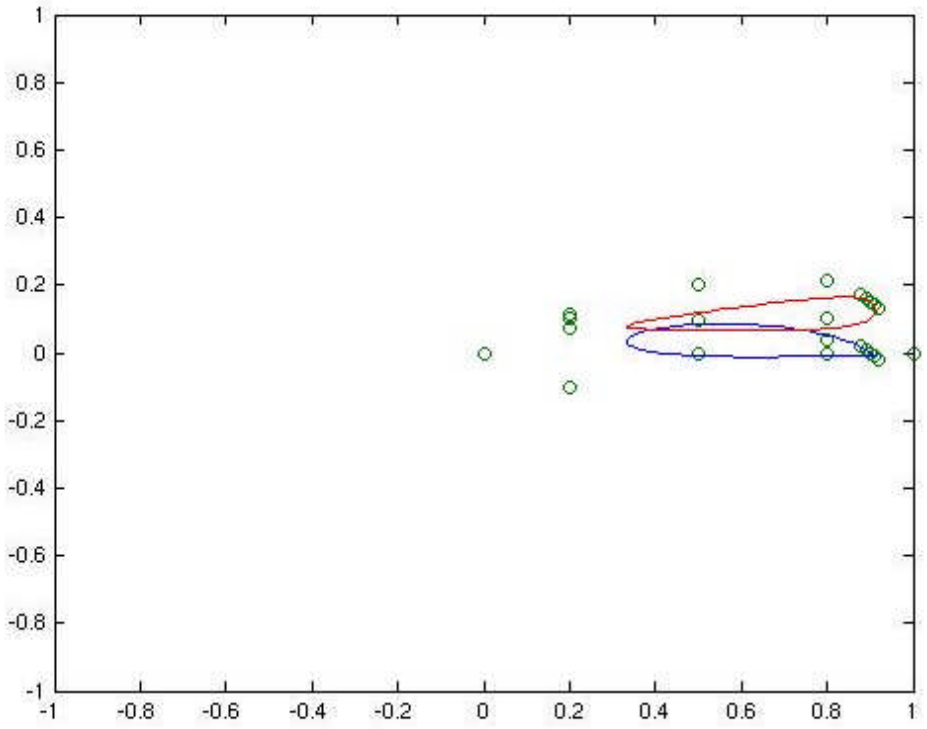

Figure 107: Optimum profile representation
after 100 initial sample points and 150 iterations.

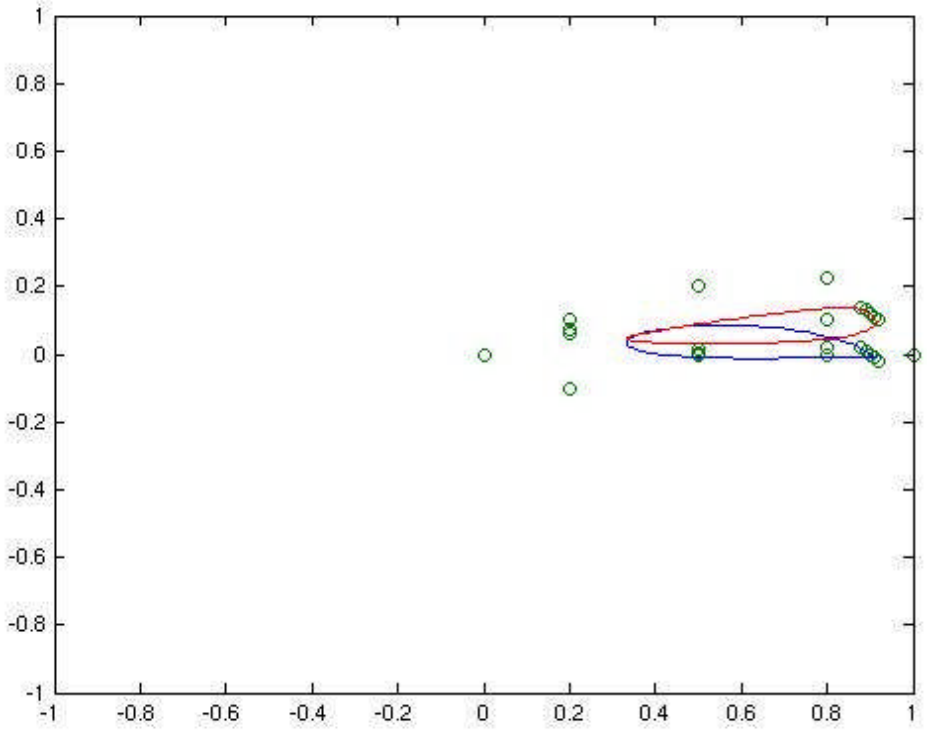

Figure 108: Optimum profile representation
after 250 initial sample points and 150 iterations.

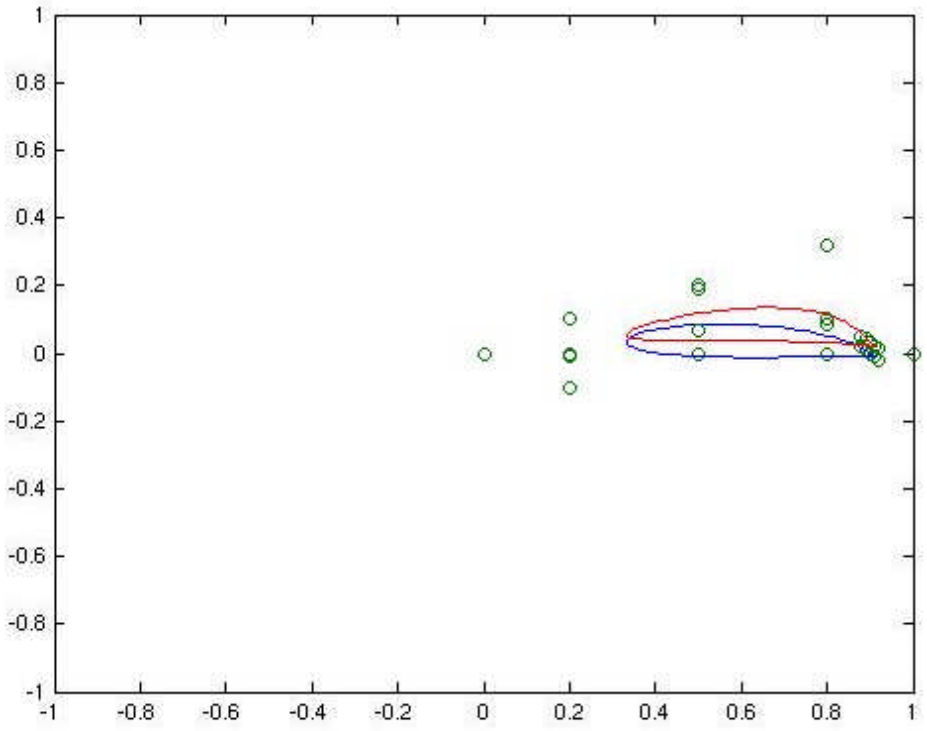

Figure 109: Optimum profile representation
after 400 initial sample points and 150 iterations.

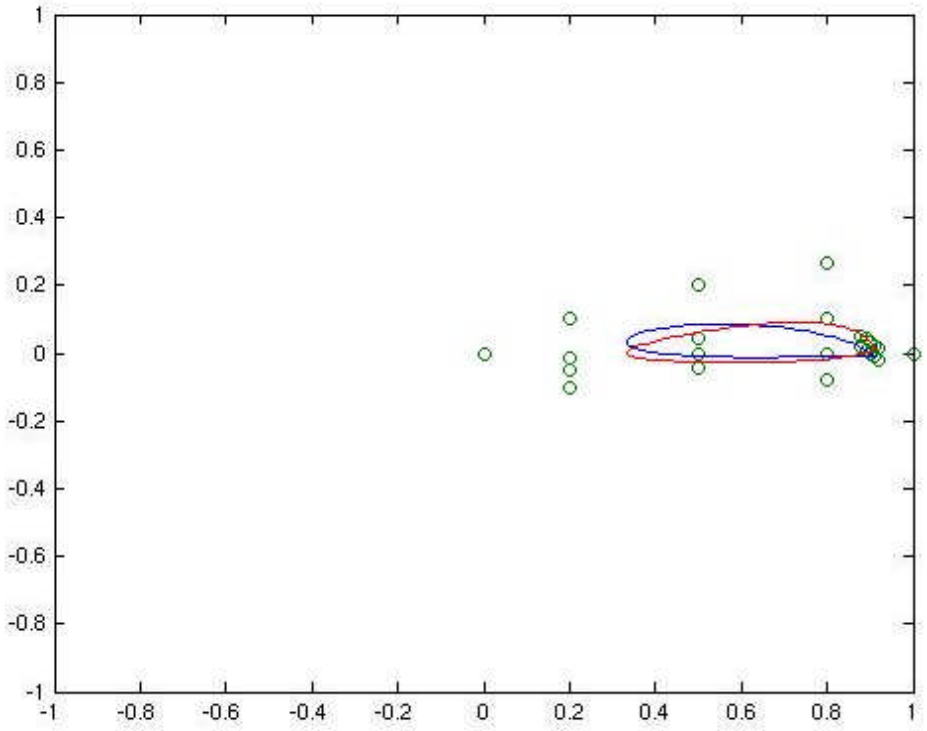

Figure 110: Optimum profile representation
after 600 initial sample points and 150 iterations.

Discussion

The results show that with increase numbers of initial sample points the estimated optimum profile becomes closer to the datum. This is as expected since an increased number of initial sample point should improve the accuracy of the Kriging meta model so that on the first pass, an improved optimum estimate should be produced. However, there is still a large variation between the estimated optimum and the real optimum (the datum) even with 600 initial sample points.

It is concluded that this is due to the limited controllability of the single Bezier curve. The single curve, with 7 design parameters has insufficient controllability to produce the desired curve. The effect of this is that each control point has little effect on the resultant profile and as a result, a large range is required for each point. This results in a large design space, despite the small number of design variables. The initial study demonstrated that 39,000 generations had to be made before the profile fell within a given tolerance of 0.2, demonstrating the requirement of the optimisation process. In this case, minimising the number of design variables has resulted in a loss of controllability, and an inefficient parameterisation method.

6.4.3 Cubic Spline parameterisation

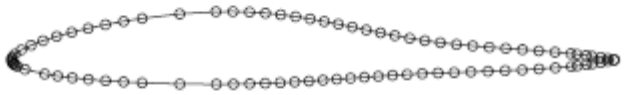

Figure 111: Airfoil representation by polynomial interpolation of a set of points
(Samareh 1999)

The cubic spline has been widely used as a method of airfoil parameterisation since it is simple to construct but retains the ability to produce complex shapes. Spline curves are also widely used in commercial CAD packages allowing for compatibility between off the shelf software and constructed optimisation and parameterisation procedures, an advantage for some applications. Using this method, coordinates are directly used to fit an airfoil shape, the points are then joined using interpolation methods *(Figure 111)*.

Song and Keane (2004) use B-spline interpolation of 34 control points to define an airfoil profile *(Figure 112)* where the y coordinates of the points are design variables while the chordwise coordinates are fixed. This method is compared to the approach

of using a set of numerically derived basis functions where only 5 design variables are involved. Their study compares both flexibility and robustness of each method and concludes that the B-spline approach is more accurate albeit with higher computational cost. The basis function approach produces less accurate results but overall is more efficient.

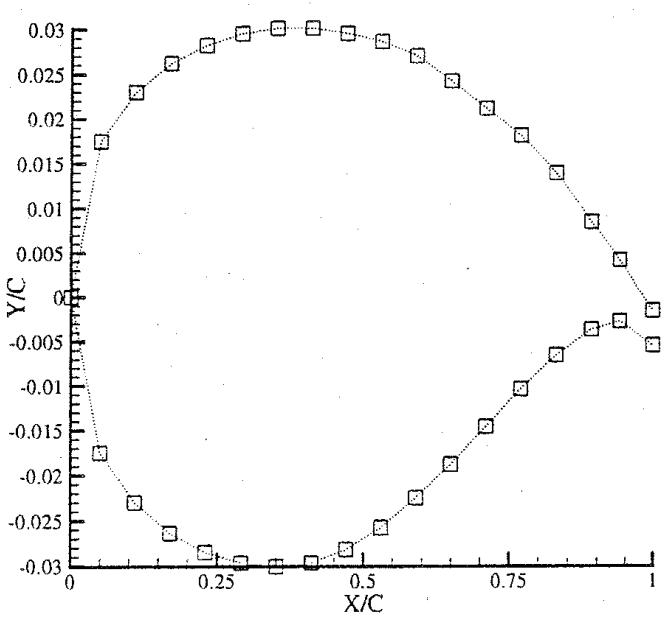

Figure 112: Airfoil parameterisation using B-spline interpolation of 34 control points (Song and Keane, 2004).

In Samareh's (1999) survey of shape parameterization techniques he refers to this method of parameterisation as the discrete approach where the boundary points between cubic spline segments are used as design variables. The benefits of this method are given as the ease of implementation and the ability to produce complex shapes since the only limit to the shape produced is the number of design variables used. Although for this reason, the number of design variables can become large resulting in high computational cost. With a high number of independent parameters, it is also difficult to maintain a smooth geometry and although methods can be taken to improve this, such as the use of multipoint constraints, this adds computational cost to the parameterisation method.

Since this method of parameterisation allows free movement of the airfoil profile without constraint by some type of numerical function, the resulting profile can be difficult to manufacture. This is mentioned by Braibant and Fleury (1983) who acknowledge the difficulty in imposing realistic constraints on the manufacturing feasibility of shape optimal designs. Overall, Samareh reports that the discrete method is well suited to 2D studies and that the main benefits of this parameterisation

approach are the local control, analytical sensitivity, short setup time and adaptable to existing grids/CAD software packages.

After an initial parameterisation methods review, Barrett (2007) decides on an interpolating segmented cubic polynomial spline for the benchmark airfoil parameterisation in their investigation. This benchmark method is compared to a method of using aerodynamic flow features of representing airfoil designs rather than geometry. Details of this approach are not discussed here but spline curves were chosen to represent the benchmark case based on evidence of accuracy and suitability to two dimensional study. *Figure 113* shows the parameterisation method used by Barrett to describe the airfoil. The airfoil profile is described by 11 data points which are interpolated by the curve resulting in 10 cubic spline segments. The x and z positioning of the data points are the design variables with some points being fixed in the x direction as can be seen in the diagram. These have been chosen based on the aim to maintaining the ability to produce smooth airfoil profiles while minimising the number of design variables.

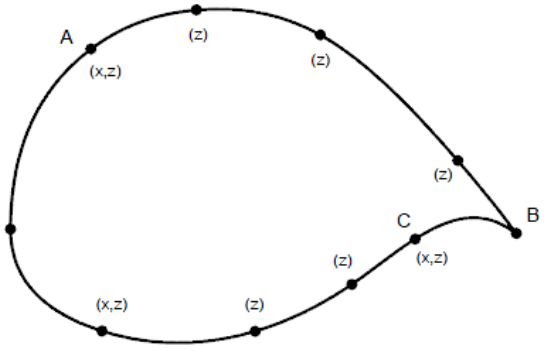

Figure 113: Benchmark airfoil parameterisation using polynomial splines with 13 variables (Barrett, 2007).

A slightly different approach was investigated by Sóbester and Kean (2007) and then later Sóbester and Barrett (2008) who explored the parameterisation of an airfoil using two Ferguson parametric splines, originally defined by Ferguson (1964). This method uses the magnitude and orientation of the tangent vectors to the spline curves to control the curvature of the airfoil. Since the vectors at the leading edge, T_A^{lower} and T_A^{upper} in *Figure 114*, will always be positioned vertically upwards and downwards respectively, this results in six design variables to define the airfoil. Sóbester and Barrett compare this method of airfoil parameterisation with two other parameterisation methods using B-Splines and Non-uniform Rational B-Splines (NURBS), both with minimum design variables. The study concludes that although the flexibility of this method is limited, it is still capable of producing a range of airfoil geometries with minimum design variables.

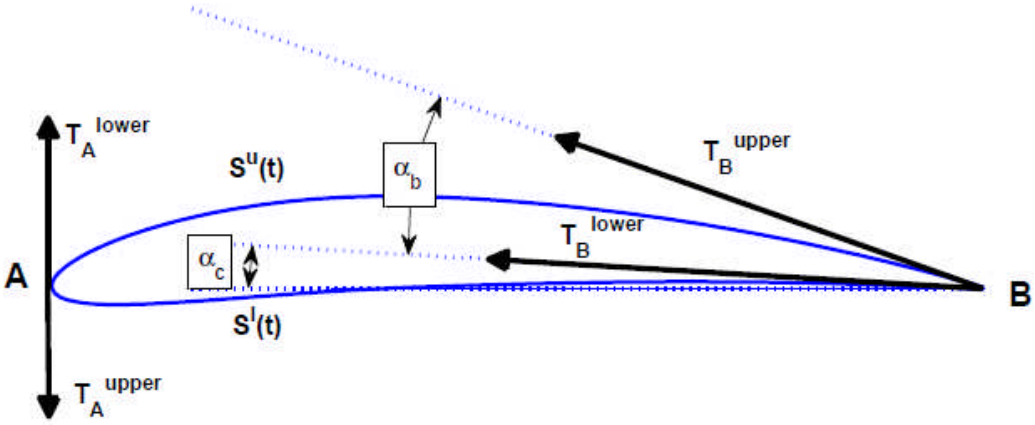

Figure 114: 6 variable cubic spline parameterisation using end conditions
(Sóbester and Barrett, 2008)

The examples given above demonstrate the suitability of cubic spline parameterisation for airfoil profiles. In numerous cases, this method has been employed in the literature for airfoil parameterisation for optimisation techniques. The main benefits of this method are given as the high accuracy achievable and the adaptability to complex shapes. Also, the high controllability and capability for local control. These benefits do come with the cost of the requirement for a large number of design variables, especially with complex shapes and along with this, the difficulty in ensuring smooth airfoil profiles and designs suitable for manufacture.

6.4.4 Conclusion

A general literature survey of profile parameterisation methods has been performed. This initial investigation highlighted the fact that the method of parameterisation used is highly dependent on the problem at hand. The underlying requirement is the need for an efficient parameterisation method which is ultimately a balance between flexibility, robustness and computational expense.

As a result of this initial investigation, three methods were chosen for further consideration however parameterisation using standard airfoil parameters was quickly deemed unsuitable. This method did not have the required flexibility to produce the unusual profiles anticipated for optimum bi-directional performance.

This left two parameterisation methods for investigation using either the Bezier parametric curve or the cubic spline. There is a large amount of literature on both methods and related content was analysed in order to assess the pros and cons of each and the suitability to guide vane parameterisation.

In the literature, Bezier curve based parameterisation methods have generally been used for global optimisation problems, particularly when objectives have been concerned with specific pressure distributions along airfoil profiles. These methods are well suited to this application where a low number of design variables are needed to have complete control over the curvature of the surface of an airfoil profile. Using this method, gentle curves are easily produced and there is no worry about creating irregular profiles as with the spline curve method. However, when this type of parameterisation method is used to produce precise geometries, the accuracy is reported as low, requiring an increased number of design variables, increasing complexity. It is evident that this parameterisation method is less well suited to this type of problem.

The investigation conducted by the author demonstrated the low accuracy of the Bezier curve method and with the small number of design variables used, the flexibility of the method was poor. The different weighting between end points and control point also added complexity to the process.

The spline curve parameterisation method demonstrates good accuracy for generating specific geometries and for local control but is less well suited to the production of airfoil surfaces where the objective is to produce a specific or optimum pressure distribution. This is due to the potential for irregular shapes to be produced. Measures can be taken to reduce this risk but again this adds complexity.

Each parameterisation method is suited to different applications and it can be seen that they could be used separately and in turn for a multi stage parameterisation process. This would involve performing an initial global optimisation using Bezier curve parameterisation and then performing more local optimisation using cubic spline methods. The bi-directional optimisation is concerned with the modification of an existing profile to produce geometry with optimum performance in reversing flows. It is anticipated that it is subtle changes to geometry that will improve performance in the reverse direction since the constraint of IGV operation is ever present for successful turbine operation. Taking this into account, the cubic spline curve method has been deemed more suitable for the task at hand.

6.5 Parameter Study

The datum guide vane profile was parameterised using two separate spline curves, one for the pressure surface and one for the suction surface each sharing a fixed point at the leading and trailing edge. End conditions were set to ensure continuity at the leading and trailing edge. At the leading edge this ensured that the spline end points were perpendicular to the incoming flow and equal and opposite.

The aim of this parameterisation process was to minimise the number of control points required to reproduce the original geometry while ensuring enough flexibility was maintained to allow for manipulation of the profile. The initial control point coordinates were taken from the original geometry and additional points were added until the reproduction of the datum geometry was satisfactory. Additional points were added to the aft-section of the suction surface since this is the area that was crucial to the performance of the IGV and the overall turning produced.

The final profile is described by 19 control points of which 9 are on the pressure surface and 10 are on the suction surface. This results in 19 spline curves describing the profile by interpolation between the points. Since the leading edge and trailing edge points are fixed, this gives the potential of 17 points being variable in either the x or y direction resulting in 34 design variables. It is not intended to vary all of the design variables at once, rather to fix the majority of the design variables and perform the optimisation process on a local area of the profile.

The objective of the optimisation procedure is to reduce the total pressure loss caused by the inlet and outlet guide vanes while meeting the turning requirement of the IGV. This is done by maintaining the same boundary conditions as the datum cases matched to the 3D CFD simulations earlier and modifying the guide vane profile geometry. Although the overall performance of the turbine is hard to predict accurately in this way, this method gives a direct comparison of the relative performance between guide vane geometries. This allows for a great many more CFD simulations to be performed within a given time than would be possible if the whole device was being simulated. Once the 2D optimisation has been conducted, the optimum profiles are compared with full scale 3D simulations to achieve an accurate performance prediction for the whole turbine device.

A parameter study was conducted to investigate the influence of varying the position of the control points on the pressure surface towards the trailing edge. As well as investigating the influence of individual parameters, the parameter study also presents the opportunity to test the capabilities of the meshing procedure.

During optimisation, each profile variation is meshed automatically using Turbogrid in batch mode. Since large variations in parameters are likely to present difficulties in automated meshing it is necessary to identify the limits of the meshing procedure so that the optimisation procedure runs smoothly without errors. The procedure can then be either adjusted to accommodate these higher variations or the parameter range can be reduced if the large deviation has an adverse effect on performance. This can be decided for each parameter and the geometry generation procedure is gradually made more robust as each parameter is analysed. The automated meshing procedure implemented uses the same process as for the MEGV optimisation so will not be repeated here.

6.5.1 Pressure surface trailing edge

The trailing edge of the guide vane profile has been identified as an area for potential performance improvement. In reverse flow, separation occurs at the trailing edge due to the poor angle of incidence with the flow exiting the rotor axially. Improvement has been demonstrated with the use of rounded trailing edge profiles over sharp trailing edges. This however is the extent to which the problem had been explored and it was expected that greater performance improvement could be achieved.

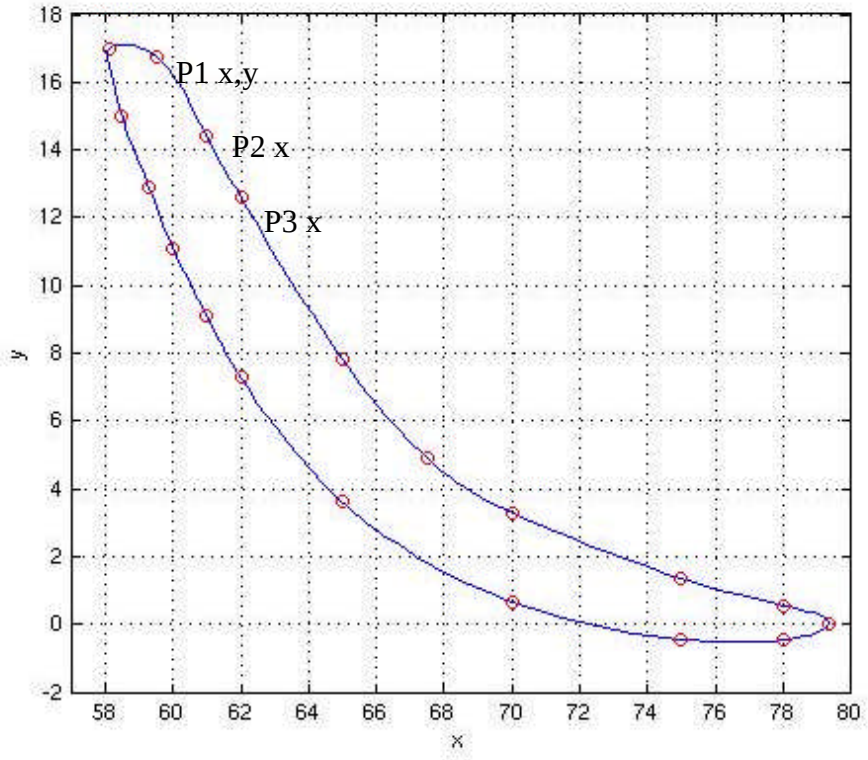

Figure 115: Datum profile parameterisation using spline curve, showing variable parameters.

Parameter	Min	Nom	Max	
P1x	59.0	59.5	64.5	cm
P1y	16.0	16.75	20.0	cm
P2x	60.0	61.0	67.0	cm
P3x	61.0	62.0	68.0	cm

Table 22: Parameter initial range and values.

The three control points, P1, P2 and P3 were investigated *(Figure 115).* Each control point was given an initial range and varied individually at equal intervals across the full range. P1 was variable in both the X and Y direction whereas P2 and P3 were varied only in the X direction. This produced 4 variables for investigation for this section of the guide vane profile. *Table 22* shows the initial range and values for each parameter. The profiles that were investigated are plotted in *Figure 116* below demonstrating the extent of the manipulation of the profile. For each profile variation, total pressure loss was measured across the IGV and OGV and the sum was recorded. The IGV turning angle at the exit to the stator row was also recorded, the results are presented below.

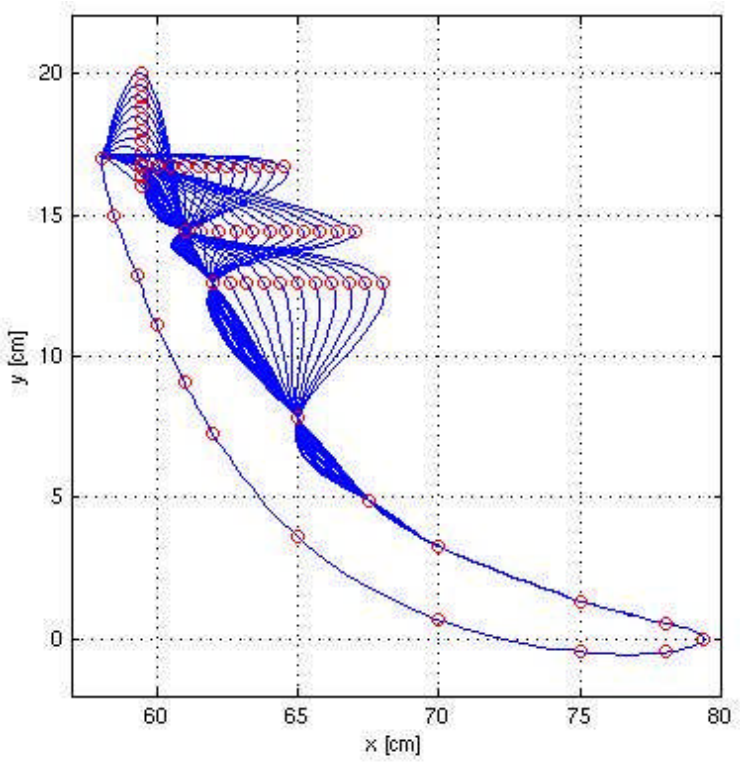

Figure 116: Pressure surface, trailing edge parameters investigated individually.

Results and discussion

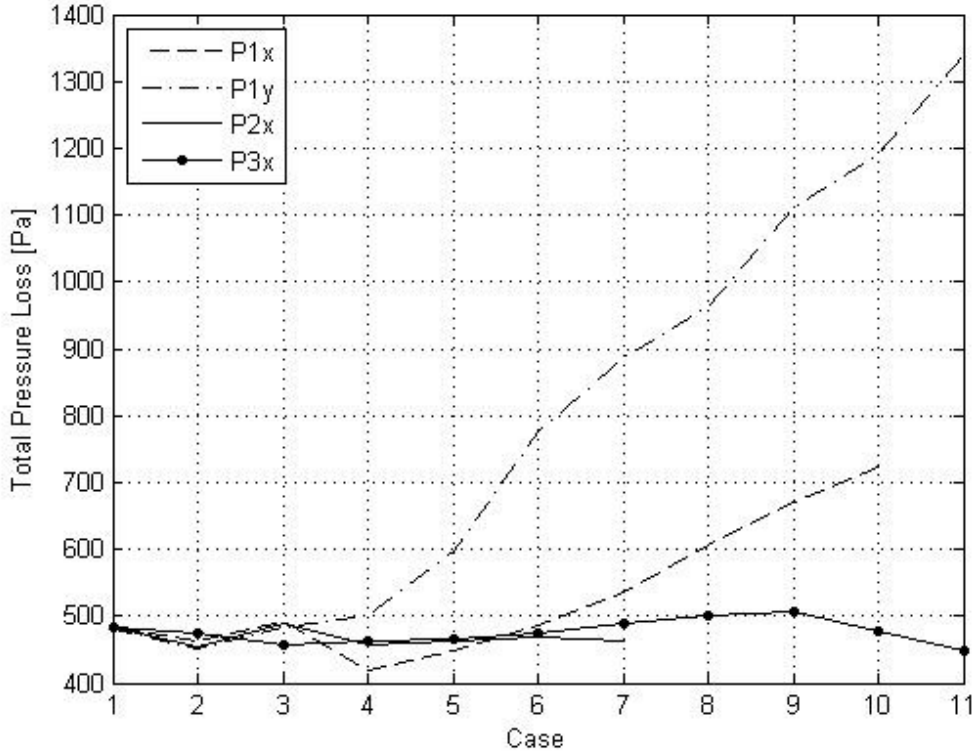

Figure 117: Plot of total pressure loss
across the full range of variation for each parameter.

Parameter	Min	Range	Max	
P1x	418.61	305.83	724.44	Pa
P1y	450.08	889.98	1340.06	Pa
P2x	453.46	34.85	488.31	Pa
P3x	447.85	59.77	507.62	Pa

Table 23: Range of total pressure for each variable parameter investigated.

The plot of total pressure loss for the variation of the parameters *(Figure 117)* shows the overall effect each of these parameters has on the profile performance. These values are also presented in *Table 23* above. The variation in flow angle at the exit of the IGV is plotted in *Figure 118* and the values displaying the range for each parameter are shown in *Table 24*. Overall, the variable parameter P1y has the largest effect on the total pressure loss across the guide vane rows. Increasing the value of this parameter has the effect of increasing the length of the trailing edge of the profile. This reduces the pitch of the stator row, effectively reducing the size of the passage for reverse flow over the OGV. For this reason, it is not surprising that the observed increase in total pressure occurs.

P1x has a smaller but still significant effect on total pressure loss with a range of 305.83 Pa. There was difficulty in the automated mesh production for the final case, case 11, of the investigation of the P1x parameter. At this value, when the parameter was varied towards the upper limit, the deformation of the geometry was too great for the scripted meshing procedure. This resulted in negative volumes within the mesh structure and as a result, the mesh was discarded. When this occurred, it presented the option to either modify the meshing procedure to accommodate this large amount of deformation or to reduce the range for this variable parameter. After examining the results, it was decided that reducing the range of this parameter was possible since increasing the value further seemed to increase the total pressure loss. Examining the plot of IGV turning angle also showed that with high values of P1x, the turning angle was above the desired 67.2º and was increasing. The high values of P2x, above case 7, also produced extreme geometries that were difficult to mesh and as a result, the range of this value was also reduced.

Overall, varying each of these parameters in turn had no beneficial effect on the total pressure loss across the guide vanes. The parameters closest to the trailing edge, P1x and P1y, had the largest influence on the total pressure loss whereas the parameters closer to the middle of the pressure surface had less effect. In terms of IGV turning angle, variation of the parameters in the x direction, increasing TET had a larger effect than variation of P1 in the y direction. It was decided to vary a number of parameters simultaneously to see if a more beneficial profile could be produced.

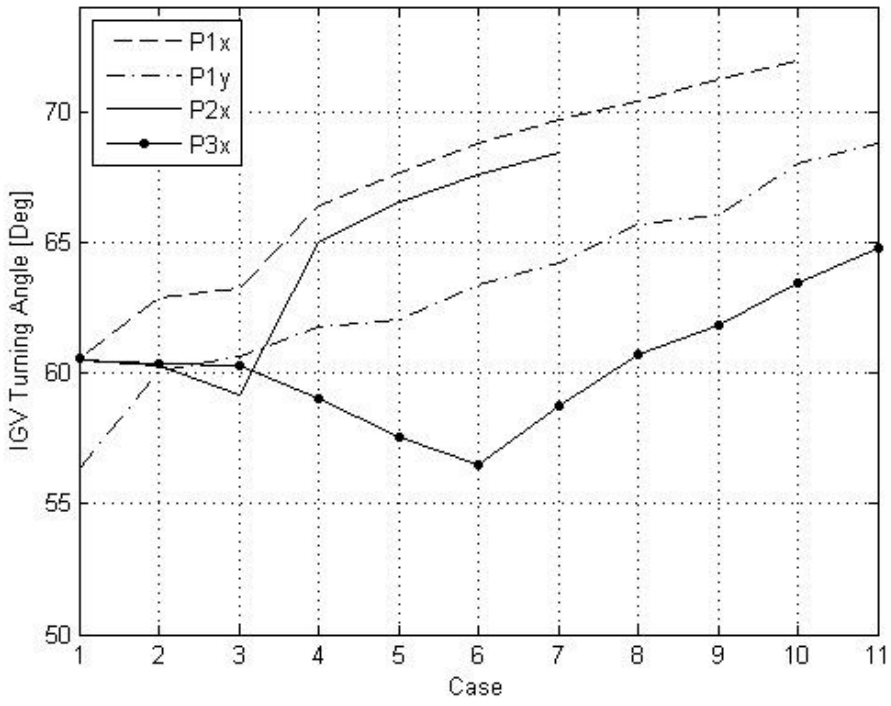

Figure 118: Plot of IGV exit flow angle
across the full range of variation for each parameter.

Parameter	Min	Range	Max	
P1x	60.53	11.41	71.94	Degrees
P1y	56.29	12.49	68.78	Degrees
P2x	59.17	9.28	68.45	Degrees
P3x	56.50	8.26	64.76	Degrees

Table 24: Range of IGV turning angle for each variable parameter investigated.

Trailing edge profile optimisation

The parameter study of the control points at the trailing edge demonstrated the effect of varying each parameter in turn has on the profile performance but did not demonstrate any significant improvement in terms of performance. To achieve greater variation of the trailing edge geometry it was decided to vary P1x and P1y simultaneously to test the theory that trailing edge modification could reduce the total pressure losses.

Using the information gathered from the parameter study, an optimisation procedure was set up after reducing the parameters in order to avoid meshing errors. The range used for each parameter is presented in *Table 25*.

Parameter	Min	Datum	Max
P1x	59.0	59.5	64.0
P1y	16.0	16.75	18.0

Table 25: Trailing edge control point parameter values.

A two variable optimisation process was conducted, starting with an initial design space of 21 sample points, distributed by a Halton sequence. The initial geometries investigated are shown in *Figure 119*, each one of these profiles was generated then meshed automatically using the pre-written script controlling Turbogrid in batch mode. As before, CFXPre was used for pre-processing and then the cases were solved using CFX. Each profile was post processed and a fitness value assigned based on performance, this data was then used to produce the Kriging estimate of the design space. The Kriging model was accepted as being valid as the root mean square error was less than 20%, no additional sample points needed to be added. *Figure 120* shows the Kriging estimate of the design space plotted as a contour plot, the black points show the initial sample points investigated.

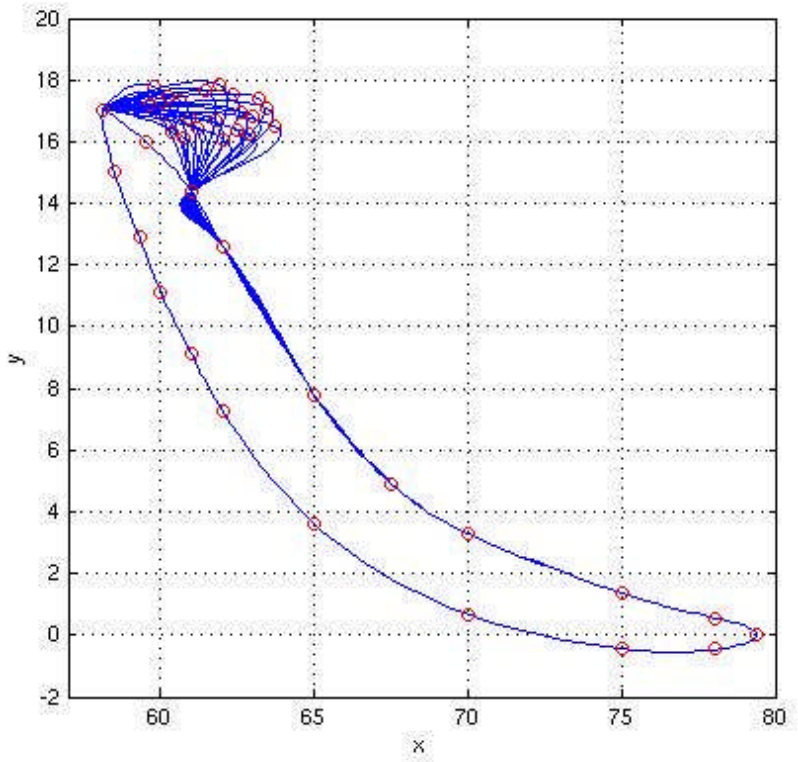

Figure 119: Initial sample points for 2 variable optimisation.

	Turning angle	Total Pressure Loss [Pa]			
	[º]	IGV	OGV	Total	Improvement
Datum	60.5	51.5	432.0	483.5	-
Optimum	64.3	67.2	342.0	409.2	15%

Table 26: 2 variable optimisation results with comparison to the datum values.

The optimum was predicted at P1x = 61.64 cm and P1y = 16.35 cm with a fitness value of 384.6 Pa. This optimum profile was produced and a CFD case was simulated to check the comparison with the predicted optimum and the performance prediction of the CFD. Values calculated from the CFD simulation are shown in *Table 26* with direct comparison to the datum profile. Predicted total pressure loss from the CFD case gave a value of 409.2 Pa, an error of 6.1% from the estimated optimum performance. Overall, the CFD results predict an improvement of 15% from the datum geometry with increased turning angle at the IGV.

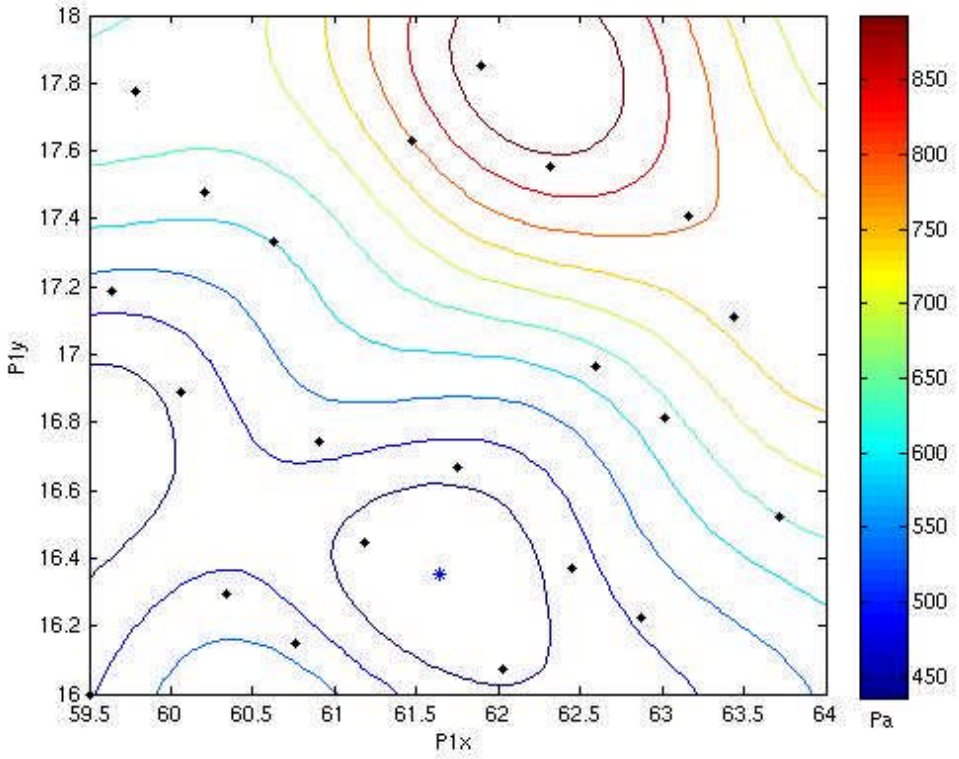

Figure 120: Kriging estimate of the response surface of two control points,
P1x and P1y varied at the pressure surface trailing edge.
Black points show initial sample points, blue star shows optimum.

These results produce the geometry shown in *Figure 121* where the optimum profile shape is plotted as well as the datum NGV profile. Here as well, the variation in the control point P1 can be seen.

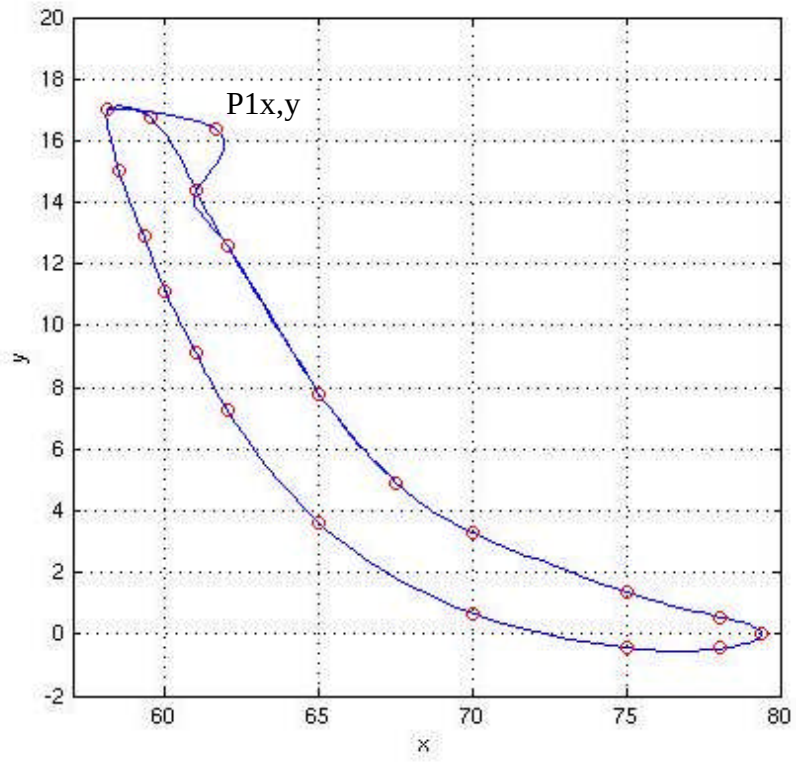

Figure 121: Plot of optimum profile compared with datum geometry.

Discussion

The optimisation process of the positioning of the P1 control point, close to the trailing edge of the guide vane profile has produced an unusual profile shape. The CFD simulations predict superior performance to the datum geometry but due to the unconventional profile, it is necessary to investigate the profile further. This has been done by first looking at the profile operating as an IGV and then examining the OGV performance, this examination is displayed below.

The flow across the IGV stator row can be visualised from the plot of total pressure shown in *Figure 122*. This compares the datum NGV profile with the optimum design using the same scale to plot total pressure. Two things are immediately obvious from the comparison, the higher operating pressure of the optimum profile and the increase in the size of the wake produced from the trailing edge. The higher operating total pressure suggests that the optimum profile cases a greater obstruction to the flow than the NGV profile. On closer inspection, the increased trailing edge thickness reduces the size of the gap between stators, this is the reason for the increase in obstruction and operating pressure.

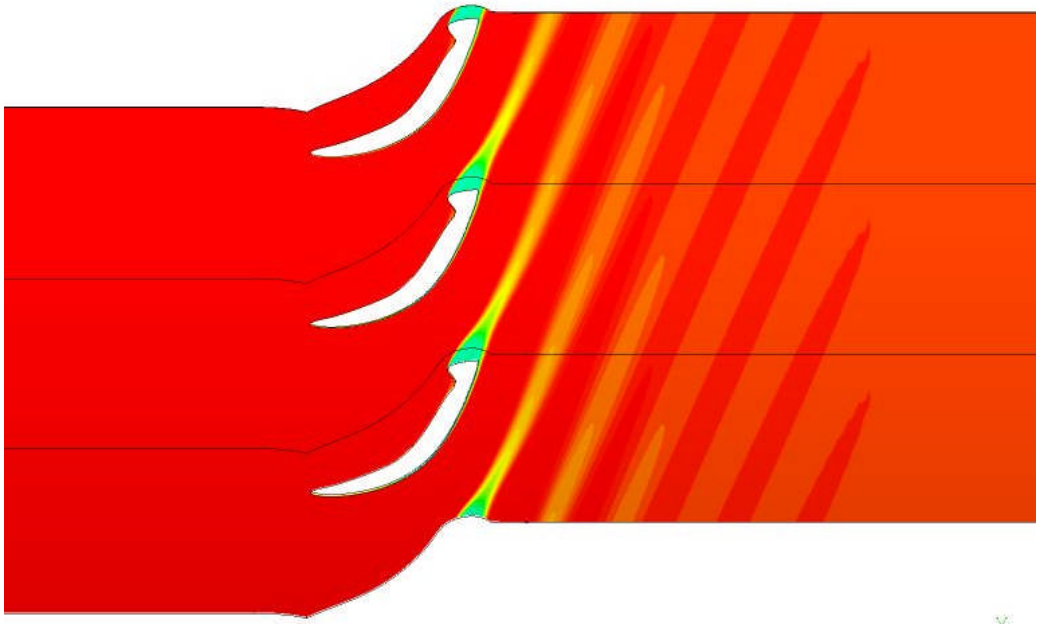

Optimum

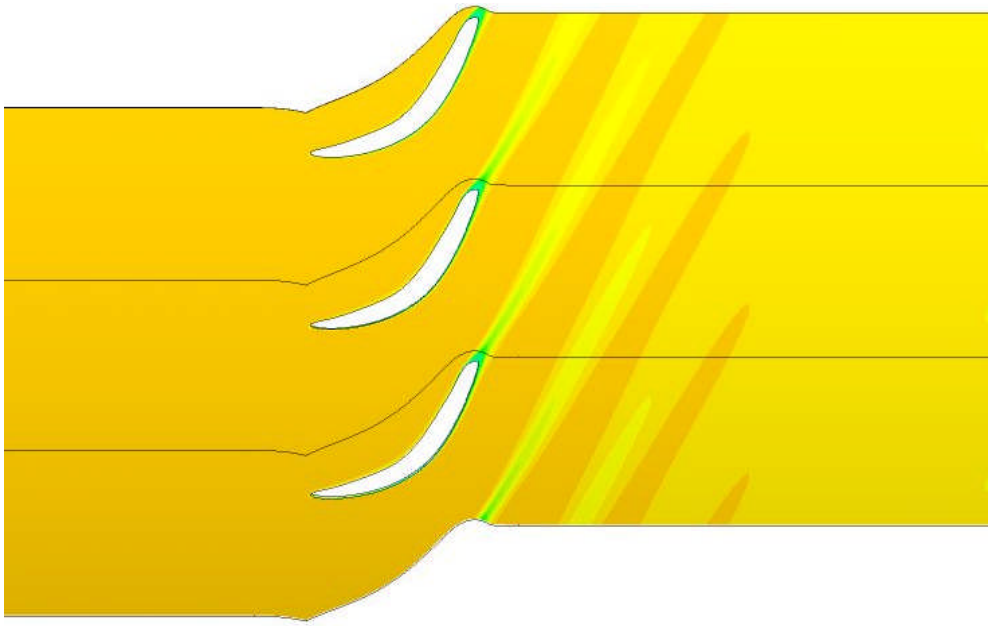

Datum

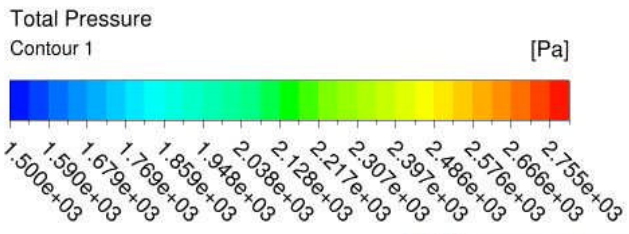

Figure 122: Plot of total pressure around IGV stator row
for Datum NGV and optimum profile presented with the same range.

The bulbous profile on the pressure surface at the trailing edge produces the increased turning angle since the flow separates from the trailing edge at the thickest point of the profile. This creates a large wake which changes the direction of the flow once it has left the surface of the profile, this results in the increased turning angle.

It is interesting that both an increase in IGV turning angle and a reduction of total pressure loss has been achieved by the modification of the trailing edge profile. Up until now, in the work presented in this thesis, increased turning angle has resulted in increased total pressure loss due to the added obstruction presented by a stator row designed to produce high turning. The addition of a raised section on the trailing edge appears to have changed that however it is unclear how this profile will react to a variation in flow rate.

Overall, the CFD plots show that the optimum profile performs less well than the datum geometry as an IGV resulting in higher obstruction and an increased wake. The positive effect does come from the increased turning angle however. Plot of pressure distribution, comparing the two profiles is presented in *Figure 123*.

The pressure at the suction surface of the optimum profile closely follows that of the datum profile since the geometry in unmodified in this area. Towards the trailing edge of the suction surface, the area of separation on the optimum profile can be seen by the harsh pressure gradient on the blade loading plot. This results in a lower pressure coefficient on the pressure surface before the pressure becomes similar again between the two profiles at the fore section of the pressure surface.

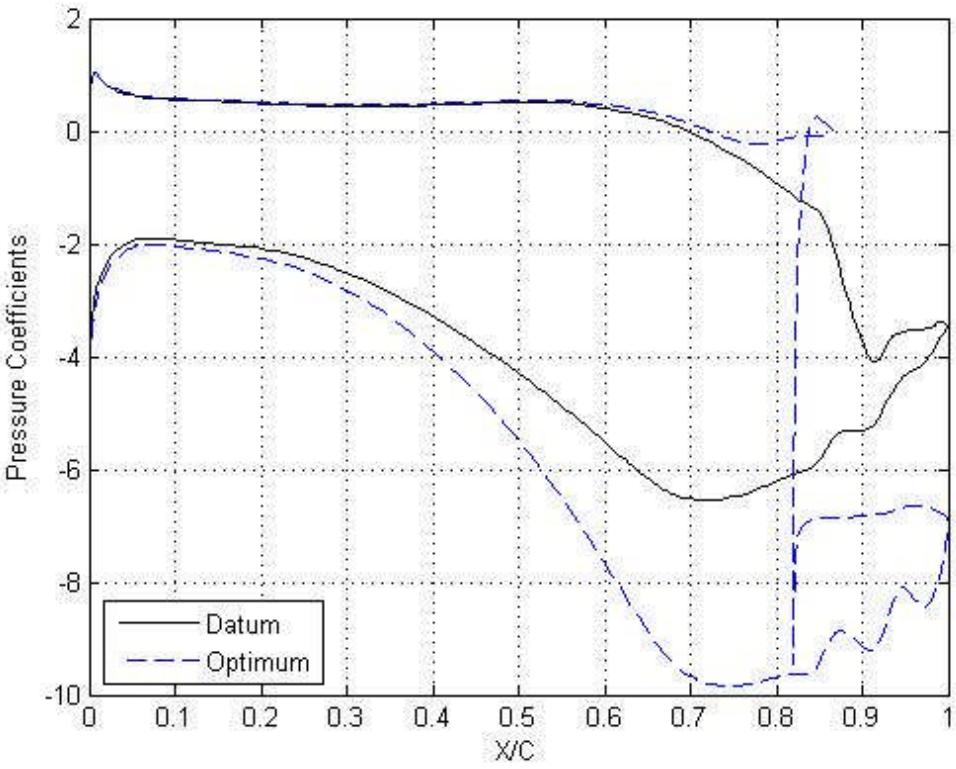

Figure 123: Datum and optimised profile pressure distribution

Plotted streamlines show the behaviour of the flow at the trailing edge of the profile, presented as a direct comparison between the optimum profile and the datum *(Figure 124).* Both plots are coloured by fluid velocity using the same scale. The wake produced as a result of the increased trailing edge thickness can be seen as well as the recirculation that occurs in this area of low pressure. The area upstream of the trailing edge raised section on the pressure surface is also of interest and the plot shows that the fluid velocity slows in this region but there is no recirculation. Overall, fluid velocity increases past the bulbous trailing edge along with the flow angle as discussed earlier.

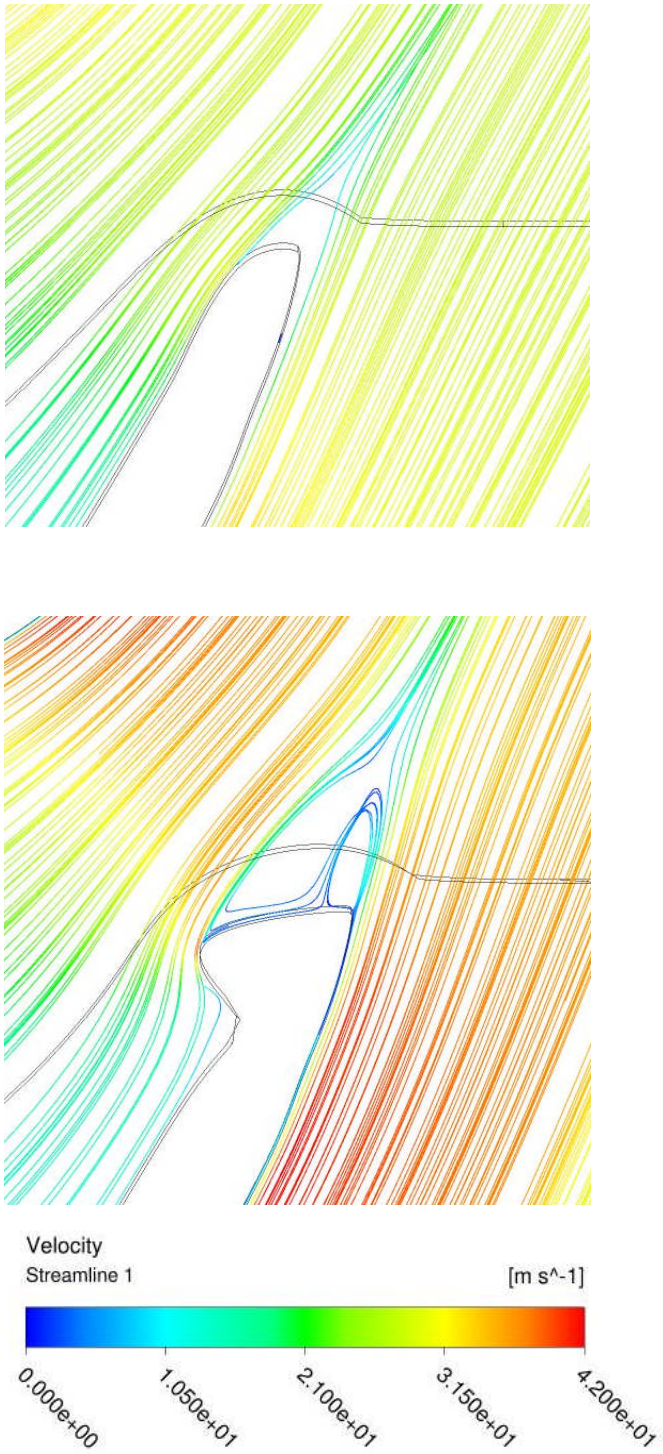

Figure 124: Velocity streamlines of flow at trailing edge
of optimum profile and NGV profile, streamlines coloured by velocity.

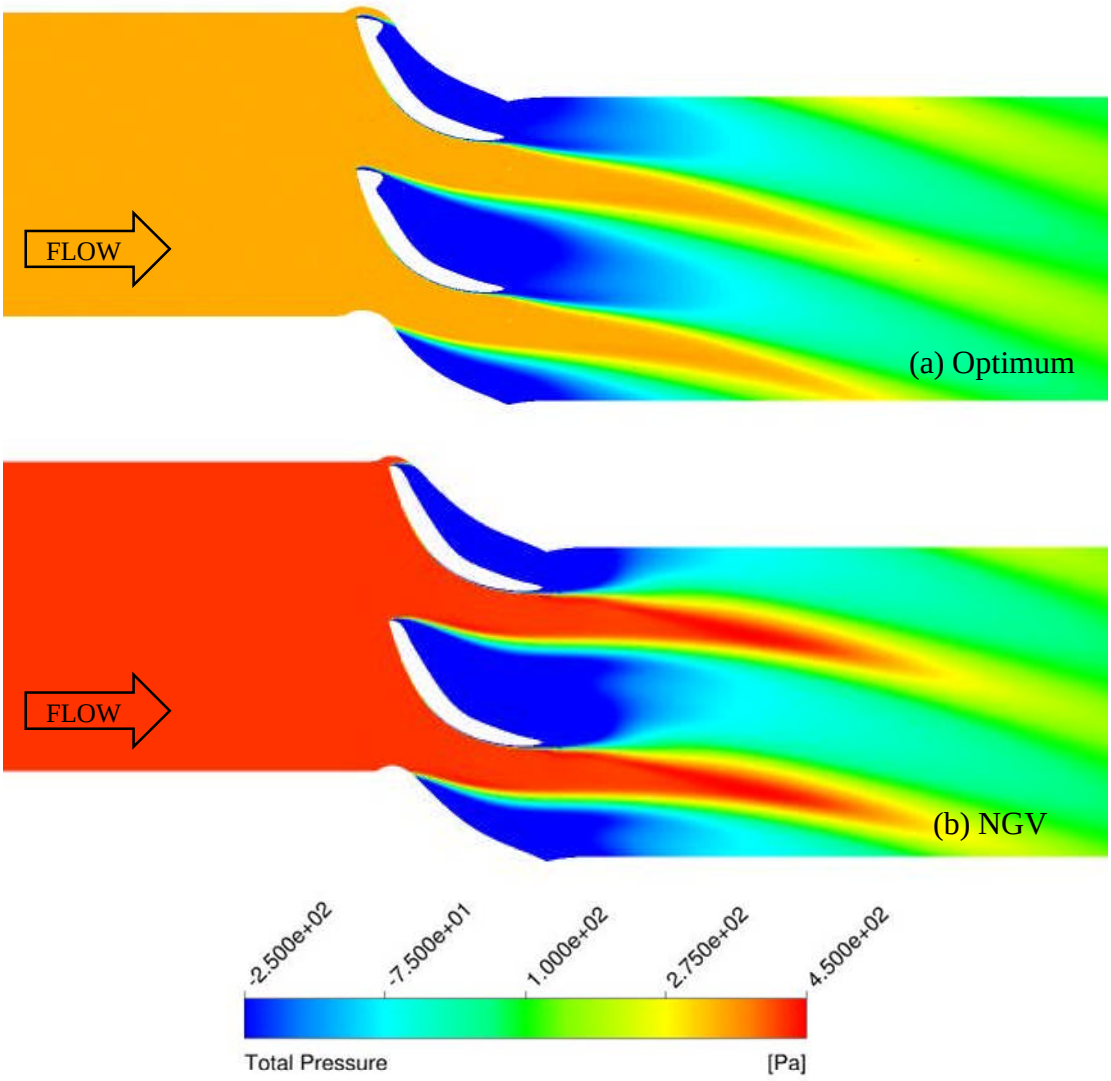

Figure 125: Total pressure contour plot of flow around OGV
for Optimum profile and datum NGV.

A plot of total pressure around the OGV of the optimum geometry is shown in *Figure 125* with the datum NGV profile shown for comparison. The same pressure range is used for each plot and it can be seen that the pressure upstream of the NGV profile is higher than for the optimum profile. This indicates a reduced obstruction at the OGV stator row with the optimum profile. Examining the trailing edge, it appears that the wake produced by the NGV profile is wider than for the optimum profile due to the trailing edge geometry affecting the way the flow passes the tip of the profile. The thicker trailing edge, draws the flow around the trailing edge more successfully, resulting in a wider flow stream and reduced obstruction.

Comparing the pressure distribution around the OGV profiles (*Figure 126)* shows that the fore section of the trailing edge behaves in a similar way despite the variation in operating pressure across the two profiles. Overall, the optimum profile operates at a higher pressure coefficient than the datum geometry.

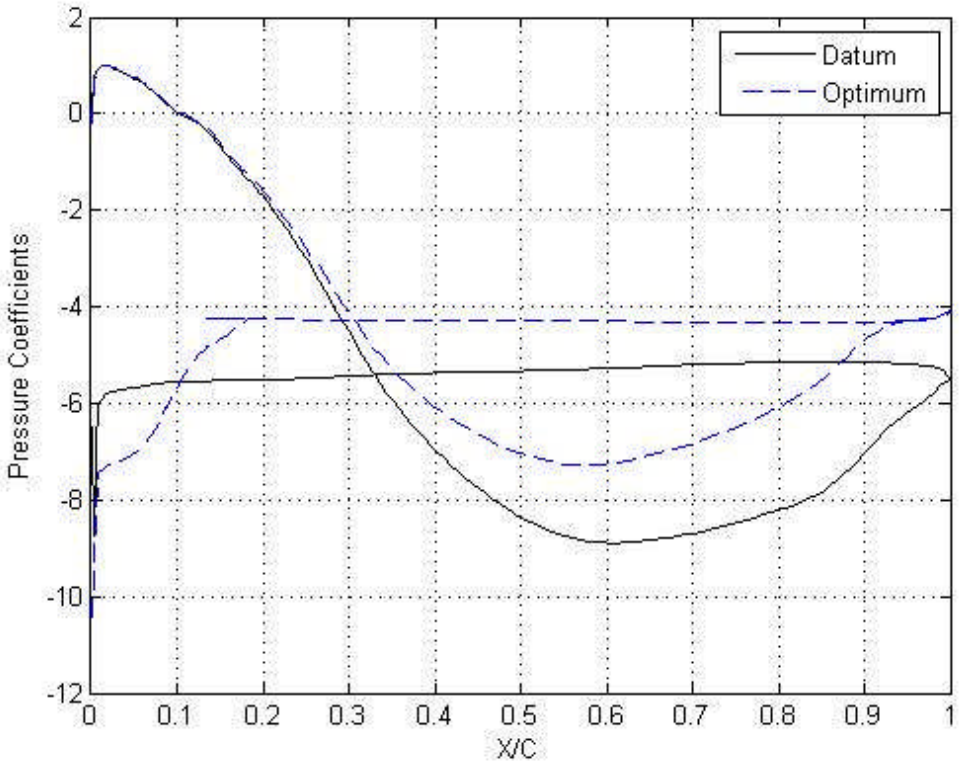

Figure 126: OGV pressure distribution comparison.

The plots of stream lines coloured by velocity *(Figure 127)* demonstrate the behaviour of the flow past the OGV stator row and in the area of low pressure downstream. It can be seen that two re-circulation zones are present in the wake of the datum profile whereas one larger recirculation zone can be seen in the wake of the optimum profile. Comparing the velocity through the nozzle between stator profiles, it can be seen that the flow velocity is reduced past the optimum profile. It also appears that the flow stream passing through the passage between stators is wider for the optimum profile despite identical stator count and hence pitch.

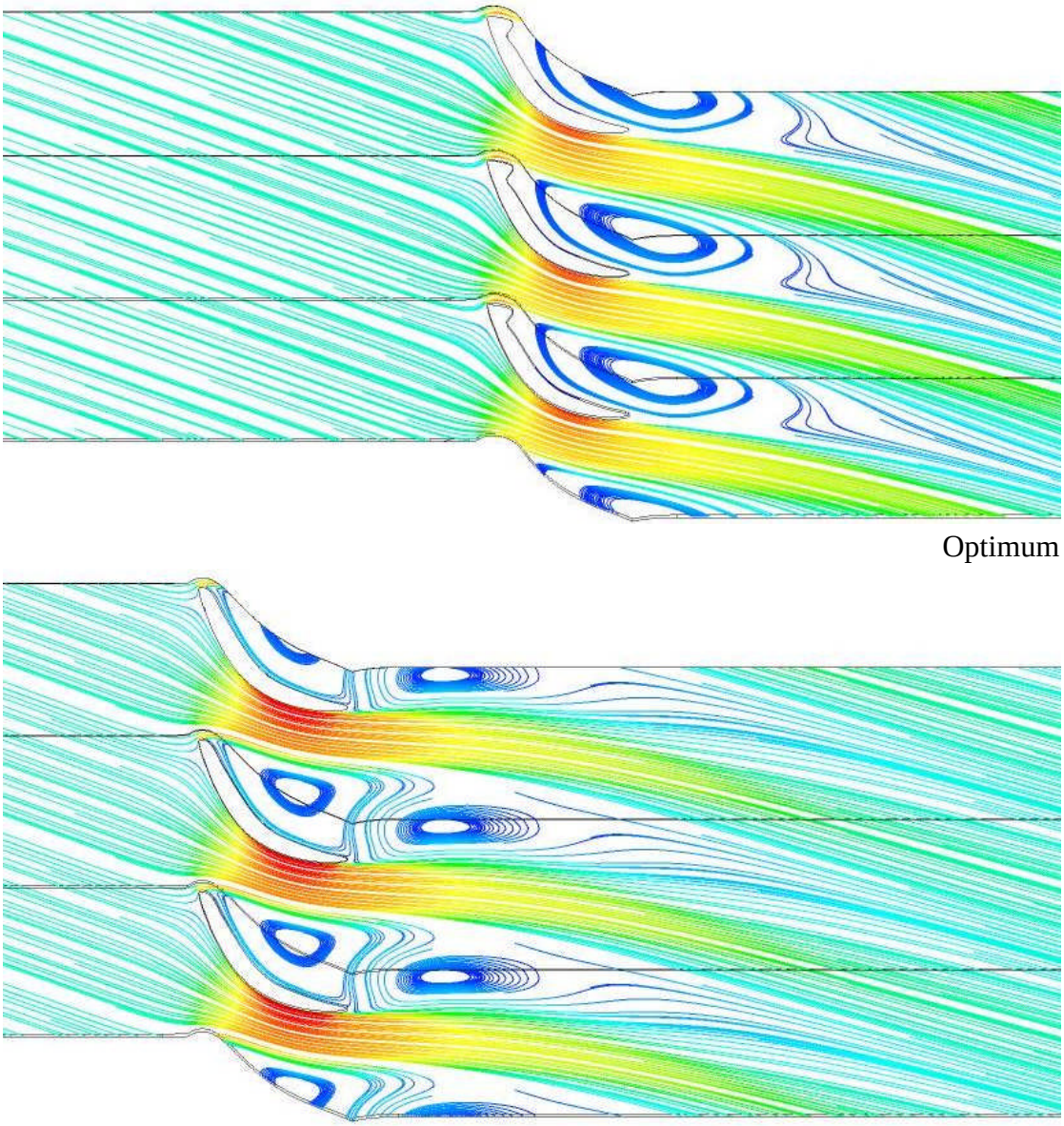

Figure 127: Comparison plot of streamlines coloured by velocity for OGV stator row.

Examining the flow behaviour around the trailing edge more closely *(Figure 128)* shows that the increased trailing edge thickness has a beneficial effect on the reverse flow around the trailing edge. In both cases, the flow impinges on the aft section of the trailing suction surface at the same point due to the incoming flow angle. This

creates a high pressure point and the flow splits to either travel around the profile via the suction surface or via the pressure surface. The air that takes the route past the pressure surface flows around the trailing edge of the profile. At the trailing edge of the datum profile, the flow separates from the surface as it passes the trailing edge and the wake is formed. At the thicker trailing edge of the optimum profile, the flow passes the trailing edge point and remains attached to the bulbous trailing edge profile. It can be seen from the streamline plot that this delays the separation of the flow from the surface of the stator, allowing the flow to pass around the trailing edge more easily, resulting in a lower flow velocity and reduced wake size.

Overall, measured performance shows a 15% reduction in total pressure loss for the optimum profile in comparison to the datum geometry. Examination of the CFD results show the reason for this improvement and despite the unconventional profile, IGV function is acceptable despite slightly reduced effectiveness. OGV performance is superior to the datum geometry and as a result, combined performance shows an improvement. This is a promising result from small profile variation and demonstrates the potential for further performance improvements from unconventional profile shapes found using bi-directional optimisation.

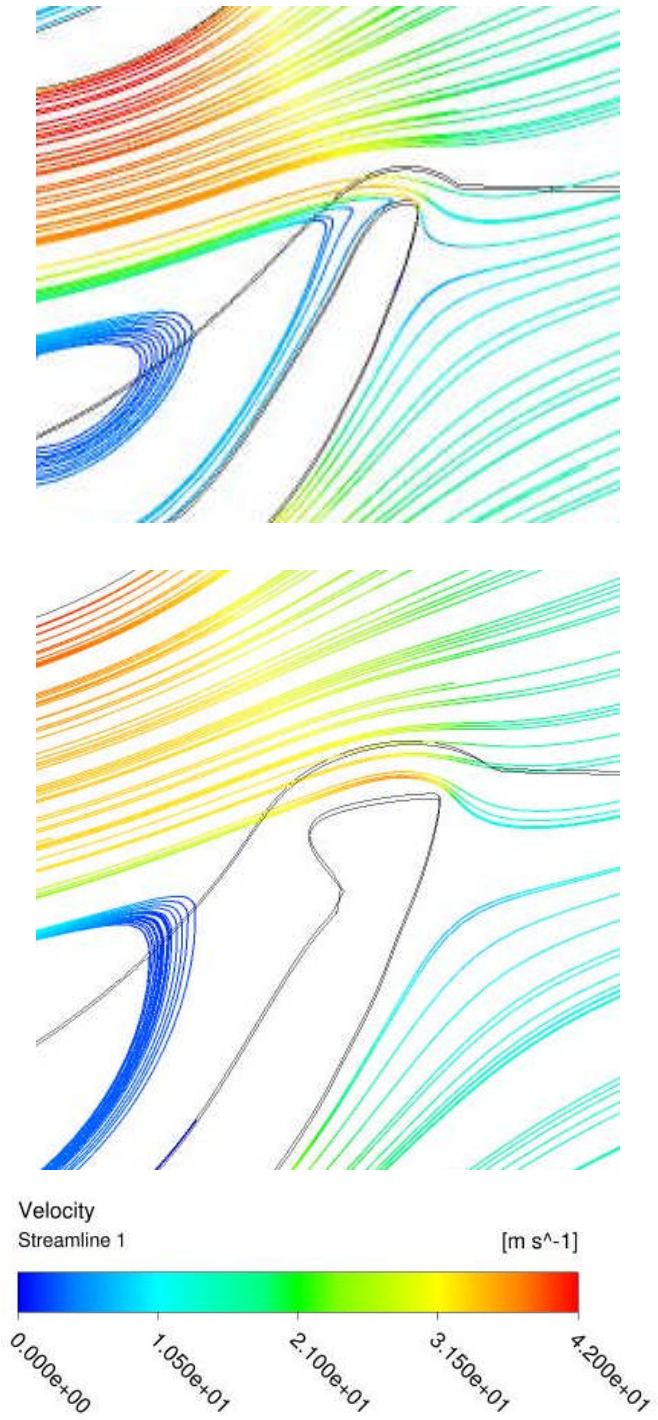

Figure 128: Plot of streamlines showing flow around profile trailing edge in the reverse direction. Streamlines coloured by velocity.

6.6 Global Optimisation

Based on the success of the two variable optimisation conducted above, it was decided to conduct a further optimisation process incorporating all 4 variable parameters that had been investigated previously. Free movement of all of these parameters simultaneously allows greater flexibility of the profile not just in the trailing edge section of the profile but the complete aft section of the pressure surface.

Parameter	Min	Nom	Max	
P1x	59.0	59.5	64.0	cm
P1y	16.0	16.75	18.0	cm
P2x	60.0	61.0	64.6	cm
P3x	61.0	62.0	68.0	cm

Table 27: Variable Parameter range and limit values.

Initially 41 sample points were generated using the Halton sequence to distribute these sample points evenly within the design space. The design space was bound by the variable parameter limits shown in *Table 27*, the limits that had been decided on based on the parameter study investigated earlier.

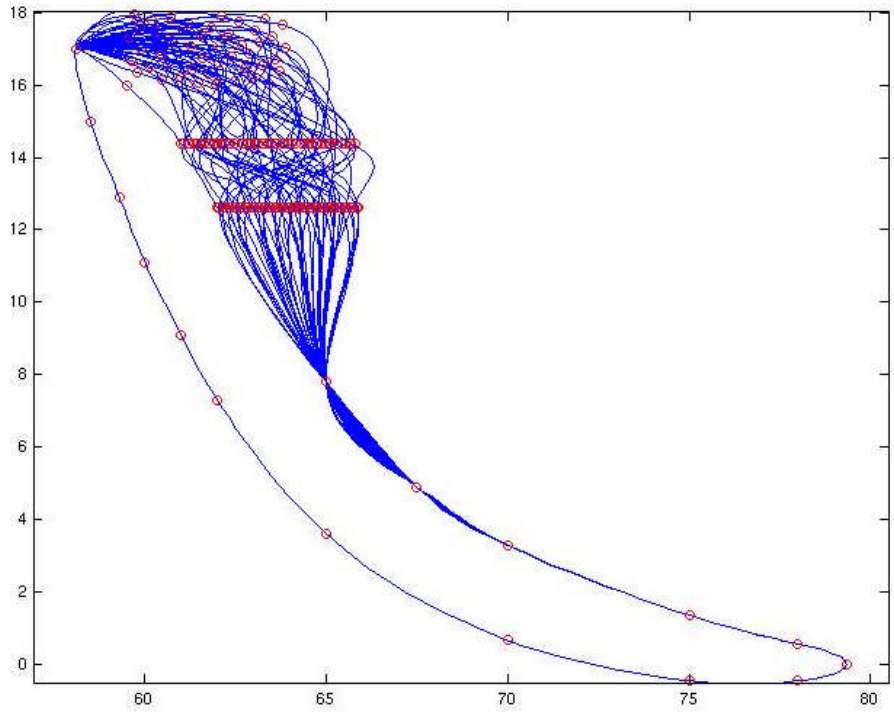

Figure 129: Initial geometry variation for 4 variable optimisation.

Each of these generated sample points within the design space described a different combination of control point locations. These control point locations were used to generate the profile geometry using the spline script written in Matlab. Each of these geometries was then generated and used to construct a meshed domain for CFD analysis. *Figure 129* is a plot of each of these initial geometries, demonstrating the range of geometries that are simulated in the initial search of the design space.

Parameter	Datum	Optimum
P1x	59.5	61.2
P1y	16.75	16.8
P2x	61.0	64.4
P3x	62.0	63.1

Table 28: Optimum geometry parameter values.

Each of the CFD cases was simulated and post processed and a fitness value was assigned to each sample point based on the performance of that geometry variation. These values were used to construct the Kriging estimate of the design space. An additional 9 sample points were added to the design space and further geometry variations produced and CFD simulations. On addition of the fitness values of these additional points to the Kriging model, the cross validation error was less than 20% so the model was deemed acceptable. The optimum values for the variable control points are shown in *Table 28* with the optimiser predicting an optimum fitness value of 346.1 Pa. The geometry was generated using these control point coordinates resulting in the profile in *Figure 130*. This profile had a predicted total pressure loss of 354.3 Pa according to the CFD results, an error of 2.3% from the predicted optimum.

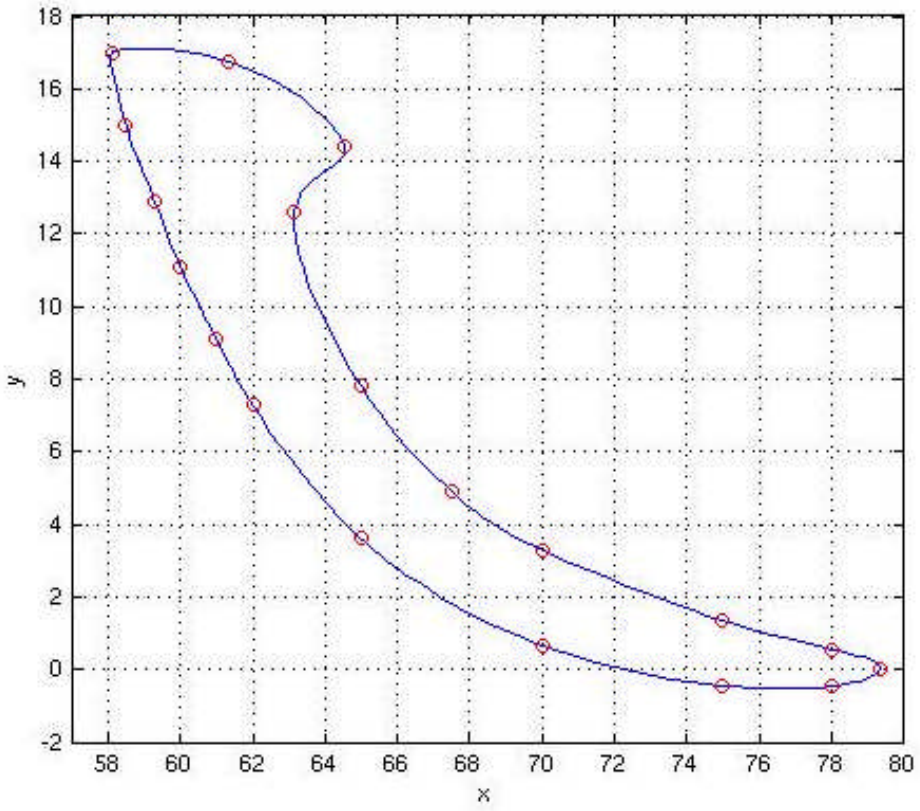

Figure 130: Optimum profile showing control points in red.

The result of this optimisation of the trailing edge section of the pressure surface has resulted in a highly unusual profile with the 2D CFD predicting a 26.7% reduction in total pressure loss across the guide vane rows when compared with the NGV datum geometry. A direct comparison between the performance of the two geometries is presented in *Table 29* along with a breakdown of the total pressure loss across the IGV and OGV. The turning angle at the exit to the stator row is also presented.

	Turning angle	**Total Pressure Loss [Pa]**			
	[º]	**IGV**	**OGV**	**Total**	**Improvement**
Datum	60.5	51.5	432.0	483.5	-
Optimum	67.2	92.9	261.4	354.3	26.7%

Table 29: 4 variable optimisation results with comparison to the datum values.

The results show that the performance of the IGV is poor compared with the datum geometry with increased total pressure loss over the IGV stator row. However, the superior performance of the OGV with dramatically reduced total pressure loss means that overall, a significant reduction in total pressure loss is achieved. The turning angle at the exit of the IGV stator row has increased by 6.7º to 67.2º due to the variation in the trailing edge geometry and it is likely that this is contributing to the increased total pressure loss across the IGV. Simulation of the datum turbine has

shown that the turbine performance is less sensitive to an increase in inlet flow angle than it is to a reduced angle. The increased inlet angle was thought to be acceptable at this point considering the reduction in total pressure loss being achieved. The full effect on power transfer to the turbine was examined when full 3D CFD simulations of the geometry were performed. These are discussed in the next section.

At this point the 2D simulations of the optimum profile were examined to investigate the performance of this highly unusual profile. The first thing to be considered was the performance of the IGV with the bulbous trailing edge and the effect this had on the flow downstream of the stator row. It was also necessary to examine the OGV and establish the reason for the significant reduction in total pressure. It was hoped that examination of the geometry in this way would demonstrate the reason that the optimisation procedure had converged on this final profile.

6.6.1 Optimum inlet guide vane

A plot of total pressure around the IGV stator row is shown in *Figure 131*, presented next to the datum geometry for comparison. The larger wake produced by the trailing edge can be seen along with increased flow angle downstream of the stator row, this can be seen by the angle of the wake. As before, in the results for the two variable optimisation, the increased trailing edge thickness has reduced the passage between the stators and this has resulted in a higher operating total pressure across the stators. This, combined with the increased turning angle accounts for the increase in total pressure across the optimum IGV compared to the datum.

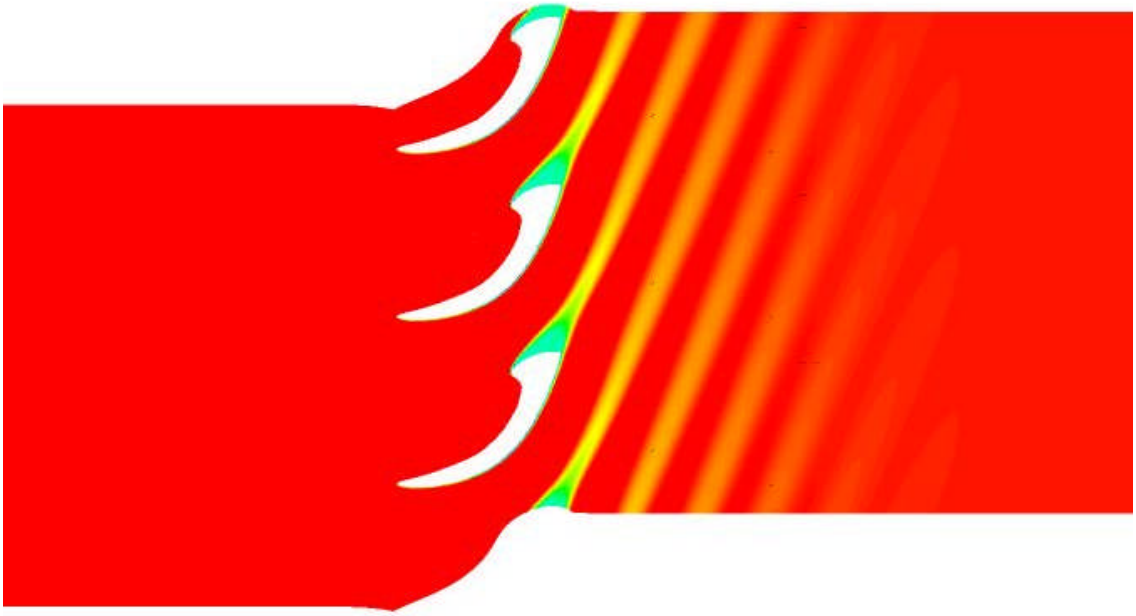

Optimum

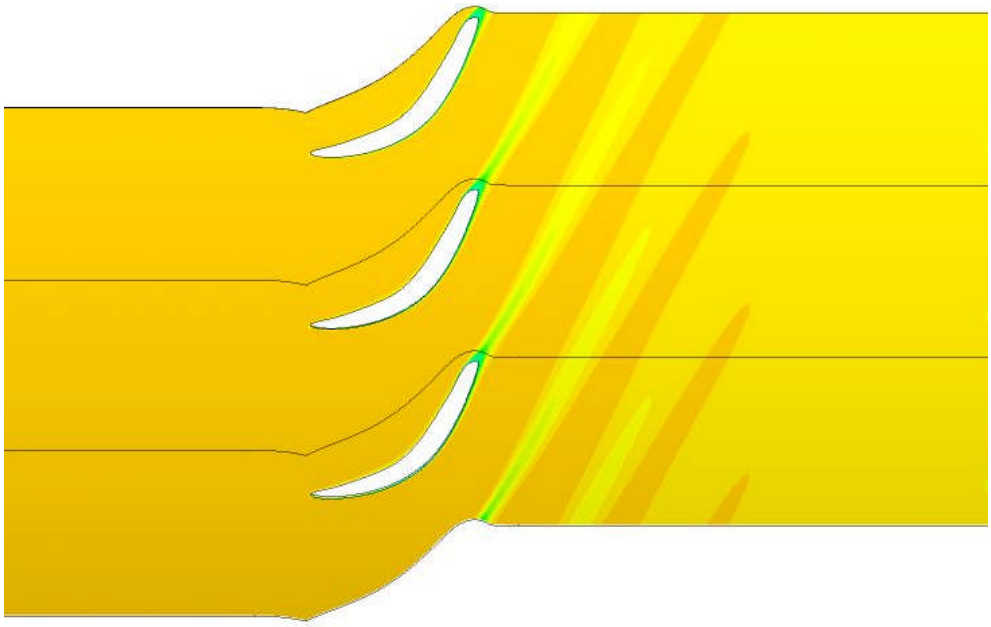

Datum

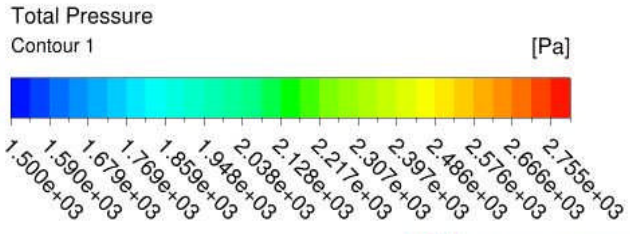

Figure 131: Plot of total pressure around IGV stator row for Datum NGV and optimum profile presented with the same range.

Initial observation of the optimum profile gave rise to concern over the flow around the bulbous trailing edge of the IGV. *Figure 132* shows a plot of streamlines of the flow around the bulbous trailing edge, coloured by flow velocity. It can be seen that air flowing along the pressure surface flows around the bulbous profile without any recirculation occurring (a). The flow then separates from the profile at (b) and the wake is formed with recirculation occurring within the area of low pressure. This area of low pressure also has an effect on the flow leaving the suction surface at the trailing edge. As the flow leaves the suction surface, the flow stream is drawn towards the low pressure region, reducing the deviation from the profile and hence increasing the turning effect. The two flow streams then meet further downstream where a constant exit angle is maintained.

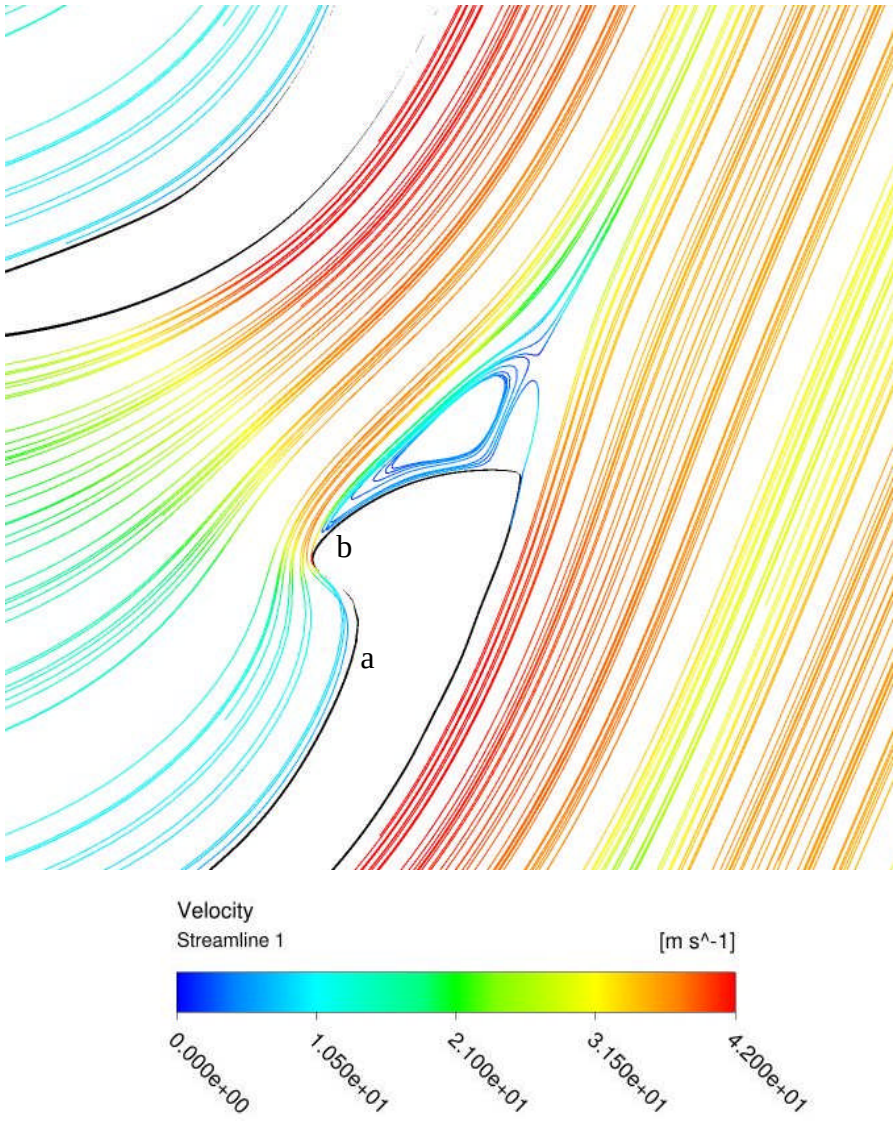

Figure 132: Plot of flow streamlines around bulbous trailing edge of IGV, coloured by velocity

A plot of total pressure around the OGV is shown in *Figure 133* with the datum geometry presented for direct comparison. The same scale is used to present both profiles and the reduction in total pressure upstream of the stator row can be seen for the optimum profile compared to the datum. The fluid stream passing between the stators is noticeably wider for the optimum stator row and it can be seen that this is a result of the trailing edge profile.

When the flow passes the thin trailing edge of the datum profile, the flow separates and a wide wake is produced. This is not the case for the optimum profile where the bulbous trailing edge accepts the flow stream as it passes. The flow remains attached for the majority of the bulbous section and this has the effect of reducing the size of the wake as well as drawing more fluid around the trailing edge through the gap between the stators. The plot of total pressure shows that this has the effect of reducing the build-up of pressure upstream of the stator row hence reducing the obstruction of the OGV.

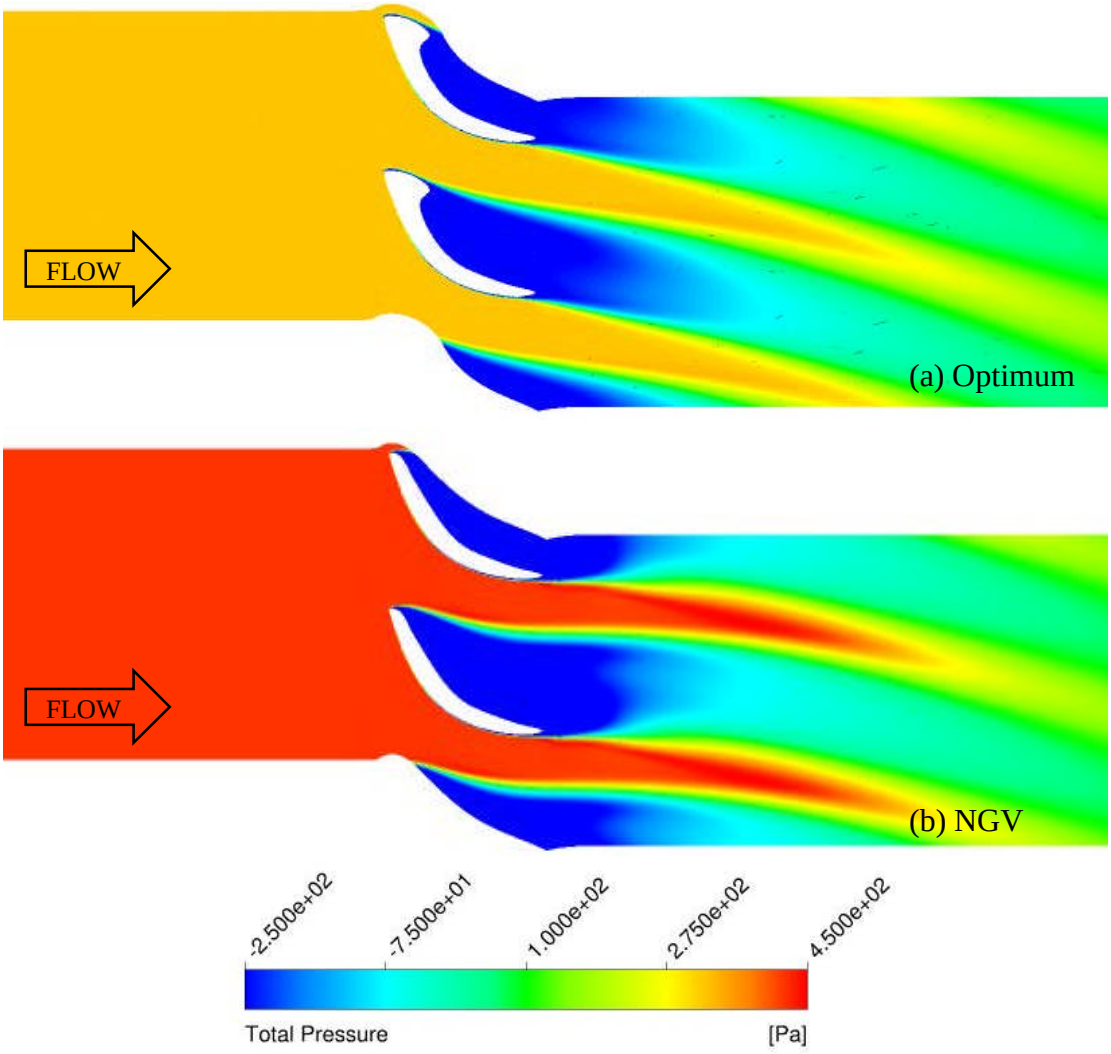

Figure 133: Total pressure contour plot of flow around OGV for Optimum profile and datum NGV.

A plot of streamlines, coloured by flow velocity, around the OGV stator row is shown in *Figure 134*. This represents the CFD estimate of the fluid behaviour at a specific time interval in the transient simulation. The recirculation within the wake can be seen as well as the beneficial interaction of the fluid stream with the bulbous trailing edge.

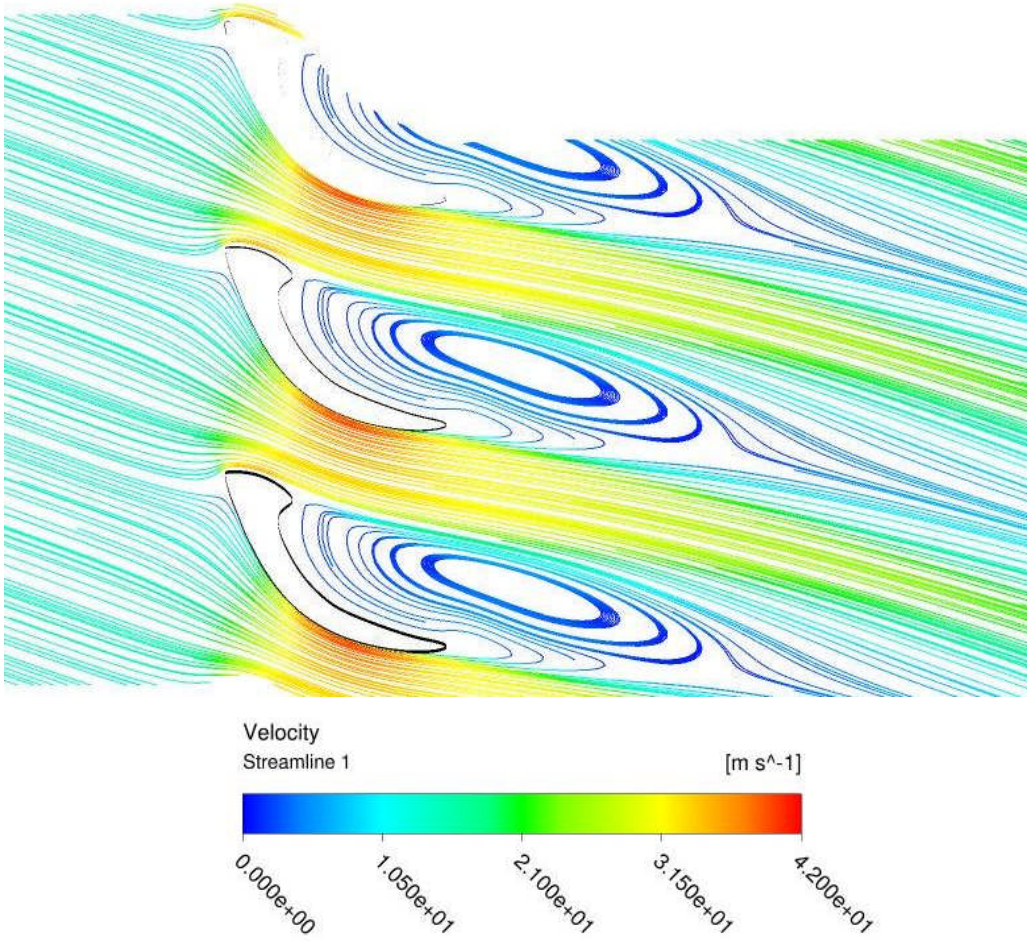

Figure 134: Plot of streamlines, coloured by velocity, showing flow across OGV stator row.

The 4 variable optimisation of the aft section of the pressure surface of the guide vane profile has demonstrated significant performance improvement as well as a truly unique bi-directional profile. Examination of the 2D CFD results demonstrate why this profile performs well in reversing flow and it can be seen why the geometry manipulation has ended in this way for these flow conditions. However, these 2D CFD simulations are a representation of the flow within the full turbine and it is necessary to simulate the optimum geometry in 3D in order to improve the validity of this performance prediction. Also, the optimisation procedure and the optimum simulations above have all been performed at the design condition with a value of 2500 Pa total pressure at inlet. The next stage is to examine the performance of the optimum geometry across a range of flow rates, this is presented in the following section.

6.7 3D Comparison

To provide a direct comparison between the optimum geometry and the datum, a full 3D CFD case was set up. All geometry, boundary conditions and mesh densities were kept the same, the only difference between these cases was the guide vane geometry. In order to produce a full turbine characteristic, the same range of flows was used for the boundary conditions as had been used for the 3D NGV geometry simulations and the Ct14b geometry simulations of the datum turbine.

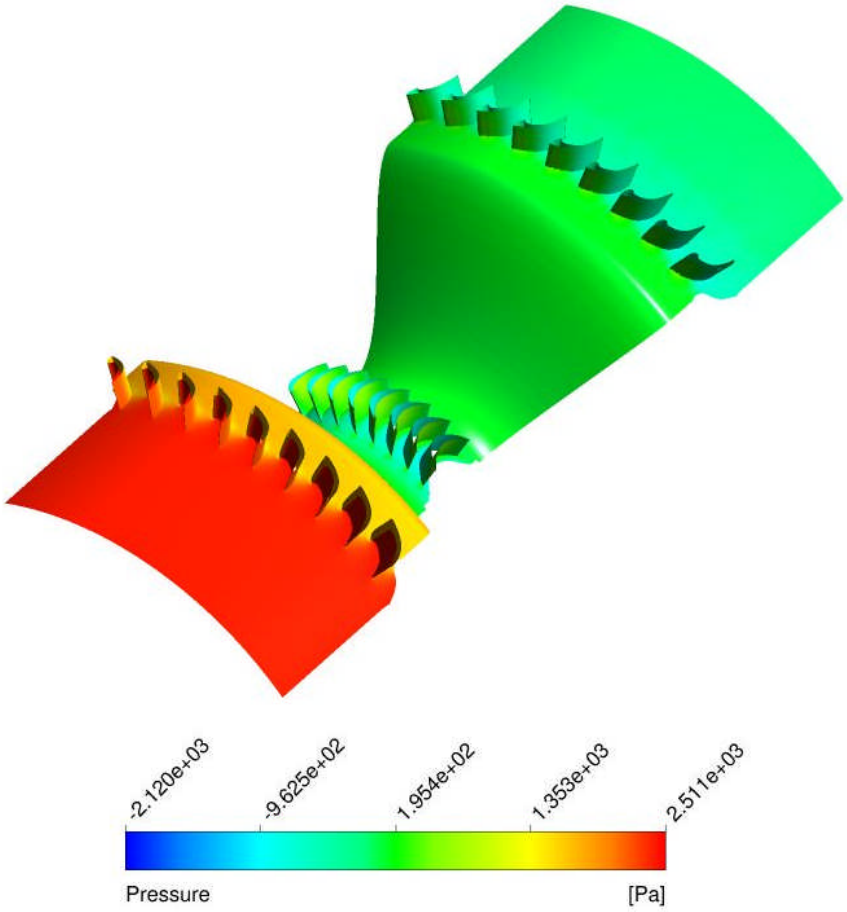

Figure 135: Plot of static pressure through the turbine showing a section of the 3D device.

A section of the simulated turbine is shown in *Figure 135* with the static pressure variation through the device plotted on the surface of the hub stator and rotor profiles. The case presented is the design condition, with an inlet total pressure of 2500 Pa. The range of inlet conditions used are given in *Table 30* with the corresponding mass flow for each component measured from the CFD. The resulting flow coefficient for each case is also given for each case along with the rotor angular velocity.

Case	Φ	ω (rad s^{-1})	TP Inlet (Pa)	m (kg s^{-1})
1	0.30	89.01	500	0.81
2	0.53	89.01	1000	1.41
3	0.71	89.01	1500	1.90
4	0.88	89.01	2000	2.34
5	1.02	89.01	2500	2.73
6	1.16	89.01	3000	3.09
7	1.40	89.01	4000	3.74
8	2.19	89.01	8000	5.83

Table 30: Values of total pressure inlet for 3D simulations.

The full turbine characteristic is plotted in *Figure 136* with direct comparison to the datum geometry and the NGV geometry. Peak efficiency occurs at the design point with an inlet total pressure of 2500 Pa and a flow coefficient of 1 producing an efficiency of 66.7%. This is a substantial improvement over the NGV geometry peak efficiency of 60.1% and more importantly, a significant improvement over the datum Ct14b geometry peak performance of 62.8%. The optimum geometry shows a performance improvement over the majority of the turbine operating range up until the flow coefficient becomes close to 2. After this point performance of the optimum geometry reduces, dipping under the performance of the NGV and Ct14b.

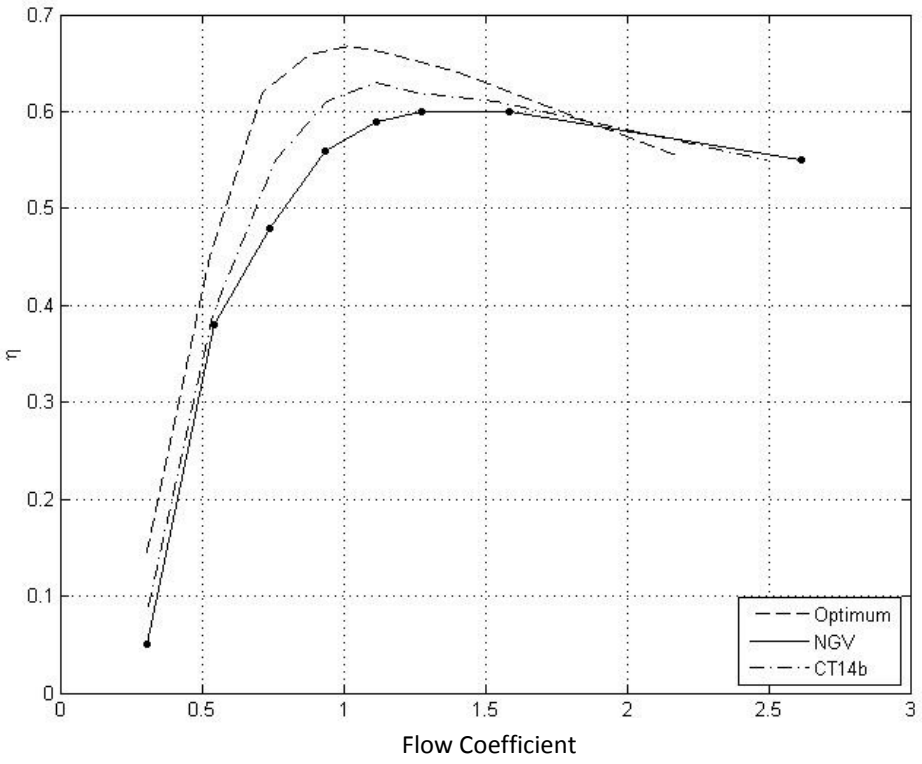

Figure 136: Plot of full turbine characteristic,
compared to datum and NGV geometry performance.

The reason for this reduction in performance at high flow rate is unclear from the overall turbine characteristic so each component has been examined in turn to find the cause. Figure 137 shows a plot of the percentage of total pressure loss that occurs across the IGV and the OGV for each of the guide vane geometries investigated in 3D. The results are produced from measurements taken upstream and downstream of the guide vane geometry within the CFD domain. The measurements have been taken from the same position for each case for consistency. The dotted lines show the pressure loss across the IGV for each set of data and it can be seen that a much greater pressure loss occurs across the optimum IGV profile when compared to the other profiles. This pressure loss gradually increases as flow rate increases. In comparison, the superior performance of the optimum profile when acting as an OGV can be clearly seen and it appears that the total pressure loss across the OGV reduces as flow rate increases. This does not however explain the reduced performance of the OGV profile displayed in the full turbine characteristic.

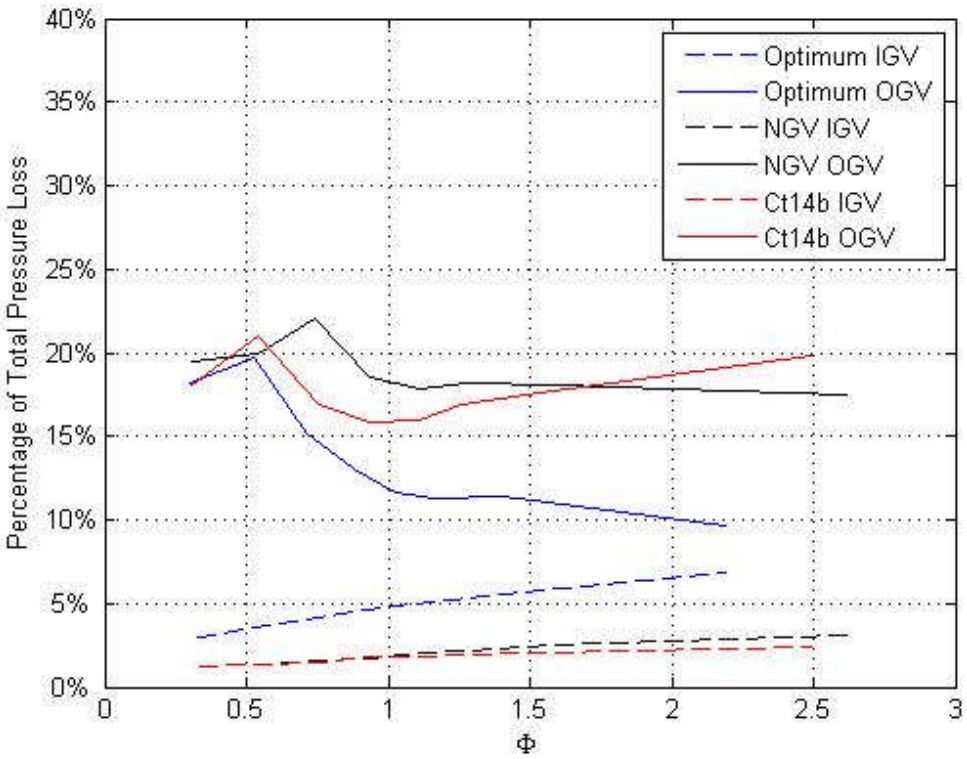

Figure 137: Plot of percentage of total pressure loss across IGV and OGV for three guide vane geometries.

The reverse flow over the optimum profile was further examined and a total pressure plot for each flow condition is presented on the following two pages *(Figure 138)*. These plots show just the OGV section of the outlet duct for the 3D CFD simulations performed and each uses the same colour scale for plotting. The plots demonstrate how the reverse flow interacts with the guide vane profile.

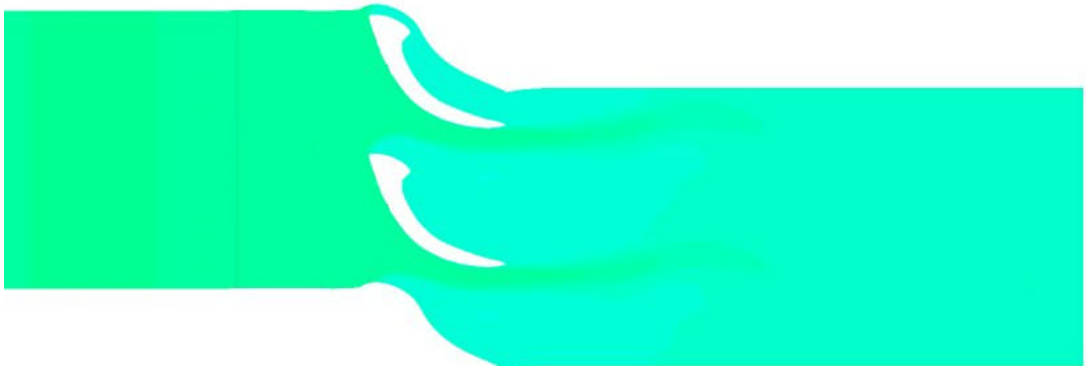

Case 1, Φ = 0.30

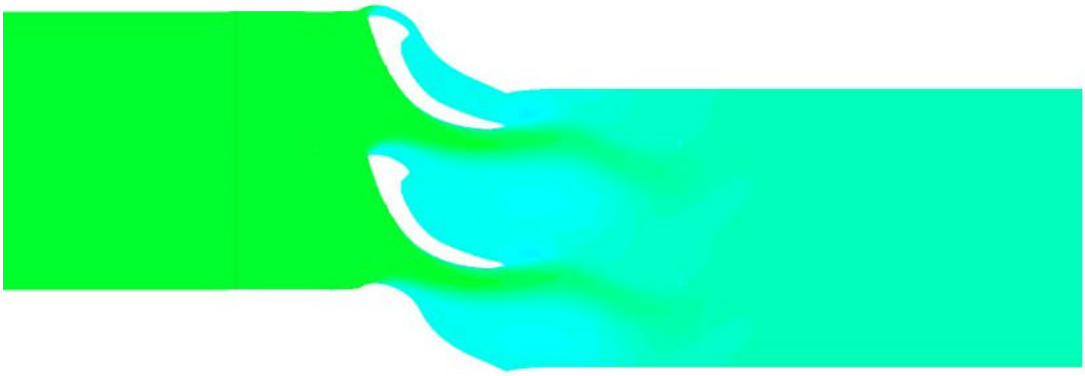

Case 2, Φ = 0.53

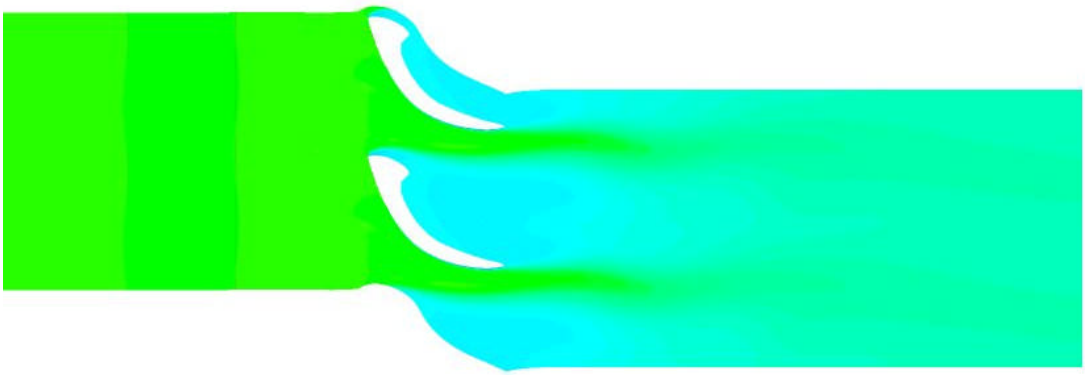

Case 3, Φ = 0.71

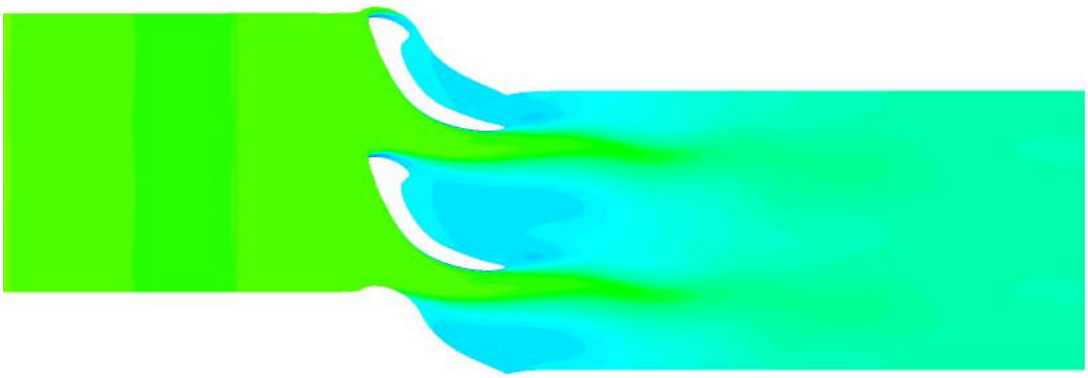

Case 4, Φ = 0.88

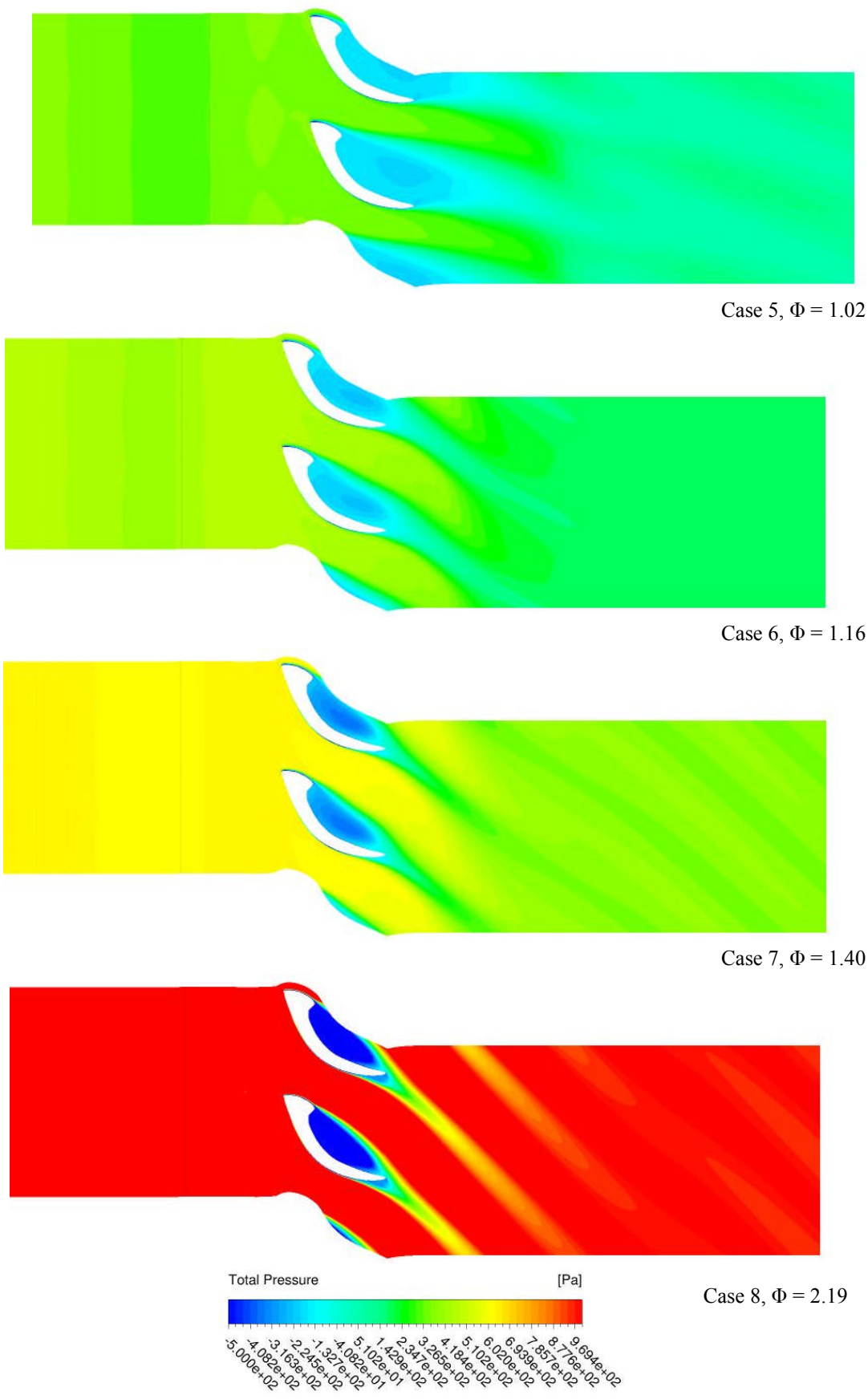

Figure 138: Total pressure plots of flow around OGV for 8 flow conditions.

Analysing the plots from the low flow condition of 500 Pa total pressure at inlet, the bulbous trailing edge of the profile does not have a beneficial effect on the flow. This explains the similar performance shown in the above plot for OGV total pressure around a Va/U of 0.5. As the flow increases, the beneficial effect of the bulbous trailing edge can be seen as the flow becomes attached to the profile, drawing air through the passage between stators. With further increase in flow rate, the effect of the bulbous trailing edge becomes stronger, changing the direction of the flow stream as it passes the OGV stator row. The exit flow angle continues to increase and is measured as 50º to the horizontal at the outlet of the final case with the highest flow rate.

Analysis of the optimum guide vane geometry across a range of flows has demonstrated that the bulbous trailing edge profile is beneficial around the design point condition. However, at higher flow rates, the profile increases the amount of swirl in the outlet flow which leads to increased losses. *Figure 139* plots the total pressure measured at the outlet for each geometry, across the flow range. This is measured as a percentage of total pressure at inlet. The increased total pressure at outlet can be seen for the optimum profile at the high flow condition where the results deviate from the relationship demonstrated by the other datum geometries. The added swirl in the outlet flow increases the total pressure at outlet and since these losses are unrecoverable, this affects the turbine performance, explaining the turbine characteristic plots above.

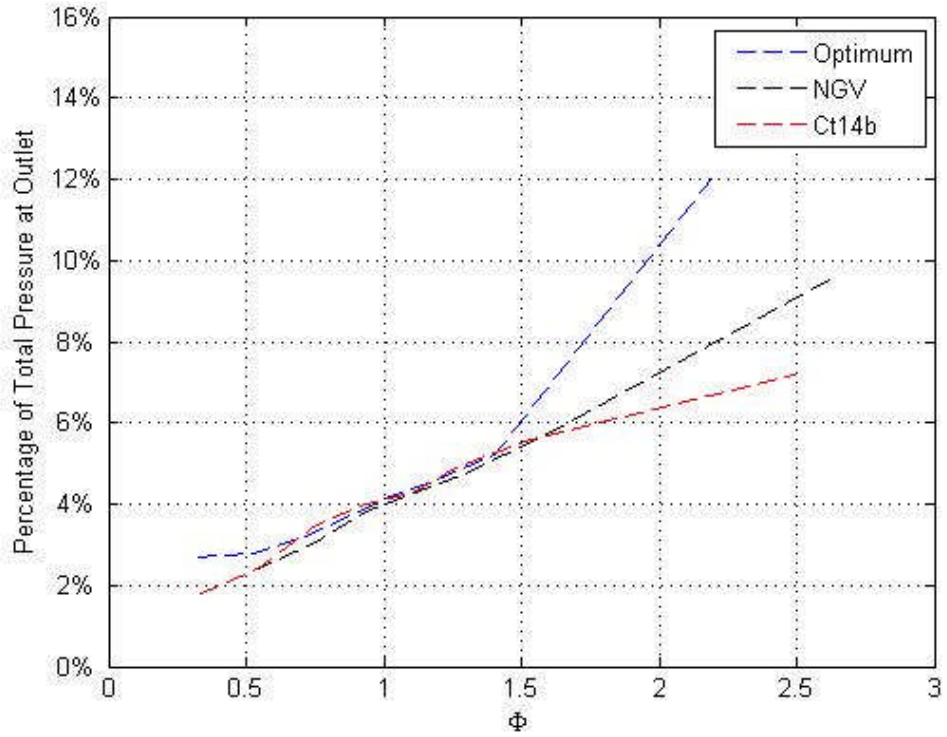

Figure 139: Plot of percentage of total pressure at outlet against flow coefficient.

Overall, the optimum guide vane profile demonstrates superior performance to the datum geometry, especially at the design condition showing the effectiveness of the optimisation procedure and the potential for significant performance improvements through designing for reversing flow.

6.8 Conclusions

The study of bi-directional stator optimisation investigates a novel method of stator design for bi-directional turbines. This method uses optimisation techniques to produce a profile designed for reversing flow conditions. The method developed, successfully produced a unique guide vane profile with improved performance over the datum geometry.

Up until this point, stators designed for unidirectional operation had been used in bidirectional turbines and the reverse flow over the OGV was the source of pressure losses in the flow. The investigation demonstrated that by optimising the stator profile for reciprocating flow, performance improvement could be achieved and a unique guide vane profile was produced.

A parameterisation study was conducted, resulting in the decision to use two cubic splines to parameterise the guide vane due to the capability of this method to allow local control. A bi-directional optimisation procedure was developed using a representation of the geometry in 2D CFD for performance prediction. Care was taken to ensure that the 2D CFD accurately represented the 3D simulations. This was done by conducting full scale 3D simulations of the initial geometry used for the optimisation. The results of these simulations were used to setup the conditions for the 2D cases. Highly similar results were produced, giving confidence in the method of representing the geometry as a 2D problem.

The optimisation procedure produced a unique guide vane profile with an unusual trailing edge profile, designed specifically for the reversing flow present in the datum turbine. This optimum profile demonstrated a 26.7% improvement over the starting geometry used for the optimisation, using total pressure loss as a measure of performance. This demonstrated the capability of the optimisation method used and the method of parameterisation.

The optimum geometry was tested using 3D CFD by replacing the datum guide vane geometry with the optimum guide vane profile. A full characteristic of the turbine was simulated, testing the optimum guide vane geometry across a range of flows.

Comparison of these results with the datum turbine demonstrated an improvement in peak efficiency of 6.2% to 66.7% with improved performance across the majority of the operating range. Close examination of the flow around the OGV shows that at high flow velocity, swirl is induced in the flow by the OGV stator row, this accounts for the reduction in performance at high flow rates.

The improvement in efficiency is significant and demonstrates the viability of designing stators with consideration of the reversing flow condition that they will be operating in. The optimisation method, parameterisation method and the CFD representation used has been successful in producing an optimum guide vane geometry. This research demonstrates that if designed appropriately, the use of an unconventional stator for an unconventional problem can have significant benefits to the function of the device.

7 Commercial Considerations

7.1 Introduction

Although research into the extraction of ocean waves commenced over 40 years ago, the take up of this method of power generation has been slow. The reason for this has been thought to be the immaturity of the technology and the associated risk as well as the low efficiency of potential devices. Mainly though, it is the fact that extracting power from waves has remained an uneconomic method of generating electricity and until it becomes economically viable, it is likely that the technology will remain at this pre-commercial stage. However, in recent years we have seen investment in wave energy development projects by large energy companies such as the case of E.ON Energy funding a Pelamis project at EMEC. Also, the acquisition of Wavegen by Voith in 2005 shows interest in the sector from large engineering firms. This type of collaboration shows that these larger firms are starting to see the potential of wave power as devices start to demonstrate their capability in the water.

In this chapter, an assessment of the global wave energy resource is conducted before identifying a number of specific countries as potential locations for wave energy development. A brief marketing audit is conducted for these locations and then the gathered data is used to perform a PEST analysis of an organisation wishing to enter the marine renewable market. A SWOT analysis is then performed on Dresser Rand's HydroAir device, taking these locations as potential sites for deployment and operation of the device as part of an OWC power plant.

The HydroAir device is currently at the scaled prototype stage of development and has yet to be tested in real sea conditions successfully. For this reason, a number of the scenarios considered while conducting the marketing audit and planning process are hypothetical. Nevertheless, conducting this investigation into the potential future development of the device sets the research presented in this thesis into some sort of

commercial context as well as positioning the device within the wave power industry at this time.

7.2 Potential Markets

Estimates of the global size of the wave energy market have varied widely over the years. Overall, these estimates agree that the potential market is very large indeed but variations arise between sources due to decisions on the point at which it becomes uneconomical to extract power from the available resource. In this section, the global potential of the wave energy market is discussed by first looking at wave power as a global resource and then at selected individual countries as potential markets.

Global estimates

An early report from the World Energy Council (WEC) estimated a global wave power resource of >2TW (WEC, 1993). More recently, a Carbon Trust White Paper (Carbon Trust, 2003) predicted the total wave power resource to be >18,000 TWh/year with the range of 2,000 – 4,000 TWh/year being given as the practical resource potential for this sector.

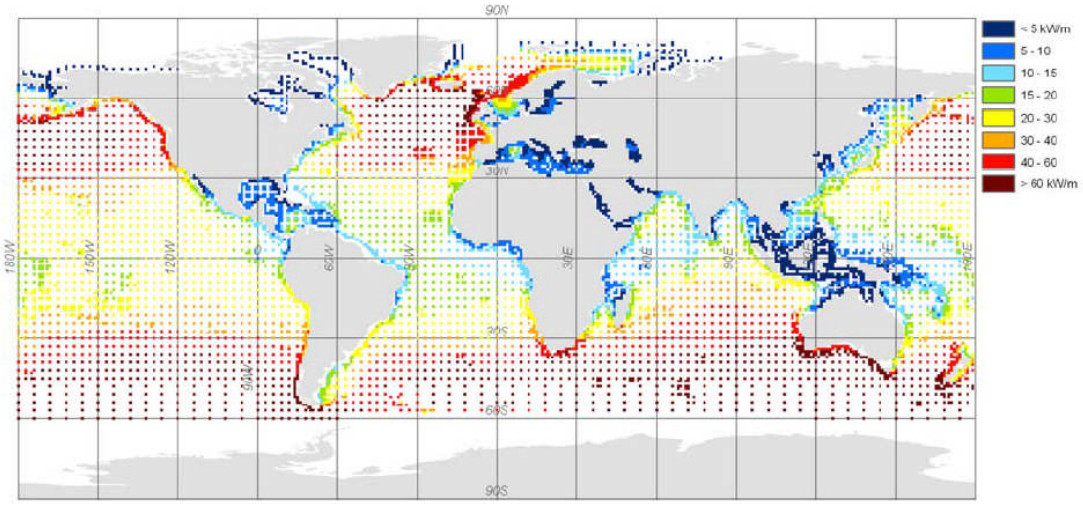

Figure 140: Theoretical global wave power resource (Mørk et al., 2010).

Mørk et al. (2010) conducted an evaluation of the global wave energy potential from satellite altimeter data and buoy data from the WorldWaves database *(Figure 140)*.

After removing areas of very low power levels (P≤5kW/m) they investigated annual and seasonal power distributions. Their study concludes an estimate of 3.7TW which is in line with earlier estimates. Their seasonal investigation demonstrates that seasonal variations are much greater in the northern hemisphere which could prove a disadvantage for the sector.

The potential revenue from this kind of global resource again has varied predictions. The Carbon Trust estimated that the revenue from wave and tidal stream energy could reach £60 billion – £190 billion in their Future Marine Energy Report (Carbon Trust, 2006). In the long term, the World Energy Council have estimated that the global wave power market could be as large as £500 billion. A report commissioned by the Department of Energy in 1999 estimated that the deployment of 2,000 TWh/year wave energy capacity worldwide would require investment in excess of £500 billion (Thorpe, 1999).

Overall, global estimates show that there is great potential for generating power from waves and with that comes a huge potential market. However, the immaturity of the technology means that as yet, there is still uncertainty in the sector and accurate predictions of the overall market potential are still not possible.

A number of specific markets have been identified from the global wave energy data above as potential targets for the HydroAir device and for this reason, they are considered in more detail below along with the UK.

7.2.1 UK

Resource

As discussed earlier, the accessible wave energy resource around the UK is estimated at 42 TWh/y (Carbon Trust, 2012) as the UK benefits from a lengthy coastline and active seas. However, compared to other potential wave power markets, these areas of high wave resource are often in sparsely populated areas, away from infrastructure creating additional difficulties in supplying power generated from ocean waves.

Government Support

The UK government offers a number of incentives to renewable energy developers designed to facilitate the meeting of ambitious energy targets. The Feed-In Tariff (FIT) scheme was launched in 2010 and is a method of incentivising renewable

generation by offering cash back based on the amount of power generated. Currently, the FIT in the UK does not cover wave energy projects as they are not widely used at the scale covered by the tariffs. Wave energy may be considered in the future if there is a take up of small scale generation methods.

The Renewables Obligation (RO) is designed to encourage production of electricity from renewable sources by putting a requirement on electricity suppliers in the UK. Suppliers are awarded Renewable Obligation Certificates (ROCs) for each MWh of electricity they produce from renewable sources and must achieve a certain number of ROCs per year. If they do not achieve this number, they are required to pay a buy-out fee, set at £38.69 per MWh for 2011-2012. The money from the buy-out fees is then re-distributed to the companies that met their ROs. At this time, the value of a ROC to a company was £42.27 (figures from Ofgem (2013)).

In the 2013 RO amendment, wave power generation up to 30MW will receive 5 ROCs per MWh, higher than the previous rate of 2 ROCs per MWh in the UK. This is providing that they become operational between 1st April 2013 and 1st April 2017. This amendment will bring the rest of the UK up to the same level as Scotland who have offered 5 ROCs for wave projects since 2009. Ofgem's report also shows the number of ROCs issued during 2011 – 2012, with 127 ROCs being issued in Scotland compared with 0 ROCs for England. The data also shows that two sites qualify for the RO in Scotland with a combined capacity of 1.2MW.

Current Projects

Current projects that have reached the demonstration phase are the Limpet OWC, now operated by Voith Hydro that has been discussed earlier. Other test projects are deployed at the EMEC test centre and these include the Pelamis P2 and Aquamarine's Oyster device. Outside of EMEC, a large number of wave and tidal sites have been leased by The Crown Estate with a total potential capacity of approximately 1.8GW (The Crown Estate, 2012). Sites have been leased to various developers but as yet, no devices have been deployed. Wave Hub is an offshore testing facility for wave power devices, connected to the grid and located off the south west coast of England.

7.2.2 Spain

Resource

The north coast of Spain offers great opportunities for wave power, especially around Galicia and Cantabria. One of the main advantages is the fact that there is a relatively short distance between where the power is generated and where it must be supplied due to the dense population along the coast. Early resource estimates from the Ministry of Energy and Industry gave a wave energy potential of 37.6 GW in 1979 (Chozas, 2009) but a more recent estimate reduces this figure to 21 GW (Mingo, 2007) with an average wave power of 30 kW/m at the Cantabrian Sea.

Government support

Support from central government in Spain is reported to be low with high costs and complicated bureaucratic processes being held responsible for delaying projects (Carlin et al. 2007). However, a feed-in tariff incentive is in place for renewable projects. Wave energy is grouped in the same category as geothermal, tidal and sea-thermal in terms of feed-in tariff classification. Current rates are 6.89c€/kWh for the first 20 years. The result of this slow progress at a central level has resulted in marine energy projects being driven at a more local level. There is evidence of this in the Basque Country, through the Basque Energy Board (EVE) and also in the Galicia and Cantabria regions.

Current projects

Mutriku – Basque country

The Mutriku wave energy plant is the first commercially operated wave energy plant to use OWC technology in Europe. It is owned and operated by Ente Vasco de la Energia (EVE) and the turbines are supplied by Voith Hydro after first being tested at their LIMPET site in Scotland. The Mutriku plant is a 440m long breakwater, housing 16 turbines and is rated at 300kW (Torre-Enciso et al., 2009). The construction of the breakwater was already scheduled and an additional $3 million was required to incorporate the OWC technology. The plant had been operational since 2011.

Bimep – Biscay Marine Energy Platform

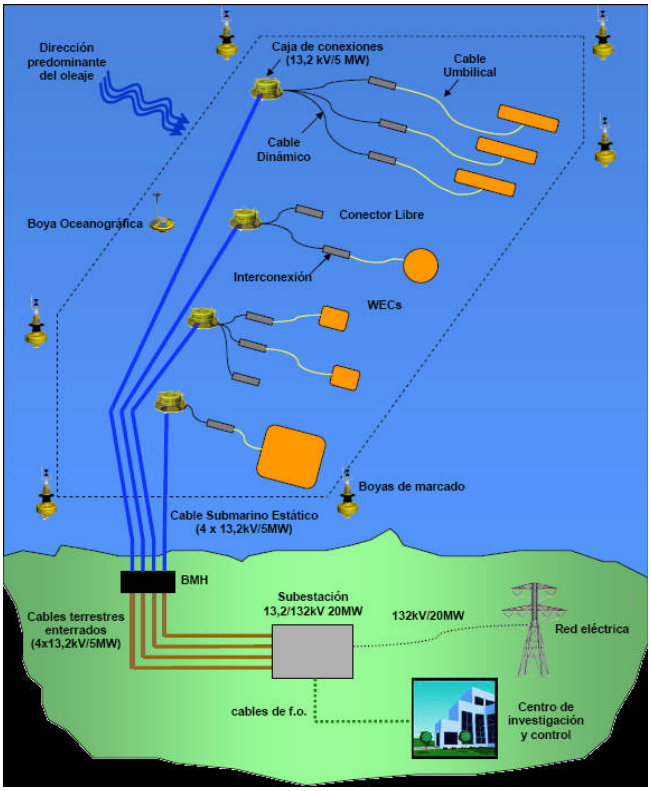

Figure 141: Concept drawing for BIMEP (Ruiz-Minguela, 2012).

The Biscay Marine Energy Platform (BIMEP) is a wave energy test site, currently in the planning stage, for location in the Bay of Biscay. Investment of €20 million has come from EVE and the Spanish Energy Agency national body (IDEA). The planned site covers 5.2km^2 of the sea surface and is located 1.7km off shore. At the site, the energy flux has been measured at 21kW/m. There are plans for 4 testing berths, capable of testing a wide range of wave energy converters, connected to the shore by 13.2kV/5MW subsea lines *(Figure 141)*. Onshore, a 20MW substation is connected to the grid. The project was initiated in 2008 and is currently under construction. Completion is planned for the end of 2013 (Ruiz-Minguela, 2012).

Iberdrola Energias Marinas de Cantabria – Santoña

Iberdrola Energias Marinas de Cantabria is a joint venture between IDEA, the local regional development agency SODERCAN, the global oil major TOTAL and Ocean Power Technologies (OPT) with the aim of building a grid connected wave power station on the north coast of Spain. The project commenced in 2006 and by 2008 a single OPT PowerBuoy (Point absorber) had been tested at the site in Santoña. Plans to install 9 PowerBuoys at the site to supply approximately 1.39MW of electricity into the Spanish grid are yet to be realised.

7.2.3 Portugal

Resource

Portugal has a high energy resource with good natural conditions and infrastructure near the coast. For this reason, Portugal is considered to be among the leaders of the upcoming ocean energy industry (Ramalhosa and Lyra, 2011). Portugal has one of the largest Exclusive Economic Zones (EEZ) of the European continent and this was recently extended to cover 2,150,000 km^2 in 2009. The Wave Energy Centre (WavEC) give resource estimates of around 15 GW on the continent and around 6 GW on the islands with an average annual flux of wave energy of 40 kW/m (WavEC, 2004).

Government support

The National Energy Strategy, ENE 2020, was established in 2010, covering all energy production but focussing on the importance on generation from renewables in Portugal. This resulted in the Portuguese government setting objectives for wave energy generation to install 250 MW by 2020 (Ramalhosa and Lyra, 2011). Also in 2010, the plans for a wave pilot zone off the coast at S. Pedro de Moel were finalised. The planned zone has an area of 320 km^2 across water depths from 30 – 90m. The wave pilot zone was proposed to attract R&D to Portugal by providing a site where tests and demonstrations can be carried out and licensing procedures could be facilitated. The pilot zone was still in the development stage at the time of writing.

A feed-in tariff is available in Portugal as an incentive to wave energy project developers. This was originally introduced in 2001 but abolished in 2005 after not being used. It was then re-introduced with modifications in 2007 and currently stands at 24-26 c€/kWh (240-260€/MWh) for technological demonstrations. This tariff is limited to devices under 4MW and with a total of 20MW installed nationally. Beyond this level, the tariff for pre-commercial scale projects, up to 100MW is 15 c€/kWh. After this, in the commercial phase, there is a subsidised tariff of approximately 10 c€/kWh but varies as values are calculated for each specific project (Brito-Melo, 2009).

Current Projects

Despite a large energy resource and early interest in wave energy technologies, current wave energy projects in Portugal are limited. The Pelamis 750kW Project was considered to be the world's first commercial wave power project and was fully

developed by 2008. However, financial and technical problems put an end to Pelamis in Portugal. The Pelamis P2 is now being tested in Scotland with support from E.ON Energy and Scottish Power Renewables.

The Pico plant built on the Azores archipelago in 1999 experienced operational and technical difficulties after construction and there was limited financial capacity to resolve these issues. After operation of the plant was taken over by WavEC in 2004, a significant number of testing hours were achieved. However, currently the plant requires considerable investment to prevent collapse due to corrosion and a campaign has been launched to raise the capital and save the plant. As a result, the plant is not currently operational.

A number of wave power development projects are in progress in Portugal but are in the research and development stage, such as MARTIFER's Flow project and FDO – Ambiente e Energia's joint venture with Spanish company Hidroflot. Both developers have demonstrated their interest in applying for a licence for demonstration projects in the Wave Pilot Zone.

7.2.4 USA – West coast

Resource

The west coast of the USA offers significant wave energy resources with considerable potential for contributing to US renewable energy supplies. Total average wave energy off the US coastlines, including Alaska and Hawaii, has been estimated at 2,100 TWh/yr. In the northwest, wave energy could produce 40 – 70 kW/m according to the Minerals Management Service (MMS) (Rosenfeld et al., 2008). This also corresponds to data presented by Mørk et al. above. This number is broken down for different coastal regions for the US by Hagerman and Scott (2011) who quote 590 TWh/year for the West Coast.

Government Support

The Energy Policy Act (EPAct), passed in 2005 was intended to combat growing energy problems through tax incentives and loan guarantees for renewable energy production. The Production Tax Credit supports generation for the first 10 years of a projects commercial operations. The Investment Tax Credit supports businesses making investments in renewable energy production property and equipment allowing

tax credits of up to 30% on eligible investments in marine technologies (Rosenfeld et al., 2008).

Legislation and incentives for renewables vary across different states in the USA. California has one of the most stringent Renewable Portfolio Standards (RPS), similar to an RO, with a target of 33% renewable production from its major utilities by 2017. In terms of carbon emissions, Governor Arnold Schwarzenegger signed into law in 2006 that 1990 levels will be met by 2020.

The Oregon RPS states that 25% energy generated by large utilities must be from renewable sources by 2025 and 5 - 10% for smaller utilities. Oregon also has a Business Energy Tax Credit (BETC) in place which allows for a tax credit of up to 35% of eligible project costs, taken over 5 years and capped at $10 million.

Current Projects

There are currently no operating wave power devices off the west coast of the United States although permits are being issued for demonstration sites as can be seen in the Federal Energy Regulatory Commission (FERC) diagram below *(Figure 142).* Two wave preliminary permits have been issued in the state of Oregon and one has been issued in the south of California. Of these, the OPT collaboration with Oregon Wave Energy Partners and others is the most advanced with plans for a 1.5 MW, grid connected wave power station, 2.5 miles off the Oregon coast. A single OPT PowerBuoy pilot device was planned for deployment in 2013 but due to further jurisdiction complications, this has been delayed.

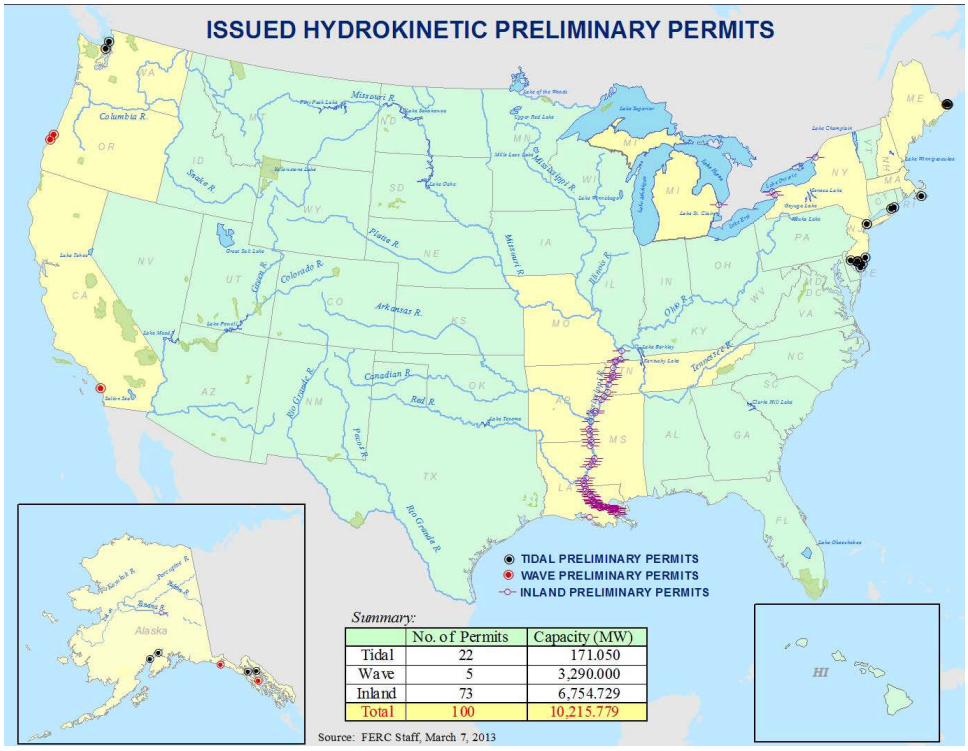

Figure 142: FERC Issued Hydrokinetic Preliminary Permits Map (FERC, 2013).

In California, no wave energy projects have reached the demonstration phase since the promising Finavera project's point absorber, AquaBuoy, sank in 2007. As a result of this, the states most powerful utility Pacific Gas and Electric (PG&E) withdrew all funding and backed out of all other wave energy projects. The Canadian company, Finavera, have now turned to wind energy.

7.3 PEST Analysis

The PEST analysis, standing for Political, Economic, Social and Technological, has been used to assess the external factors affecting an OWC based wave energy developer in the current climate. The above information, gathered from investigating potential markets has been used in the study. The initial analysis, displayed in a grid format can be seen in *Appendix A*, each section is discussed in more detail in the following sections.

7.3.1 Political

Increasing evidence of man-induced climate change has resulted in political agreement that reductions in carbon dioxide and other greenhouse gases must be achieved. International agreements have been set up with this as the main objective. The Kyoto Protocol is an international agreement to reduce carbon emissions, originally adopted in Japan in 1997 and agreed by 189 countries. However, the USA signed the protocol but did not ratify it, meaning it is not legally binding. In 2011, after an update had been agreed, Canada, Japan and Russian pulled out of the agreement, stating that they would now take on further Kyoto targets. China and India are not required to reduce their emissions levels as they are classed as developing countries. However, China is now the biggest emitter of CO_2, second to the USA. The UK is still legally bound to the target of reducing carbon emissions by 20% from 1990 levels by 2020. Carbon trading schemes have been introduced as a result of the Kyoto protocol such as the European Union Emissions Trading Scheme (EU ETS) and ROCs in the UK.

Security of Supply

Security of energy supplies is an increasing concern for countries in the EU as most are net importers of energy in the form of gas and oil. Gas is primarily imported from Russia and Oil primarily comes from the Middle East. This creates reliability on uncertain markets and political uncertainty overseas gives concern over the stability of future oil prices. This had been less of a concern for the UK when extensive supplies of Gas and Oil were available in the North Sea. Production from these reserves has since peaked and the UK is increasingly reliant on imports. This is why the current ‘dash for gas’ has received criticism as it will increase the UK’s dependence on imported natural gas as well as diverting funds and infrastructure development away from renewables and back into fossil fuel technologies.

Increasing global energy demand from emerging economies such as China, India and Brazil also adds uncertainty to future oil and gas prices. The global economic downturn has seen this increased demand slow but it is likely to resume within the medium term bringing with it the possibility of large increases in energy prices.

Investment in domestic renewable energy generation brings with it security of supply which is attractive for governments. Although wave power is still in the early stages of development, this fact is likely to benefit the sector in the future.

7.3.2 Economic

Generating electricity from renewable sources is generally more costly than conventional fossil fuel methods, this is most certainly the case for wave energy. For this reason, the reduction of carbon emissions through adoption of green technologies will involve significant investment. The data gathered above shows a number of methods adopted to support renewables developers economically and reduce the costs required to meet climate change objectives.

Support mechanisms

In the UK, wave power is currently eligible to receive five ROCs for every MWh of energy generated. This amounts to a subsidy of around £210/MWh a substantial amount since the current wholesale price for electricity is somewhere around £50/MWh. This amount is now level with Scotland where wave power has been eligible to receive 5 ROCs since 2009. The high wave resource available in Scotland as well as the high level of support has seen wave energy increase greatly there over the last decade. This is also due to the development of the EMEC test facility. It is hoped that the increased subsidy across the UK will increase the number of wave energy projects in England, bringing other leased sites into use as well as the WaveHub test site in Cornwall. Despite the increase, developers have a short window of opportunity, needing to have demonstration devices in the water and producing electricity within the next four years.

Of the other countries researched, Portugal currently offers the feed-in tariff scheme of 240-260€/MWh, a similar level to that of the UK. In comparison, the Spanish feed-in tariff rate is much lower at 68.9€/MWh. The USA does not support feed-in tariffs and it is not possible to make a comparison for the information found on production tax credits.

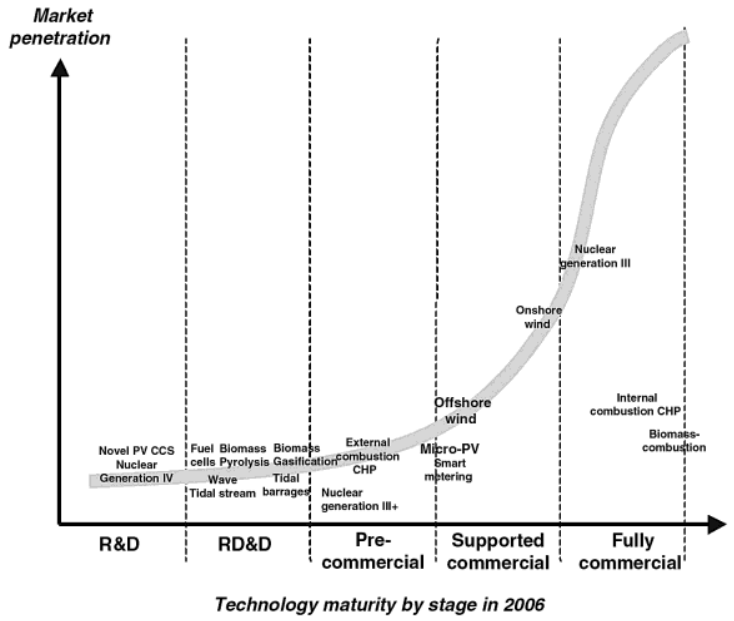

Figure 143: Renewable technology maturity (Jamasb et al., 2006)

Jamasb et al. (2006) present the development stages of renewable technologies on the diffusion of innovation curve, based on their maturity and level of market penetration in 2006. On the x-axis, technology maturity is presented from initial concept to fully commercial. On the y-axis, market presentation or the level at which the technology has been adopted by the market.

The development stages are described as below:

- R&D includes research undertaken within industry as well as at universities, covering basic research and engineering/application focused study.
- RD&D (research, development and demonstration) includes full scale working devices as early prototypes in single units or in small numbers.
- Pre-commercial covers broad development, when previously demonstrated devices are installed for the first time either in greater numbers or at a larger scale.
- Supported commercial is the stage where technologies are rolled out in greater numbers but are still supported by government (such as ROCs) or private finance.
- Commercial technologies can compete within the institutional framework, unsupported.

It can be seen that Jamasb et al. positioned wave and tidal energy in the RD&D stage in 2006. By reviewing the development stages presented here, it can be seen that wave technology is still in the early stages of development and continued economic support is required to advance the technology towards becoming fully commercial.

Finance and Investment

The current financial situation means that it is difficult for companies to raise finance. It is also true that stories of failure and the high risk attached with deploying devices offshore do not help companies attract equity finance. However, a number of utilities are backing wave power development with E.ON Energy and ScottishPower Renewables both investing in the Pelamis P2 device. Each power company has deployed one P2 machine, side by side, at EMEC in order to test the device's operation in a wave farm. Scottish and Southern Energy plc. invested in Aquamarine Power in 2007. The company has now deployed their second generation Oyster device at EMEC. This is also true in Spain where, due to low governmental support, the current projects discussed above are privately funded by either utility companies such as EVE or technology developers. This investment shows growing interest and confidence in wave energy technology. Also, that the support mechanisms, at least in Scotland, are sufficient to temp utility companies into investment.

Fuel Prices

The projected cost of oil is likely to have a significant influence on the uptake of low-carbon technologies. On one hand, low-carbon power has lower running costs that are not affected by volatile fuel prices. However, high oil prices will increase the cost of engineering and services that are required for development and deployment of marine renewables, increasing initial investment costs. In the long run, higher oil prices will likely increase the uptake of marine renewables but this will require a change in the balance of the industries costs as well as a significant increase in investment (Yago et al. 2008).

Wave power is a variable resource and although it is less predictable than tidal energy, it is more predictable than wind. This requires power companies to develop ways of coping with the variable supply, as has been done with wind energy. Despite this, when waves are present, the force generating the electricity is free and it always will be. The instability of oil and gas prices means that although a utility company can predict how much energy can be produced from a conventional thermal power station, they cannot be sure how much this energy will cost. The predictability of future costs is a benefit for renewables whereas the unpredictability of the resource is an undesirable factor.

Infrastructure

The addition of renewable energy systems to the energy mix in the UK is increasing stress of the national grid. In the case of marine renewables and offshore wind, power needs to be delivered from offshore locations, to major centres of population for the power to be used. In the UK, the locations with the greatest wave resource, the Scottish Highlands and the south west of England, are also the least populated. If a significant amount of the UK's energy requirements are going to be met by marine renewables then large investment in infrastructure will be required.

In the other energy markets analysed such as Spain and the USA west coast, active wave sites were much closer to densely populated areas on the coast so it is likely that less investment would be required to deliver the power to these areas. Once wave power reaches commercialisation, the upgrading of the national grid is something that could hold further development back and may make one market more attractive than the other in the long run.

7.3.3 Social

In the UK, customers have the freedom to choose their energy supplier and generally this is done based on cost. However, with growing evidence of climate change and increased awareness of environmental issues, energy companies are using their green credentials to attract new customers. There is a growing number of consumers who are willing to pay more for electricity that has been produced from renewable sources and this has brought about companies such as Good Energy who were the first dedicated 100% renewable electricity supplier. In general though, people are still looking for the best deal, but how green an energy supplier is perceived to be can be a final deciding factor.

Like many large development projects, renewables can face strong opposition and companies must be aware of the impact on all potential stakeholders. In the case of wave power, stakeholders include fisherman, surfers, environmental groups and those involved in the tourist industry. A number of studies have been conducted on the impact of wave power devices on local wildlife and conclusions are generally that with careful planning the impact it is likely to be low. One such study is being conducted at EMEC where the lobster population is being monitored at one of their test sites. The fact that many of the proposed offshore or nearshore wave energy devices will have little or no visual impact from the shore is a significant advantage over wind power.

7.3.4 Technological

Although the concept of extracting power from ocean waves has been around for a long time, the majority of the technologies employed are immature. Continued investment in research and development is required as well as learning from demonstration devices deployed at sea. There is no short-cut for this and it will take time for the technology to reach maturity, the sooner devices reach the demonstration stage, the better.

Wave energy technology is competing against other renewable technologies as well as conventional fossil fuel methods of producing electricity. The added complexity of the harsh marine environment means that wave power devices have to overcome the problem of efficient power extraction as well as survivability, increasing the difficulty of being competitive. Currently, there are many, vastly different, wave energy technologies under development across the world and at this time, it cannot be said which devices will be successful in making the transition to commerciality. It will be necessary to achieve cost savings through improved manufacturing methods and innovative design in order to become cost competitive within the sector and with other methods of power generation.

7.4 SWOT Analysis

While the PEST analysis assess the external factors affecting a company or product, the SWOT analysis, standing for Strengths, Weaknesses, Opportunities and Threats is used to assess both internal and external factors that are important to achieving an objective within the company. The SWOT framework has been used to assess the factors important to the commercialisation of an OWC turbine, using Dresser Rand's HydroAir Variable Radius Turbine as an example. The initial analysis, displayed in a grid format can be seen in *Appendix B.* Each section is discussed in more detail below, starting with the internal factors (Strengths and Weaknesses) and followed by the external factors (Opportunities and Threats).

7.4.1 Strengths

Dresser-Rand has been among the largest global suppliers of rotating machinery and services for over 100 years. Their expertise cover centrifugal and reciprocating compressors, gas and steam turbines, expanders and control systems, supplying oil and gas, chemical, petrochemical, and process industries worldwide. This well recognised brand with proven technological expertise and client focused operations goes a long way in the development of a new product such as HydroAir.

The HydroAir turbine is a new product for D-R and although it falls within the broad description of rotating machines, the design, construction and indeed the problem which it is designed to overcome are vastly different to the other products in D-R's portfolio. The investment in R&D of new products creates risk and strategic marketing planning is required to monitor this risk across the company as a whole.

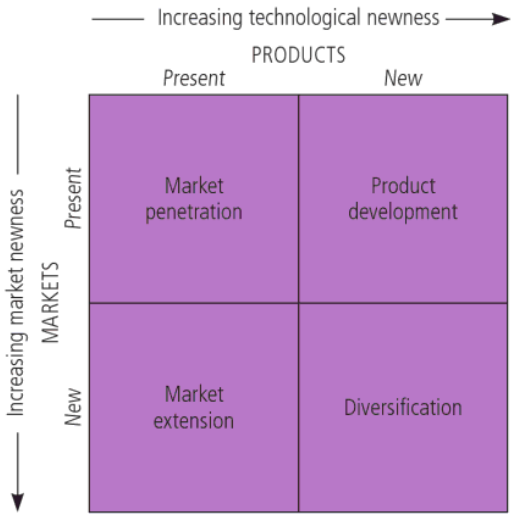

Figure 144: Ansoff matrix, taken from McDonald and Wilson (2011)

The Ansoff matrix is a tool used to analyse marketing objectives for new and current products as well as assessing the overall risk within an organisation. The framework displays a companies competitive position in two dimensions only – products and markets. The grid above *(Figure 144)* demonstrates that there are four possible courses of action for the company. These are selling existing products to existing markets (Market penetration), Extending existing products to new markets (Market extension), developing new products for existing markets (Product development) and developing new products for new markets (Diversification) (McDonald and Christopher, 2003).

HydroAir is a new product aimed at existing energy markets. However, the current market for turbines for OWCs is not present due to the immaturity of the technology and the lack of infrastructure for wave energy projects. For this reason, HydroAir is positioned in the Diversification segment of the Ansoff matrix. Diversification is the highest risk strategy for businesses but if successful, offers the greatest rewards. The advantage of diversification is that the risk should be disconnected from the firm so that if the new product should fail, this should not affect other products in the portfolio.

Before embarking on a high-risk diversification strategy, it is desirable for a company to have a balanced portfolio so that if the new venture should fail, the company can get itself out of trouble. A healthy company would have products spread around the Ansoff matrix. For D-R, the continued supply of gas turbines and compressors to existing oil and gas markets would be their low risk strategy for market penetration. An example of market extension would be the supplying of Combined Heat and Power (CHP) systems to the growing Biogas sector. Continued development of existing products and services would be necessary to remain ahead of the competition.

The international recognition of a large company and security of a balanced portfolio backing up research and development helps with the marketing of a device and again, reduces the risk of diversification. It can be seen that preference would be taken towards a device developed by a multi-national engineering company with substantial backing rather than a start-up company with a bright idea and limited funds.

The HydroAir project has demonstrated significant performance improvements over other bi-directional impulse turbines presented in the literature. Currently, this is based on numerical data and experimental data recorded at the test facility. It is unfortunate that no performance data has been recorded from offshore tests, this is due to the failure of the Oceanlinx demonstration project in Australia. Despite this, the predicted high performance is a strong factor for the commercialisation of the HydroAir device. The patenting of the VRT concept and further modifications ensure that competitive advantage is secured for the duration of the patent.

7.4.2 Weaknesses

The main weakness of the HydroAir project is the fact that there are no performance results from offshore testing. Despite impressive results from numerical analysis, the device has not been tested in real sea conditions, though it has been tested in simulated sea conditions at the test facility. In this respect, HydroAir is behind

competing wave power devices that have scaled prototypes in the water as demonstration devices.

The inherent design of the VRT requires an increase in the overall diameter of the device. The result of this is that compared to other turbines of similar power rating, the HydroAir device is large. In an OWC, a large part of the damping in the system is due to the airflow restriction imposed by the turbine and as a result, the size is dependent on the damping requirement for the specific OWC device. However, it is desirable to reduce the overall size of the turbine to increase marketability of the device. It is reported that D-R has designed a new version of HydroAir, reducing the overall size by 50%.

The HydroAir turbine is part of a system that makes up an OWC wave power device. This means that the successful commercialisation of the HydroAir turbine is reliant on the successful development of a buoy/chamber that requires a bi-directional turbine. Currently, there are few OWC buoy developers globally and this presents a weakness in the development strategy of HydroAir.

Taking a wider view of the company, the development of a new product presents weaknesses internally that must be overcome if and when the product reaches the point of commercialisation. These cover things such as new manufacturing techniques and the use of new materials. During the early stages of development, integrating these methods into the company's current procedures is costly and adds to the complexity of the project. It is not until the project has progressed in to the early commercialisation stage that the lessons learned can be put into practice and economies of scale can be realised to reduce production costs.

7.4.3 Opportunities

The global wave energy market is enormous and currently untapped at a large commercial scale and this offers great opportunity for the HydroAir device. Accompany this with the growing demand for energy and requirements for reduced carbon emissions and the future looks promising for HydroAir. There is currently no clear leader in the wave power sector with a growing number of devices either at or close to the testing phase of development. This is an exciting time for the sector and presents great opportunities for all involved.

Currently there are only two major players in the development of turbines for OWCs and these are D-Rs HydroAir and Voith Hydro's Wavegen turbine. Although the Voith turbine has had extensive testing in the LIMPET device and then in the

commercial development at Mutriku, no performance results have been published so it is not possible to compare the two devices in terms of performance.

HydroAir is being developed in the UK so is well placed to take advantage of the test sites available. The opportunity for collaboration has been presented in the partnership between D-R and Ocean Energy, announced in 2010. Since this time, Ocean Energy have finished testing their OE Buoy

The fact that the HydroAir turbine is only a component of an OWC power device presents the opportunity for collaboration. D-R and Ocean Energy Limited have agreed a partnership to develop OWC devices to produce commercial electricity, this was announced in 2010. Ocean Energy have been testing their quarter scale prototype OE Buoy successfully in Galway Bay, Ireland for three years. The rigorous testing has demonstrated the survivability of the technology and has helped the developers move on to the next stage. Ocean Energy and D-R now plan to deploy a full-scale device at the WaveHub test site in Cornwall in 2013.

7.4.4 Threats

The HydroAir project is a unique product, designed for a unique application. The commercial success of HydroAir rides not only on the success of wave energy but specifically, on the success of OWC technology. If, for some reason, OWC technology became obsolete, that would be the end of HydroAir and this presents a potential threat to the project. Fortunately, this does not appear very likely for the near future but scenarios such as wide adoption of nuclear as a low-carbon energy source or a definite leader in wave power technology with low costs and high efficiency could endanger the future of the technology.

Currently infrastructure in the UK is not setup for the deployment and support of large scale marine renewable energy projects. In the short term, this is not an issue but could delay commercialisation is infrastructure upgrading does not keep up with the advancement of the technology.

Support mechanisms in the UK are currently favourable for marine renewables and this is encouraging investment from private companies. However, lack of commitment from government or a sudden change in direction, such as towards natural gas or nuclear can have a serious effect on the confidence of investors. Wave power is at a crucial stage of development and needs all the help it can get to reach commercialisation.

7.5 Discussion

With a vast global resource and great potential market, the future looks promising for wave power technology. However, the difficulty of the problem and limited financial resource to solve it means that wave power is still, in general, in its infancy.

The specific markets investigated show good intentions in terms of support structures and planned test sites. However, outside the UK, these test sites are still in the development stage. The research gathered on current projects shows that few have actually reached the demonstration stage of development. It seems what the sector really needs is devices to be in the water and prove their performance capabilities in real ocean conditions.

The support mechanisms identified are available to marine energy projects but only once they start producing power. While this does provide incentive, a large amount of funding is required to get a device to the RD&D stage at which point it can start producing power and making use of support mechanisms in place. This means that without private funding or interest from large utilities, devices will find it hard to meet this funding gap.

Scotland is currently leading the marine renewable energy market in terms of installed capacity and power generated. This demonstrates that the combination of high wave resource, generous support mechanisms and a designated test site can produce results and advance technology. The rest of the UK has recently increased the number of ROCs per MWh to the same level as Scotland so it is expected that this will aid development in the rest of the country. Of the markets researched, the UK appears to be the strongest due to high levels of support and wave resource. Also the availability of wave test sites in both Scotland and the south west of England. Portugal offers equal support mechanisms and has a high wave resource but lacks a test facility at the time of writing. The financial situation in Portugal also adds uncertainty at this time.

Focussing on HydroAir, the strong brand of D-R gives an advantage over smaller competitors but at this time, the capabilities of the device need to be demonstrated offshore to win the trust of potential customers. Currently, the lack of buoy developers or other potential marketing channels is hindering the process of collaboration and the opportunity for demonstration. There is the opportunity for market creation, such as buoy or breakwater development, but this adds increasing risk onto the HydroAir development project.

The collaboration with Ocean Energy does offer the opportunity for offshore demonstration and if successful will bring the device up to the front of the competition.

8 Conclusions

The work presented in this thesis investigates methods of improving the performance of bi-directional impulse turbines for OWCs by reducing the losses associated with the OGV stator row. Two unique guide vane concepts have been investigated making use of optimisation methods coupled with CFD as a method of performance prediction. The optimisation procedure has been developed specifically for reversing flow. The research has demonstrated improvement in total-to-static efficiency of the datum turbine and this has been demonstrated by full scale 3D numerical analysis.

In this section, conclusions are drawn for each of the main sections of the thesis.

8.1 Datum Turbine

A numerical study of the datum turbine was conducted using 3D steady-state RANS CFD. This study was used to gain knowledge of the function of the datum turbine as well as to validate the CFD method used in the research. The results of this study were compared with previous simulations conducted on the datum device which had in turn been validated by experimental data obtained from the reciprocating test rig.

The results showed good agreement with previously performed simulations with an error of 0.2% of peak efficiency. This close agreement demonstrated the effectiveness of the CFD method to be used as a design tool and the results and method presented were used as a base for comparison for the subsequent research conducted.

8.2 MEGV Concept

A novel concept of reducing OGV losses in a bi-directional impulse turbine by employing MEGVs has been investigated. The initial representation resulted in a set of design constraints for the concept which were used to design a MEGV configuration for optimisation.

After a parameter study was conducted, a parameterisation scheme was established for the starting geometry. This scheme allowed a wide range of MEGV configurations to be examined automatically by optimisation using CFD. The parameter study demonstrated that this was a multi-variable problem and the design variables had to be varied simultaneously for performance improvement to be realised.

Geometry was represented as a 2D slice at mid span, simulating only the guide vane and part of the duct of the turbine. This was done to reduce the size of the domain, reducing the run time and computational cost of each simulation.

Results of 2D, multi-variable optimisation showed significant improvement in performance from the geometry used as the starting point of the optimisation. This proved the effectiveness of the design constraints used to define the problem as well as the optimisation technique that had been used.

Numerical assessment of the performance of the optimum geometry was conducted, simulating the datum turbine in 3D, replacing the datum guide vanes with the optimum guide vane geometry. The results of the 3D simulations showed an increase in efficiency over the operating range of the turbine however, this was much lower than had been predicted by the 2D representations of the geometry.

The 3D results showed the limitations in the method that had been used to represent the MEGV guide vane problem in 2D. It was concluded that the main reason for the variation between the 2D and 3D results was due to the limited cross-validation between the two methods that were performed during the optimisation process.

The improvement in the performance of the 2D representation demonstrates the potential of the MEGV concept and further investigation is recommended, this is discussed in the following chapter. The knowledge gained through conducting this optimisation procedure was used to improve the method, this method was then applied in the subsequent research.

8.3 Bi-directional stator profile optimisation

The novel concept of optimising a stator profile for reciprocating flow has been investigated. This involved the parameterisation of a stator profile and adaption of an optimisation technique using CFD as a method of performance prediction. The investigation demonstrated that designing a stator for bi-directional flow in this way is beneficial to the performance of bi-directional turbines. A unique stator profile was produced than increased the total-to-static efficiency of the datum turbine.

A study of profile parameterisation methods was conducted. Cubic splines were chosen as the method of parameterisation due to the control of local profile manipulation this offered. Investigation of the variable parameters demonstrated that this method of parameterisation was suitable, allowing controlled manipulation of the trailing edge.

The 4 variable optimisation procedure conducted resulted in a unique stator profile that achieved the requirements of both the IGV and OGV for the turbine. The 2D simulations showed significant performance improvements over the geometry used at the starting point of the optimisation. 3D simulations were conducted for the optimum geometry resulting in an increase in peak efficiency of 6.2% with improved performance across the majority of the operating range of the turbine.

8.4 Commercial considerations

In order to put the research presented in this thesis into some sort of commercial context, an analysis of the market for a wave energy device was conducted. This was done by first assessing the global wave energy resource then investigating specific locations with respect to the local resource, government support and current wave energy projects. The information gathered was used to conduct a PEST analysis of the external factors affecting a company wishing to develop wave energy. A SWOT analysis was then performed for the HydroAir turbine, analysing the internal and external factors affecting the device at the current stage of development.

The study identifies the huge wave energy resource available globally and the large potential market due to increasing global energy demand. However, the fact that the technology is in the early stages of development means there is a long way to go until large scale wave energy farms are developed.

The markets analysed in more detail, Spain, Portugal, the west coast of the USA and the UK demonstrate promise for marine renewables with attractive support mechanisms in place as well as plans for test sites to aid development, if they were not already in place. However, it was clear that there was a gap in available funds for early research since support mechanisms would only generate returns once a device was in the water, producing electricity. This gap needs to be filled with private investment and in the current financial market, this is not readily available.

Of the potential markets investigated, the UK was identified as the strongest location for the development of a wave energy device. This is due to the strong support mechanisms, available, high wave resource and access to wave energy test sites in both Scotland and the south west of England.

The SWOT analysis of the HydroAir device demonstrated key strengths to be the high performance of the device and the D-R brand. This presents opportunities for collaboration and the opportunity to win contracts for future energy production. However, the fact that the device is only part of an OWC power plant means that the development of other critical components should be considered. Currently this limits the market for HydroAir and is the main current threat to the fast development of the device. HydroAir needs to quickly move on to the next stage of development to demonstrate the performance of the device offshore in real sea conditions. This is necessary to keep up with the competition as a number of other wave energy converters are already in the RD&D stage, generating power at test sites in the UK.

9 Suggestions for Further Work

Although the research presented here has demonstrated methods of improving the performance level of bi-directional impulse turbines, there is still potential for further improvement. This chapter presents a number of other potential areas for exploration in the continued development of impulse turbines for OWCs.

9.1 Guide vane development

The potential for unconventional guide vane profiles and configurations to improve the performance of bi-directional impulse turbines has been demonstrated in the research. There is potential for further improvement by developing the optimisation tool further, a number of suggested optimisations are presented below:

The MEGV configuration shows potential but is restricted by that fact that conventional, single direction airfoil type profiles are used. It is recommended that the profile parameterisation procedure developed in the research is combined with the MEGV parameterisation. This combination has the potential to maximise the performance of the MEGV configuration as well as reduce the swirl experience at high flow velocities with the profile optimisation method.

It is recommended that both the MEGV optimisation and the profile optimisation are performed in 3D. This will allow for additional parameters to be investigated such as lean, twist and sweep.

9.2 Global turbine optimisation

Optimisation has already played an important role in the HydroAir project, initially being employed by Banks in the development of his ImpOpt design and optimisation system. In this research, the optimisation procedure was adapted for the guide vane profile and configuration. There is the potential for further development of the tool, incorporating the capability of guide vane profile design along with the other turbine parameters.

This global optimisation process would explore the possibility that with improved guide vane profiles, the offset of the VRT could be reduced, reducing the overall size of the turbine. Reducing the size of the turbine would increase marketability as well as reducing the cost of manufacture.

9.3 Flow Control

Active flow control has been suggested as a method of reducing the separation that occurs on the OGV of a bi-directional impulse turbine and a number of concepts for implementing this on the VRT are presented in Freeman et al. (2008). Active flow control (AFC) makes use of an external energy source to manipulate the flow, usually in the form of sucking or blowing devices. In the concepts suggested, the flow was diverted from upstream of the turbine, to the OGV.

Flow control is not a new concept, Ackeret, et al. (1926) experimented with the function of an airfoil after removing the boundary layer through slots in the airfoil surface using suction. More recently, Collis et al. (2004) have analysed a large range of AFC applications involving blowing devices to change the characteristics of fluid flow. Despite the long period of research into AFC, the physical phenomena behind the concept are not fully understood and experimental research shows irregular and sometimes unrepeatable results. Functioning AFC designs are able to show improved fluid flow properties, especially in terms of boundary layer re-generation and control.

As AFC requires some kind of external source of energy, the overall benefit of the system must be realised. This means that the overall increase in performance of the turbine as a result of AFC must be worthwhile to cover the extra energy required to create this improvement in performance. It may be possible to duct the flow from the upstream air flow, to the nozzle for an AFC device, in which case an external source of energy would not be required. This would however use energy from the upstream

flow, reducing the potential power available to the turbine, so the required energy must be recovered by the turbine as a result of reduced losses.

In the research conducted in this thesis, it was ensured that the minimum thickness of the guide vane profiles proposed did not go below 3mm. This was the value, set by Herring (2007) as the minimum thickness at which flow control could still be incorporated into the guide vane profile. This means that the concept of using AFC to reduce the separation at the OGV could be incorporated into the new guide vane profiles in future investigation.

References

Abbott, I.H. and von Doenhoff, A.E. (1949). Theory of wing sections including a summary of airfoil data. McGraw-Hill

Ainley, D.G. and Mathieson, G.C.R. (1957). A Method of Performance Estimation for Axial-flow Turbines, (6th Ed.), Aeronautical Research Council R. & M. 2974.

Ansoff, I. H. (1957). Strategies for Diversification, Harvard Business Review, Vol. 35, pp.113-124

ANSYS (2010). CFX Solver Theory Guide. Release 13.0. Technical report. ANSYS Inc.

ANSYS (2009). Introduction to CFX – Chapter 8 – Transient Simulations. ANSYS Inc. Inventory #002598.

Banks, K. (2009). Optimisation of bidirectional impulse turbines for wave power generation. PhD thesis, School of Engineering, Cranfield University.

Barrett, T.R. (2007). Aerodynamic Design Optimization Using Flow Feature Paramterization, PhD Thesis, University of Southampton.

Bet, F. and Grassmann, H. (2003). Upgrading conventional wind turbines. Renewable Energy 28:71-78

Boccotti, P., Filianoti, P., Fiamma, V., Arena, F. (2007). Caisson breakwaters embodying an OWC with a small opening - Part II: A small-scale field experiment. Ocean Engineering 34:820–841

Braibant, V. and Fleury, C. (1983). Shape optimal design using B-splines. Computer Methods in Applied Mechanics and Engineering, Vol. 44 pp. 247-267.

Brito-Melo, A. (2009). Portugese Pilot Zone. WavEC - Wave Energy Centre Presentation at Energiuka 2009, Oslo.

Brito-Melo, A., Gato L.M.C, Sarmento A.J.N.A., (2002). Analysis of Wells turbine design parameters by numerical simulation of the OWC performance, Ocean Engineering 29:1463–1477

Carbon Trust, (2012). UK Wave Energy Resource, AMEC Environment & Infrastructure UK Limited, Doc Reg No. B/C001/29603/003.

Carbon Trust (2006). Future Marine Energy (CTC601). Technical report, The Carbon Trust.

Carbon Trust (2003). Building options for UK renewable energy (CT-2003-08). Technical report, The Carbon Trust.

Carlin, M., Brown, S. and Doyle, D (2007). Spain, Overseas Market Introduction Service (OMIS). UK Trade & Investment report. Ref. 0459.

Cebeci, T., Shao, J.P., Kafyeke, F., Laurendeau, E. (2005). Computational fluid dynamics for engineers. Horizon, Springer.

Charcosset, C. (2009). A review of membrane processes and renewable energies for desalination. Elsevier, Desalination 245:214-231

Collis, S.S., Joslin, R.D., Seifert, A., Theofilis, V. (2004). Issues in active flow control: theory, control, simulation and experiment. Progress in Aerospace Sciences 40:237-289

Deb, K., (2011). Multi-Objective Optimization Using Evolutionary Algorithms: An Introduction. KanGAL Report Number 2011003, Indian Institute of Technology Kanpur.

Deb, K., Pratap, A. Sameer, A. and Meyarivan, T. (2002). A Fast Elitist Multi-Objective Genetic Algorithm: NSGA-II. IEEE Transactions on Evolutionary computation, Vol. 6, No. 2.

Deb, K. (2001). Multi-objective optimisation using evolutionary algorithms. Wiley.

Deb, K., Agrawal, S., Pratab, A., and Meyarivan, T. (2000). A fast elitist non-dominated sorting genetic algorithm for multi-objective optimization: NSGA-II. Technical report, Kanpur Genetic Algorithms Laboratory, Indian Institute of Technology Kanpur.

Deng, Y., Duan, Z. and Zhan, H. (2007). Aerodynamic optimization of multi-element airfoils by genetic algorithms. West-East High Speed Flow Field Conference, Moscow, Russia.

Denton, J.D. and Dawes, W.N. (1999). Computational fluid dynamics for turbomachinery design. Journal of Mech. Eng Science, IMECHE Proc. Part C Vol 213, No. C2, 107-124.

Dhanasekaran, T.S. and Govardhan, M., (2005). Computational Analysis of Performance and Flow Investigation on Wells Turbine for Wave Energy Conversion, Renewable Energy, 30:2129-2147

Dixon, S., (2005). Fluid Mechanics and Thermodynamics of Turbomachinery. Elsevier.

Dresser Rand, (2009). Insights, Spring 2009, Dresser Rand publication.

Ferguson, J., (1964). Multivariable Curve Interpolation. Journal of the Association for Computing Machinery, Vol. 11, No. 2, 1964, pp. 221-228.

Fernandez Chozas, J. and Soerensen, H.C. (2009). State of the Art of Wave Energy in Spain. IEEE Electrical Power & Energy Conference.

Folley, M. and Whittaker, T. (2009). Analysis of the near shore wave energy resource. Renewable Energy, Published online.

Folley, M., Curran, R., Whittaker, T. (2006). Comparison of LIMPET contra-rotating wells turbine with theoretical and model test predictions. Ocean Engineering 33:1056-1069

Freeman, C., Herring, S., and Banks, K. (2008). Impulse turbine for use in bi-directional flows. International Patent: WO/2008/012530.

Hagerman, G. and Scott, G. (2011). Mapping and Assessment of the United States Ocean Wave Energy Resource. Electric Power Research Institute. Technical Report.

Herring, S. (2007). Design and evaluation of turbines for use in OWC power plants. PhD thesis, School of Engineering, Cranfield University.

Hicks, D.C., Mitcheson, G.R., Pleass, C.M. and Salevan, J.F. (1989). Delbouy: Ocean wave-powered seawater reverse osmosis desalination systems. Elsevier, Desalination, 73:81-94
Hicks, R. and Henne, P. (1978). Wing design by numerical optimization. Journal of Aircraft, 15:407-413.

Horlock, J. (1966). Axial Flow Turbines: Fluid Mechanics and Thermodynamics. Butterworth.

Howell, A.R. (1945a). Design of axial compressors. Proceedings of the Institution of Mechanical Engineers, Vol. 153.

Howell, A.R. (1945b). Fluid dynamics of axial compressors. Proceedings of the Institution of Mechanical Engineers, Vol. 153.

Hoyle, N. (2006). Automated Multi-Stage Geometry Parameterization of Internal Fluid Flow Applications. PhD thesis, School of Engineering Sciences, University of Southampton, UK.

Hussey, J., and McNelis, B. (2012). UK Market Opportunities, Asian Wave and Tidal Energy Conference Series.

International Herald Tribune, (2009). Waves Start to Make Ripples in Renewable Energy World, Energy Report, published 20th October.

Jackson, C.D., Moore, J.R. and Cooper, W.S. (2008). Atlas of UK Marine Energy Resources: Technical Report. BERR, R1432

Jamasb, T., Nuttall, W.J., Pollit, M.G. and Maratou, A. (2006). Technologies for a low-carbon electricity system: an assessment of the UK's issues and options. In: Grubb, M., Jamasb, T. and Pollit, M.G. (2008) Delivering a Low-Carbon Electricity System-Technologies, Economics and Policy. Cambridge University Press. Chapter 3.

Khan, M.J., Bhuyan, G., Iqbal, M.T., Quaicoe, J.E. (2009). Hydrokinetic energy conversion systems and assessment of horizontal and vertical axis turbines for river and tidal applications: A technology status review. Applied Energy 86:1823-1835

Keane, A.J. and Nair, P.B. (2005). Computational Approaches to Aerospace Design: the Pursuit of Excellence. First Edition, John Wiley & Sons, UK.

Kinoue, Y., Kim, T., Setoguchi, T., Mohammad, M., Kaneko, K., Inoue, M. (2004). Hysteretic characteristics of monoplane and biplane Wells turbine for wave power conversion. Energy Conversion and Management, 45:1617-1629.

Krohn, D., Mathews, S., Adams, J. and Valpy, B. (2012). Renewable UK & BVG Associates, Marine Energy in the UK, State of the industry report 2012. Renewable UK.

Lawn, C.J. (2003). Optimization of the power output from ducted turbines. Proceedings of the Institution of Mechanical Engineers, Part A: Journal of Power and Energy, Vol. 217, 107-117.

Lépine, J., Guibault, F., Trépanier, J.-Y., and Pépin, F., (2001). Optimized Nonuniform Rational B-Spline Geometrical Representation for Aerodynamic Design of Wings, AIAA Journal, Vol. 39, No. 11.

Lophaven, S., Nielsen, H., and Sndergaard, J. (2002). DACE: A Matlab Kriging Toolbox. Technical report, IMM, Technical University of Copenhagen.

Mackay, D.J.C., (2009). Sustainable Energy – without the hot air, UIT Cambridge Ltd.

Maeda, H., Santhakumar, S., Setoguchi, T., Takao, M., Kinuoue, Y., and Kaneko, K. (1999). Performance of an impulse turbine with fixed guide vanes for wave power conversion. Renewable Energy, 17:533-547.

Maier, W. (2012). Voith Hydro Ocean Current Technologies, Asian Wave and Tidal Energy Conference Series.

McCroskey, M.J. (1987). A Critical Assessment of Wind Tunnel Results for the NACA 0012 Airfoil. U.S. Army Aeroflightdynamics Directorate, NASA, N258-1

McDonald, M. and Wilson, H. (2011). Marketing plans: How to prepare them, how to use them. Seventh edition, West Sussex: John Wiley & Sons, Inc.

McDonald, M. and Christopher, M. (2003). Marketing: A Complete Guide. Palgrave Macmillan.

McGlumphy, J. (2008). Numerical Investigation of Subsonic Axial-Flow Tandem Airfoils for a Core Compressor Rotor. Dissertation, Virginia Tech.

Meckesheimer, M., Booker, A., Barton, R., and Simpson, T. (2002). Computationally Inexpensive Metamodel Assessment Strategies. AIAA Journal, Vol.40, No. 10, p.2053-2060.

Menter, F. (1994). Two-equation eddy-viscosity turbulence models for engineering applications. AIAA Journal, Volume 32; No. 8; 1598-1605

Mingo, L. (2007). Environment, normalization and regulatory frame. Promotory enterprises vision. Spanish Renewable Energies Association (APPA).

Mollison, D. (1986). Wave climate and the wave power resource. In Hydrodynamics of Ocean Wave-Energy Utilization, Springer, 133-156.

Mørk, G., S. Barstow, A. Kabuth, M. T. Pontes. (2010). Assessing the global wave energy potential, Proc. of 29th International Conference on Ocean, Offshore and Arctic Engineering, ASME, paper 20473.

Morris, R. (2012). The Benefits of a Marine Renewable Test/Demonstration centre, EMEC Ltd., UK. Asian Wave and Tidal Energy Conference Series.

Mortel, F. (2003). Cranfield Team F1: The front wing. Cranfield University, School of Engineering, MSc Thesis.

Natanzi, S., Teixeira, J.A. and Laird, G. (2011). A Novel High-Efficiency Impulse Turbine for Use in Oscillating Water Column Devices. In 9th European Wave and Tidal Energy Conference (EWTEC) handbook, Southampton, UK.

Ofgem (2013). Renewables Obligation: Annual Report 2011 – 2012.

Phillips, D.G., Flay, R.G.J. and Nash, T.A., (1999). Aerodynamic analysis and monitoring of the Vortec 7 diffuser-augmented wind turbine. IPENZ Transactions, Vol. 26, No. 1/EMCh

Queen's University of Belfast, (2002). Islay LIMPET wave power plant, Report, Contract JOR3-CT98-0312

Raghunathan, S. (1995). The Wells air turbine for wave energy conversion. Progress in Aerospace Sciences, 31:335-386.

Roberts, D.A. and Steed, R. (2004). A Comparison of Steady-State Centrifugal Stage CFD Analysis to Experimental Rig Data. ANSYS CFX User Conference.

Ramalhosa, R. and Lyra, F. (2011). Marine Renewable Energy in Portugal. UK Trade & Investment Report.

Rogers, D.F. and Adams, J.A.. (1989). Mathematical elements for computer graphics. Second edition. McGraw-Hill.

Rosenfeld, M., Beverly, Xu., Meadors, L. and Carlstrom, M. (2008). Overseas Market Introduction Service on wave energy technologies and projects on the west coast of the United States. UK Trade & Investment Report.

Ruiz-Minguela, P. (2012). Biscay Marine Energy Platform (bimep). GMREC V Open water testing panel presentation. TECNALIA, Spain.

Samareh, J.A. (1999). A Survey of Shape Parameterization Techniques. CEAS/AIAA/CASE/NASA Langley International Forum on Aeroelasticity and Structural Dynamics, CP-209136, pp.333-343.

Saravanamuttoo, H., Rogers, G., Cohen, H. and Sraznicky, P. (2009). Gas Turbine Theory. Sixth Edition. Prentice Hall. P.344

Sasena, M. (2002). Flexibility and efficiency enhancements for constrained global design optimization with Kriging approximations. PhD thesis, University of Michigan.

Setoguchi, T., Takao, M., Kinoue, Y., Kaneko, K., Santhakumar, S., and Inoue, M. (1999). Study on an impulse turbine for wave energy conversion. Proceedings of the International Offshore and Polar Engineering Conference.

Setoguchi, T., Santhakumar, S., Maeda, H., Takao, M., and Kaneko, K. (2001). A review of impulse turbines for wave energy conversion. Renewable Energy, 23:261-292.

Setoguchi, T., Santhakumar, S., Takao, M., Kim, T.H., Kaneko, K. (2003). A modified Wells turbine for wave energy conversion. Renewable Energy, 28:79-91

Setoguchi, T., Takao, M. (2006). Current status of self rectifying air turbines for wave energy conversion. Energy Conversion and Management 47:2382–2396

Sheldahl, R.E. and Klimes, P.C., (1981). Aerodynamic characteristics of seven symmetrical airfoil sections through 180-degree angle of attack for use in aerodynamic analysis of vertical axis wind turbines. Sandia national laboratories energy report, SAND80-2114

Slawig, T., (2001). Domain optimization of a multi-element airfoil using automatic differentiation. Advances in Engineering Software, 32:225-237

Sóbester, A. and Barrett, T., (2008). The Quest for a Truly Parsimonious Airfoil Parameterization Scheme. 8th AIAA Aviation Technology, Integration, and Operations (ATIO) Conference, Paper ICAS2008-P2.2 (AIAA 2008-8879)

Sóbester, A. and Kean, A. J., (2007). Airfoil Design via Cubic Splines - Ferguson's Curves Revisited, AIAA Infotech at Aerospace 2007 Conference and Ex-hibit, American Institute of Aeronautics and Astronautics, Rohnert Park, California, No. AIAA 2007-2881.

Song, W. and Keane, A.J. (2004). A study of shape parameterisation methods for airfoil optimisation. 10th AIAA/ISSMO Multidisciplinary Analysis and Optimization Conference, AIAA 2004-4482.

Tang, Z.L. and Désidéri, J.A. (2002). Towards Self-Adaptive Parameterization of Bézier Curves for Airfoil Aerodynamic Design. INRIA Research Report No. 4572.

The Crown Estate (2012). The Crown Estate, Wave & Tidal Programme, Future Leasing: Industry Engagement Exercise.

Torre-Enciso, Y., Ortubia, I., Lopez de Aguileta. L.I. and Marques, J. (2009). Mutriku Wave Power Plant: from the thinking out to the reality. Proc. 8th European Wave and Tidal Energy Conference.

Washio, Y., Osawa, H. and Ogata, T. (2001). The open sea tests of the offshore floating type wave power device “Mighty Whale” - characteristics of wave energy absorption and power generation, Oceans 2001 MTS/IEE Conference: 579-585

Watterson, J. K. and Raghunathan, S. (1996). Investigation of Wells Turbine performance using 3-D CFD. Department of Aeronautical Engineering, The Queen's University of Belfast

WavEC (2004). Potential and Strategy for the Development of Wave Energy in Portugal. Wave Energy Centre – Offshore Renewables Report.

Wavegen (2003). Research into the further development of the LIMPET shoreline wave energy plant. Technical report, UK Department of Trade and Industry.

Webb, I., Seaman, C., and Jackson, G. (2005). Oscillating water column wave energy converter evaluation report. Technical report, Carbon Trust.

WEC (1993). Renewable energy resources: Opportunities and Constraints. Technical report, World Energy Council.
Wells, A. (1976). Fluid driven rotary transducer. UK Patent No. [GB]47365/76.

Whittaker T, Collier D, Folley M, Osterried M, Henry A, Crowley M. (2007). The development of Oyster - a shallow water surging wave energy converter. Proceedings of 7th European Wave Tidal Energy Conference, Porto, Portugal, 2007.

Wind Power, (2009). How can the offshore wind industry overcome O&M obstacles? published 1st January.

Venkataraman, P. (1998). Low speed multipoint airfoil design. 16th Applied Aerodynamic Conference Paper #98-2402, Albuquerque, New Mexico

Yago, M., Atkins, J.P., Bhattarai, K., Green, R. and Trotter, S. (2008). Modelling the economic impact of low-carbon electricity. In: Grubb, M., Jamasb, T. and Pollit, M.G. (2008) Delivering a Low-Carbon Electricity System – Technologies, Economics and Policy. Cambridge University Press. Chapter 15.

Appendix A – PEST Analysis

Political	Economic
• Support mechanisms • Incentives • Environmental issues • Legislation • Barriers to entry • Energy policy • Funding, grants and initiatives • International legislation / agreements (Kyoto protocol) • Regulatory bodies and processes • Trading schemes (ROCs, EU ETS) • Home market lobbying / pressure groups e.g. pro fossil fuel / nuclear power companies • Wars or conflicts • Fuel taxation • Security of supply • Global energy demand	• Viability • Support mechanisms • Subsidy • Feed in tariffs • Availability of finance • Oil prices • Collaboration • Investment • Uncertainty of resource • Predictable future costs (not affected by oil price) • Investment in infrastructure (Grid, gas pipelines etc.) • Interest and exchange rates • International trade / monetary issues • Market cycles - renewables
Social	**Technological**
• Green issues • Climate change evidence • Liberal energy market • Stakeholder impact • Environmental concerns • Noise factor • Media coverage • Image of wave power / OWC technology	• Immature technology • Efficiency • Viability • Survivability • Competing technology development • Other renewables cost effectiveness • Continued research funding • Associated technologies • Dependent technologies • Replacement technology / solutions • Patents • Size constraints

Appendix B – SWOT Analysis

Strengths	Weaknesses
• Unique turbine design • Patented technology • Proven Turbine expertise • High Efficiency • Recognised international company • Financial backing • Global reach • Internationally recognised • Proven Quality • Proven customer service • Partnership • University collaboration • Engineering council funding • Renewable energy – predictable future costs • Low visual impact of OWC technology • Scalable / modular design	• New product • New manufacturing techniques • Diversification • New Markets • No offshore testing results • Previous failed testing • Immature technology • Size • High cost • Reliant on development of other technologies (OWC Buoy) • Part of a system • Noise factor of OWC technology
Opportunities	**Threats**
• Growing renewables market • Increasing global energy demand • Large global wave resource • Little competition from OWC turbine developers • Niche target markets • Current leader in experimental performance • No current clear leader in wave energy market • Continued product development • Partnership – Universities, developers • Wave energy test sites (EMEC, WaveHub) • Demonstration Units • Offshore industry development	• Immature technology sector • Immature supply chain • Political effects • Favouring of other low-carbon technologies • Competitiveness with other renewables • Reduction of governmental support • Competing devices • OWCs deemed unsuitable • Funding • Environmental opposition